ADVANCES IN SYNTHESIS OF CO- AND TER- POLYCARBONATES AND POLYESTERS FROM NON-PETROLEUM FEEDSTOCKS AND KINETIC STUDIES OF LIGAND SUBSTITUTION FROM MANGANESE HALF-SANDWICH COMPLEXES

A Dissertation

by

ROSS RIVERS POLAND

Submitted to the Office of Graduate Studies of
Texas A&M University
in partial fulfillment of the requirements for the degree of

DOCTOR OF PHILOSOPHY

May 2012

Major Subject: Chemistry

Advances in Synthesis of Co- and Ter- Polycarbonates and Polyesters from Non-Petroleum Feedstocks and Kinetic Studies of Ligand Substitution from Manganese Half-Sandwich Complexes

ADVANCES IN SYNTHESIS OF CO- AND TER- POLYCARBONATES AND POLYESTERS FROM NON-PETROLEUM FEEDSTOCKS AND KINETIC STUDIES OF LIGAND SUBSTITUTION FROM MANGANESE HALF-SANDWICH COMPLEXES

A Dissertation

by

ROSS RIVERS POLAND

Submitted to the Office of Graduate Studies of
Texas A&M University
in partial fulfillment of the requirements for the degree of

DOCTOR OF PHILOSOPHY

Approved by:

Chair of Committee,	Donald J. Darensbourg
Committee Members,	François P. Gabbaï
	Timothy Hughbanks
	Jaime Grunlan
Head of Department,	David H. Russell

May 2012

Major Subject: Chemistry

ABSTRACT

Advances in Synthesis of Co- and Ter- Polycarbonates and Polyesters from Non-Petroleum Feedstocks and Kinetic Studies of Ligands Substitution from Manganese Half-sandwich Complexes.

(May 2011)

Ross Rivers Poland, B.S., Rose-Hulman Institute of Technology

Chair of Advisory Committee: Dr. Donald J. Darensbourg

This dissertation is written in two parts. The first pertains to polycarbonate and polyester synthesis using relatively benign processes.

The synthesis of polycarbonates from the coupling of CO_2 and epoxides catalyzed by transition metal catalysts has long been studied in the DJD group. The benefits of this process are that it utilizes comparatively benign reagents, can be performed using no extraneous solvent, and is 100% atom efficient. A method potentially useful for achieving more desirable polycarbonate properties is to produce an epoxide A/epoxide B/CO_2 terpolymer, thus allowing more fine "tuning" of properties to what one may desire while simultaneously influencing relative epoxide reactivity to potentially increase catalytic turnovers. Specifically, the coupling of propylene oxide and cyclohexene oxide with CO_2 to yield a random copolymer with tunable properties has been studied *via* a Fineman-Ross analysis. Propylene oxide was found to be

incorporated into the resultant polymer chain with anywhere from 4-10 times the preference of cylcohexene oxide.

Although it has been reported as early as 1969, the copolymerization of epoxides and cyclic anhydrides catalyzed by transition metal complexes to yield polyesters *via* a chain-growth mechanism has recently gained much attention. This robust method of polyester synthesis can utilize rather inexpensive reagents to synthesize an array of polyester products which have a wide range of T_g values (-30°C – 90°C), achievable through simple monomer selection.

The second part of this dissertation deals with the kinetic study of ligand substitution from manganese carbonyl metal fragments. Some time ago it was postulated that complexes of the $(Cp)M(CO)_2L$ variety undergo ligand substitution *via* a associative mechanism allowed by a haptotropic η^5-η^3 shift in the η^5 ligand. Through kinetic studies and theoretical modeling, an approximate activation energy barrier of ~34 kJ/mol has been calculated for the ring slip of (2,5-dimethylpyrrole)Mn to occur. Additionally, further kinetic studies were performed in which Tp, a ligand electronically similar to Cp, was compared to MnCp complexes.

DEDICATION

I dedicate this dissertation to my family. My parents, Shep and Mary Poland, have invested countless hours and dollars ensuring that I "do OK" in life. Regardless of my shortcomings or failures along the way, they never have wavered in their support of me and for that I cannot thank them enough.

ACKNOWLEDGEMENTS

To quantify my earliest interest in science, I'd have to go all the way back to a book my parents bought me when I was 2 or 3 years old entitled The Way Things Work, by David Macauly. If you're a parent, go immediately to the nearest book retailer and purchase this for all your current and future children. This book introduced me to the concept that there was more to everything in the universe than *it just works*. My desire to understand the logic behind the various processes that govern our world probably stems from my parents reading (and rereading) this book to me at a very early age, although I didn't necessarily understand that my inquisitiveness constituted a sort of research

Years later, science became more than the title of a class in school which was supposed to terrify me. I excelled in most of my classes, but apparently displayed an above average interest in my science classes. In the fifth grade, I won the science fair by presenting several experiments I learned in the Boy Scouts. In the eighth grade my friend Brent's father, Anthony Martin, was my teacher for Earth Science, in which I learned about weather patterns, plate tectonics, and why astronauts don't get hot even though they may technically be closer to the sun than I am. Mr. Martin's class was the first one that really piqued my interest in science as something I could *do*. My freshman science teacher in high school, Yvonne Naiser, was the first to introduce me to the periodic table, the concept of an electron as more than "the one that's negative", and the Bohr model of the atom. I had never been so engaged in a subject prior to this; I don't believe

I missed a single point from any assignment in that grading period. Two years later I enrolled in Chemistry, taught by the ever-intimidating Allen Coats. It was during this time that I learned of thermodynamics, some light molecular orbital theory (the day he finally got me to understand the concept of a pi bond is still one of my more satisfying intellectual achievements), and the structure of organic molecules; and during which I fully embraced my future as a chemist. Mr. Coats instructed me in chemistry for two years, encouraged me academically, in some cases protected me from the bureaucracy of high school (in one famous instance he denied a summons to the central office because, as he put it, "Chemistry 2 is not some bullshit class, pull him out of athletics"), and gave me confidence in my abilities by referring me as a tutor to multiple students. Without Mr. Coats I'd probably be an engineer right now, and that's terrible. By the time I arrived at my alma mater, Rose-Hulman Institute of Technology, I was already planning my foray into the graduate world. Notably, Drs. Rebecca Devasher and Bruce Allison aided me greatly in my academic career by being my earliest research advisors. Rebecca Devasher is the first person who introduced me to organometallic catalysis and "green" chemistry. Dr. Allison is the first person to introduce me to the concept of utilizing CO_2 for more than exhaling. If they hadn't taken a chance on me, it's doubtful that I would have had an opportunity to attend such a great graduate school as Texas A&M.

A number of non-science teachers have influenced me greatly as well by teaching me to be a well-rounded person intellectually. My high school English teachers and tennis coaches, Roben Eller and Carol Grogan, have had faith in me for years and have encouraged me as a student, an athlete, and a person for most of my life. Drs.

Richard House, Mark Minster, and Julia Williams at Rose-Hulman taught me almost every class for my minor in language and literature. At times when I was worn down by constant focus on chemical structures and equations, these folks were able to take my mind elsewhere, to fantastic places created by authors that I probably never would have heard of otherwise.

During my academic pursuits I've made more friends than I can count, all of whom have helped me to relax and not take life too seriously throughout it all. Chad Schulz has known me for longer than anyone barring my parents. David Aaronson has constantly been the level head that I go to for advice. Brent Martin is a guy I could not see for two years (God forbid) and wouldn't miss a beat when we got back together. Spike Miller is the first friend I made at Rose-Hulman. Much thanks is due to him and his beautiful wife Kimberly for always giving me a home away from home, whether it's the Psycho Closet or Brookings, SD. Jordan Wysong and Michael Rasche were the greatest roommates a guy could ask for. I don't understand how we managed to live together for almost three years while remaining friends, but I'm glad it's worked out this way. I want to thank Jeremy Haefele for being my Sonka buddy, it's the greatest bar in the world. I want to apologize to Anthony Sloan for slacking off on starting a band with him. Maybe once I'm done writing this thing I'll have a little more time to dedicate to serious riffing. Thanks to Brian Eoff for being an awesome roommate, for following the Rockets with me, and for not understanding a damn thing about chemistry. Thanks to the TAMU Chemistry softball team (Mike, Kenton, Tyler, Larry, Dan, Amy Alissa,

etc…) for the mostly mediocre brand of softball we played and for the (much more needed) companionship during some emotionally rough times.

The DJD and MYD groups have been a constant source of support and inspiration. First and foremost, thanks to Dr. Jeremy Andreatta for being my mentor during my earliest times at Texas A&M. The others, Dr. Wonsook Choi, Dr. Eric Frantz, Dr. Shawn Fitch, Dr. Adriana Moncada, Dr. Osit Karroonnirrun, Sheng-Hsuan Wei, Sam Kyran, Joanna, and Andrew Yeung (from DJD) and Dr. Kayla Green, Dr. Jen Hess, Dr. Scott Brothers, Danielle Crouthers, Jason Denny, and everyone else in MYD have all kept me company, advised me on research, or aided me in some manner, and for that I'm very thankful. A special thanks goes to Marcetta Darensbourg for much advice given over the course of my Texas A&M career. Extremely special thanks go to the beautiful Ms. Stephanie Wilson. We've truly made some memories following Aggie Athletics, marathoning TV series, and having a great time doing basically anything. You've invested a ridiculous amount of time in helping me with my research, my research presentations, and this dissertation. I can't thank you enough.

Finally, I want to thank my advisor, Don Darensbourg. Thanks for putting up with me as patiently as you did for the past several years. I've learned an incredible amount from you about how to be an effective scientist. Thank you.

Before I run out of room, I need to squeeze in the following people: Metallica for writing the album "…And Justice for All", ISIS for writing the album "Oceanic", Ron Howard for producing "Arrested Development", J.J. Abrams for producing "Lost", Dash Harris, Hakeem Olajuwon, Shane Battier, and Andre Agassi.

TABLE OF CONTENTS

Page

ABSTRACT iii

DEDICATION v

ACKNOWLEDGEMENTS vi

TABLE OF CONTENTS x

LIST OF FIGURES xiii

LIST OF TABLES xxii

CHAPTER

I INTRODUCTION 1

Carbon Dioxide as a Pollutant and as a Reagent 1
Industrial Synthesis of Polycarbonate 5
Polycarbonates from Copolymerization of CO_2 and Epoxides 9
Metal Catalyzed CO_2/epoxide Coupling 12
Tuning Properties of Polycarbonates through Terpolymerization 19
Polymers from Renewable Resources 20
Polyesters from Epoxides and Cyclic Anhydrides 22
Synthesis of One-Pot Block Terpolymers 24
Metallocenes in Industrial Chemistry 27
Manganese Cyclopentadienyl Complexes 28
RapidScan and StepScan FTIR 29
Ring-Slip Mechanism 31
Tp: An Electronic Cp Mimic 33

II COPOLYMERIZATION OF PROPYLENE OXIDE AND CYCLOHEXENE OXIDE WITH CO_2 BY CHROMIUM(III) (SALAN) CATALYSTS 34

Introduction 34
Experimental 36
Results and Discussion 41
Conclusions 55

III TERPOLYMERIZATION OF MULTIPLE EPOXIDES WITH CO_2 57

Introduction 57
Experimental 58
Results and Discussion 62
Future Work 74
Conclusions 75

IV SYNTHESIS OF POLYESTERS FROM THE ALTERNATING COPOLYMERIZATION OF CYCLIC ANHYDRIDES AND EPOXIDES 77

Introduction 77
Experimental 79
Results and Discussion 81
Future Work 94
Conclusions 95

V QUANTIFYING THE ENERGY BARRIERS OF THE RING SLIP OF 2,5-DIMETHYLPYRROLE MANGANESE CARBONYL COMPLEXES 97

Introduction to collaboration with Texas A&M Qatar 97
Introduction 98
Experimental and Theoretical Methods 101
Results and Discussion 103
Theoretical Modeling 118
Conclusions 123

VI KINETIC AND THEORETICAL COMPARISONS OF TRIS(PYRAZOLYL)BORATE AND CYCLOPENTADIENYL MANGANESE COMPLEXES 126

Introduction 126
Experimental and Theoretical Methods 130
Results and Discussion 134
Conclusions 156

VII CONCLUSIONS 158

REFERENCES 163

APPENDIX A 177

APPENDIX B 184

VITA 192

LIST OF FIGURES

		Page
Figure 1.1	Greenhouse gases and their absorption bands	2
Figure 1.2	Atmospheric CO2 concentration measured at Mauna Loa, Hawaii, displaying an overall rising trend despite annual fluctuations.....	3
Figure 1.3	Phase diagram of CO_2	4
Figure 1.4	Commonly produced plastics. A – Polyethylene, B – Polypropylene, C – Polystyrene, D – Polyethyleneterephthalate.....	6
Figure 1.5	Top - Industrial synthetic route to BPA polycarbonate Lexan®. Bottom – synthetic replacements for phosgene as carbonyl source. Left – dimethyl carbonate. Right – diphenyl carbonate.....	6
Figure 1.6	Schematic of ATR-FTIR Spectroscopy and a ReactIR1000 setup at Texas A&M in lab of Prof. Donald J. Darensbourg	7
Figure 1.7	General scheme for polycarbonate synthesis from CO2 and generic epoxides. n = polycarbonate, m = polyether linkages.....	10
Figure 1.8	Mechanism of CO_2/epoxide copolymerization to afford polycarbonates	13
Figure 1.9	Representative three dimensional plot of poly(cyclohexylene carbonate) formation catalyzed by (salen)Cr(III)Cl	15
Figure 1.10	A – Representative (salan)CrX catalyst. B – (S,S,S)-stereoactive catalyst reported by Lu, et al. C – Pendant amine arm catalyst reported by Lu, et al. D – representative (salen)CoX catalyst, ligand architecture is identical to that of (salen)CrX. E – salen catalyst with ammonium salt pendant arms reported by Lee, et al. X = 2,4-dinitrophenolate, Y = [X-H-X].....	16
Figure 1.11	Standard (salen)CrX binding mode, left. Salan binding mode, right. Square is representative of substrate binding site.	17
Figure 1.12	Examples of regiochemistry in PPC. Top – Head to head linkage. Middle – Tail to tail linkage. Bottom – Head to head linkage.....	18

Figure 1.13	Industrial synthesis of PET from terephthalic acid and ethyelene glycol.....	22
Figure 1.14	Scheme of epoxide/cyclic anhydride coupling to afford polyester…	23
Figure 1.15	Epoxides and anhydrides used thus far in polyester synthesis.	25
Figure 1.16	Potential mechanism of block-polyester-*co*-polycarbonate terpolymer formation	26
Figure 1.17	Synthesis of polyester-block-polycarboante from CO_2, anhydride, and epoxide.	26
Figure 1.18	Typical metallocene Ziegler natta catalyst, M = Ti, Hf, Zr	27
Figure 1.19	General scheme of CO displacement from $CpMn(CO)_3$	28
Figure 1.20	RapidSCAN and StepSCAN setup at Texas A&M Qatar in laboratory of Dr. Ashfaq Bengali. Top photo: tunable CO laser used as IR source for StepSCAN experiments. Bottom photo: YAG laser photolysis setup used in both RapidSCAN and StepSCAN .... experiments.	30
Figure 1.21	Ligand substitution by “ring-slip” mechanism. The dimethylpyrrole ligand is able to disrupt its aromaticity and shift from *η5* to *η3,* allowing the ligand to substituted through an associative, rather than dissociative, mechanism.	32
Figure 2.1	Proposed structures of complex 1 employed as catalyst in the ..... copolymerization processes.	35
Figure 2.2	Head-to-tail (HT) regiochemistry of poly(propylene carbonate).....	42
Figure 2.3	Synthesis of (salan)CrN_3	43
Figure 2.4	(a) X-ray structure of dimeric complex obtained from crystallization of complex 1. (b) Truncated model of one of the metal fragments . containing the H2O molecule, with stick drawing for better clarity.	44
Figure 2.5	*In situ* infrared monitoring of copolymer production from CHO and CO_2 as catalyzed by complex 1 in the presence of varying quantities of $PPNN_3$.....	46

Figure 2.6 (a)Three-dimensional stack plots of the infrared spectra collected every 3 min during the coupling reaction of CHO and CO_2 (60^o C and 500 psi pressure) in the absence of $PPNN_3$. (b) Reaction profile of this catalytic system. 48

Figure 2.7 Photographs of the isolated poly(cyclohexylene carbonate) after one methanol precipitation: (a) using (salen)CrCl as catalyst and (b) using complex 1 as catalyst. 49

Figure 2.8 Carbonyl region of the 13C NMR spectra (125 MHz, CDCl3) generated from the copolymerization of rac-PO/CO2 at 22 oC and 1.5 MPa for 16 h: head-to-tail (HT); tail-to-tail (TT); head- to-head (HH). 49

Figure 2.9 Diblock copolymer of poly(propylene carbonate) and poly(cyclohexylene carbonate) 52

Figure 2.10 ^{1}H NMR spectrum in methine and methylene regions of diblock ... copolymer of poly(propylene carbonate) and poly(cyclohexylene .. carbonate). (b) ^{13}C NMR spectrum in carbonate region of diblock . copolymer of poly(propylene carbonate) and poly(cyclohexylene .. carbonate). The m-centered tetrads (isotactic) appear at 153.7 ppm and r-centered tetrads (syndiotactic) appear at 153.1 ppm. 53

Figure 2.11 ^{1}H NMR spectrum in methine and methylene regions of terpolymer prepared from a 1.5 ratio of propylene oxide to cyclohexene oxide. Ratio of corresponding monomers (PO:CHO) in terpolymer is ..... approximately two to one. 53

Figure 2.12 Triblock copolymer of poly(propylene carbonate), poly(cyclohexylene carbonate), and poly(vinylcyclohexylene carbonate). 54

Figure 2.13 ^{1}H NMR spectrum in the methine, methylene, and vinyl regions of triblock copolymer of poly(propylene carbonate), poly(cyclohexylene carbonate), and poly(vinylcyclohexylene carbonate). 55

Figure 3.1 (a) X-ray structure of (salalen)CrCl·H_2O. (b) X-ray structure of .... $[(salen)Cr(OH)]_2$. 63

Figure 3.2 Copolymerization of cyclohexene oxide and CO2 in the presence of complex **2a** and an equivalent of PPNN3. **2a** (blue): No catalyst pretreatment. **2b** (green): catalyst pretreatment at 60 oC. **2c** (red): . Catalyst pretreatment at 110 ^{o}C. 64

Figure 3.3 Epoxides 3 and 4 are able to be coupled with CO2, unlike epoxide 5 66

Figure 3.4 Reactivity ratios, the relative tendencies of the monomers (M1 and **M2)** to self-propagate or cross propagate. –O-P = growing polymer chain..... 68

Figure 3.5 Fineman-Ross plot of CHO/PO/CO2 terpolymerization reaction at 25 ^{o}C. The r_1 and r_2 values are 0.172 and 1.11, respectively, with an R^2 value of 0.9995..... 70

Figure 3.6 Comparison of rates of copolymer formation for the copolymerization of CHO/CO_2 at 40 ^{o}C (blue) and 60 ^{o}C (red) *vs* terpolymerization of CHO/PO/CO_2 at 40 ^{o}C (green) and 60 ^{o}C (purple)..... 71

Figure 3.7 Growth of peak at 1750 cm^{-1} for copolymerizations of CHO and CO_2 catalyzed by complex **2a** and $PPNN_3$ at 3.5 MPa of CO_2 in toluene solvent as a function of temperature monitored by ATR-FTIR spectroscopy..... 72

Figure 3.8 Kinetic plots of $\ln[(A_\infty)/(A_\infty-A_t)]$ *vs* time for the data presented in . **Figure 3.7,** where A_∞ and A_t represent the absorbance of the copolymer band at 1750 cm^{-1} at time equals infinity and t, respectively. Second-order rate constants are 1.59 x 10^{-2} sec^{-1}-M^{-1} at 70.0 ^{o}C, 7.37 x 10^{-3} sec^{-1}-M^{-1} at 60.0 ^{o}C, and 1.22 x 10^{-3} sec^{-1}-M^{-1} at 40.0 ^{o}C. 72

Figure 3.9 Eyring plot of rate constant data *vs* temperature shown in **Figure 3.8,** with an R^2 value of 0.9997..... 73

Figure 3.10 *In situ* infrared spectroscopy monitoring of copolymerization of PO/CO_2 in toluene at 40 ^{o}C utilizing catalyst **2a** and $PPNN_3$ at 3.5 MPa of CO_2 pressure. 74

Figure 4.1 Scheme describing generic reaction of epoxide with anhydride to produce polyester 77

Figure 4.2 Anhydrides and epoxides used in study 81

Figure 4.3 *N,N'-bis(3,5-di-tert-butylsalicylidine)-1,2-cyclohexane* ..... diaminochromium(III)chloride. 82

Figure 4.4 Growth of polyester peak at 1748 cm-1 as monitored by *in situ* ATR-FTIR spectroscopy for various combinations of catalyst and cocatalyst. (Green line) [Cr]:[Cl]:[PA]:[CHO] = 1:1:200:200, (Red line) [Cr]:[Cl]:[PA]:[CHO] = 1:0:200:200, (Blue line) [Cr]:[Cl]:[PA]:[CHO] = 0:1:200:200. Cr = (salen)CrCl, Cl = PPNCl, PA = phthalic anhydride, CHO = cyclohexene oxide..... 82

Figure 4.5 Cocatalyst Study – Reactions were performed using the following conditions: 64 mg catalyst (1 eq, 4.05 mM), appropriate cocatalyst, 200 eq PA (3 g), 200 eq CHO (2 mL), and 18 mL toluene (solvent) at 80 ^{o}C. Cations not listed are PPN^{+} (bis(triphenylphosphine)iminium) salts. DNP- = 2,4-dinitrophenoxide. **A.** Absorbance of polyester band at 1738 cm^{-1} *vs* time. **B.** Determination of rate constants from the $\ln(A_\infty/A_\infty-A_t)$ *vs* time, where A_∞ and A_t are absorbances of polyester band at 1738 cm^{-1} at t_∞ = infinity and t = time, respectively. 83

Figure 4.6 ^{1}H NMR Spectrum of PACHO. (a) PA phenyl appears at 7.65 ppm. (b) H adjacent to ester functionality in CHO appears at 5.25 ppm. 85

Figure 4.7 Scheme describing competitive incorporation of CO_2/anhydride into polyester-block- polycarbonate 86

Figure 4.8 Copolymerization of equimolar quantities of cyclohexene oxide and phthalic anhydride in the presence of 4.05 mM (salen)CrCl and one equivalent of PPNN3 in 2.5 mL of toluene at 80 ^{o}C. **A.** Absorbance of the growth of the 1738 cm^{-1} band of the polyester *vs* time. **B.** Plot of $\ln(A_\infty/A_\infty - A_t)$ *vs* time. 87

Figure 4.9 First-order plots for the copolymerization of PA and CHO as a function of temperature. 88

Figure 4.10 Eyring plot of the PA and CHO copolymerization reaction, with $R^2 = 0.980$. 88

Figure 4.11 *In situ* FTIR analysis of block copolymerization process. Reaction conditions used were (salen)CrCl/PPNCl/PA/CHO = 1:3:200:200 under 500 psi CO2, 80oC with 19 mL toluene (solvent, volume totaling 25 mL). Deconvolution was performed by ReactIR ic10 software. Green line = polyester growth (1738 cm^{-1}, red line = anhydride consumption (1770 cm^{-1}), and blue line = polycarbonate growth (1750 cm^{-1}). The three-dimensional surface of the reaction is shown in the insert on the right. 89

Figure 4.12 Scheme describing competitive CO_2/anhydride incorporation into . polyester-block- polycarbonate..... 90

Figure 4.13 Comparison of Epoxides: Polymer growth vs. time – Reactions were performed in sealed NMR tubes using 2.0 mL d_8 toluene as solvent. 200 eq appropriate epoxide was added to tube, then was dissolved in a stock solution of 1.8 mL d8 toluene, 300 mg CHA (200 eq), 6.3 mg (salen)CrCl (1 eq), and 5.7 mg PPNN3 (1 eq). The tubes were then heated to 80oC and allowed to react until 100% conversion was achieved. 91

Figure 4.14 Scheme describing potential photochemical crosslinking mechanism of MAPO polymer 93

Figure 5.1 Proposed ring-slip mechanism for ligand substitution in (indenyl)Rh complex..... 101

Figure 5.2 Scheme of photolytic CO removal, subsequent solvent replacement, and solvent displacement by the incoming ligand, L..... 104

Figure 5.3 Difference spectra obtained upon photolysis of a cyclohexane solution of (η^5-DMP)$Mn(CO)_3$ in the presence of THF at 293 K. The positivepeaksareduetotheformationofthe(η^5-DMP)$Mn(CO)_2$(THF) complex, and the negative peaks are associated with depletion of parent upon photolysis. 105

Figure 5.4 Reaction of the initially formed (η^5-DMP)$Mn(CO)_2$(Br-hex) complex with 2,6-lutidine in cyclohexane at 303 K. Photolysis was conducted in the presence of [1-bromohexane] = 2.85 M and [2,6-lutidine] = 0.43 M in cyclohexene solution. Spectra were obtained at 600 ms intervals. The CO band at 1950 cm^{-1} is a composite of the E vibrational mode of the parent tricarbonyl and the A_1 mode of the Br- hex solvate. 107

Figure 5.5 Plot of k_{obs} versus [THF] for the reaction of (η^5-DMP)$Mn(CO)_2$(CyH) with THF in cyclohexane at several temperatures. 107

Figure 5.6 Plot of kobs versus [THF] for the reaction of X$Mn(CO)_2$(η^2-Bz) [X = η^5-DMP, Cp] with THF at 323 K in cyclohexane solvent. The similar slope for the two plots suggests the lack of a significant rate enhancement upon replacement of Cp with the DMP ligand. The intercept for the DMP system is larger than for Cp although, as

explained in the text, this does not imply a different displacement mechanism. 108

Figure 5.7 Rates describing the displacement of olefin from manganese center by picoline. 112

Figure 5.8 Plot of kobs versus [2-picoline] at 358 K for the displacement of cyclooctene from the DMP and Cp complexes by 2-picoline in heptane. Note that while the plot is linear for the DMP system, as shown in the inset, kobs does not vary with [2-picoline] for the Cp complex. 113

Figure 5.9 Mechanism describing dual associative/dissociative pathways of olefin substitution from (DMP)$Mn(CO)_2$ fragment 117

Figure 5.10 Calculated structures for the (a)(η^5-DMP)$Mn(CO)_2$(THF) and (b) $CpMn(CO)_2$THF molecules. The geometries and THF binding strengths are similar for both complexes. 118

Figure 5.11 Enthalpy diagram for the displacement of CO from (η^5-X)-$Mn(CO)_3$ PH_3 where X = Cp and DMP. The η^3 transition state is energetically more accessible for the DMP system. 121

Figure 5.12 Enthalpy profile for the substitution of THF from the (-DMP)-$Mn(CO)_2$ fragment by C_2H_4. Unlike CO displacement, the dissociative channel for THF substitution has a lower enthalpy than the associative pathway 123

Figure 5.13 Calculated structures of the (η^3-DMP)$Mn(CO)_2$(THF)(η^2-C_2H_4) .... transition state and intermediate. 124

Figure 6.1 Ligand substitution in $TpMn(CO)_2L$ and $CpMn(CO)_2L$ complexes 128

Figure 6.2 Difference spectra obtained 12.5 μs after photolysis of a cyclohexane solution of $TpMn(CO)_3$ in the presence of cyclooctene (2.11 M) and THF (0.45 M) at 296 K. Negative peaks are associated with depletion of the parent upon photolysis. Positive peaks are due to the CO stretching bands of the $TpMn(CO)_2$(η^2-cyclooctene) 1960/ 1884 cm^{-1}) and $TpMn(CO)_2$(THF) (1851 cm^{-1}) complexes. The second CO band for the THF species is not observed in this experiment, due to overlap with the parent band. Under some conditions, however, it is observed at 1946 cm^{-1}. 129

Figure 6.3 Mechanism of photolytic CO displacement and subsequent ligand replacement by cyclooctene and THF in $TpMn(CO)_2$, the THF adduct of which is more stable than the cyclooctene adduct. 130

Figure 6.4 Photolysis of (a) $TpMn(CO)_3$ and (b) $CpMn(CO)_3$ conducted in the presence of cyclooctene (2.11 M) and THF (0.45 M) in cyclohexane at 296 K. 135

Figure 6.5 Plot of k_{obs} vs [THF] at several temperatures for the displacement of cyclooctene from $TpMn(CO)_2(\eta^2$-cyclooctene by THF. The cyclohexane solution was 3.1 M in cyclooctene with the appropriate amount of THF added. The saturation behavior of k_{obs} suggests a dissociative mechanism of ligand displacement from the Mn center. 136

Figure 6.6 Mechanism of cyclooctene displacement by THF from $TpMn(CO)_2$ 137

Figure 6.7 EyThe dissociation of cyclooctene from $CpMn(CO)_2(\eta^2$-cyclooctene) and $TpMn(CO)_2(\eta^2$- cyclooctene).The plots have been extrapolated to more clearly demonstrate the difference in slopes, which is related to the binding enthalpy difference in the Cp and Tp systems. The y intercepts for both systems yield similar positive $\Delta S^{\neq}$ values, consistent with a dissociative displacement mechanism. 141

Figure 6.8 Space filling models of (a) $TpMn(CO)_3$ and (b) $CpMn(CO)_3$ 142

Figure 6.9 Relative stabilities of $CpMn(CO)_2(THF)$ and $TpMn(CO)_2(THF)$ complexes at 293 K. Photolysis of the parent tricarbonyl complexes in pure THF was conducted in the absence of other ligands, and the absorbances at 1860 and 1852 cm^{-1} for the Cp and Tp analogues, respectively, were monitored. 144

Figure 6.10 Photolysis of (a) $TpMn(CO)_3$ and (b) $CpMn(CO)_3$ in neat $HSiEt_3$ at 295 K. The Tp spectra were obtained at 0, 1, 7, 10.5, 14, and 17.5 ms after photolysis. For $CpMn(CO)_3$ only the spectra after 250 μs and 17.5 ms after photolysis are shown. The second CO band of the parent tricarbonyl complexes is not shown. 146

Figure 6.11 Difference spectra obtained upon photolysis of a cyclohexane/$HSiEt_3$ (100:4) solution of $TpMn(CO)_3$ purged with N_2 at 297 K. The spectrum was obtained 1 s after photolysis. The positive peaks at 2180, 1977, and 1914 cm^{-1} are due to the $TpMn(CO)_2N_2$ complex. 147

Figure 6.12 Reaction of the initially formed $TpMn(CO)_2(HSiEt_3)$ complex with THF at 295 K. Photolysis was conducted in the presence of $HSiEt_3$

(1.9 M) and THF (0.25 M) in n-heptane. Spectra were obtained 0, 122, 244, 366, 488, and 1000 μs after photolysis. 149

Figure 6.13 Calculated BVP86 geometries for $CpMn(CO)_2(HSiEt_3)$ and $TpMn(CO)_2(HSiEt_3)$ 150

Figure 6.14 Plot of kobs vs [THF] at different temperatures for the displacement of HSiEt3 from the $TpMn(CO)_2(HSiEt_3)$ complex by THF. The n-heptane solution was 1.9 M in $HSiEt_3$ with the appropriate amount of THF added. The limiting behavior of kobs indicates a dissociative mechanism for the reaction. 151

Figure 6.15 Relationship between the MnL bond dissociation enthalpy and the length of the MnN_{trans} bond relative to the average MnL_{cis} bond length in $TpMn(CO)_2L$ complexes. 153

LIST OF TABLES

Page

Table 1.1 Thermal and mechanical properties of relevant polycarbonates..... 11

Table 2.1 Copolymerization of Cyclohexene Oxide and Carbon Dioxide by Complex 1a a All reactions performed at 3.4 MPa CO_2 and 60 ^oC. b The rate is expressed in terms of the turnover frequency (TOF, mol of epoxide consumed/ (mol catalyst h)). c Determined by using gel permeation chromatography in THF, calibrated with polystyrene standards. 45

Table 2.2 Copolymerization of *rac*-Propylene Oxide and Carbon Dioxide Using Complex 1. All reactions performed with 1 equiv of $PPNN_3$ in rac-PO and 1.5 MPa CO_2 at included temperatures. [a] The rate is expressed in terms of the turnover frequency (TOF (mol of epoxide consumed (mol of catalyst h)$^{-1}$) = turnovers/h). [b] Determined by using ^{13}C NMR spectroscopy. [c] Determined by using gel permeation chromatography in THF, calibrated with polystyrene standards. [d] Only propylene carbonate obtained (3.4 MPa of CO_2 used). 50

Table 3.1 Mole fraction ratios of cyclohexene oxide and VCHO in the feed (F) and in the resultant copolymer (f). a – determined by ^1H NMR spectroscopy..... 67

Table 4.1 Tabulated values for the rate constants, k from the cocatalyst study. Reactions performed with PA:CHO:(salen)CrCl – 200:200:1 in toluene at 80 ^oC. $k = k_{obs}/[catalyst]$, where [catalyst] = 4.05 mM. ... 83

Table 4.2 Temperature Dependent Rate Constants for the Copolymerization of PA and CHO.Reaction conditions: (salen)CrCl/$PPNN_3$/PA/CHO = 1:1:200:200, where the [(salen)CrCl] = 4.05 x 10^{-3} M in toluene solution. Determined by GPC in tetrahydrofuran using monodisperse polystyrene standards..... 89

Table 4.3 GPC and DSC data for selected polyesters. [a]Sample was synthesized using both $PPNN_3$ and (salen)CrCl. [b]Sample was synthesized using only PPNCl as initiator. 92

Table 5.1 CO Stretching Frequencies for the $XMn(CO)_2(Solv)$ [X = η^5-*DMP* or Cp] Complexes in Cyclohexane Solvent at 298 K. In some cases the position of only one band is listed since the remaining band is obscured by the CO absorbance of the parent tricarbonyl..... 106

Table 5.2 Comparison of the kinetic parameters for the DMP and Cp systems.a For a given solvent (Solv) and incoming ligand (L) the slopes of the kobs versus [L] plots were used to determine the ratio, k_{DMP}/k_{Cp}, at 293 K. In all cases the relative rate constants for a given solvate were obtained with the same incoming ligand L. *a* Calculated values. *b* Ref 143. *c* Ref 146 110

Table 5.3 Calculated enthalpic parameters for the reaction: (η^5-DMP)$Mn(CO)_2$-(solv) + L→(η^5- DMP)$Mn(CO)_2$L. The enthalpy of the associative transition state (η^3-TS) and η^3 intermediate (η^3-I) for two Solv/L combinations along with the Mn-Solv binding enthalpies are presented. 115

Table 6.1 Experimental CO Stretching (cm^{-1}) and Force Constants (102 N/m) for a variety of $XMn(CO)_2L$ (X = Tp, Cp) complexes at 298 K in cyclohexane solution with some THF added to aid in the solubility of the Tp system. *a* Neat $HSiEt_3$. Unlike other ligands, *vCO* values for the $HSiEt_3$, eomplexes are different since the natures of silane binding to the Tp and Cp metal center are somewhat different (vide *infra)*. 132

Table 6.2 Rate constants obtained from fits to the k_{obs} vs THF data for the reaction: $TpMn(CO)_2L + THF \rightarrow TpMn(CO)_2THF + L$ at several temperatures 138

Table 6.3 Mn-L bond dissociation enthalpies in $XMn(CO)_2$-L complexes.[a] Bond dissociation enthalpies have been calculated using zero-point corrected energies and thermal enthalpy corrections at 298.15 K. All values are in kcal/mol and were obtained using the BVP86 functional.[b] Reference 32. [c]Reference 37. [d]Reference 35. [e] Reference 24. [f]This work. 152

I. INTRODUCTION

Carbon Dioxide as a Pollutant and as a Reagent

Carbon dioxide, CO_2, is a naturally occurring gas prevalent in the atmospheres of many non-gas giant planets, most notably Venus and Mars. CO_2 is a relatively minor component of Earth's atmosphere, accounting for roughly 0.039% by mole fraction,[1] yet it is becoming a topic of great controversy and importance due to its ability to absorb infrared radiation (**Figure 1.1)**. In what is commonly known as the "greenhouse effect," light emitted from the sun comes into contact with the earth, some of which is absorbed and some of which is reflected. Infrared radiation, when absorbed, excites the vibrational modes of chemical bonds and is retained as kinetic energy.[2] Although many gases contribute, CO_2 is the gas most frequently associated with the greenhouse effect.[3]

Typically a product of aerobic respiration, CO_2 has been released into the atmosphere at greater amounts on an annual basis due to mankind's increasing dependence on fossil fuels.[3,4] Evidence shows that the CO_2 produced by industrial processes is not reabsorbed into the carbon cycle as quickly as it is produced. Studies such as the one performed at Mauna Loa, Hawaii have shown that the atmospheric concentration of CO_2 has increased over time (**Figure 1.2**). This is presumably because of mankind's ever increasing use of fossil fuels in combustion processes. The replacement of petroleum as an energy resource is a very controversial topic because of

---

This dissertation follows the style of *The Journal of the American Chemical Society*.

matters of convenience, financial incentives, and the overall infrastructure of a society as it is constructed. Each of these topics individually affect government policies, as it is a

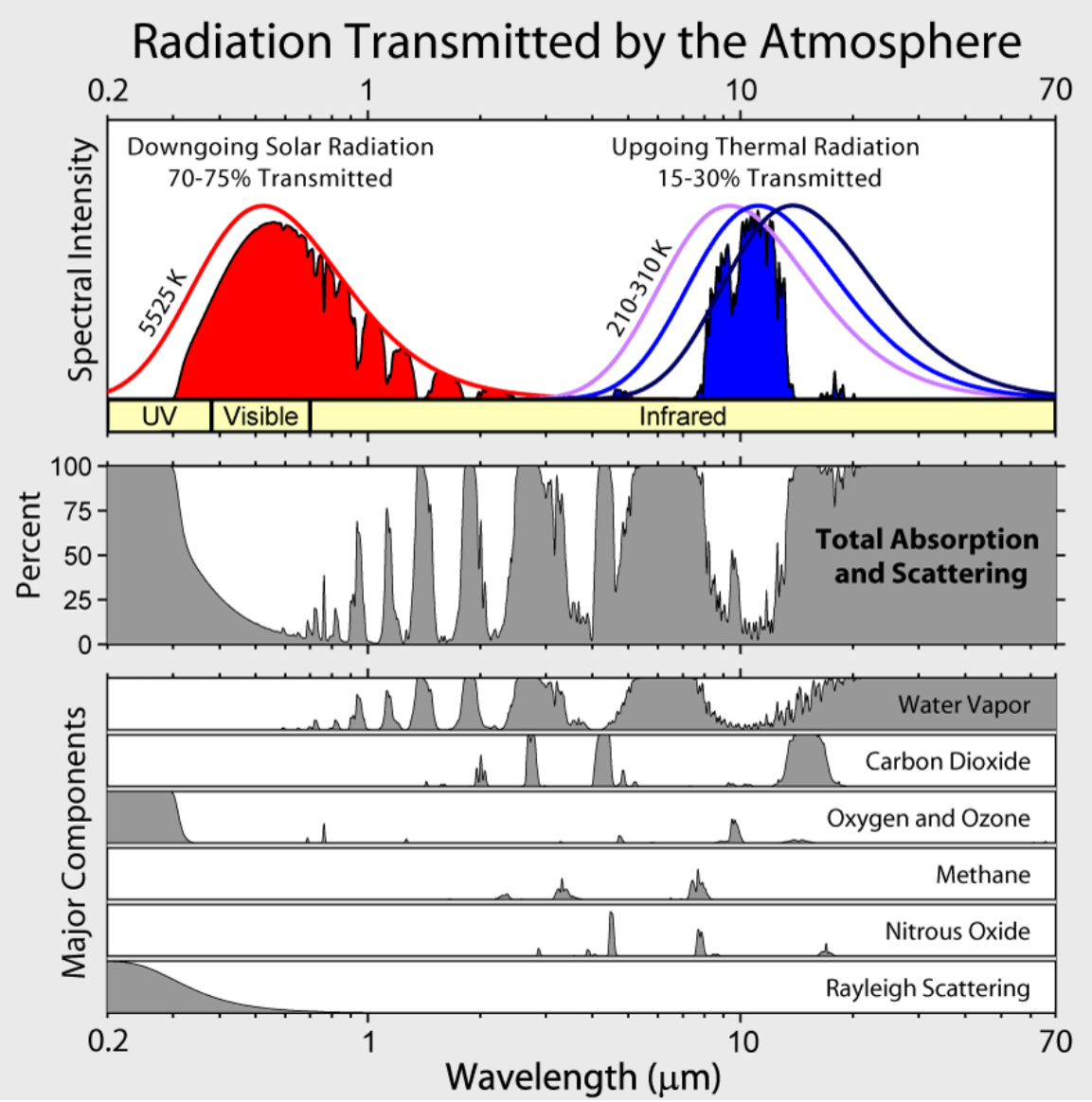

Figure 1.1. Greenhouse gases and their absorption bands.[2]

fact that the vast majority of our CO_2 production comes from consumption of non-renewable resources.[3] Because fossil fuels are a finite resource, the tapping of other sources of carbon is a highly important topic worldwide.[5] The utilization of CO_2 as a chemical reagent not only reduces the reliance on petrochemical resources but also represents a potential destination for CO_2 sequestered from the atmosphere.[6]

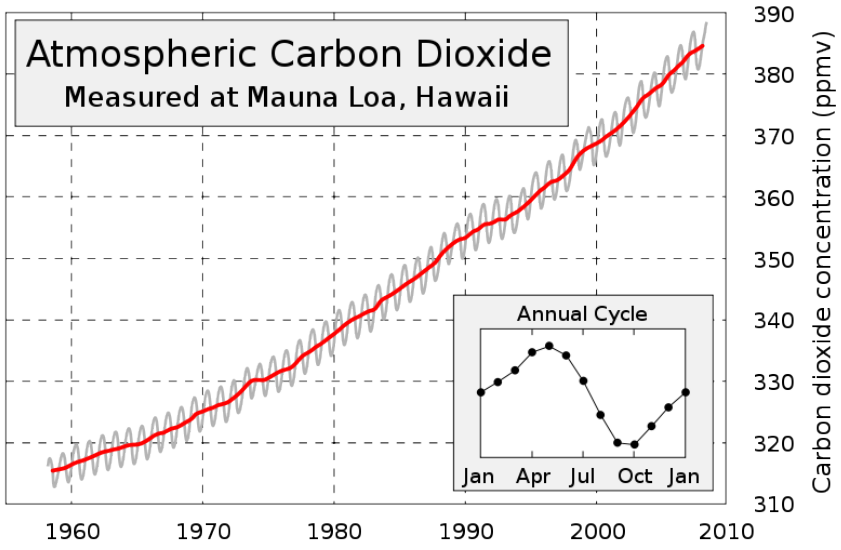

Figure 1.2. Atmospheric CO_2 concentration measured at Mauna Loa, Hawaii, displaying an overall rising trend despite annual fluctuations.[7]

Global usage of petrochemical resources has risen at continually increasing rates, and is predicted only to continue to do so.[8] Because of this, the consumption of carbon-based resources and the amount CO_2 exhaust produced by humanity is expected to increase as well. Many scientists have embraced the problem of CO_2 pollution by attempting to utilize it as a chemical reagent. Quite a few successful results have led to

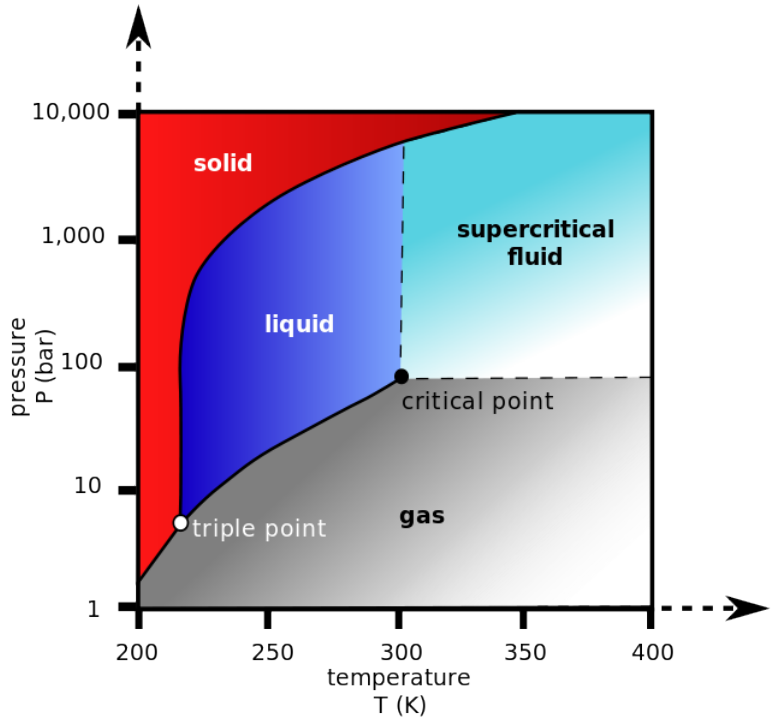

Figure 1.3. Phase diagram of CO_2.[9]

the use of CO_2 as a reagent for the industrial synthesis of urea,[10] methanol,[11] and aspirin.[4] As well as being used as a chemical reagent, CO_2 has proven useful for use as a solvent for chemical reactions due to its easily achievable liquid and supercritical phases (**Figure 1.3**)[12,13] and uses as a compressor gas, an inert gas, and as a food additive in carbonated beverages. Despite the many discovered uses of CO_2, the worldwide production of the gas continues to outweigh the amount used in these previously mentioned applications.[8] It is because CO_2 is a nearly endlessly abundant, renewable resource that the utilization of CO_2 as a viable C1 feedstock represents a potential step towards energy independence from fossil fuels.[3,8,14,15]

The laboratories of Donald J. Darensbourg at Texas A&M University have long studied the utilization of CO_2 as a reagent for polycarbonate plastic synthesis through the coupling reaction of CO_2 with cyclic ethers such as epoxides or oxetanes.[16–18,19–22] It should be noted that though this process does utilize CO_2 as a reagent, this research is not intended to reduce atmospheric CO_2 concentrations through sequestration(I still don't like the use of sequestration here, but I guess I can't come up with anything better), it is merely serving as a means to usefully apply this abundant C1 feedstock.

Industrial Synthesis of Polycarbonate

"One word: plastic." As predicted in the movie The Graduate, plastics have become a huge economic cornerstone for the United States, as the plastics industry is one of the few that has recently seen yearly increases in its trade surplus.[23] The most commonly produced plastics are polyethylene (PE), polypropylene (PP), and polyethylene terephthalate (PET) (**Figure 1.4**).[24] These three plastics are seen in nearly every facet of society, including grocery bags, food and beverage containers, electronic casings, and clothing. Each of these is produced in massive quantities and the vast majority of resources used in their production, ethylene, propylene, and terephthatlic acid, respectively, are petroleum based.[24] Another widely used plastic, although produced on a smaller scale than the plastics mentioned previously, is bisphenol-A polycarbonate (BPAPC). This refers to the plastic produced from the polycondensation of bisphenol-A (BPA) and phosgene, dimethyl carbonate, or diphenyl carbonate (**Figure 1.5**).

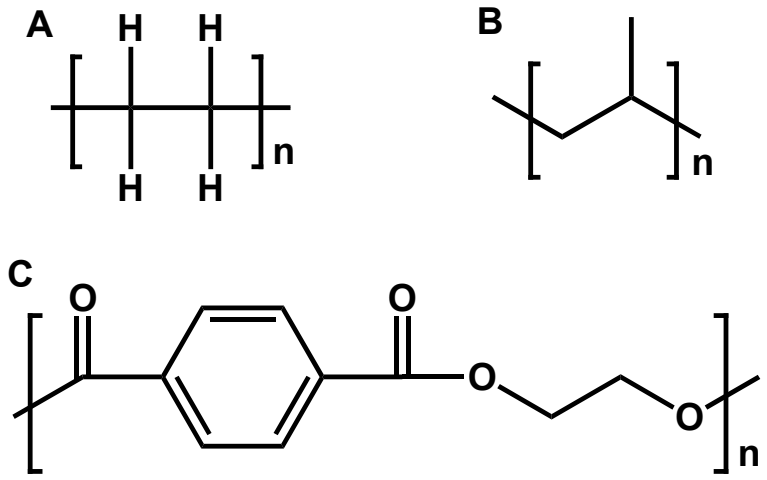

Figure 1.4. Commonly produced plastics. A – Polyethylene, B – Polypropylene, C – Polystyrene, D – Polyethyleneterephthalate

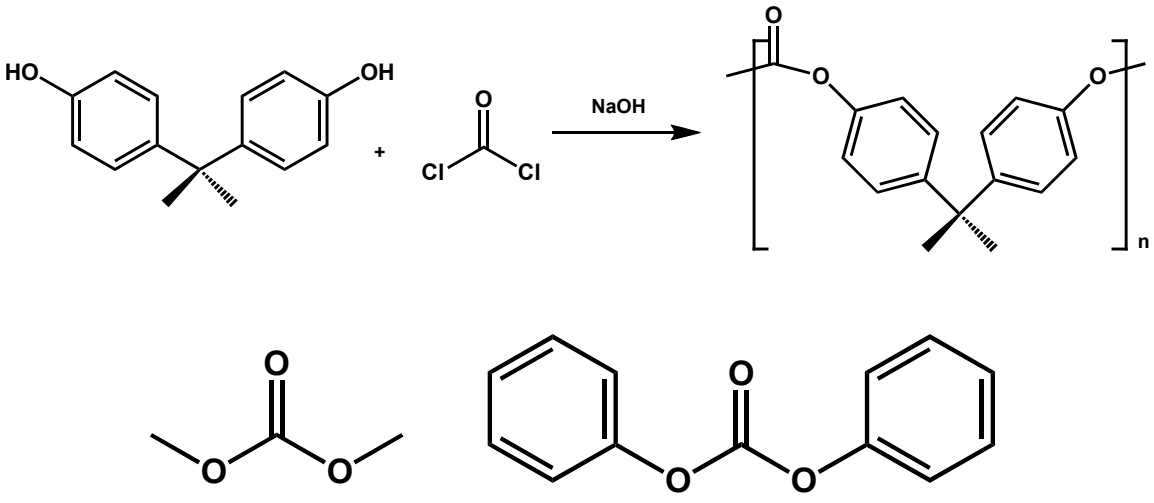

Figure 1.5. Top - Industrial synthetic route to BPA polycarbonate Lexan®. Bottom – synthetic replacements for phosgene as carbonyl source. Left – dimethyl carbonate. Right – diphenyl carbonate.

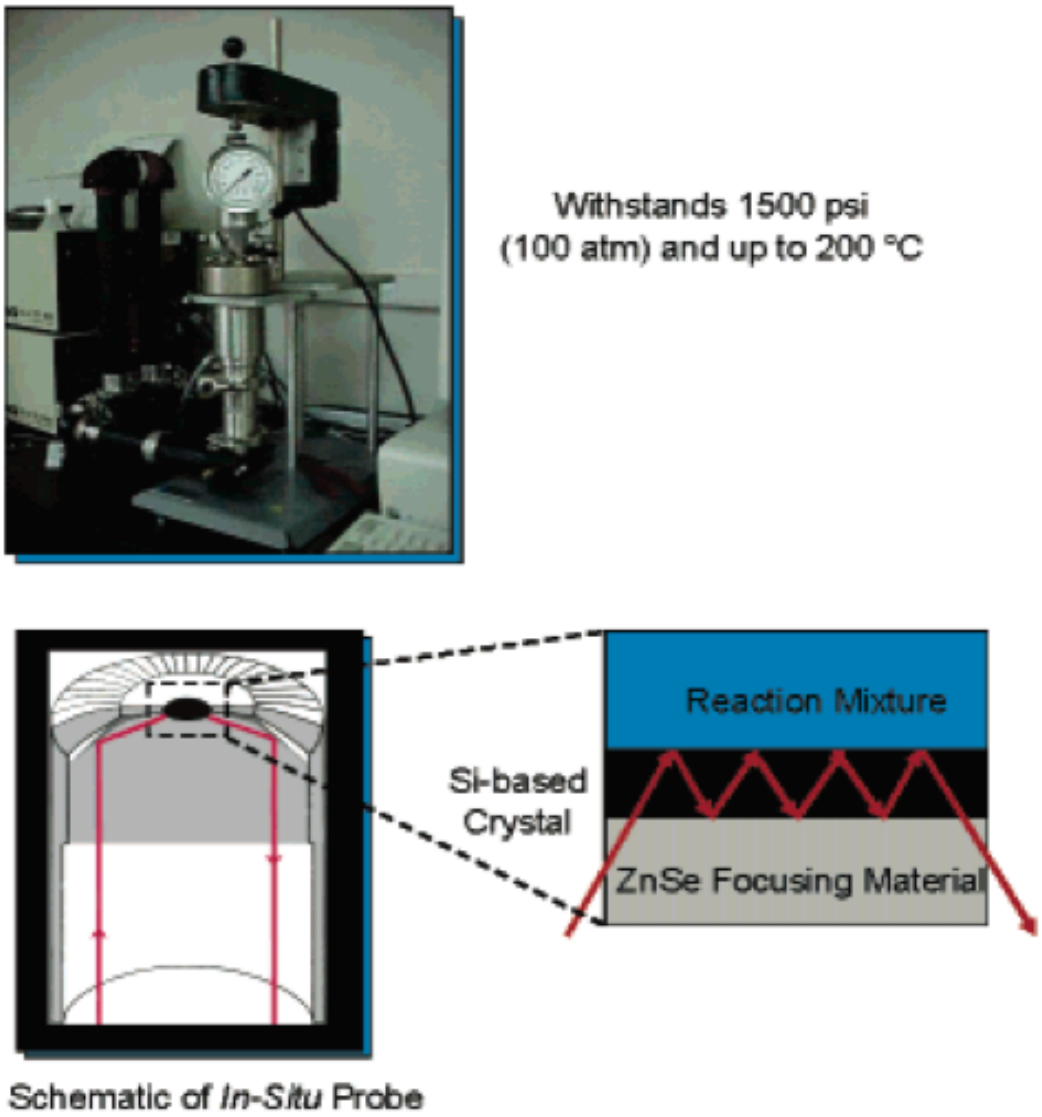

Figure 1.6. Schematic of ATR-FTIR Spectroscopy and a ReactIR1000 setup at Texas A&M in lab of Prof. Donald J. Darensbourg

BPA polycarbonate is an engineering thermoplastic with excellent mechanical and thermal properties including a tensile strength of ~75MPa and a T_g of 145^{o}C.[24] These properties make it an extremely useful plastic for a wide variety of applications,

including data storage media (CDs, Blu-ray discs), computer casings (white Macbook), and various automobile and airplane parts. The process used to synthesize BPAPC, however, is inherently inefficient due to low atom economy and the use of extraneous solvents. The process, which historically uses phosgene as a carbonyl source for the polycondensation reaction, must be run using CH_2Cl_2 as a solvent and NaOH as a proton sink. The solvent and materials not included in the final product all contribute to the extraneous waste generated by the process.

In addition to concerns regarding the efficiency of the production of BPAPC, the monomers used in its synthesis, BPA and phosgene, are both environmental and health safety concerns.[25,26] BPA is a matter of controversy due to claims that it may leach into liquids if used as a container for foodstuffs.[27] BPA is a known endocrine disruptor and is linked to adverse health effects. Some studies indicate that BPA may leach into water at elevated temperatures, which has led to much debate regarding the use of BPAPC in food and drink storage applications. The human response to BPA is still a matter of research, but many world governments have taken steps to reduce or eliminate entirely the presence of BPA from materials used in food storage.[28] Additionally, phosgene is a toxic gas that was used as a chemical weapon in World War I. Its status as a Schedule 3 chemical weapon under the Chemical Weapons Convention is still active today.[29] The presence of phosgene at BPA polycarbonate plants is a major cause for concern due to safety regulations of the gas. The combination of low atom economy, toxicity of reagents involved, and waste produced from the process make the production of BPA

polycarbonate one that can be both dangerous to plant workers and quite harmful for the neighboring environment if any spills were to occur.

Recent advances in the synthesis of BPAPC have resulted in the replacement of phosgene gas with dimethyl or diphenyl carbonate (**Figure 1.5**).[4,30] In particular, diphenyl carbonate as a co-monomer is very useful because it isolable as a pure solid. Because both BPA and diphenyl carbonate are solids, the polymerization can be run in melt conditions and without NaOH. The resultant polymer of the melt process is also much easier to purify due to the lower amount of chlorinated impurities leftover from phosgene. As an added bonus, diphenyl carbonate and dimethyl carbonate can be produced using CO_2 as a starting material.[31] Despite the advantages to BPAPC production by diphenyl carbonate utilization, the predominant method of its synthesis is still accomplished using phosgene as a carbonyl source.

Polycarbonates from Copolymerization of CO_2 and Epoxides

An alternative method of polycarbonate synthesis, which is easily characterized using technology in the Donald J. Darensbourg research laboraties at Texas A&M (**Figure 1.6**), is the copolymerization of CO_2 with cyclic ethers (**Figure 1.7).** This process is effective in that it is 100% atom efficient, it requires no extraneous solvent, and it is a chain-growth process allowing ease of molecular weight control. Despite the advantages, this method for polycarbonate production has yet to yield a product that surpasses the mechanical and physical properties of BPA polycarbonate (**Table 1.1)**. The main issue is inherent in the process: because epoxides and oxetanes are used as monomers, it is impossible to synthesize BPAPC and will likely be nearly impossible to

synthesize a structurally similar replacement that replicates its excellent properties while maintaining its lack of brittleness.[32,33]

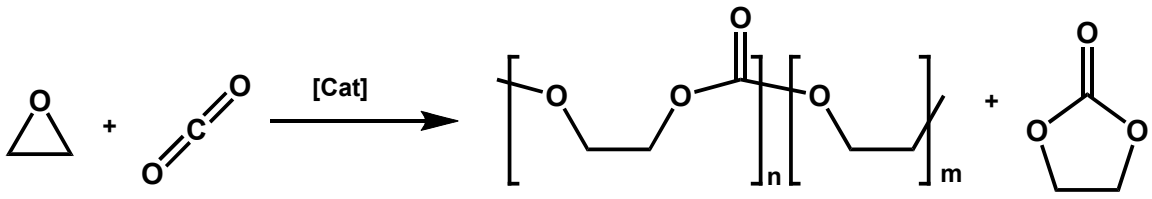

Figure 1.7. General scheme for polycarbonate synthesis from CO_2 and generic epoxides. n = polycarbonate, m = polyether linkages.

The two most-studied monomers for polycarbonate synthesis are cyclohexene oxide (CHO) and propylene oxide (PO). The polymer produced from CHO/CO_2 coupling, poly(cyclohexylene carbonate) (PCHC), has physical and thermal properties that approach those of BPAPC (**Table 1.1)**. Unfortunately, it is rendered almost completely useless in commercial applications due to its extreme brittleness, reaching only 1-2% elongation at break.[32] Thus far the PO/CO_2 and ethylene oxide/CO_2 coupling products, poly(propylene carbonate) (PPC) and poly(ethylene carbonate) (PEC), are the only epoxide/CO_2 based polycarbonates to be produced industrially.[34] It is currently used in electronic applications as it can easily be used as a coating which can be burned away, as a packing material, and as a lining for metal cans for cold beverage storage. PPC, though not brittle, has a T_g over 100 ^oC lower than that of BPAPC and a tensile strength that is a small fraction of BPAPC's. Recent innovations in the catalyst system used to produce PPC have resulted in reports of stereoregular, isotactic PPC exhibiting a 12 ^oC

increase in T_g,[35] unfortunately still well short of the BPAPC benchmark in terms of use as an engineering thermoplastic.

There are currently very few epoxides for which the CO_2 coupling process has proven to yield excellent products reproducibly and efficiently. Interesting monomers which have long been of interest due to a variety of reasons include styrene oxide (SO), due to its inclusion of a bulky phenyl ring,[36] and limonene oxide (LO), due to it being derived from a renewable resource.[37] Both have been reported to undergo CO_2 coupling to afford their respective polycarbonates. Unfortunately, neither has yet been reported to undergo polymerization with an acceptably high turnover frequency (TOF, where TOF = moles product / (moles catalyst * time in hours)).

Table 1.1. Thermal and mechanical properties of relevant polycarbonates

Polymer	T_g (^oC)	Tensile Strength (MPa)
BPA Polycarbonate[19]	145	55-75
Poly(cyclohexene carbonate)[38]	115	~40
Poly(propylene carbonate)[38]	~35	~30
Poly(styrene carbonate)[36]	~80	N/A
Poly(indene carbonate)[33]	~135	N/A

Much of the research of the Darensbourg group is concerned with identifying new epoxide monomers potentially useful for synthesizing polycarbonates with

interesting properties and various techniques to improve the properties of polycarbonates which are currently produced.[39,33]

Metal Catalyzed CO_2/Epoxide Coupling

In 1969, Inoue and coworkers reported the coupling of CO_2 and propylene oxide catalyzed by diethyl zinc, in water, with a very low turnover frequency.[40] Subsequent studies by the Darensbourg group and Zheng exhibited that zinc glutarate was a more effective catalyst for the coupling of PO and CO_2. In 1986, Inoue reported the first single-site metal catalyst effective at catalysis of epoxide and CO_2 coupling.[41] The catalyst, tetraphenylporphyrin aluminum (X), was able to produce polycarbonates from CO_2 and ethylene oxide (EO), PO, or CHO at very mild conditions with a high catalyst loading, but the resulting polymers had a narrow polydispersity index indicating that the aluminum complex facilitated polymer formation through a single-site mechanism (**Figure 1.8)**. In the decades since, much research has been devoted to the development of more active and selective catalyst systems. Popularized by Jacobsen, (salen)M(III)X complexes have achieved excellent reactivity and selectivity for CO_2/ epoxide copolymerization (**Figure 1.9**).[42–44] This (salen) ligand architecture is of particular interest to this dissertation, as it is predominantly the catalyst used in the subsequent studies.

(salen)CrCl, has been shown to catalyze the copolymerization of CHO and CO_2 very effectively, with TOFs exceeding 1000 h^{-1}.[19] The polymerization is hypothesized to

proceed *via* a single-site mechanism with a polymer chain propagating from the Cr center.

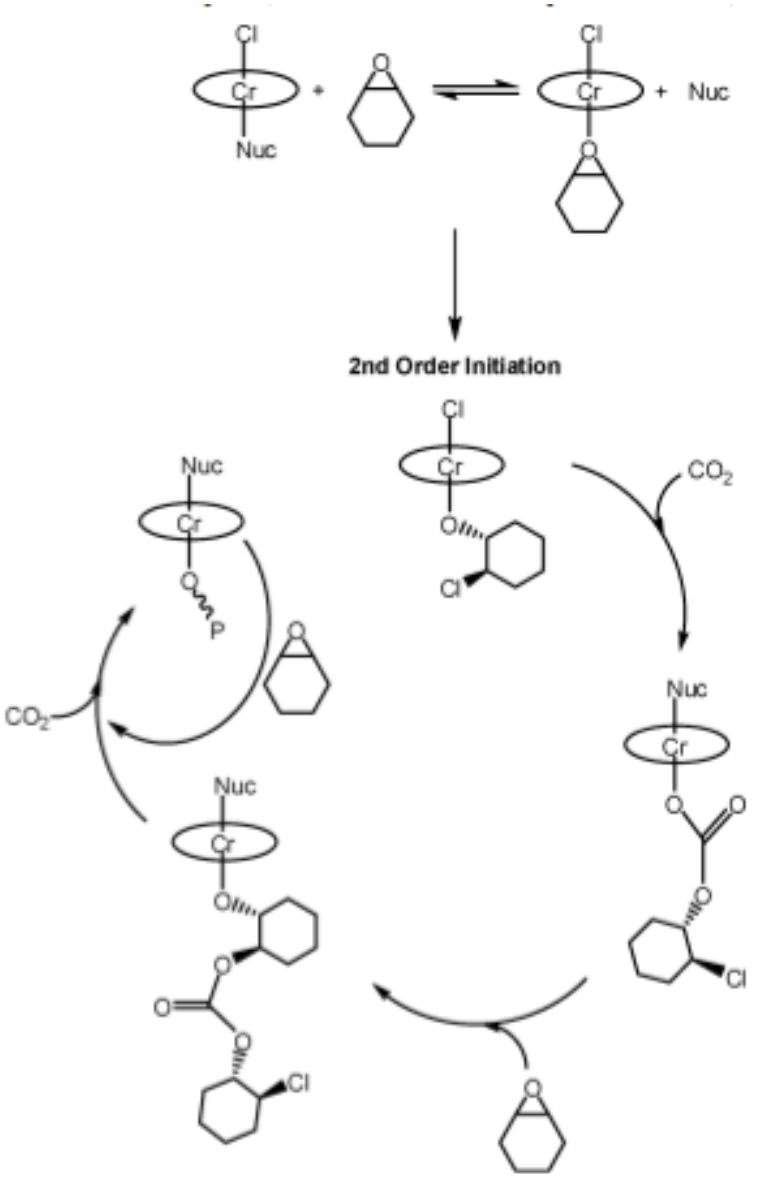

Figure 1.8. Mechanism of CO_2 and epoxide copolymerization to afford polycarbonates[19]

The initiation step involves an epoxide molecule undergoing anionic ring-opening, which is facilitated by the presence of a cocatalyst. The cocatalyst, typically an anionic salt such of either bis(triphenylphosphine)iminium (PPNX) or tetraalkylammonium (nR_4NX) salts with X = N_3^- or Cl^-, is present in the reaction mixture with the catalyst. Following epoxide ring-opening, a metal-oxygen bond is formed, which quickly undergoes CO_2 insertion. Due to the high rate at which CO_2 inserts into this bond, the epoxide ring-opening is considered to be the rate-limiting step.[19] (salen)CrX, while very effective as a catalyst for CHO/CO_2 coupling, has exhibited little effectiveness towards other epoxides. Under conditions of PO/CO_2 copolymerization, PPC formation has been reported, but mild conditions are required to achieve good selectivity and thus low TOFs are observed.[45] In an effort to modify the salen architecture to better facilitate the formation of polycarbonates from novel epoxides, Lu and coworkers synthesized a saturated version referred to as salan (**Figure 1.5, Figure 1.10**).[45,46] (salan)CrCl, has proven to be a more effective catalyst for the coupling of terminal aliphatic epoxides (PO, HO, etc…) as well as alicyclic ones such as CHO.

The mechanism of (salan)CrX cataylzed epoxide/CO_2 copolymerization is similar to that of (salen)CrX with regard to it being a single-site catalyst with a similar initiation step requiring anionic epoxide ring-opening.

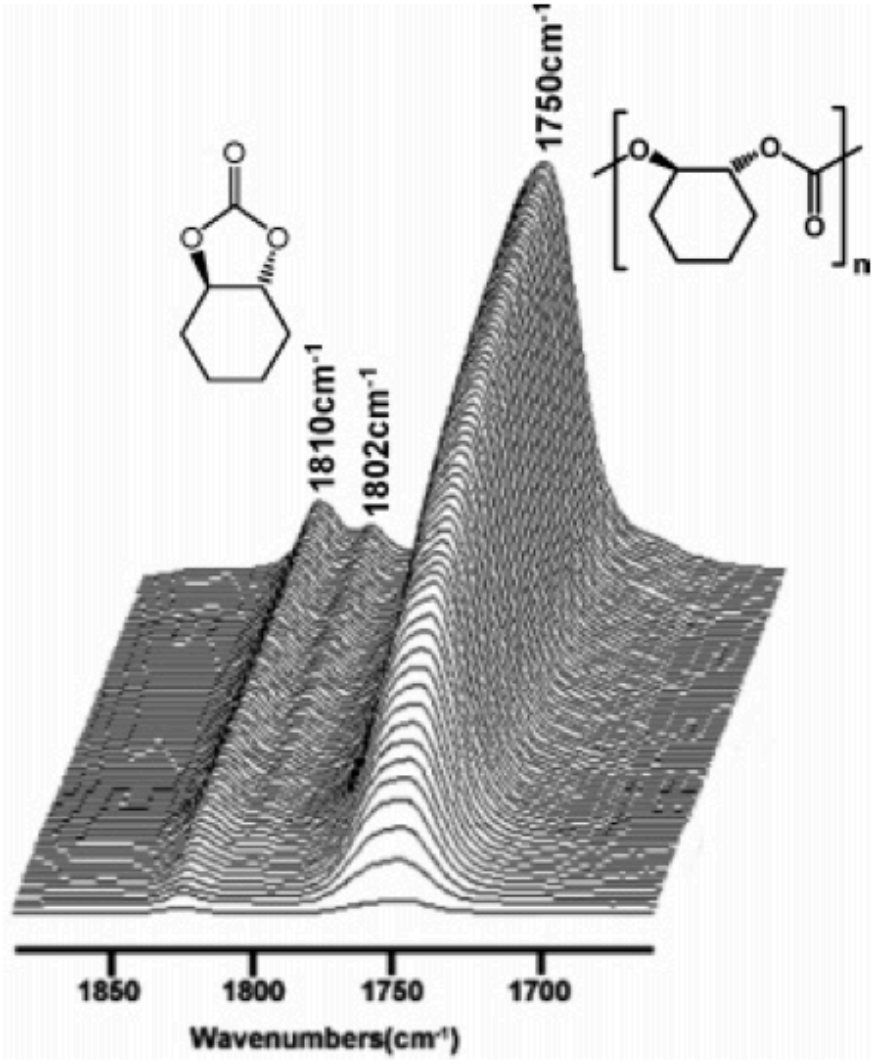

Figure 1.9. Representative three dimensional plot of selective poly(cyclohexene carbonate) formation catalyzed by (salen)Cr(III)Cl

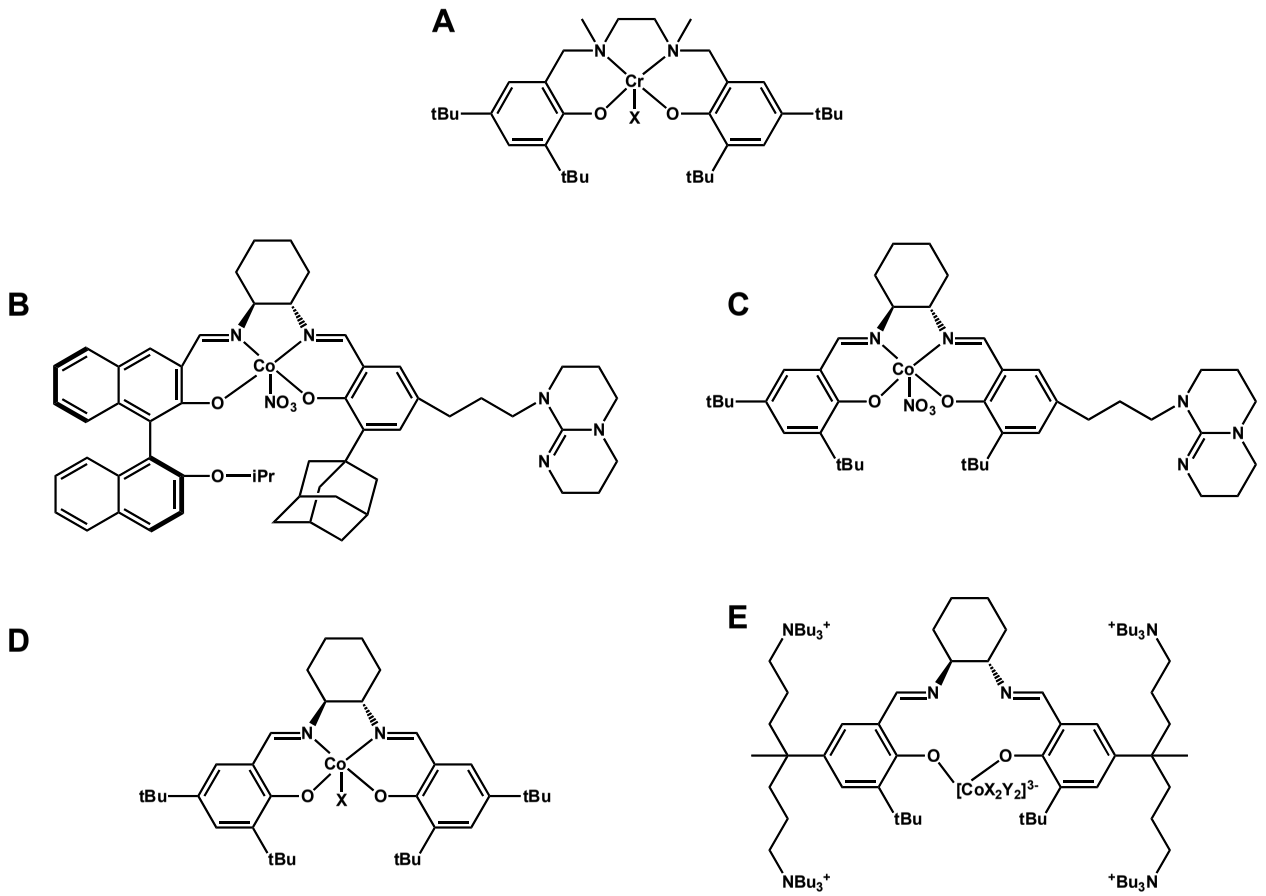

Figure 1.10. A – Representative (salan)CrX catalyst. B – (S,S,S)-stereoactive catalyst reported by Lu, et al. C – Pendant amine arm catalyst reported by Lu, et al. D – representative (salen)CoX catalyst, ligand architecture is identical to that of (salen)CrX. E – salen catalyst with ammonium salt pendant arms reported by Lee, et al. X = 2,4-dinitrophenolate, Y = [X-H-X].

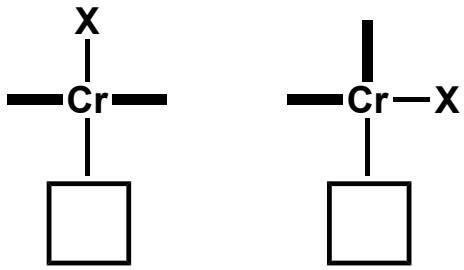

Figure 1.11. Standard (salen)CrX binding mode, left. Salan binding mode, right. Square is representative of substrate binding site.

The main difference in the two catalysts is the flexibility of the salan ligand. Because the imine bond is saturated in salan, the ligand is able to adopt a cis-β coordination scheme, resulting in a catalyst with an active site adjacent to the ancillary anion bound to the catalyst (**Figure 1.11**).[45] The rigid salen architecture adopts a planar coordination scheme, resulting in active site and anion position *trans*- across the Cr center. The proximity of the ancillary anion accomplishes allowing the catalyst to function at lower temperatures, and thus allows greater selectivity for polymer.

A thermodynamic barrier exists between the polycarbonate and the cyclic carbonate product produced from the CO_2/epoxide coupling process. While the polymeris the kinetic product, the five membered cyclic carbonate byproduct is thermodynamically more stable.[47] Extensive kinetic studies of the coupling of CO_2 and various epoxides have been performed by *in situ* ATR-FTIR spectroscopy, utilizing a setup like those seen in **Figures 1.6** and **1.8.** These studies have shown that the activation energy of polymer formation is typically lower than that of cyclic formation, allowing selective polymer synthesis through temperature management. Unfortunately,

for many epoxides of interest, this "activation gap" is narrow enough to make selective polymer formation extremely difficult. Modification of the catalytic system used in the polymerization studies can cause the activation gap to widen or shrink depending on how the catalyst interacts with the monomers. Advances in this area have focused on the stabilization of the growing polymer chain, typically by adding functionalized "arms" to the catalyst architecture. The Co(III) based catalysts reported thus far with these stabilizing arms contain a built- in ammonium cocatalyst that helps keep the growing polymer chain coordinated to the metal center, preventing detachment and backbiting to cyclic carbonate.[48]

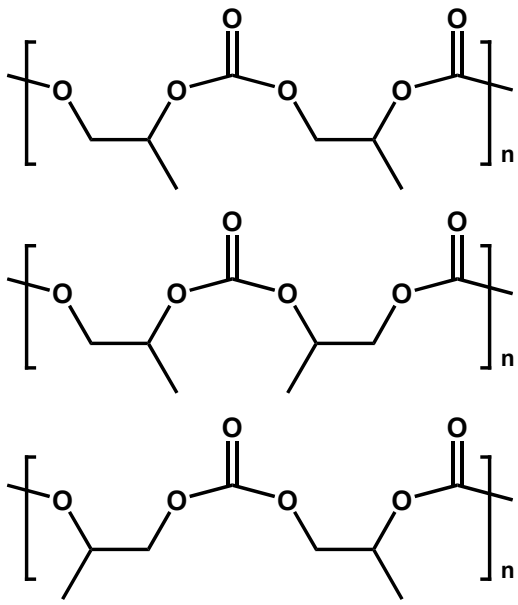

Figure 1.12. Examples of regiochemistry in PPC. Top – Head to head linkage. Middle – Tail to tail linkage. Bottom – Head to head linkage.

Another important facet of catalyst design is the inclusion of functionalities which influence the stereochemistry and regiochemistry of the resulting polymer. In the case of polycarbonates synthesized from CO_2 and epoxides, regiochemistry is caused by site-specific ring-opening of an asymmetric epoxide, such as PO. If subsequent PO molecules are opened at the same site, *e.g.* O-methylene C bond cleavage followed by subsequent O-methylene C bond cleavage, the pendant methyl groups are oriented in a "head-to-tail" fashion (H-T) and result in a H-T linkage (**Figure 1.12)**. Repeated H-T linkages result in isotactic PPC, alternating H-H and T-T results in syndiotactic PPC, and no selectivity for H-T or H-H results in atactic PPC. Stereochemical selectivity in epoxide/CO_2 copolymerization is typically achieved through steric design of the catalyst ligand architecture. Using a previously mentioned pendant-arm modified (salen)CoX catalyst, Lu and coworkers were able to synthesize 100% isotactic, stereoregular PPC.[35] The resulting polymer is reported to have exhibited a monumental 12 ^{o}C increase in T_g, from 35 ^{o}C for atactic PPC to 47 ^{o}C for the isotactic polymer. The monomer used, resolved *(R)*-PO, is forced to interact with the metal center in a stereospecific orientation. This results in 100% of the PO molecules opening at the methylene position, yielding only H-T linkages. The (salan)CrX catalyst, a precursor to Lu's excellent catalyst, is also effective in selectively synthesizing isotactic PPC.[48]

Tuning Properties of Polycarbonates through Terpolymerization

An effective method of achieving a desirable set of properties in a polycarbonate plastic is to "tune" its composition by performing a terpolymerization reaction, in which

a mixture of two or more different epoxides is copolymerized with CO_2.[38,45,49–51] The terpolymerization of epoxides with CO_2 is useful in that a very wide range of physical properties is attainable by controlling the mole fraction of epoxides introduced into the polymerization. Through the use of monomers which, when individually co-polymerized with CO_2, yield a wide glass transition (T_g) range, any value of T_g can be achieved within this range *via* terpolymerization. This process presents advantages over blending individual polymers in that extra steps which may use further reagents and solvent can be eliminated because the terpolymerization process is a one-pot procedure. One-pot and "click" chemistry methods are a pertinent topic of chemical research due to their potential applications in industrial scale-ups. Every step in an organic synthesis reaction requires more solvent, more reagents, and results in more product lost to purification techniques.[38,45,49–51] The overall efficiency of chemical reactions is improved by removing extraneous purification and modification steps. The studies presented in this dissertation discuss the terpolymerization of polycarbonates in the context of the Fineman-Ross equation, which is used to determine the reactivity ratios of multiple epoxide monomers in the CO_2/epoxide coupling process.[52] These reactivity ratios are calculated by comparing the initial mole fraction of the monomer loading and the resulting mole fraction of the polymer at an early point in the coupling process.

Polymers from Renewable Resources

The three most produced polymers worldwide are polyethylene, polypropylene, and polyethylene(terephthalate), all of which are produced from petrochemical

resources.[24] Polyethylene(terephthalate) (PET) in particular, due to its numerous applications, good physical properties, and ease of recyclability, is a very important plastic. Its major uses include use as a blend in many types of clothing and as a plastic bottles used in packaging soda and other beverages. The overall reaction used in its synthesis is the homopolymerization of ethylene terephthalate, which is itself produced from terephthalic acid and ethylene glycol (**Figure 1.13**).[24] Another method of synthesis is the copolymerization of dimethylterephthalate and ethylene glycol, with methanol produced as a byproduct. All of the previously mentioned terephthalate derivate monomers are isolated from fossil fuels and are very cheap due to the widespread production of PET. Unfortunately, the process used to produce this exceedingly useful plastic utilizes a step-growth mechanism. This means that molecular weight control is somewhat difficult and that the reaction does not achieve high yields until very late in the reaction process. This necessitates a maximum amount of energy input for the overall reaction if high yield is necessary. In addition, the step-growth mechanism production of PET is not 100% atom efficient, as water is produced in the reaction. Although water is a benign byproduct, it must be purified according to EPA standards prior to being reintroduced into the environment by conventional disposal means. Extra use of resources, both monetary and chemical, to purify waste water is an added inefficiency to the process of PET production. Additionally, recent research has indicated that PET used in food containers may be a potential health concern because of the potential leaching of endocrine disruptors into water and/or food.[48] Recent research has shown that it is possible to synthesize polymers similar to PET from cyclic

anhydrides and epoxides. This process presents several advantages over the production of PET in that the process is 100% atom efficient, it is a chain growth process, produced polymers can exceed thermal properties of PET, and it has potential for utilization of renewable resources.

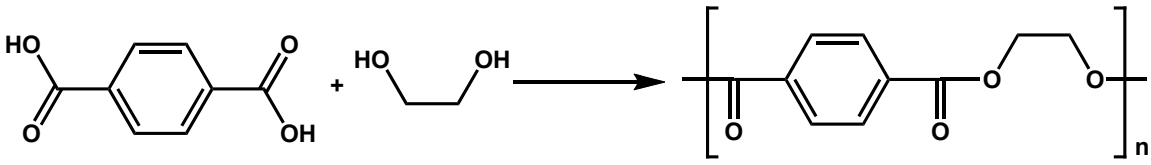

Figure 1.13. Industrial synthesis of PET from terephthalic acid and ethylene glycol

Polyesters from Epoxides and Cyclic Anhydrides

The reactivity of anhydrides with epoxides is well documented. A classic example is the use of cyclic anhydrides as a curing agent in epoxies typically used as adhesives. While these epoxies are useful for adhesion, they are not typically used in a similar, diverse number of applications like PET because they are thermosets and thus difficult to process. The reaction of cyclic anhydrides with epoxides to afford polyesters, however, has recently become a well-visited topic due to its chain-growth nature. Inoue and coworkers first documented this phenomenon in 1968,[54] and extrapolated the reactivity to include epoxides with CO_2, with CO_2 acting as an anhydride of carbonic acid. Indeed, according to the prior introduction, this extrapolation was correct in predict the ability of CO_2 to copolymerize with epoxides to yield polycarbonates. The coupling of epoxides with cyclic anhydrides, however, yields

polyester as the only product (**Figure 1.14**). Initial reports of polymer isolation use anionic initiators such as diethyl zinc to promote polymerization,[55] sometimes even utilizing water as a solvent. More recent studies have focused on introducing transition metal complexes in an attempt to develop a process with a single-site catalyst facilitating chain-growth polymerization.[41,55,56] Of the complexes used, the most effective has proven to be a Jacobsen-type chromium(III) salen catalyst. Studies employing the (salen)CrX catalyst have resulted in polyesters with narrow molecular weight distributions and high molecular weights.[57–61] In addition to being promoted in relatively benign media at modest temperatures with potential for melt polymerizations, the process is extremely robust for a wide variety of monomers. The compatibility of the process with such a wide variety of monomers enables fine-tuning of physical properties of the polymer with a range of over 100 ^{o}C in T_g simply through monomer selection (**Figure 1.15**). Another benefit of this process is that, per unit mass, the anhydride monomers are typically very low in cost. In fact, some anhydrides, such as succinic anhydride (SA), are produced from renewable resources. It is possible to synthesize a polyester consisting entirely of renewable resources, such as an alternating copolyester of SA and limonene or α-pinene oxide.

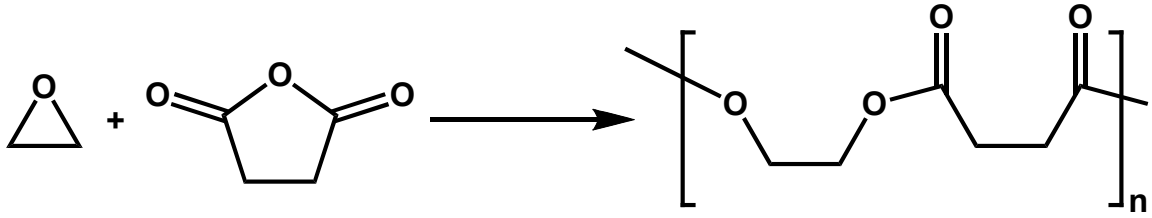

Figure 1.14. Scheme of generic epoxide/anhydride coupling to afford polyester.

This is of note because the analogous CO_2/epoxide coupling reactions featuring these renewable epoxides have proven to be extremely difficult to perform with viable results. In one instance, Coates and coworkers were able to synthesize poly(propylene maleate) (MAPO) by the alternating copolymerization of maleic anhydride (MA) and PO.[60,62] Through a post-polymerization modification, the polymer was then isomerized to poly(propylene fumarate), an extremely important polymer for biomedical applications which, by its standard step-growth synthesis, is extremely difficult to synthesize with acceptable molecular weight.[60] The chain-growth mechanism of MAPO synthesis makes acceptable molecular weights much easier to achieve.

Synthesis of One-Pot Block Terpolymers

As mentioned previously, the reaction of an epoxide with CO_2 can be compared to the reaction of an epoxide with an anhydride if CO_2 is considered to be a carbonic acid anhydride.[63] This analogy has led researchers to attempt to "combine" the two processes in an attempt to utilize CO_2 in the synthesis, thereby both reducing the cost per weight of the polymer and potentially improving its properties through addition of carbonate linkages.[55] This attempt at terpolymerization, while successful, yielded a very interesting result: when catalyzed by a single-site metal catalyst, the reaction would selectively copolymerize epoxides and anhydrides, initially yielding only polyester (**Figure 1.16, 1.17**).

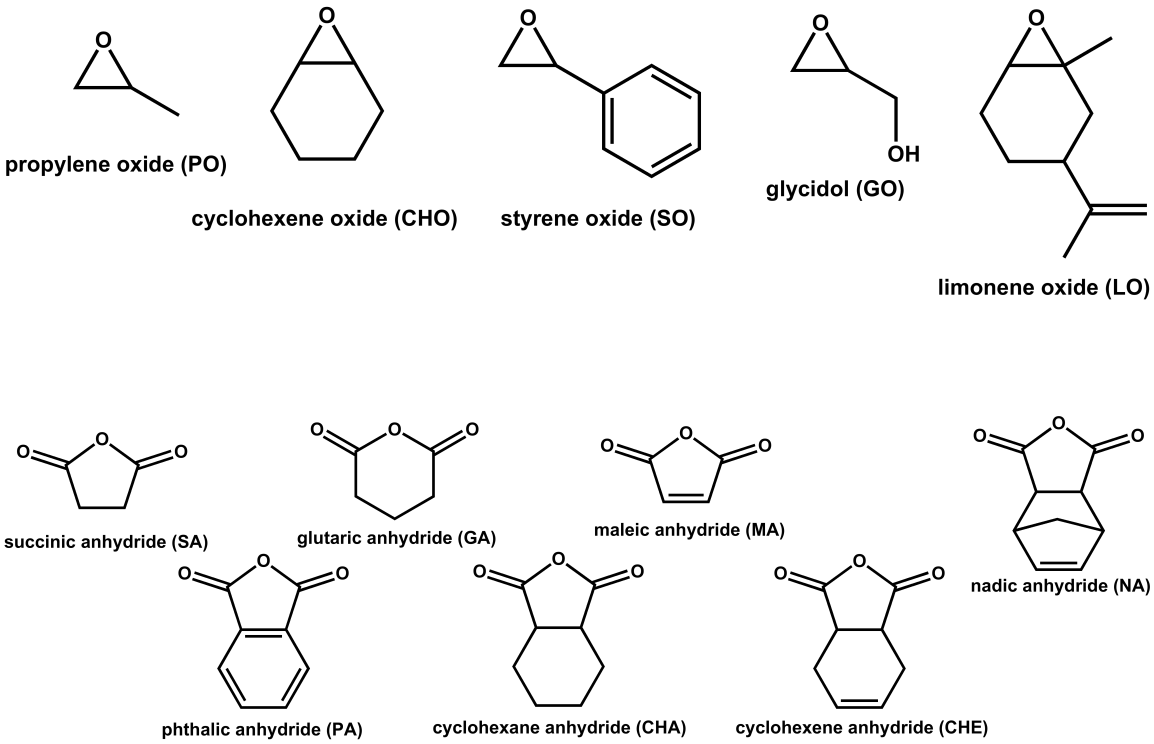

Figure 1.15. Epoxodes and anhydrides used thus far in polyester synthesis.

However; in an excess of epoxide, upon exhausting the available anhydride, CO_2 is then incorporated into the polymer, yielding a one-pot polyester-block-polycarbonate product.

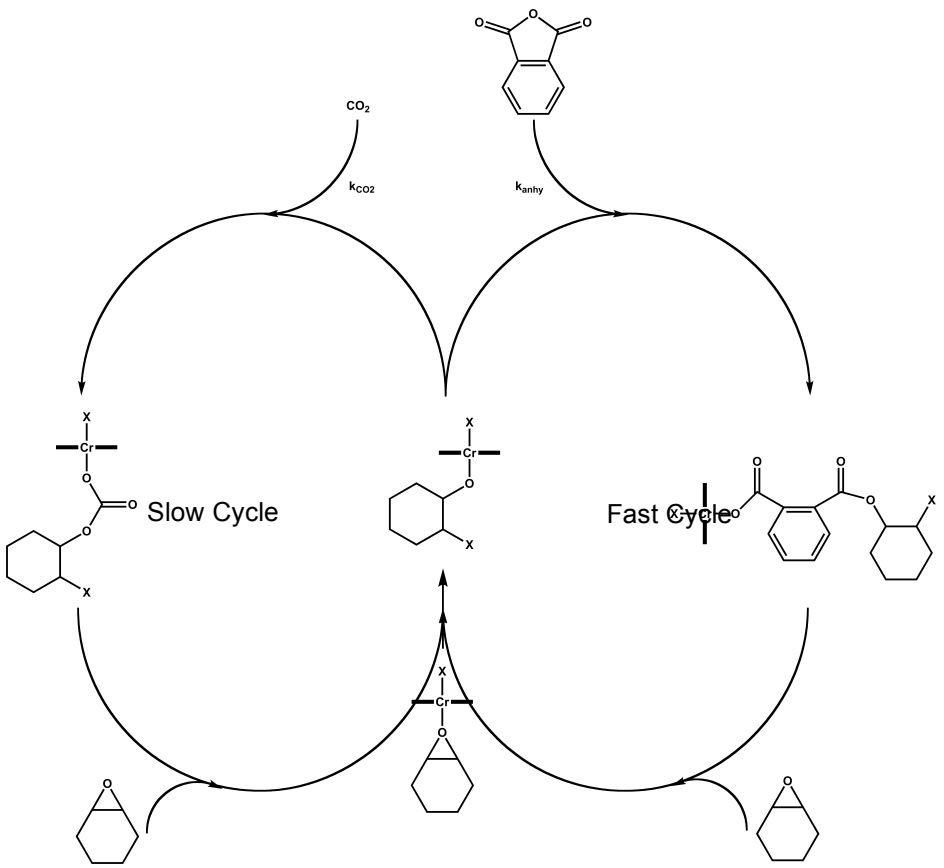

Figure 1.16. Potential mechanism of block-polyester-*co*-polycarbonate terpolymer formation.

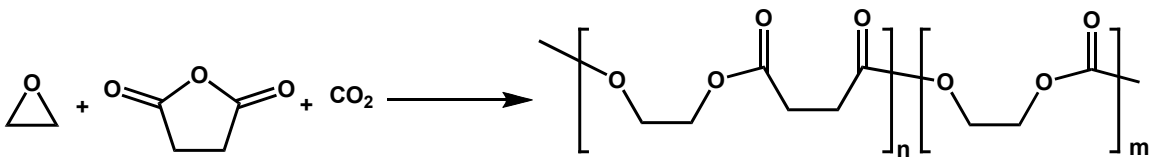

Figure 1.17. Synthesis of polyester-block-polycarbonate from CO_2, anhydride, and epoxide.

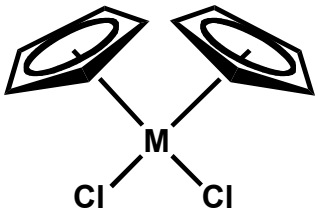

Figure 1.18. Typical metallocene Ziegler Natta catalyst, M = Ti, Hf, Zr

Metallocenes in Industrial Chemistry

Metallocenes are a class of organometallic compounds defined by a metal atom being bound to at least one multidentate ligand, typically one such as η^5-cyclopentadienyl. The first discovered metallocene complex is ferrocene,[64] a complex described as a "sandwich complex"[65] due to the complex's resemblance to the Earl's delicacy. Of interest to our research is the "half sandwich" or "piano stool" complex. As the name implies, the ligand is characterized by a single η^5 ligand occupying three *cis*-imaginary sites around an octahedrally coordinated metal atom with others occupied by carbonyls. An example of an industrially useful half-sandwich complex is the Ziegler-Natta catalyst. The Ziegler-Natta is are a very important class of metallocene catalyst used in industrial production of polyolefins such as polyethylene and polypropylene (**Figure 1.18**). The catalysts, usually of the form $CpMCl_2$, typically utilize titanium, zirconium, and hafnium as their metal binding sites. Although the catalytic activity of the zirconocene complex had been reported much earlier, it wasn't until the mechanism and catalyst design was fully understood that it became a commercially viable option for

PP production.[66] As other metallocene catalysts are frequently useful in organic transformations, their study is indeed very important.

Manganese Cyclopentadienyl Complexes

Over 40 years ago Angelici et al. performed studies in which the displacement of various ligands from the $CpMn(CO)_2$ fragment was studied.[64] This study consisted of removal of a CO molecule from $CpMn(CO)_3$ *via* photolysis, (**Figure 1.19**) replacement of the CO with a second ligand (typically and olefin), and subsequent displacement of the olefin ligand with a phosphine.

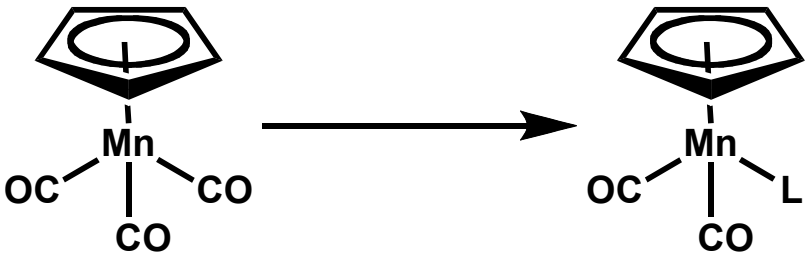

Figure 1.19. General scheme of CO displacement from $CpMn(CO)_2$

Kinetic measurements were performed in the olefin displacement step of the reaction in order to determine relative binding enthalpies of a range of olefin ligands.[67] Due to the technological limitations of the era in which the studies were performed, olefins are approximately the weakest binding ligand that was observable on the timescale that the Angelici study was capable of. The displacement of truly weakly coordinating ligands

such as alkanes and weak O-donors were impossible to observe due to the instability of the complex. Advances in FT-IR technology have made observation of "fast" reaction possible, such as the interaction and lifetime of weakly coordinating ligands to the $CpMn(CO)_2$ fragment and their displacement by stronger ligands.

RapidScan and StepScan FTIR

In the formative years of organmetallic carbonyl chemistry, studies invoking infrared as an analytical technique for kinetic measurements suffered from the relatively long timescale necessary to perform the measurements. Typically, to perform a kinetics study, it was necessary for a researcher to initiate the reaction and then remove aliquots from the reaction mixture, insert them into an infrared cell, place that cell into the instrument, and then collect data. This routine would be performed periodically throughout the experiment until completion. While this sort of technique is still quite common in chemical research, it does limit the sort of reactions that can be monitored.[68] For instance, observation of any sort of weakly binding ligand to a recently photolyzed $CpMn(CO)_2$ fragment was practically impossible due to the short lifetime of the complexes involved. New techniques have allowed researchers to observe reactions on a much faster timescale using FT-IR.

Two of these techniques, RapidSCAN and StepSCAN, will be discussed. The laboratories of Dr. Ashfaq Bengali of Texas A&M Qatar (**Figure 1.20**) utilize these two techniques for their studies, which encompass Chapters IV and V of this dissertation.

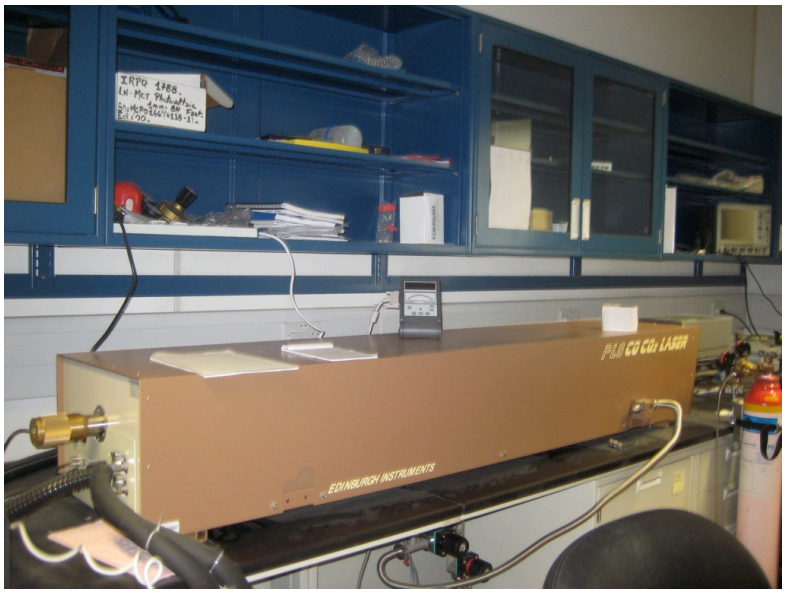

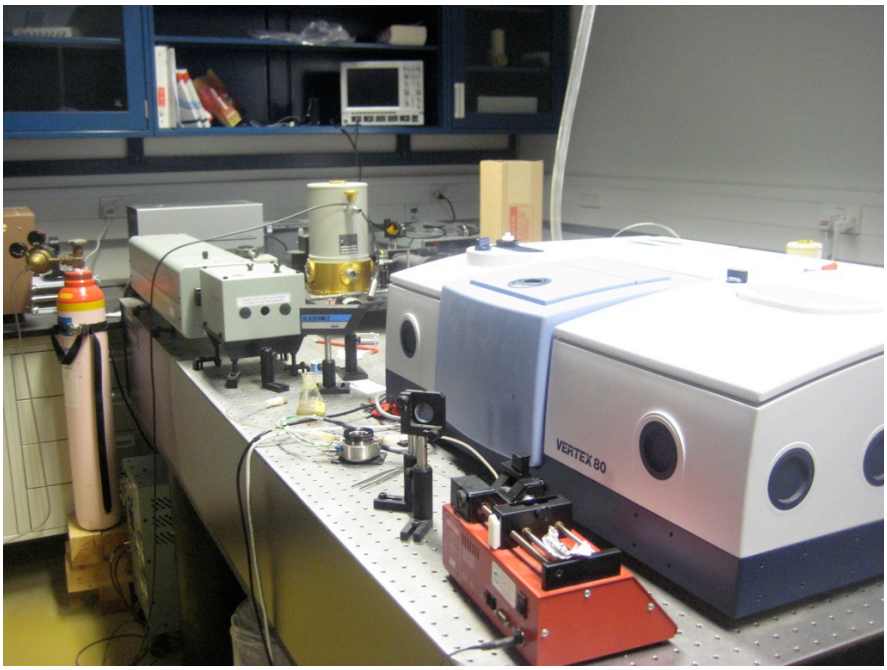

Figure 1.20. RapidSCAN and StepSCAN setup at Texas A&M Qatar in laborator of Dr. Ashfaq Bengali. Top photo: tunable CO laser used as IR source for StepSCAN experiments. Bottom photo: YAG laser photolysis setup used in both RapidSCAN and StepSCAN experiments.

RapidSCAN is a technique, due to fast oscillations of the moving mirror in the FT-IR setup, able to collect data on the millisecond (10^{-3} s) timescale. In the experiment, a sample is photolyzed using a Nd:YAG laser while inside the sample holder and in the presence of the incoming ligand. It is appropriate to think of Rapidscan merely as a very fast version of the ATR-FTIR setup.

StepSCAN is a more complicated technique allowing observation of chemical transformations on the microsecond (10^{-6} s) timescale, and ironically takes much longer than a Rapidscan experiment. In the Stepscan setup, the reaction is performed multiple times, each experiment having observed a small portion of the infrared spectrum. After performing enough observations to encompass the desired IR spectrum, the data is recombined into three-dimensions. The FT-IR setup, in this case, utilizes a rapidly moving moving-mirror again, but in addition the fixed mirror moves a small amount for each observed instance of the reaction, allowing the range of wavenumbers observed to be narrowed and observed more quickly. A pump is used to flow the reaction solution through the sample holder at a constant rate, which is

photolyzed repeatedly as the instrument observes the reaction. All things considered, although StepSCAN is able to observe reaction on a timescale three orders of magnitude faster than RapidSCAN, it does end up taking far longer to complete the experiment.

Ring-Slip Mechanism

It has been postulated that ligand substitution in CpMn complexes proceeds by what is called a "ring-slip".[69–71] This mechanism is characterized by disruption η^5 character of the Cp ligand, the ring "slipping" to an η^3 coordination scheme, and

subsequent binding of the incoming ligand, resulting in an associative process (**Figure 1.21**). The "slipped" intermediate, although it has yet to be isolated or observed, is hypothesized to be stabilized due to its 18-electron nature. The proposed associative displacement mechanism is known as the "indenyl" effect. (η^5-indenyl)M carbonyl complexes had been shown to undergo substantial rate increases for ligand substitution when compared to their Cp analogues. This was typically thought to occur due to the stabilization of the (η^3-indenyl)Mn intermediate in the ring-slip mechanism due to the benzene ring's aromaticity. This theory has been dispelled; however, because the η^5-indenyl complex is actually able to undergo the ring-slip due to a weaker η^5-L bond.[72–76] In addition to this, calculations have shown that an η^3-Cp complex would be very unstable and thus would likely warrant a high activation energy to be observed.

Recently, due to the advances in fast FT-IR technology already discussed previously, it has become possible to measure very fast displacement of ligands from metal complexes.

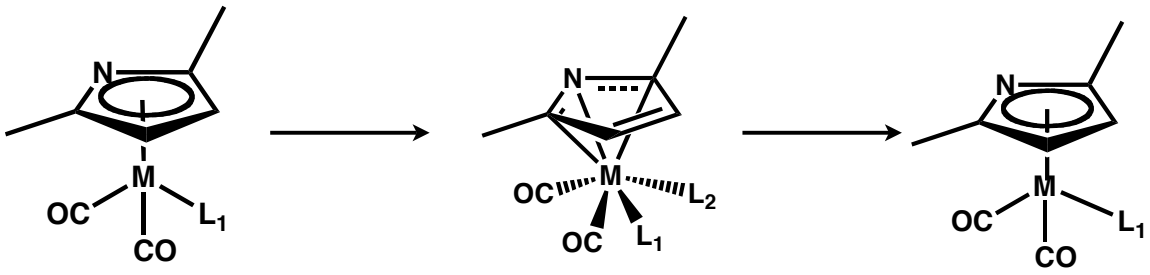

Figure 1.21. Ligand substitution by "ring-slip" mechanism. The dimethylpyrrole ligand is able to disrupt its aromaticity and shift from η^5 to η^3, allowing the ligand to substituted through an associative, rather than dissociative, mechanism.

Tp: An Electronic Cp Mimic

The trispyrazolylborate (Tp) ligand,[77] a bulky tridentate ligand, is reported to be electronically similar to Cp based on the FT-IR analysis of its carbonyl complex.[78] Recent studies have shown that although this complex does have similar IR stretches, ligand substitution and stability of olefin complexes are vastly different for manganese Cp and Tp.

II. COPOLYMERIZATION OF PROPYLENE OXIDE AND CYCLOHEXENE OXIDE WITH CO_2 BY CHROMIUM(III) (SALAN) CATALYSTS*

Introduction

Much effort has been made to develop effective, regio- and stereoselective catalysts for the coupling of carbon dioxide and epoxides to selectively provide polycarbonates with minimal ether linkages. To this aim we have focused on the use of salen(salicylaldimine) derivatives of chromium(III) and cobalt(III).[44,79,19] It has become apparent that ligands with greater donor character than salen, namely, tmtaa(tetramethyltetraazaannulene)[80,81] and salan(*N,N'*-disubstituted bis(aminophenoxide))[46], provide more active chromium(III) sites for this catalytic process. The latter salan ligand system with its sp^3-hybridized amino donors represents a saturated version of the pervasive salen ligand. An additional feature of metal complexes of the salan ligand which might dramatically impact catalytic behavior and control polymer stereochemistry is the potential of this ligand system to afford a cis-coordination geometry as depicted in the cartoons in **Figure 2.1**.[82]. Indeed, Lu and co-workers have shown chiral (salan)CrX complexes in the presence of ionic quaternary ammonium salts to catalyze the copolymerization of racemic propylene oxide to afford a copolymer with very high head-to-tail linkages and moderate enantioselectivity.[46]

---

*Reprinted (adapated) with permission from Darensbourg, D. J.; Ulusoy, M.; Karroonnirum, O.; Poland, R. R.; Reibenspies, J. H.; Cetinkaya, B. *Macromolecules* **2009,** *42,* 6992–6998.

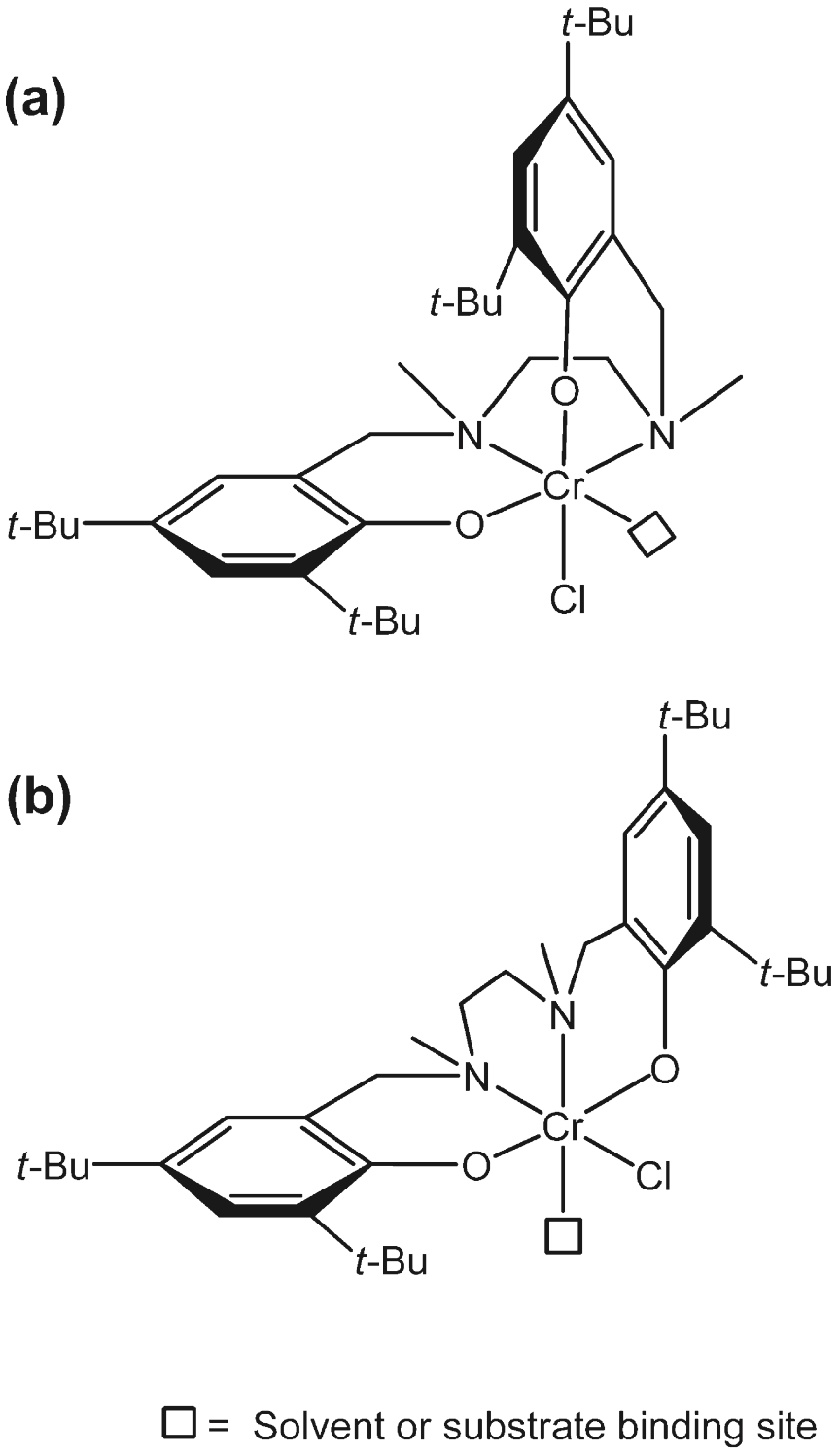

Figure 2.1. Proposed structures of complex 1 employed as catalyst in the copolymerization processes.

These studies will focus on utilizing complex 1 (**Figure 2.1**) as a catalyst in the presence of the [PPN][N_3] salt (PPN= bis(triphenylphosphoranylidine)) as ionic initiator for the copolymerization of propylene oxide, cyclohexene oxide, and 4-vinylcyclohexene oxide with carbon dioxide. The syntheses of di- and triblock polycarbonates of the corresponding copolymers will also be described.

Experimental

Method and Materials. Syntheses were performed under pure argon with rigorous exclusion of air and moisture using standard Schlenk techniques or in an argon-filled glovebox. Cyclohexene oxide (CHO) and propylene oxide (PO) were purchased from TCI America, and vinylcyclohexene oxide (VCHO) was purchased from Aldrich. All epoxides were freshly distilled from CaH_2 prior to use. The solvents Et_2O, pentane/hexane, CH_3CN, THF, and CH_2Cl_2 were purified by an MBraun Manual Solvent Purification System packed with Alcoe F200 activated alumina desiccant. [PPN][N_3] was prepared according to the published procedure.[83] Bone-dry CO_2 supplied in a high-pressure cylinder and equipped with a liquid dip tube was purchased from Scott Specialty Gases. All ^1H and ^{13}C NMR spectra were performed in $CDCl_3$. ^1H NMR spectra were recorded at 295 K using an Inova Varian spectrometer at 500 MHz, and ^{13}C NMR spectra were recorded at 295 K at 125 MHz. Chemical shifts are given in ppm relative to TMS and coupling constants (J) in hertz. Infrared spectra were recorded on a Mattson 6021 Fourier transform FTIR spectrometer with a MCT detector. Analytical elemental analysis was provided by Canadian Microanalytical Services Ltd. High-

pressure reaction kinetic measurements were performed using an ASI ReactIR 1000 reaction analysis system with stainless steel Parr autoclave modified with a permanently mounted ATR crystal (SiComp) at the bottom of the reactor (purchased from Mettler Toledo). The starting 3,5-di-tert-butylsalicylaldehyde was prepared from commer- cially available 2,4-di-tert-butylphenol according to the literature procedure.[84] The H_2salen ligand (salen = *N,N*-bis(3,5-di-*tert*-butylsalicylidene)-1,2-ethylenediimine) was synthesized as previously described.[85]

Synthesis of Tetrahydrosalen Ligand. To 0.01 mol of the H_2salen ligand in 20 mL of glacial acetic acid was added 0.03 mol of $NaBH_4$ in CH3CN over a 2-3 h period, during which time the solution became colorless. 20 mL of water was added to the reaction mixture, and it was neutralized via the addition of 2 N NaOH. The product was extracted with 150 mL of CH_2Cl_2, dried with $MgSO_4$, and isolated as a solid upon solvent removal under vacuum. The ligand was stirred in 5.0 mL of cold methanol for 10 min and isolated by filtration. Crystalline product was obtained in 67% yield upon layering a saturated solution of the product with methanol. ^{1}H NMR: 1.28 (s, 18H, tBu); 1.40 (s, 18H, tBu); 2.87 (s, 4H, CH2); 3.96 (s, 4H, CH2); 6.85 (s, 2H, Ar-CH); 7.22 (s, 2H, Ar-CH).

Synthesis of Salan Ligand. The salan ligand was synthesized from the tetrahydrosalen ligand according to the published method.[46,82] The product was obtained in 74% yield upon crystallization by layering methanol over a saturated methylene chloride solution of the compound. ^{1}H NMR: 1.27 (s, 18H, tBu); 1.39 (s, 18H, tBu); 2.26 (s, 6H, CH3); 2.63 (s, 4H, CH2); 3.66 (s, 4H, CH2); 6.80 (s, 2H, Ar-CH); 7.19 (s, 2H,

Ar-CH). Alternatively, the salan ligand was synthesized according to the route reported in the literature.[86,87,88,89] After washing with cold methanol, the product was dried and analyzed by ^{1}H NMR, ^{13}C NMR, and elemental analysis. Anal. Calcd (%) for $C_{34}H_{56}O_2N_2$: C, 77.86; H, 10.69; N, 5.34. Found: C, 77.68; H, 10.92; N, 5.25.

Synthesis of (salan)CrCl(1). 1.0 mmol of salan ligand and chromium(II) chloride (1.1 mmol) were dissolved in 10 mL of THF and stirred under argon at ambient temperature for 24 h. The reaction mixture was exposed to air and stirred an additional 24 h. After pouring the reaction mixture into 100 mL of diethyl ether, the organic layer was separated and washed with aqueous saturated NH4Cl (3 100 mL) and brine (3 100 mL) followed by drying over Na_2SO_4. After filtration to remove solid impurities and drying agent, solvent was removed in vacuo, yielding a green powder. No further purification was performed. Anal. Calcd (%) for $C_{34}H_{54}N_2O_2CrCl$, $(H_2O)_3$: C, 65.00; H, 8.98; N, 4.46. Found (%): C, 64.33; H, 9.29; N, 4.35.

Synthesis of (salan)CrN3(2). 0.5 mmol of (salan)CrCl complex was dissolved in 10 mL of CH_3CN. In another Schlenk flask, 0.5 mmol of $AgClO_4$ was dissolved in an equal volume of CH_3CN. The (salan)CrCl solution was then cannulated into the silver perchlorate solution. Immediate precipitation of AgCl was observed, and the reaction was allowed to stir overnight. 1.5 mmol of NaN_3 was added, keeping exposure to air at a minimum. The reaction was stirred for an additional 24 h. The mixture was diluted with distilled diethyl ether and the organic portion washed with water to remove $NaClO_4$ and excess NaN_3, dried with Na_2SO_4 and the solvent removed in vacuo, yielding a dark green powder with a νN_3 vibrational mode at 2062.9 cm^{-1}.

Copolymerization of Epoxides (CHO or PO) with CO_2. Measurements of the copolymerization processes at high pressure were carried out using a stainless steel Parr autoclave modified with a SiComp crystal to allow for attenuated total reflectance spectroscopy using infrared radiation (ASI ReactIR 1000 in situ probe). The (salan)CrCl (50 mg) and $PPNN_3$ were dissolved in CH_2Cl_2 and stirred for 1 h. The CH_2Cl_2 solvent was evaporated to dryness in vacuo, and epoxide (CHO or PO) was added to the catalyst and stirred for 10 min. The Parr autoclave reactor was dried in vacuo at 80^o C and cooled down to room temperature before the reaction mixture was injected into it. A 128-scan background spectrum was collected and followed by immediate charging with 3.4 MPa CO_2 pressure. With a reaction temperature of 60^o C being maintained, a single 128-scan spectrum was collected every 3 min during the reaction time. Profiles of the absorbance at 1750 cm^{-1} (polycarbonate) with time were recorded after baseline correction. After cooling and venting the reactor in a fume hood, the polymer was extracted with dichloromethane. The polymer was precipitated with hexane to remove unreacted CHO. The polymer was purified by dissolving it in methylene chloride and precipitating it out with acidified methanol. Molecular weight determinations (M_w and M_n) were carried out in THF solutions using a Viscotek gel permeation chromatograph equipped with refractive index and right-angle and low-angle light scattering detectors.

Diblock Copolymerization of Epoxides (PO and CHO) with CO_2. 50 mg of (salan)CrCl and an equimolar (49 mg) amount of $PPNN_3$ were dissolved in CH_2Cl_2 and stirred for 1 h at ambient temperature. The CH_2Cl_2 was evaporated to dryness in vacuo, 2.9 mL (1/500, cat./PO) of PO was added to the catalyst, and the solution was stirred for 10 min.

The Parr autoclave reactor was dried in vacuo at 80° C and cooled down to room temperature before the reaction mixture was injected into it. The reactor was maintained at 25° C for 16 h, followed by venting the excess CO_2. Immediately 5.0 mL (1/500, cat./CHO) of CHO was injected under an inert atmosphere into the reactor. The reactor was pressurized with CO_2 (3.4 MPa) and heated at 60° C for 4 h. After cooling and venting the reactor in a fume hood, the diblock copolymer was extracted as a dichloromethane solution. The diblock copolymer was precipitated with hexane and again with acidified methanol. Molecular weight determinations (M_w and M_n) were carried out in THF solutions using gel permeation chromatography.

Triblock Copolymerization of Epoxides (PO, CHO, and VCHO) with CO2. The same procedure for preparing the diblock copolymer (with same catalyst and cocatalyst ratio, also 1.94 mL (1/333, cat/PO) of PO and 3.33 mL (1/333, cat./CHO) of CHO was used as monomers) was carried out followed by immediately venting the CO_2. 4.2 mL (1/333, cat./VCHO) of VCHO was injected under inert atmosphere into the reactor. The reactor was pressurized with CO_2 (3.4 MPa) and heated at 60° C for 4 h. The same purification method was performed after cooling the reactor to room temperature and venting the excess CO_2 in a fume hood.

Differential Scanning Calorimetry Measurements. Glass transition (T_g) temperatures were measured using a Mettler Toledo polymer DSC equipped with a liquid nitrogen cooling system and 50 mL/min purge of dry nitrogen gas. Samples, (~6 mg) were weighed into 40 μL aluminum pans and subjected to two heating cycles. The

first covered the range from 25^{o} C to 140^{o} C at 5^{o} C/min and was then cooled back to 25 ^{o}C. The second heating cycle covered 25 to 200 at 2^{o} C/min.

Results and Discussion

It is well-established that alicyclic epoxides (e.g., cyclohexene oxide) in the presence of various metal catalysts react with carbon dioxide to selectively afford copolymers at much harsher reaction conditions than the coupling of aliphatic epoxides (e.g., propylene oxide) with CO_2. This is due to the difference in activation energies for copolymers vs. cyclic carbonate formation, E_a being much greater in the case of cyclohexene oxide copolymerization with CO_2.[47,90] With regard to the copolymerization of propylene oxide and CO_2, regio- and stereo-selectivity for copolymer formation are also important qualities of an effective catalyst system. Relevant to this latter point, Coates and co-workers have demonstrated a chiral (salen)CoX catalyst in the presence of PPNX salts provides high regioregularity (95% head-to-tail) (**Figure 2.2**) and good control of polymer tacticity from isotactic to syndiotactic.[91] Reaction conditions were generally 22^{o} C and 3.4 MPa.

In this report, the N,N'-dimethyl substituted H_2salan ligand was synthesized following the general procedures in the literature. The route described in reference 9 is a more facile one-pot preparation achieved by the reaction of 3,5-di-tert-butylphenol, paraformaldehyde, and N,N'-dimethylethylenediamine in methanol 50^{o} C. The corresponding (salan)CrCl was prepared from the H_2salan ligand and anhydrous $CrCl_2$ following oxidation with air or directly from $CrCl_3(THF)_3$. Replacement of the chloride

ligand by azide was achieved via the standard procedure employed for the preparation of the analogous (salen)CrN_3 derivative (**Figure 2.3**).[92] However, strikingly unlike the (salen)CrN_3 complex, addition of excess $PPNN_3$ (20 equiv) to a solution of (salan)CrN_3 over a prolonged reaction time (2 days) did not afford a stable bis-azide complex, (salan)$Cr(N_3)_2^-$.[93]

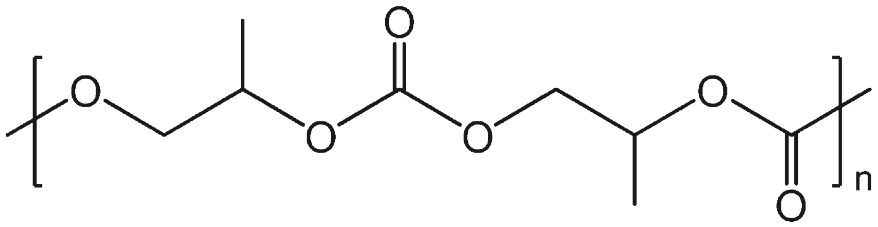

Figure 2.2. Head-to-tail (HT) regiochemistry of poly(propylene carbonate).

In an attempt to crystallographically characterize complex 1, crystals of a close derivative of complex 1 were isolated from the reaction solution. The crystals obtained were shown by X-ray crystallography to be a dimeric metal complex where the anion is a bridging sulfate group, originating from the drying reagent sodium sulfate, with the sixth coordination sites of the two chromium(III) centers occupied by methanol and water, respectively (**Figure 2.4**). Included in **Figure 2.4** is a model of one of the metal centers, illustrating the geometry of the metal-salan framework (**Figure 2.4b**). The importance of this structure is that, unlike the salen ligand, the salan ligand adopts a *cis*-coordination mode with the anion and neutral ligand occupying positions *trans* to oxygen and nitrogen donors, respectively (**Figure 2.1a**). Similarly, the crystal structure

of the (salan)AlMe derivative displays a distorted trigonal-bipyramidal coordination geometry with *cis* arrangements of oxygen atoms and of nitrogen atoms.[94]

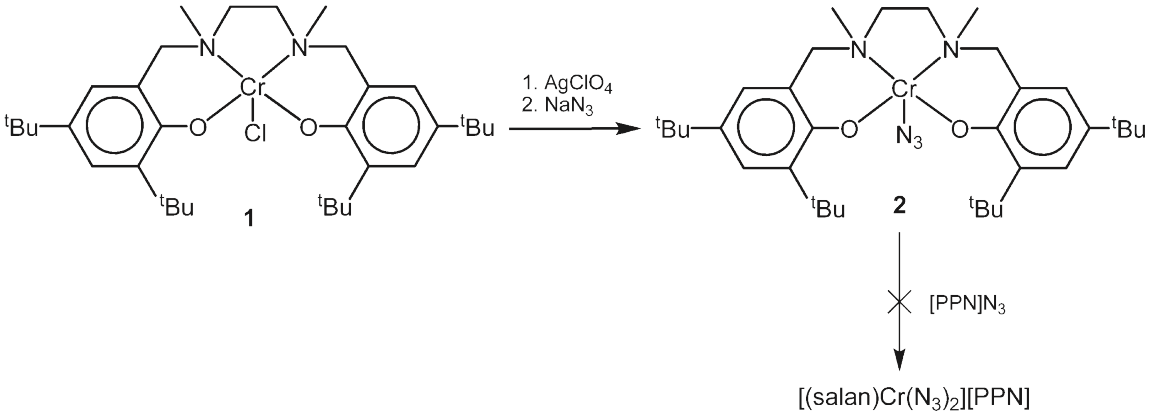

Figure 2.3. Synthesis of (salan)N_3 Complex

The copolymerization of cyclohexene oxide and carbon dioxide was initially examined employing (salan)CrCl (1) with varying quantities of $PPNN_3$ for comparison with our earlier studies involving the corresponding (salen)CrCl catalyst systems. Because the quaternary organic salt, $PPNN_3$, is insoluble or very sparingly soluble in epoxides at room temperature, pretreatment of 1 with $PPNN_3$ is required to ensure the system achieves the greatest possible catalytic activity.

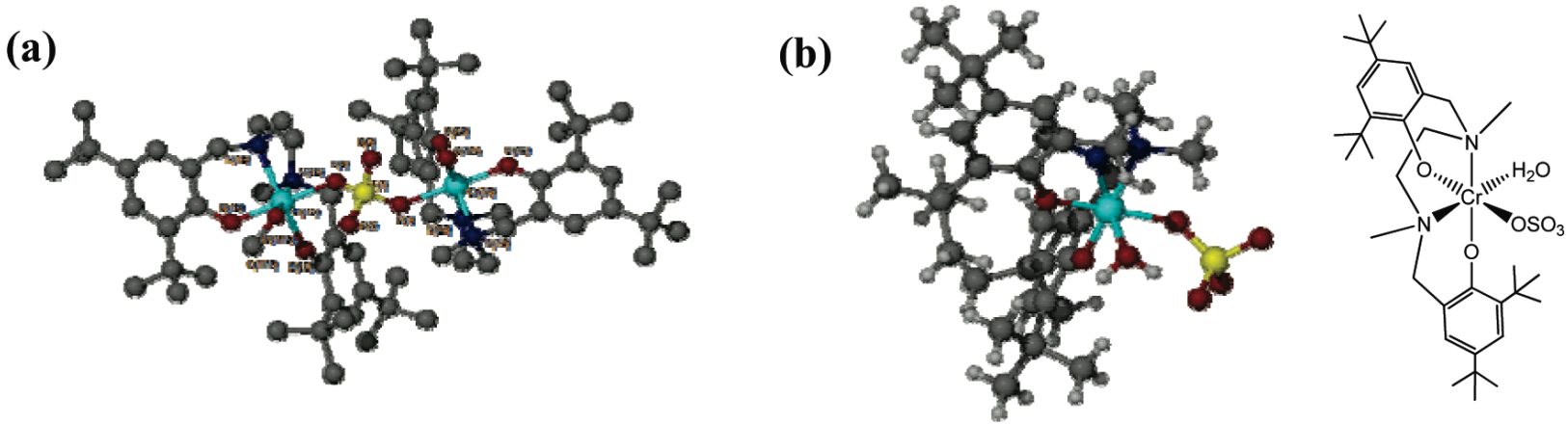

Figure 2.4. (a) X-ray structure of dimeric complex obtained from crystallization of complex 1. (b) Truncated model of one of the metal fragments containing the H2O molecule, with stick drawing for better clarity.

In a typical copolymerization experiment, complex 1 and the desired equivalents of $PPNN_3$ were dissolved in methylene chloride and stirred for 1 h at ambient temperature. Upon removing the methylene chloride under vacuum cyclohexene oxide was added with stirring, and the solution was cannulated into the stainless steel reactor. Following the copolymerization reaction, the polymer was dissolved in methylene chloride and precipitated upon addition of acidified methanol. **Table 2.1** summarizes the results of a series of copolymerization reactions carried out under various reaction conditions for the formation of poly(cyclohexylene carbonate). It is noteworthy that TOFs as reported here and elsewhere in the literature are highly dependent on reaction time. That is, the highest TOFs are obtained during the initial period of high polymer production.

Table 2.1. Copolymerization of Cyclohexene Oxide and Carbon Dioxide by Complex 1a
a All reactions performed at 3.4 MPa CO2 and 60^{o} C. b The rate is expressed in terms of the turnover frequency (TOF, mol of epoxide consumed/ (mol catalyst h)). c Determined by using gel permeation chromatography in THF, calibrated with polystyrene standards.

Entry	$PPNN_3$ (equiv)	Time(h)	CHO/Cat (mole ratio)	TOF	M_n (kg/mol)	PDI (M_w/M_n)
1	2	2	1250	321	11.9	1.10
2	2	4	1250	240	15.8	1.19
3	2	17	1250	61	27.2	1.10
4	1	4	2500	405	19.5	1.19
5	1	10	1250	95	21.7	1.10
6	0	10	1250	14	3.92	1.31

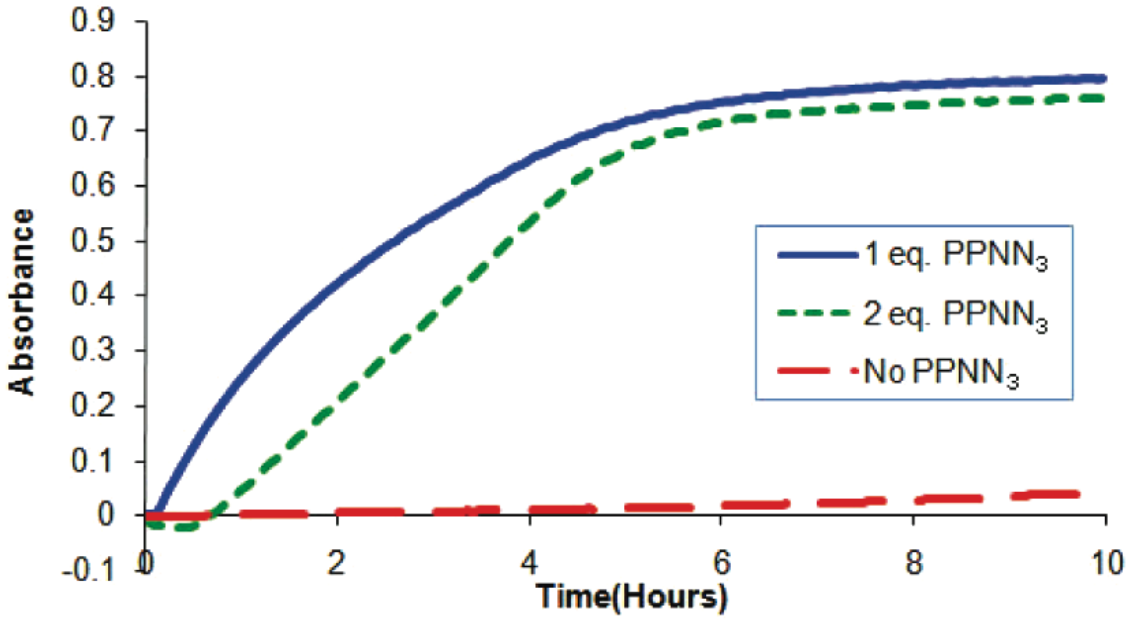

Figure 2.5. In situ infrared monitoring of copolymer production from CHO and CO2 as catalyzed by complex 1 in the presence of varying quantities of PPNN3.

As evident from **Table 2.1**, complex 1 is a very effective catalyst for the copolymerization of cyclohexene oxide and CO_2. In general, reaction of cyclohexene oxide and CO2 was carried out at 60^{o} C and 3.4 MPa CO_2 pressure to afford poly(cyclohexylene carbonate) in good yield with narrow molecular weight distributions.

For example, entry 4 in **Table 2.1** for the process starting with 20 mL of cyclohexene oxide following 10 h of reaction time provided 18.1 g of purified copolymer (60% yield) with a polydispersity of 1.19. Interestingly, an increase in catalytic activity is noted for 1 equiv of quaternary organic salt over 2 equiv (entries 2 and 4 in **Table 2.1**). This is in contrast to what is observed in our previous studies utilizing (salen)CrX or (tmtaa)CrX as catalysts, where 2 equiv of cocatalyst optimizes the rate of copolymer formation. It is however consistent with the cis-(salan)CrN_3 complex not undergoing reaction with an additional equivalent of azide, whereas (salen)CrN_3 readily forms a stable (salen) $Cr(N_3)_2^-$ complex in the presence of added azide ions. In a related observation, Lu and co-workers have recently shown that the (salan)Cr^+ ion adds one molecule of DMAP, whereas (salen)Cr^+ coordinates two molecules of the amine. The reaction profiles depicted in **Figure 2.5** illustrate the effect of adding various quantities of $PPNN_3$ on the catalytic system. From these profiles it is apparent that the decrease in rate of copolymer production is due to an inhibition process involving the added equivalent of $PPNN_3$. On the other hand, in the absence of any $PPNN_3$ the reaction is very slow, similarly exhibiting a profile indicative of rate inhibition during the early stages of the process (**Figure 2.6**).

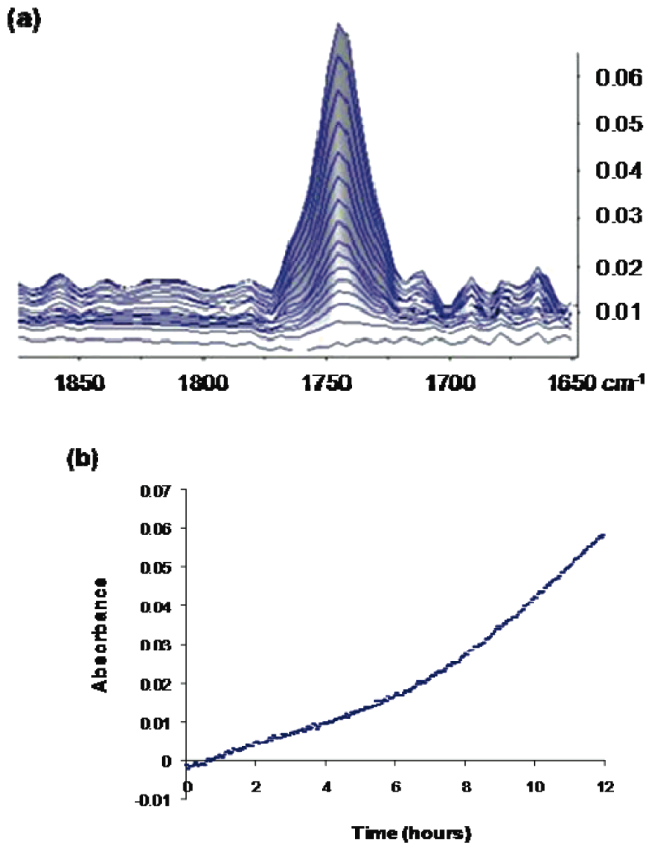

Figure 2.6. (a)Three-dimensional stack plots of the infrared spectra collected every 3 min during the coupling reaction of CHO and CO_2 (60^o Cand 500 psi pressure) in the absence of $PPNN_3$. (b) Reaction profile of this catalytic system.

For comparative purposes a catalytic run of the copolymerization of cyclohexene oxide and CO_2 carried out under identical reaction conditions as entry 1 in **Table 2.1** except utilizing the corresponding (salen)CrCl catalyst affords a somewhat lower TOF of 228 h^{-1}. However, the isolated copolymer possessed a similar molecular weight of 11,600 with a PDI of 1.11. Of notable interest, because of the increased solubility of the (salan)CrX derivatives, much more of the metal catalyst is removed from the polymer with only one methanol purification step. This is illustrated in **Figure 2.7**, where the

copolymer isolated from the process catalyzed by complex 1 is white, and the correspondingly obtained copolymer produced in the presence of the (salen)CrCl analogue is colored because of the presence of metal contaminant.

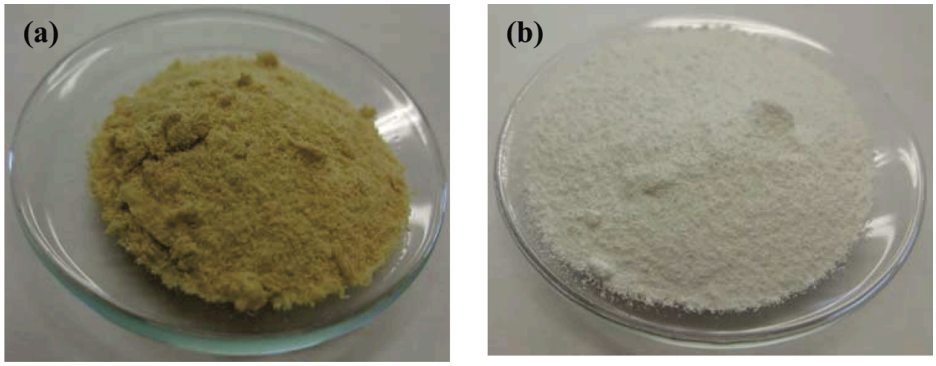

Figure 2.7. Photographs of the isolated poly(cyclohexylene carbonate) after one methanol precipitation: (a) using (salen)CrCl as catalyst and (b) using complex 1 as catalyst.

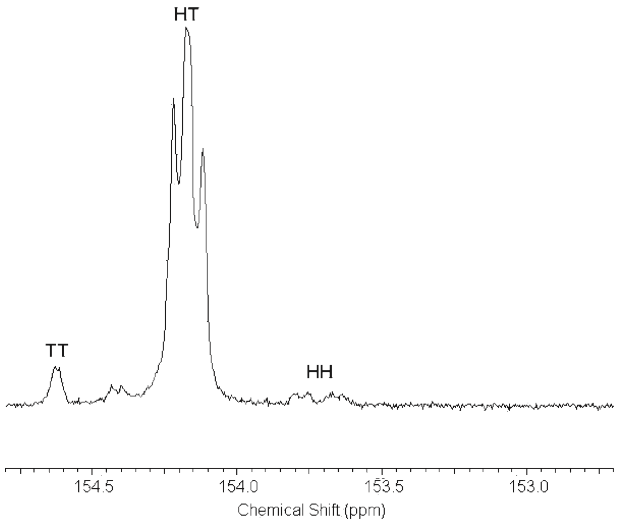

Figure 2.8. Carbonyl region of the ^{13}C NMR spectra (125 MHz, $CDCl_3$) generated from the copolymerization of rac-PO/CO_2 at 22 ^{o}C and 1.5 MPa for 16 h: head-to-tail (HT); tail-to-tail (TT); head-to-head (HH).

Table 2.2. Copolymerization of *rac*-Propylene Oxide and Carbon Dioxide Using Complex 1. All reactions performed with 1 equiv of $PPNN_3$ in rac-PO and 1.5 MPa CO_2 at included temperatures. [a]The rate is expressed in terms of the turnover frequency (TOF (mol of epoxide consumed (mol of catalyst h)$^{-1}$) = turnovers/h). [b]Determined by using ^{13}C NMR spectroscopy. [c]Determined by using gel permeation chromatography in THF, calibrated with polystyrene standards. [d]Only propylene carbonate obtained (3.4 MPa of CO_2 used).

Entry	Time (h)	Temp (^oC)	TOF[a]	Head-to-tail linkages (%)[b]	M_n (kg/mol)[c]	PDI (M_w/M_n)[c]
1	48	22	6	93	11.8	1.06
2	16	25	21	92	8.0	1.13
3	4	60	220[d]	NA	NA	NA
4	4	0	NA	NA	NA	NA

Importantly, unlike its (salen)CrX analogue, complex 1 is an effective catalyst for the selective coupling of propylene oxide and carbon dioxide to poly(propylene carbonate) at ambient temperature. This has recently been reported by Lu and co-workers for other related (salan)CrX derivatives. **Table 2.2** contains a compilation of the copolymerization reaction of propylene oxide and CO_2 catalyzed by complex 1. As indicated in **Table 2.2**, upon raising the reaction temperature to 60^o C, the coupled product of propylene oxide and CO_2 is exclusively propylene carbonate. This observation is anticipated based on our earlier studies using (salen)CrX based catalysts, where lower reaction temperature favors the production of copolymer. This result stems from the fact that the activation barrier for copolymer formation was shown to be 33 kJ/mol less than the corresponding value for cyclic carbonate production. In other words, a lowering of the reaction temperature has a much greater effect on the rate of propylene carbonate formation than the rate of poly(propylene carbonate) production. Furthermore,

for the reaction catalyzed by complex 1 at ambient temperature the process is highly selective for the production of regioregular head-to-tail linkages (**Figure 2.8**).

Further investigations of this catalyst system were for the synthesis of diblock copolymers of poly(propylene carbonate) and poly(cyclohexylene carbonate). This was achieved by first performing the copolymerization of propylene oxide and CO_2 at ambient temperature and 3.4 MPa CO_2 pressure for 16 h. Following the evacuation of carbon dioxide and unreacted propylene oxide, cyclohexene oxide was cannulated into the reactor under an inert atmosphere. The reactor was repressurized with 3.4 MPa of CO_2 and heated at 60^o C for 4 h. The resulting polymer was dissolved in methylene chloride and precipitated first from hexane, followed by precipitation from acidified methanol to yield a purified sample of diblock terpolymer (**Figure 2.9**). From ^{1}H NMR analysis the diblock polymer's composition was determined to be 53% poly(cyclohexylene carbonate) (**Figure 2.10a**). ^{13}C NMR spectroscopy revealed the poly(cyclohexylene carbonate) to be atactic and the poly(propylene carbonate) to have 94% HT carbonate linkages (**Figure 2.10b**). The diblock polymer's molecular weight (M_n) as determined by gel permeation chromatography was found to be 16,500 with a PDI of 1.08.

An interesting note that will be the subject of more far-reaching studies is our observation that whereas propylene oxide and CO_2 in the presence of complex 1 and [PPN]N_3 readily copolymerize at ambient temperature where cyclohexene oxide displays no activity, the two epoxide monomers undergo a facile terpolymerization process at ambient temperature. Indeed, the ^{1}H NMR spectrum of the resulting terpolymer shown

in **Figure 2.11** reveals an almost statistical distribution of propylene oxide and cyclohexene oxide monomers in the polymer. Relevant to this point, it was previously demonstrated that the ring-opening of a metal bound propylene oxide monomer is much easier than the corresponding process involving cyclohexene oxide.[93] A similar observation, i.e., the addition of propylene oxide greatly enhances the copolymerization of cyclohexene oxide and CO_2, was recently noted by Lu and co-workers employing a (salen)Co(III) catalyst system.[95]

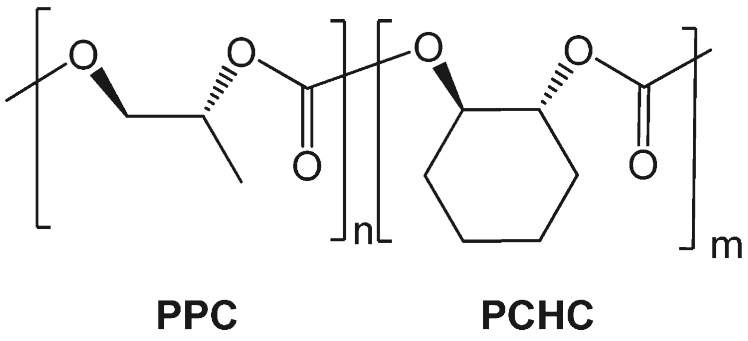

Figure 2.9. Diblock copolymer of poly(propylene carbonate) and poly(cyclohexylene carbonate)

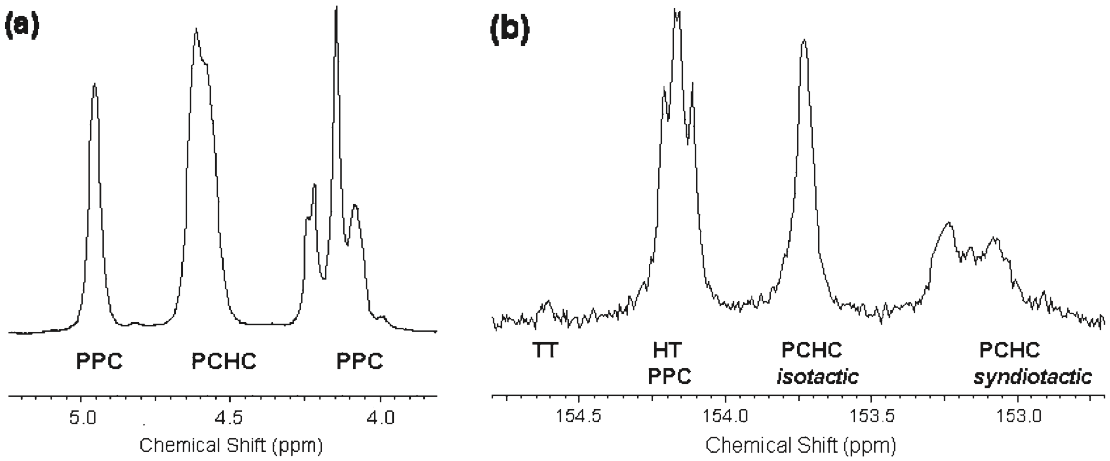

Figure 2.10. (a) ^{1}H NMR spectrum in methine and methylene regions of diblock copolymer of poly(propylene carbonate) and poly(cyclohexylene carbonate). (b) ^{13}C NMR spectrum in carbonate region of diblock copolymer of poly(propylene carbonate) and poly(cyclohexylene carbonate). The m-centered tetrads (*isotactic*) appear at 153.7 ppm and r-centered tetrads (*syndiotactic*) appear at 153.1 ppm.

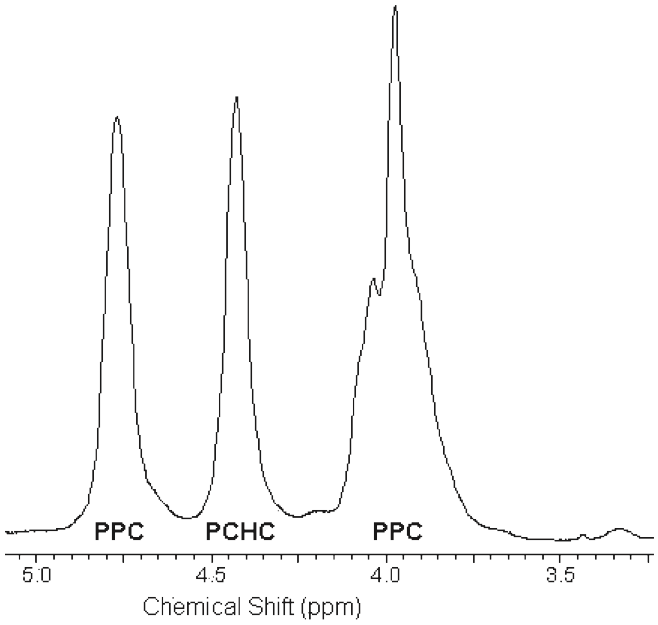

Figure 2.11. ^{1}H NMR spectrum in methine and methylene regions of terpolymer prepared from a 1.5 ratio of propylene oxide to cyclohexene oxide. Ratio of corresponding monomers (PO:CHO) in terpolymer is approximately two to one.

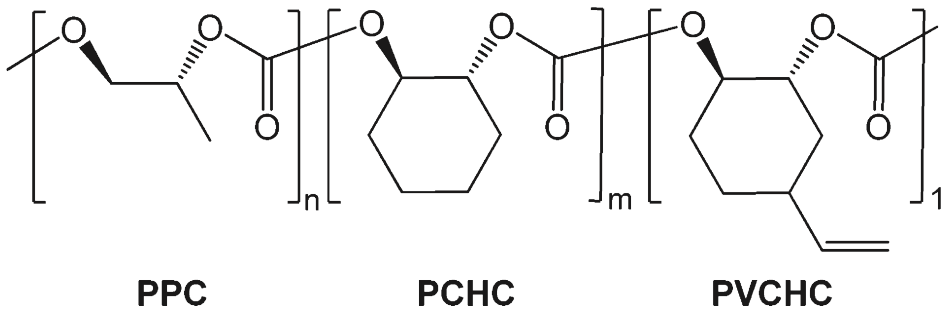

Figure 2.12. Triblock copolymer of poly(propylene carbonate), poly(cyclohexylene carbonate), and poly(vinylcyclohexylene carbonate).

In addition, a triblock polymer was synthesized in a similar manner to that utilized for the preparation of the diblock polymer (*vide supra*). That is, subsequent to preparation of the diblock polymer of poly(propylene carbonate) and poly(cyclohexylene carbonate), vinylcyclohexene oxide (4-vinyl-1-cyclohexene-1,2-epoxide) was cannulated under an inert atmosphere into the reactor. The reactor was repressurized with CO_2 to 3.4 MPa and heated at 60^o C for 4 h. Following the venting of CO_2 the polymeric residue was dissolved in methylene chloride and first precipitated from hexane and then acidified methanol to afford a purified sample of a triblock polymer (**Figure 2.12**). Because of the overlap of the proton resonances, it is difficult to be precise in the composition of the triblock polymer; however, its composition is consistent with the equal quantities of the monomers utilized in its synthesis (**Figure 2.13**). The triblock polymer's molecular weight (Mn) was found to be 22 200 with a polydispersity index of 1.08.

Conclusions

The thermal properties of the copolymers prepared in this report were determined by thermal gravimetric analysis and digital scanning calorimetry measurements. The onset of weight loss for the poly(propylene carbonate) sample was 175^{o} C with 95% loss occurring at 200^{o} C, whereas the corresponding values for poly(cyclohexylene carbonate) were found to be 253 and 275^{o} C. Similar parameters for the onset of weight loss for the diblock and triblock were noted.

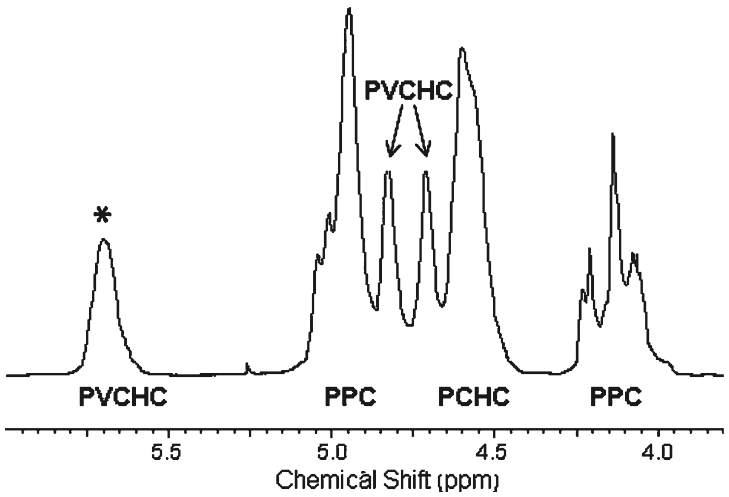

Figure 2.13. ^{1}H NMR spectrum in the methine, methylene, and vinyl regions of triblock copolymer of poly(propylene carbonate), poly(cyclohexylene carbonate), and poly(vinylcyclohexylene carbonate).

The glass transition temperatures (T_gs) of the diblock copolymers of poly(propylene carbonate) and poly(cyclohexylene carbonate), which possess long enough homocopolymer chains, displayed T_g values similar to the individual copolymers. That is, the midpoint glass transition temperatures in the diblock polymer were determined to

be 43.4 and 121.6 ^{o}C. Similar parameters for the triblock copolymer sample were found at 40.6 and 102.3^{o} C. For comparison, the T_g values of random copolymers lie between the values of the homocopolymers, poly(PPC) and poly(CHC).[38]

III. TERPOLYMERIZATION OF MULTIPLE EPOXIDES WITH CO_2*

Introduction

The copolymerization of carbon dioxide and epoxides catalyzed by transition metal complexes represents the environmentally benign synthesis of a new class of polycarbonates derived in part or wholly from renewable resources.[44,96,97,79,19,98,99,100] For example, poly(limonene carbonate) and poly(ethylene carbonate) can be produced from CO_2 and epoxides derived from citrus fruit and corn, respectively. The usage of carbon dioxide as a C1 feedstock has been thoroughly discussed based on its widespread availability, low cost, and nontoxicity.[101,102,103,8,15,104,105,106,107,108,109,110] Thus far most studies have focused on catalysts development and accompanying mechanistic investigations for the copolymerization of CO_2 and the alicyclic and aliphatic epoxides, cyclohexene oxide and propylene oxide. Although polypropylene carbonate (PPC) has applications in such areas as coatings, electronics, and ceramics; polycyclohexene carbonate (PCHC) because of its brittleness has no current commercial use.[32,50]

The utilization of other epoxides for potentially providing copolymers with CO_2 which might have desirable properties is limited by the lack of selective reactivity for copolymer formation or the availability of the epoxide monomers. On the other hand, it is possible to combine multiple epoxides in the polymerization process with CO_2 in order to "tune" the physical properties of the polymeric material, e.g., the

---

*Reprinted (adapated) with permission from Darensbourg, Donald J.; Poland, Ross R.; Strickland, Amanda. *Journal of Polymer Science Part A-Polymer Chemistry* **2012,** *50,* 127–133.

terpolymerization of propylene oxide, cyclohexene oxide, and carbon dioxide.[111,112,51,113] It is also possible to alter polymer properties through the use of polymer blends. In this report we describe rate studies for the relative reactivity of two different epoxide monomers during their terpolymerization process with carbon dioxide.

Experimental

Materials and Instrumentation. All syntheses were performed under pure argon with rigorous exclusion of air and moisture using standard Schlenk techniques or in an argon–filled glovebox. Cyclohexene oxide (CHO) and propylene oxide (PO) were purchased from TCI America, and 4-vinylcyclohexene oxide (VCHO) was purchased from Aldrich Chemicals. All epoxides were freshly distilled from CaH_2 prior to use. The solvents Et_2O pentane/hexane, CH_3CN, THF, and CH_2Cl_2 were purified by an MBraun Manual Solvent Purification System packed with Alcoe F200 activated alumina desiccant. $PPNN_3$ was prepared according to the published procedure.[83] Bone-dry CO_2 purchased from Scott Specialty Gases. All ^1H and ^{13}C NMR spectra were performed in $CDCl_3$. ^1H NMR spectra were recorded at 295 K using an Inova Varian spectrometer at 500 MHz, and ^{13}C NMR spectra were recorded at 295 K at 125 MHz. Chemical shifts are given in ppm relative to TMS and coupling constants (J) in hertz. Infrared spectra were recorded on a Mattson 6021 Fourier transform FTIR spectrometer with a MCT detector. Analytical elemental analysis was provided by Canadian Microanalytical Services Ltd. High-pressure reaction kinetic measurements were performed using an ASI ReactIR 1000 reaction analyses system with stainless steel Parr autoclave modified

with a permanently mounted ATR crystal (SiComp) at the bottom of the reactor (purchased from Mettler Toledo). Glass transition temperature (T_g) values were measured using a Mettler Toledo polymer DSC equipped with a liquid nitrogen cooling system and 50 mL/min purge of nitrogen gas. Samples (~10 mg) were weighed into 40 mL aluminum pans and subjected to two heating cycles. The starting 3,5-di-tert-butylsalicylaldehyde was prepared from commercially available 2,4-di-tert-butylphenol according to the literature procedure.[84]

Synthesis of H_2salan (1a). 5.55 g paraformaldehyde and 38.15 g 2,4-di-tert-butylphenol (1 eq) were dissolved in 300 mL ethanol. 10 mL *N*,*N'*-dmethylethylenediamine (0.5 eq) was cannulated into this mixture, which was then refluxed for 3 days. A white solid, which had precipitated, was isolated and washed with cold methanol. The pure product was characterized by ^{1}H NMR spectroscopy and elemental analysis. ^{1}H NMR: 1.27 (s, 18H, ^{t}Bu), 1.39 (s, 18H, ^{t}Bu), 2.25 (s, 6H, CH_3), 2.63 (s, 4H, CH_2), 6.79 (s, 2H, Ar-H), 7.19 (s, 2H, Ar-H). Anal. Calcd (%) for $C_{34}H_{56}O_2N_2$. C, 77.86; H, 10.69; N, 5.34. Found: C, 77.68; H, 10.92; N, 5.25.

Synthesis of H2salen (1b). The H_2salen ligand (salen = *N*,*N*'–bis(3,5-di-tert-butylsalicylidene)-1,2-ethylenediimine) was synthesized as previously described.

General method for synthesis of Cr(III)Cl Catalysts (2a-b). The appropriate $N_2O_2^{-2}$ ligand (**1a-b**, 1 mmol) and $CrCl_2$ (1.1 mmol) were added to a Schlenk flask in an argon-filled glovebox. The reactants were dissolved in 10 mL of THF and stirred overnight at ambient temperature. The following day the septum was removed, and the reaction solution was exposed to air and stirred for an additional 24 hours. In the instance of

complex **2a**, upon the removal of the solvent *in vacuo*, the remaining solid was dissolved in Et_2O, dried over $MgSO_4$, and subsequently washed with NH_4Cl (3 x 50 mL), brine (3 x 50 mL), and water (3 x 50 mL). Subsequently, the solvent was removed *in vacuo* yielding a green powder. Anal. Calcd (%) for $C_{34}H_{54}N_2O_2CrCl \cdot H_2O$: C, 65.00; H, 8.98; N, 4.46. Found (%): C, 64.33; H, 9.29; N, 4.35. Complex **2b**, (salen)CrCl, was isolated and purified as previously reported.[85]

General Procedure for Neat Copolymerization of Cyclohexene Oxide (CHO) and CO_2. A glass vial was charged with the 50 mg **2a** (1 eq) and 47 mg $PPNN_3$ (1 eq). These solids were dissolved in 10 mL CH_2Cl_2 and stirred for approximately one hour. The solvent was removed *in vacuo* and the remaining solid was dissolved in 10 mL cyclohexene oxide. After dissolution, this mixture was cannulated into a stainless steel Parr reactor at ambient temperature (the reactor had previously been heated to 100 ^oC for 8 hours under vacuum). The vial was rinsed with 10 mL CHO (totaling the volume at 20 mL, 2400 eq), which was also cannulated into the reactor. The reactor was pressurized to 500 psi of CO_2 and maintained at the appropriate temperature. Once the reaction was complete, the reactor was depressurized and a small aliquot was taken to be analyzed by ^1H NMR. The polymer mixture was dissolved in minimal CH_2Cl_2 and was purified by precipitation upon the addition of 1M HCl in MeOH. The purified polymer was dried overnight *in vacuo* and analyzed by ^1H NMR, DSC, and GPC.

General Procedure for Neat Copolymerization of Propylene Oxide (PO) and CO_2. 50 mg (1 eq) **2a**, 47 mg (1 eq) $PPNN_3$ and 20 mL PO (3500 eq) were used as

catalyst/cocatalyst/monomer. Aside from this, the method was identical to that of the copolymerization of CHO/CO_2.

General Procedure for Kinetic Experiments of CHO/CO_2 and PO/CO_2 Copolymerizations. A glass vial was charged with 50 mg **2a** (1 eq) and 47 mg $PPNN_3$ (1eq). 10 mL epoxide (1200 eq CHO, 1750 eq PO) was added to the vial which was stirred until dissolution was apparent. This mixture was cannulated into an ATR-FTIR mounted Parr stainless steel reactor. The vial was rinsed with 10 mL dry toluene, which was also cannulated into the reactor. The reactor was heated to 70^{o} C for 30-45 minutes, after which it was cooled to the desired reaction temperature and pressurized with 500 psi CO_2.

General Procedure for Terpolymerization of PO/CHO/CO_2. 50 mg **2a** (1 eq), 47 mg $PPNN_3$ (1 eq) were added to a glass vial. The two solids were dissolved in 10 mL CH_2Cl_2 and stirred for ~1 hour. Solvent was removed *in vacuo* and the resultant solid was redissolved in either CHO or PO and cannulated into the ambient temperature reactor which had previously been dried by heating *in vacuo* for 8 hours. The vial was rinsed with either PO or CHO (whichever aliquot remained in order to attain a total volume of 20 mL), and the solution was also cannulated into the reactor. The reactor was pressurized to 500 psi and maintained at the appropriate temperature during the polymerization process. In several reactions, aliquots were withdrawn for analysis from the reactor by opening a valve attached to a dip tube within the reactor. Aliquots were immediately placed on ice to prevent PO evaporation and were subsequently analyzed by ^{1}H NMR spectroscopy.

General Procedure for the Terpolymerization of VCHO/CHO/CO_2. 50 mg **2b** (1 eq), 106 mg $PPNN_3$ (2 eq), and CHO/VCHO (vinylcyclohexene oxide) with a combined volume totaling 20 mL were used as catalyst/cocatalyst/monomer 1/ monomer 2. Aside from this, the procedure was identical to the general procedure for PO/CHO/CO_2 terpolymerization.

Results and Discussion

Structure of (salan)CrCl. Complex **2a**, (salan)CrCl, in the presence of an onium salt has been shown to be an effective catalyst for the terpolymerization of PO, CHO, and CO_2.[45] As has been previously pointed out the structure of **2a** is somewhat ambiguous in the absence of crystallographic data. That is, it could exist in the *cis*-b-configuration (**Figure 3.1a**) as its (salalen)CrCl·H_2O analogy[114,115], or as a dimer structure as in (salen)CrOH (**Figure 3.1b**).[116] Elemental analysis of **2a** showed that there were no unexpected ligands available for binding to the chromium(III) center other than a water molecule. This along with our published X-ray structure of a sulfate bridged dimer of (salan)Cr(III), suggests that indeed complex **2a** might be a dimer in solution with bridging chloride ligands. Even if (salan)CrCl·H_2O as isolated is monomeric with a water molecule in the sixth coordination site, upon its dissolution into weakly coordinating epoxide solutions dimerization could readily take place. Support for such a dimeric structure is seen in *in situ* copolymerization studies (*vide infra*).

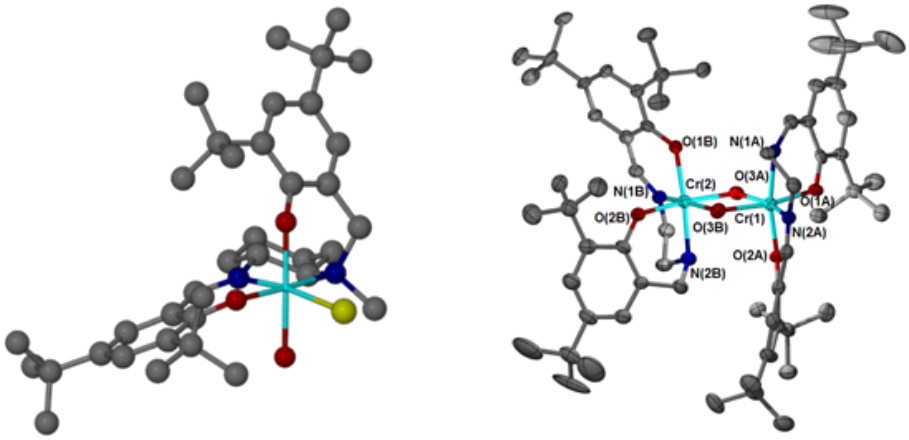

(a) **(b)**

Figure 3.1. (a) X-ray structure of (salalen)CrCl·H_2O.[9] (b) X-ray structure of $[(salen)Cr(OH)]_2$.

Further support for the catalytically active metal species originating from a more aggregated metal precursor can be seen in *in situ* infrared studies of the copolymerization process of cyclohexene oxide and CO_2. That is, the copolymerization of cyclohexene oxide/CO_2 catalyzed by complex **2a** in the presence of one equivalent of $PPNN_3$ was performed in order to monitor the process as a function of catalyst pretreatment. This procedure has the advantage of observing the reaction's progress as opposed to only noting the quantity of copolymer product after a designated reaction time.[117] In particular this allows for an examination of the reaction with regard to any initiation period or change in reaction rate. **Figure 3.2a** illustrates that for a process carried out at 60^{o} C and 3.5 MPa without any pretreatment of the catalyst, there is a three hour initiation period prior to the onset of copolymer formation.

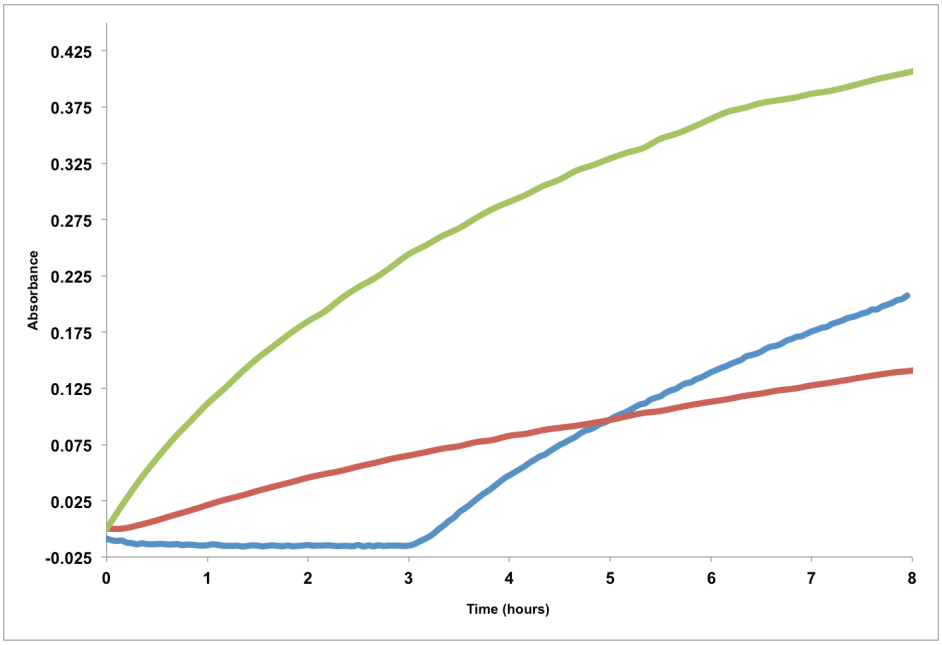

Figure 3.2. Copolymerization of cyclohexene oxide and CO_2 in the presence of complex **2a** and an equivalent of $PPNN_3$. **2a** (blue): No catalyst pretreatment. **2b** (green): catalyst pretreatment at 60 ^oC. **2c** (red): Catalyst pretreatment at 110 ^oC.

Similarly, for a copolymerization reaction of cyclohexene oxide/CO_2 performed in the presence of a small quantity of propylene oxide an extended initiation period in excess of three hours was noted. On the other hand, upon adding the catalyst/cocatalyst/(epoxide or solvent) and heating the reactor at 60^o C with stirring for 30-45 minutes followed by cooling prior to addition of CO_2 results in *no* initiation periods (**Figure 3.2b**). In the instances where coordinating (THF) or weakly coordinating (CH_2Cl_2) solvents were used, these were removed following the reflux/stirring/cooling period and prior to addition of epoxide and CO_2. From these studies we conclude that with heating the anionic cocatalyst or THF disrupts the dimeric

complex **2a** resulting in a monomeric catalytically active metal species. It was further noted that pretreatment at temperatures significantly greater than 60^{o} C led to lower rates of copolymer production, presumably due to catalyst instability (**Figure 3.2c**).

Currently there is much interest in polymeric materials produced by terpolymerization reactions between two different epoxide monomers and carbon dioxide. Investigations of these processes are stimulated by the need to produce polycarbonates with different properties than those of the respective epoxide copolymers with CO_2.[50,38,118,119] For example, through the incorporation of other monomers the T_g of poly(propylene carbonate) can be increased or decreased. That is, Lu and coworkers have synthesized terpolymers from cyclohexene oxide, propylene oxide, and CO_2 covering a range of glass transition temperatures from 42 to 118 ^{o}C. Similarly, Lee and coworkers have prepared terpolymers of propylene oxide with 1-hexene oxide or 1-butene oxide and CO_2 which have T_gs over the ranges of -15 – 32^{o} C and 9 – 33^{o} C, respectively.[49] In addition, early on it was shown that it was possible to synthesize terpolymers of propylene oxide/cyclohexene oxide/CO_2 under reaction conditions where propylene oxide and CO_2 would provide exclusively propylene carbonate.[120] Alternatively, because of reactivity differences it is often possible to incorporate a comonomer into a terpolymers under reaction conditions where the monomer alone is unreactive.[45]

At this time we wish to report quantitative studies of terpolymerization processes involving various epoxide monomers and CO_2. Because cyclohexene oxide is selectively coupled with CO_2 to afford copolymers over a wide temperature range, it is

possible to perform terpolymerization reaction of cyclohexene oxide with its functionalized derivatives to provide polycarbonates which may be postsynthetically modified. For example, the terpolymerization of cyclohexene oxide with TMSO (**Figure 3.3a**) or VCHO (**Figure 3.3b**) and CO_2 readily takes place resulting in terpolymers that can be intra- or inter-molecularly cross-linked by silsesquioxane units[19] or metathesis reactions.[121] It is important to note here that the derivative of cyclohexene oxide should not possess substituents at the *ipo*-carbon center. That is, epoxides such as limonene oxide (**Figure 3.3c**) is an extremely difficult monomer to copolymerize with CO_2 to provide poly(limonene carbonate).[37]

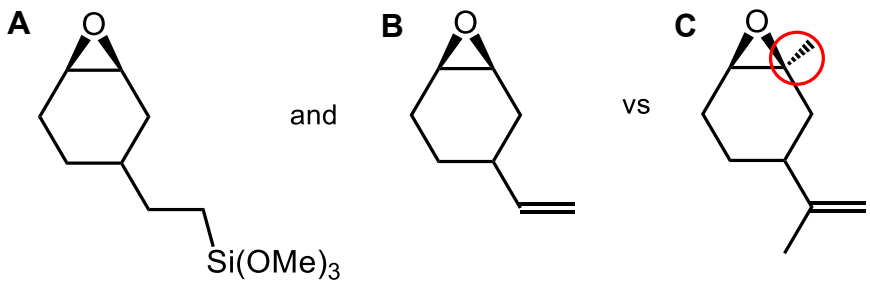

Figure 3.3. Epoxides 3 and 4 are able to be coupled with CO_2, unlike epoxide 5

The terpolymerization of cyclohexene oxide and vinylcyclohexene oxide catalyzed by complex **2b** in the presence of two equivalents of $PPNN_3$ and 3.5 MPa of CO_2 was carried out at several different epoxide feed ratios in order to quantify the relative reactivities of the two monomers. As indicated in **Figure 3.4**, r_1 and r_2 represent the relative tendencies of the epoxide monomers to self-propagate or cross-propagate.

At low conversion (<10%) we can use the Fineman-Ross equation to evaluate r_1 and r_2, where $f = m_1/m_2$ = molar ratio of monomers in copolymer and $F = M_1/M_2$ = molar ratio of monomers in feed, where M_1 = cyclohexene oxide and M_2 = VCHO(**Figure 3.4**).[53] **Table 3.1** contains the respective mole fraction ratios in the feed and resultant copolymer, and **Figure 3.5** depicts the Fineman-Ross plot. As seen in **Table 3.1** and **Figure 3.5**, there is only a slight preference for incorporation of cyclohexene oxide in the terpolymer. It is important to note here that the basicities of CHO and VCHO, and presumably their binding abilities, are the same based on the shifts in the ν_{OD} frequencies of MeOD upon hydrogen-bonding with the respective epoxide.

Table 3.1. Mole fraction ratios of cyclohexene oxide and VCHO in the feed (F) and in the resultant copolymer (f). a – determined by ^{1}H NMR spectroscopy.

Entry	F	f[a]
1	4.0	3.76
2	2.3	2.57
3	1.5	1.56
4	1.0	1.13
5	0.67	0.786
6	0.43	0.493
7	0.25	0.282

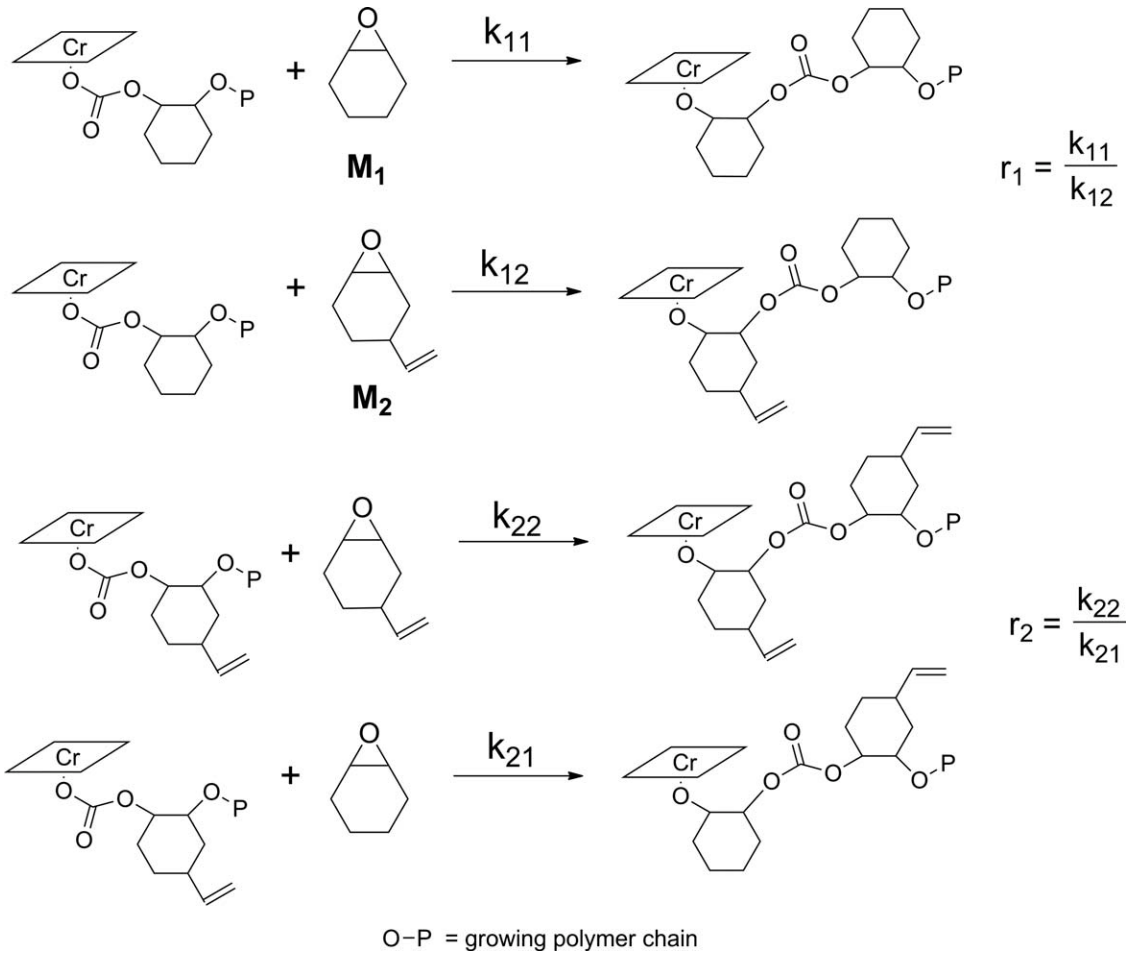

Figure 3.4. Reactivity ratios, the relative tendencies of the monomers ($\mathbf{M_1}$ and $\mathbf{M_2}$) to self-propagate or cross propagate. –O-P = growing polymer chain.

Earlier we noted that although the copolymerization of cyclohexene oxide and carbon dioxide using the binary (salan)CrCl/onium salt catalyst system did not take place at ambient temperature, in the presence of propylene oxide, cyclohexene oxide was readily incorporated in the polycarbonate at ambient temperature.[45] A similar observation was reported by Lu and coworkers employing the closely related bifunctional (Salen)CoCl catalyst.[95,122] In an effort to better quantify the relative reactivity of cyclohexene oxide and propylene oxide, the terpolymerization reaction of these two monomers with CO_2 was carried out in the presence of (salan)CrCl/onium salt catalyst at two different temperatures. Results from the Fineman-Ross plot at 25 ^{o}C shown in **Figure 3.5** provide r_1 (r_{CHO}) and r_2 (r_{PO}) values of 0.172 and 1.11, respectively. That is, whereas a propylene carbonate polymer end group will ring-open either epoxide monomer with near equal ease, a cyclohexene carbonate polymer end group has a much greater propensity for ring-opening a propylene oxide monomer over a cyclohexene monomer. On the other hand, upon raising the reaction temperature to 40 ^{o}C, r_1 = 0.869 and r_2 = 1.49. As anticipated, the cyclohexene carbonate's reactivity towards cyclohexene oxide has greatly increased relative to propylene oxide (by a factor of 5), whereas, the increase in propylene carbonate's propensity for ring-opening propylene oxide *vs* cyclohexene oxide has only increased by 1.3 times. The basicity of PO is almost identical to that of CHO.

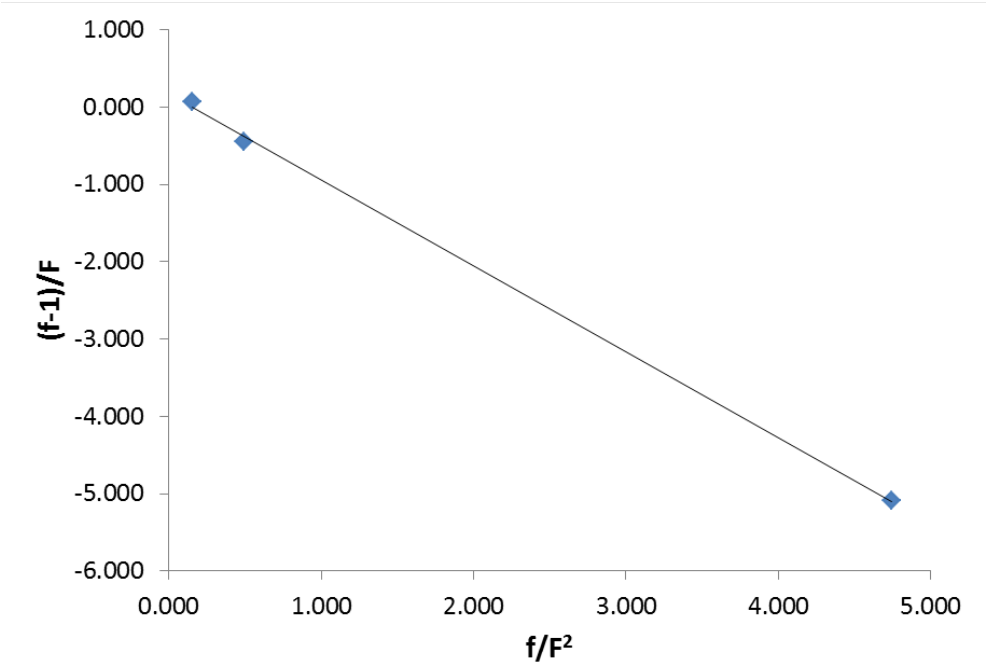

Figure 3.5. Fineman-Ross plot of CHO/PO/CO_2 terpolymerization reaction at 25 ^{o}C. The r_1 and $_2$ values are 0.172 and 1.11, respectively, with an R^2 value of 0.9995.

This behavior is further observed in comparable copolymerization and terpolymerization studies of cyclohexene oxide/CO_2 and cyclohexene oxide/propylene oxide/CO_2, respectively, as monitored by *in situ* infrared spectroscopy. Because of the limited solubility of poly(propylene carbonate) in propylene oxide the cyclohexene oxide/propylene oxide feed ratio was maintained at 9:1, while the reaction temperature was varied from 40 to 60 ^{o}C. As illustrated in **Figure 3.6**, the enhancement in the rate observed for the copolymerization of cyclohexene oxide and CO_2 upon addition of propylene oxide decreased with increasing reaction temperature.

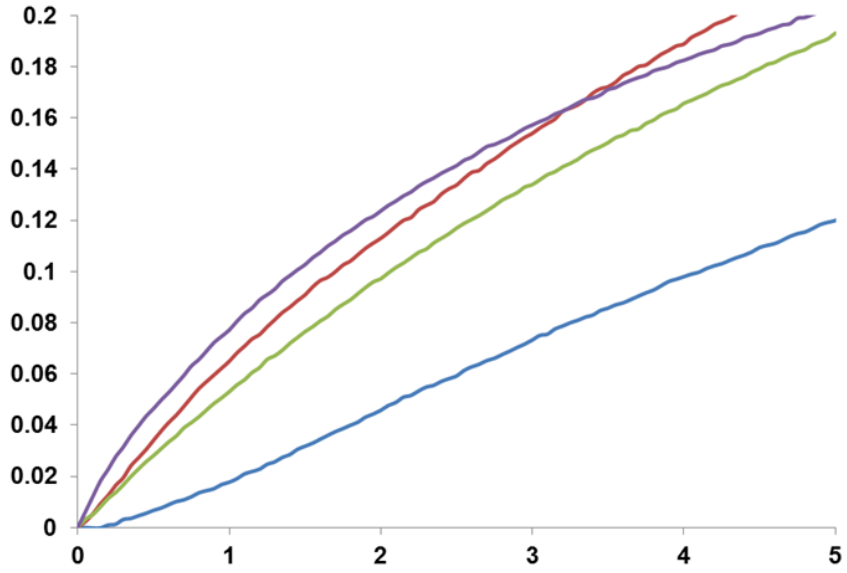

Figure 3.6. Comparison of rates of copolymer formation for the copolymerization of CHO/CO_2 at 40 ^{o}C (blue) and 60 ^{o}C (red) *vs* terpolymerization of CHO/PO/CO_2 at 40 ^{o}C (green) and 60 ^{o}C (purple).

To better ascertain the difference in reactivity of cyclohexene oxide and propylene oxide with CO_2 to provide copolymer, comparative kinetic studies were conducted for the coupling processes using the binary catalyst system of complex **2a** and $PPNN_3$. Temperature-dependent measurements in toluene solution at a CO_2 pressure of 3.5 MPa were performed using *in situ* infrared spectroscopy for monitoring the growth of the carbonate absorption of the copolymers at ~1750 cm^{-1}. **Figure 3.7** depicts the reaction profiles for copolymer production, whereas **Figure 3.8** displays the plots of $\ln[(A_\infty)/(A_\infty-A_t)]$ *vs* time. An Eyring plot of the rate constants for copolymer production at a catalyst concentration of 4.1 mM yields an enthalpy of activation $\Delta H^{\neq}$ = 73.9 kJ-mol^{-1} and entropy of activation $\Delta S^{\neq}$ = -68.8 J-mol^{-1}-K^{-1} (**Figure 3.9**).

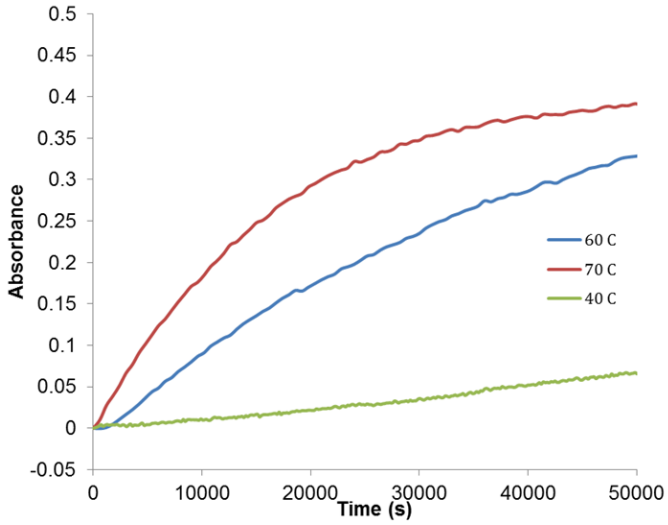

Figure 3.7. Growth of peak at 1750 cm^{-1} for copolymerizations of CHO and CO_2 catalyzed by complex **2a** and $PPNN_3$ at 3.5 MPa of CO_2 in toluene solvent as a function of temperature monitored by ATR-FTIR spectroscopy.

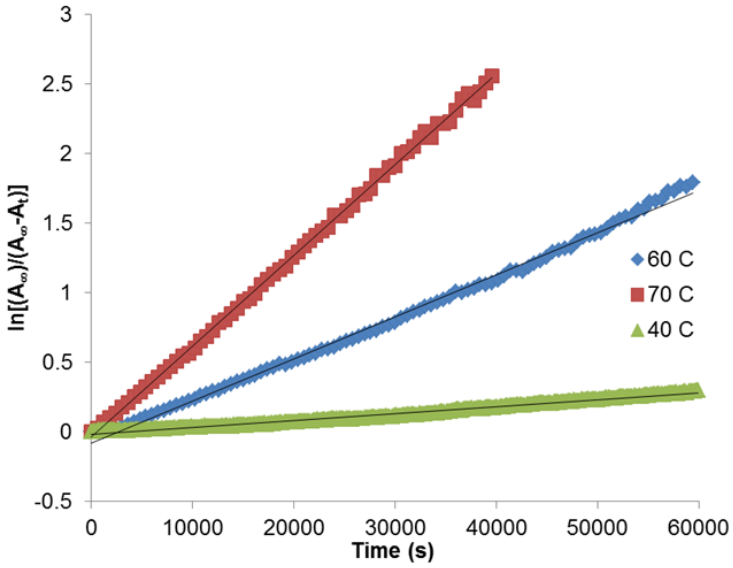

Figure 3.8. Kinetic plots of $\ln[(A_\infty)/(A_\infty-A_t)]$ *vs* time for the data presented in **Figure 3.7**, where A_∞ and A_t represent the absorbance of the copolymer band at 1750 cm^{-1} at time equals infinity and t, respectively. Second-order rate constants are 1.59 x 10^{-2} sec^{-1}-M^{-1} at 70.0 ^oC, 7.37 x 10^{-3} sec^{-1}-M^{-1} at 60.0 ^oC, and 1.22 x 10^{-3} sec^{-1}-M^{-1} at 40.0 ^oC.

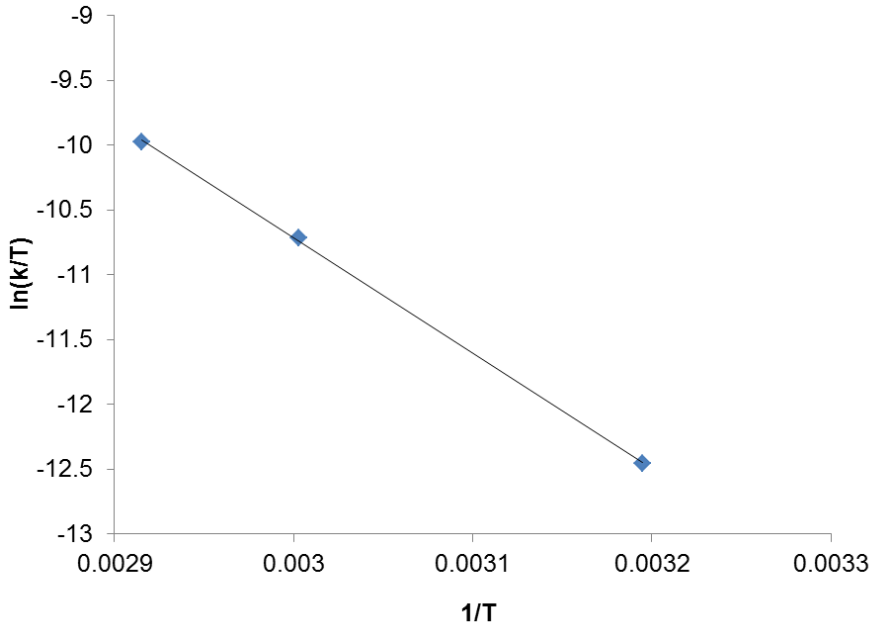

Figure 3.9. Eyring plot of rate constant data *vs* temperature shown in **Figure 3.8**, with an R^2 value of 0.9997.

Analogous kinetic studies of the copolymerization of propylene oxide and carbon dioxide were performed in toluene solution utilizing the catalyst system of complex **2a** and $PPNN_3$ at a CO_2 pressure of 3.5 MPa. The copolymerization of propylene oxide/CO_2 for the temperature range of 30 – 50 ^oC provided a $\Delta H^{\neq}$ value of 76.2 kJ/mol with a corresponding $\Delta S^{\neq}$ = -182 J/mol-K. As seen in **Figure 3.10** this coupling process is selective for propylene carbonate formation even at 40 ^oC. This is to be contrasted with reactions carried out in neat propylene oxide where the process occurs at a much faster rate and is highly selective for copolymer formation.[45]

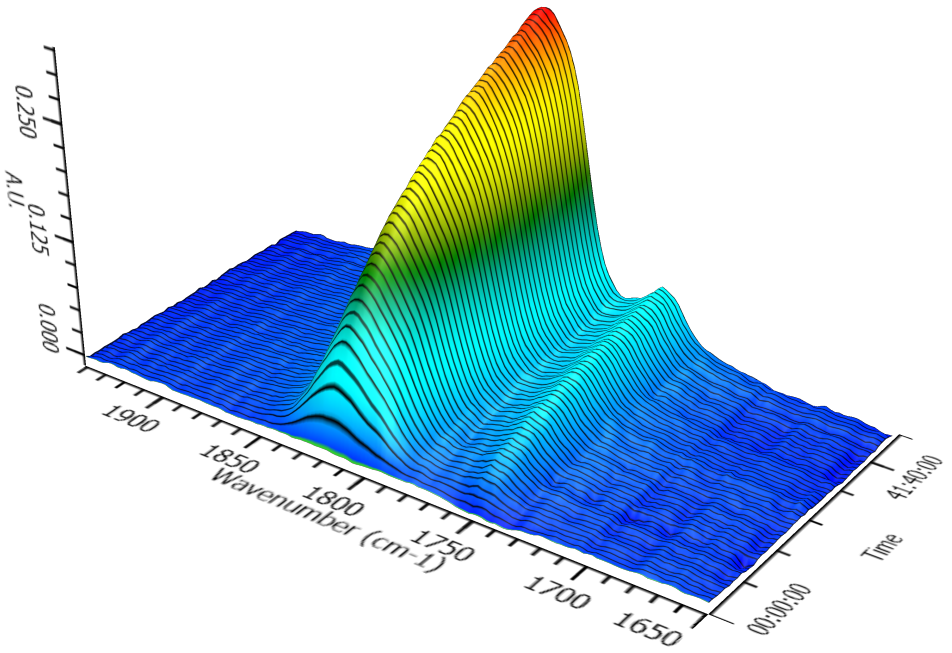

Figure 3.10. *In situ* infrared spectroscopy monitoring of copolymerization of PO/CO_2 in toluene at 40 ^{o}C utilizing catalyst **2a** and $PPNN_3$ at 3.5 MPa of CO_2 pressure.

Future Work

Further studies in this area will be focused primarily on the ability to incorporate a wider variety of epoxide monomers into terpolymerization reactions. While this study focused on PO, CHO, and VCHO, there is much interest in studying monomers with bulky functionalities, such as styrene oxide, as well as monomers isolated from renewable resources, such as limonene oxide. Much will be learned from the standpoint of studying the kinetic effects of reactive epoxides with relatively inert epoxides as well as the study of the mechanical and thermal properties of the resulting polymers.

Another area of future study is the incorporation of bifunctional epoxides into a terpolymer for use as a crosslinker. By using an appropriate mole fraction of a bifunctional epoxide such as 1,3-butylenediepoxide or bisphenol-A diglycidyl ether, it is possible to drastically alter the physical properties of a polymer without adding a post-polymerization crosslinking step. Previous studies on crosslinked polycarbonates have shown that inclusion of a small molar fraction of crosslinker can increase its expected T_g by over 100 ^oC relative to the analogous pure CO_2/epoxide copolymer.[121] Typical post-polymerization crosslinking reactions of CO_2/epoxide polycarbonates are performed after isolation of the polymer by adding a crosslinking catalyst, such as Grubbs' catalyst. This method, while very effective, requires extraneous solvent and catalyst, resulting in an overall decrease in the efficiency of the process. Additionally, the only well-studied vinyl-containing monomer is VCHO, which, when incorporated into a polymer, succumbs to similar mechanical shortfalls as PCHC in terms of brittleness. By utilizing a bifunctional epoxide as a crosslinker, no additional purification or modification is necessary.

Conclusions

These studies of the coupling reactions of cyclohexene oxide or propylene oxide with carbon dioxide in the presence of the binary (salan)CrCl/onium salt catalyst system illustrate important observations relevant to the rate and selectivity of these reactions. Firstly, the activation barriers for copolymer formation in toluene are significantly enhanced relative to those observed for the *solventless* processes.[47] This may in part be due to the less polar nature of toluene as compared to the monomer, since the transition-

state for ring-opening of the epoxide is quite polar. *NOTE*: The use of polar cosolvents is prohibited since these compete more effectively for active catalyst sites than the weakly coordinating epoxide monomers. Secondly, for epoxide monomers prone to cyclic formation, performing reactions in a cosolvent enhances the rate of cyclic carbonate formation as compared to copolymer production. That is, cyclic carbonate *vs* copolymer formation is closely linked to epoxide concentration, with the latter being retarded with decreasing epoxide monomer concentration. This phenomenon will be of greater significance when employing epoxides which are solids over the temperature range of the copolymerization reactions, and hence must be carried out in the presence of a cosolvent.[123]

IV. SYNTHESIS OF POLYESTERS FROM THE ALTERNATING COPOLYMERIZATION OF CYCLIC ANHYDRIDES AND EPOXIDES*

Introduction

It has become increasingly more apparent that there is a need to develop the synthesis of new polymeric materials which incorporate renewable resources.[124] In this regard, the synthesis of polyesters by way of ring-opening polymerization of cyclic anhydrides and epoxides offers the possibility of providing a wide variety of polyesters, including some from replenishable reserves. For example, copolymers from succinic anhydride and ethylene oxide or limonene oxide constitute polymeric materials from such sources (**Figure 4.1**).[125,58] Furthermore, many of these aliphatic polyesters exhibit a wide range of mechanical and thermal properties in addition to be biodegradable.

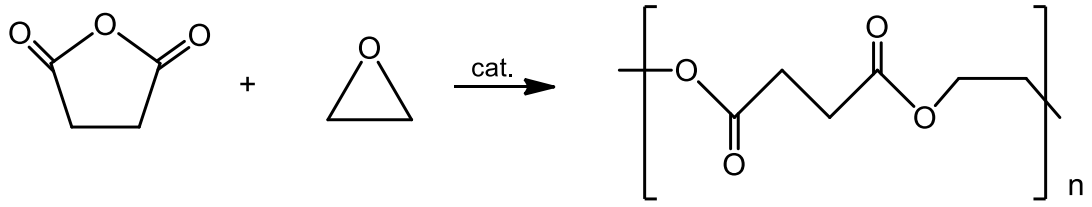

Figure 4.1. Scheme describing generic reaction of epoxide with anhydride to produce polyester

Several early publications have reported upon catalytic systems utilizing a range of metal initiators which are able to accomplish these copolymerization reactions.[56]

---

*Reprinted (adapated) with permission from Darensbourg, D. J.; Poland, Ross R.; Escobedo, Christina. *Macromolecules* **2012,** *42,* 6992–6998. Copyright 2009 American Chemical Society.

However, these processes generally display low catalytic activities and provide copolymers of relatively low molecular weights.[57,44,126] More recently, Coates and coworkers have employed (BDI)ZnOAc (BDI = β-diiminate) complexes as active catalysts for the ring-opening polymerization of epoxides and cyclic anhydrides.[127] In this manner, these researchers were able to synthesize new aliphatic polyesters in a highly alternating copolymerization of epoxides and cyclic anhydrides which afforded high molecular weight copolymers with narrow molecular weight distributions.

Because (salen)CrCl complexes in the presence of onium slats, like (BDI)ZnOAc complexes, have been very effective at coupling CO_2 and epoxides, it is anticipated that these complexes will be productive catalysts for the copolymerization of epoxides and cyclic anhydrides.[44,79,19,99] Indeed, while this work was in progress, DiCiccio and Coates presented results on the ring-opening polymerization of maleic anhydrides with epoxides catalyzed by (salen)$CoO_2CC_6F_5$ and (salen)CrCl.[60] Additional reports containing extensive MALDI-ToF-MS studies of the ring-opening co- and terpolymerization of cyclohexene oxide and a series of cyclic acid anhydrides and CO_2 catalyzed by chromium(III) porphyrinate and salen complexes have been published by Duchateau and coworkers.[61] Herein, we report kinetic studies of the copolymerization of a variety of epoxides and cyclic anhydrides catalyzed by these single-site chromium(III) catalysts. In addition *in situ* infrared monitoring of the terpolymerization of phthalic anhydride, cyclohexene oxide, and CO_2 to provide a diblock copolymer of polyester and polycarbonate, i.e., poly(ester-*co*-carbonate) will be examined.

Experimental

Reagents and Methods. Unless otherwise specified, all syntheses and manipulations were carried out on a double-manifold Schlenk vacuum line under an atmosphere of argon or in an argon filled glovebox. Propylene oxide, cyclohexene oxide, and styrene oxide were purchased from VWR and either distilled from CaH_2 or used as received. Phthalic anhydride, succinic anhydride, cyclohexane anhydride, cyclohexene anhydride, and maleic anhydride were purchased from VWR and used as received. Oxetane (Alfa Aesar) was freshly distilled from CaH_2 and stored in the freezer of the glovebox. (Salen)Cr(III)Cl was purchased from Strem. PPNCl was purchased from Aldrich and recrystallized from diethyl ether and acetonitrile. $PPNN_3$ was synthesized by mixing molar equivalents of NaN_3, followed by recrystallization from diethyl ether and acetonitrile. *n*-Bu_4NCl was purchased from VWR and recrystallized before use. (n-Bu)NX, where X = Br^-, N_3^-, or I^- was synthesized from *n*-Bu_4NCl and the appropriate salt, followed by recrystallization.

Measurements. All ^1H and ^{13}C NMR spectra were performed in $CDCl_3$. ^1H NMR spectra were recorded at 295 K using an Inova Varian spectrometer at 500 MHz, and ^{13}C NMR spectra were recorded at 295 K at 125 MHz. Chemical shifts are given in ppm relative to TMS and coupling constants (J) in hertz. High-pressure reaction kinetic measurements were performed using an ASI ReactIR 1000 reaction analyses system with stainless steel Parr autoclave modified with a permanently mounted ATR crystal (SiComp) at the bottom of the reactor (purchased from Mettler Toledo). *In situ* infrared experiments were performed using a ReactIR ic10 with a SiComp ATR crystal. T_g

values were measured using a Mettler Toledo polymer DSC equipped with a liquid nitrogen cooling system and 50mL/min purge of nitrogen gas. Samples (~10 mg) were weighed into 40 μL aluminum pans and subjected to two heating cycles, 1st cycle was at 10°C/minute from -100°C to 200°C, 2nd was at 5°C/minute over the same range of temperatures. Molecular weight determination was performed using a Viscotek GPC instrument with a low angle light scattering (LALS), right angle light scattering (RALS), and refractive index (RI) detectors with THF as eluent.

Representative ReactIR Monitored Copolymerization. A jacketed reaction vessel was charged with 64 mg (1 eq) (salen)Cr(III)Cl, 57 mg $PPNN_3$ (1 eq), and 3 g phthalic anhydride (200 eq) followed by purging with argon. 23 mL toluene was added to the flask, at which point the flask was heated to 80°C and allowed to equilibrate for 15 minutes. Once it became apparent that all phthalic anhydride had dissolved, 2mL cyclohexene oxide (200 eq) was injected into the flask, at which point the FTIR monitoring was stared. Reactions were allowed to proceed until 100% conversion was achieved.

Representative Copolymerization. A vial was charged with a stirring bar, 2 g phthalic anhydride (533 eq), 16 mg (salen)Cr(III)Cl (1 eq), and 7.5 mg *n*-Bu_4NCl (1 eq) . The vial was purged for several minute with argon, then 10 mL toluene and 1 mL cyclohexene oxide (400 eq) were injected into the vial. The vial was inserted into an oil bath heated to 80°C and allowed to react overnight. Excess anhydride and catalyst were removed by dissolution in 1.0M HCl in methanol.

Results and Discussion

The various epoxide and cyclic anhydride monomers examined in these studies are listed in **Figure 4.2**. Initially we investigated the copolymerization of phthalic anhydride (PA) and cyclohexene oxide (CHO) employing the (salen)CrCl catalyst (**Figure 4.3**) in the presence of several onium salts to optimize the catalytic activity. As illustrated in the infrared traces of polymer formation in **Figure 4.4**, the chromium (III) catalyst alone was ineffective and the onium salt alone was less effective than a combination of the two species. This is to be contrasted with the previous literature report where (salen)CrCl did not require a cocatalyst for the copolymerization of maleic anhydride and propylene oxide.[60] On the other hand, in the Duchateau studies a DMAP (4-*N*,*N*-dimethylamino-pyridine) cocatalyst was necessary in the presence of (Salophen)CrCl to impact catalytic activity.[61] In both instances the polyesters afforded exhibited narrow molecular weight distributions, with PDIs ranging from 1.07 to 1.13.

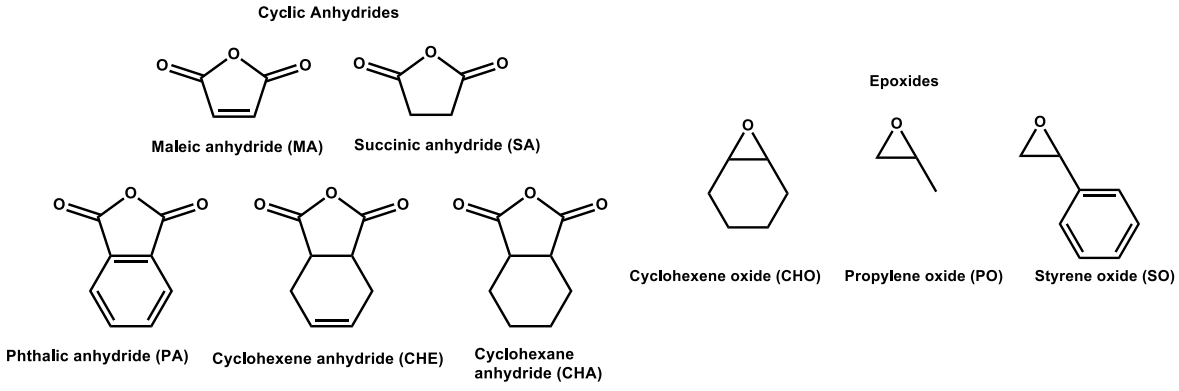

Figure 4.2. Anhydrides and epoxides used in this study.

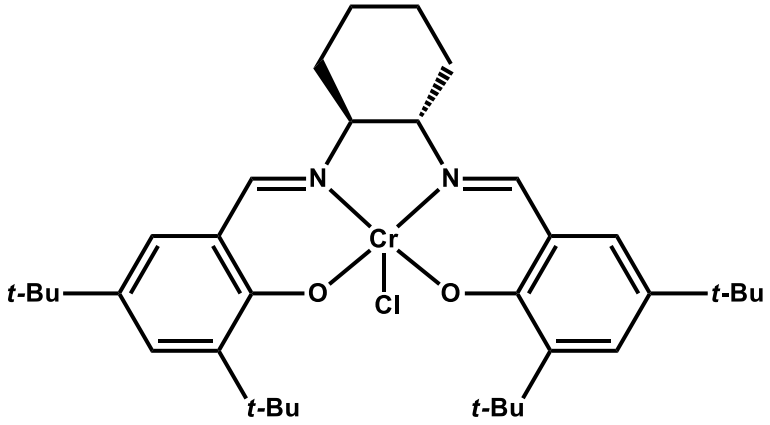

Figure 4.3. *N,N'*-bis(3,5-di-*tert*-butylsalicylidine)-1,2-cyclohexane diaminochromium(III)chloride.

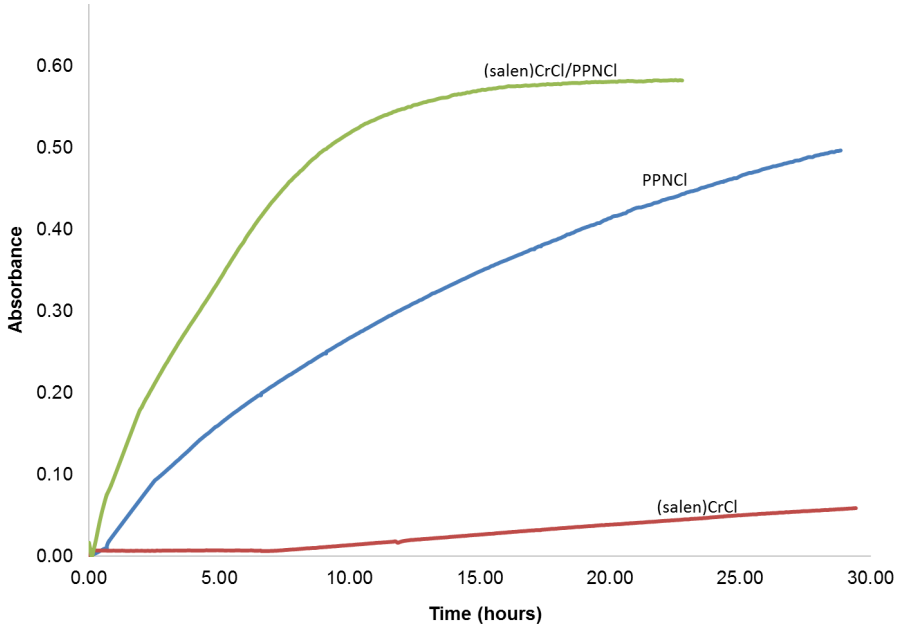

Figure 4.4. Growth of polyester peak at 1748 cm^{-1} as monitored by *in situ* ATR-FTIR spectroscopy for various combinations of catalyst and cocatalyst. (Green line) [Cr]:[Cl]:[PA]:[CHO] = 1:1:200:200, (Red line) [Cr]:[Cl]:[PA]:[CHO] = 1:0:200:200, (Blue line) [Cr]:[Cl]:[PA]:[CHO] = 0:1:200:200. Cr = (salen)CrCl, Cl = PPNCl, PA = phthalic anhydride, CHO = cyclohexene oxide.

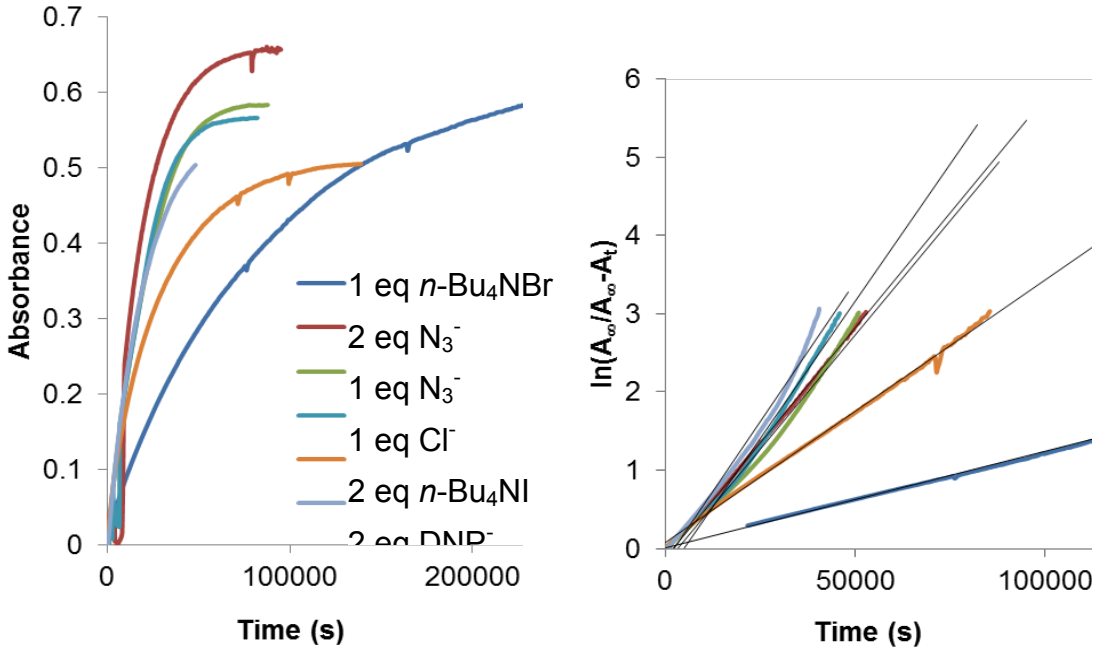

Figure 4.5. Cocatalyst Study – Reactions were performed using the following conditions: 64 mg catalyst (1 eq, 4.05 mM), appropriate cocatalyst, 200 eq PA (3 g), 200 eq CHO (2 mL), and 18 mL toluene (solvent) at 80 °C. Cations not listed are PPN^+(*bis*(triphenylphosphine)iminium) salts. DNP^- = 2,4-dinitrophenoxide. **A**. Absorbance of polyester band at 1738 cm^{-1} *vs* time. **B**. Determination of rate constants from the $\ln(A_\infty/A_\infty-A_t)$ *vs* time, where A_∞ and A_t are absorbances of polyester band at 1738 cm^{-1} at t_∞ = infinity and t = time, respectively.

Table 4.1. Tabulated values for the rate constants, k from the cocatalyst study. Reactions performed with PA:CHO:(salen)CrCl – 200:200:1 in toluene at 80 °C. $k = k_{obs}/[catalyst]$, where [catalyst] = 4.05 mM.

Cocatalyst	$k(M^{-1}\text{-}sec^{-1}) \times 10^2$
2 eq PPNDNP	1.76
1 eq PPNCl	1.73
2 eq $PPNN_3$	1.45
1 eq $PPNN_3$	1.44
2 eq *n*-Bu_4NI	0.827
1 eq *n*-Bu_4Br	0.304

Utilizing the two monomers (PA and CHO) in the accompaniment of (salen)CrCl and various anions derived from PPN^+ and *n*-Bu_4N^+ salts provided the results illustrated in **Figure 4.5** with the corresponding rate constants listed in **Table 4.1**.

Since the common PPN^+ salts of chloride and azide provide similar rates of initiation of polymerization, we have elected to use the azide anion in our comprehensive studies because of its strong ν_{N_3} absorption band in the infrared. For these investigations we have synthesized a series of polyesters employing the combination of anhydride and epoxide monomers listed in **Figure 4.2**. The appropriate monomers were dissolved in toluene and heated at 80 ^oC in the presence of (salen)CrCl and one equivalent of $PPNN_3$. The resultant polyesters were characterized by infrared spectroscopy, ^1H NMR spectroscopy, differential scanning calorimetry (DSC), and selected samples were subjected to molecular weight analysis by gel permeation chromatography. Infrared analysis of the purified polyester confirmed the location of the ν_{co} stretching frequency at 1738 cm^{-1} for all of the polyesters described herein. The $\nu_{c=o}$ vibration is significantly different from that of the cyclic anhydrides, located at approximately 1770 cm^{-1}, which allows for the monitoring of polyester formation *via in situ* ATR-FTIR analysis. The ^1H NMR spectra of the polyesters displayed chemical shifts in the 4-6 ppm range indicative of hydrogens bound to the carbons alpha to the ester group, both from the anhydride and epoxide units (**Figure 4.6**). Furthermore, analysis of the ^1H NMR spectra revealed that the copolymerization of epoxide and anhydride takes place in an almost exclusive (>99 %) alternating fashion.

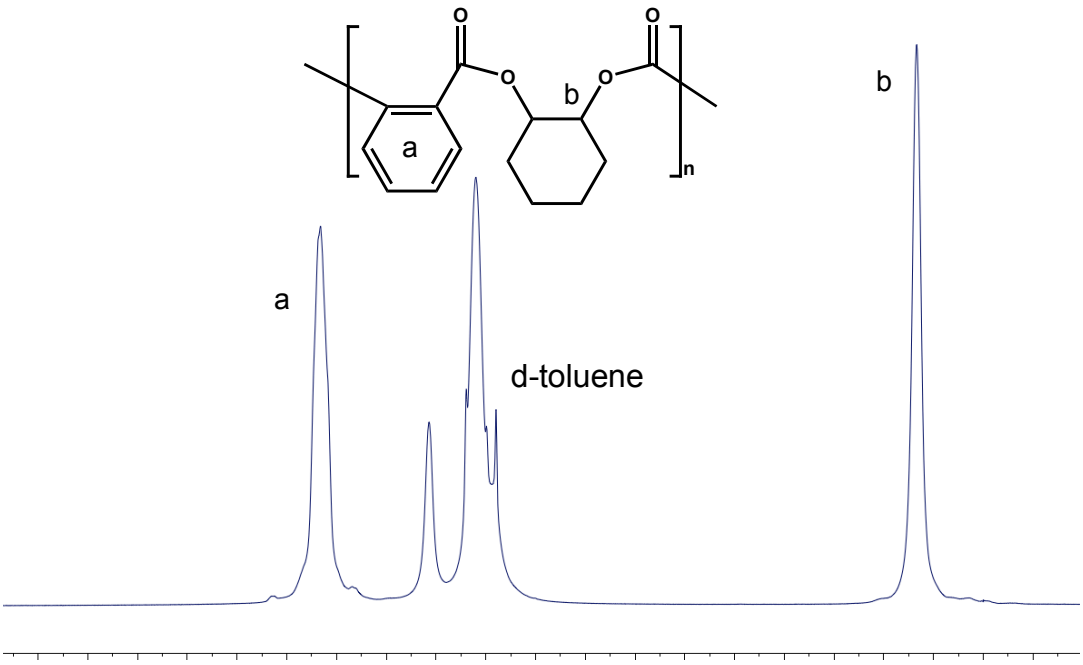

Figure 4.6. ^{1}H NMR Spectrum of PACHO. (a) PA phenyl appears at 7.65 ppm. (b) H adjacent to ester functionality in CHO appears at 5.25 ppm.

Kinetic Studies. The suggested reaction pathways for the formation of alternating copolymers from epoxides and anhydrides are summarized in **Figure 4.2**. As indicated, the rate of epoxide and CO_2 coupling to provide polycarbonates is slow relative to polyester formation (*vide infra*). This latter observation provides a one-step production of diblock copolymers of polyesters and polycarbonates as previously demonstrated by Coates and coworkers employing β-diiminate zinc catalysts,[44] and Duchateau and coworkers employing (salophen)CrCl/DMAP as catalyst (**Figure 4.7**).[61] The rate of the alkoxide anion reacting with an anhydride monomer (k_2) is generally much faster than a carboxylate anion ring-opening an epoxide (k_3), hence the latter

process is rate-determining. At constant initiator concentration, the copolymerization is first-order with respect to the epoxide monomer (**Figure 4.8**) and to the initiator at equimolar ratios of monomers. An increase in the cyclic anhydride concentration by 50% lead to only a slight change in reaction rate.

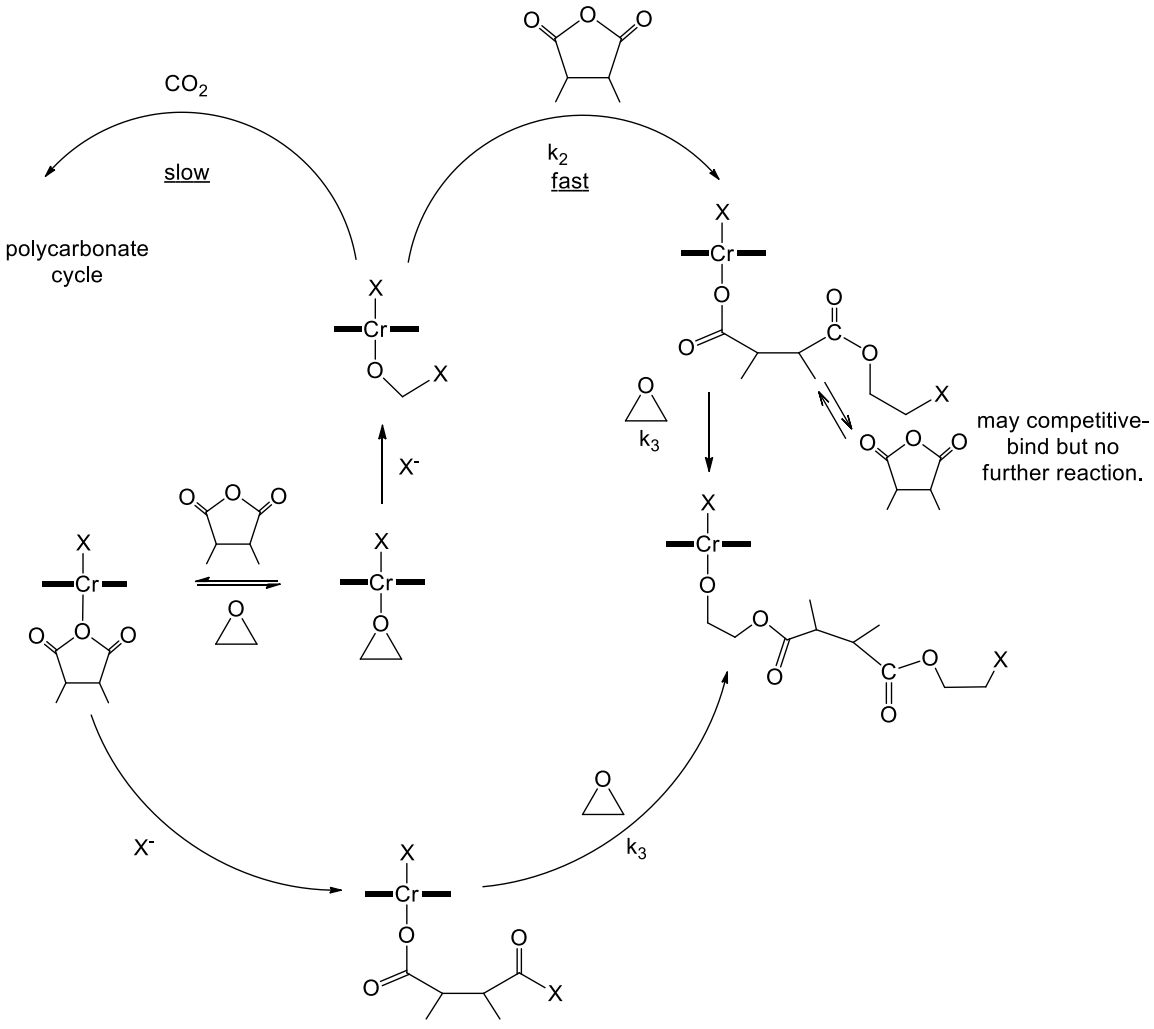

Figure 4.7. Scheme describing competitive incorporation of CO_2/anhydride into polyester-block-polycarbonate

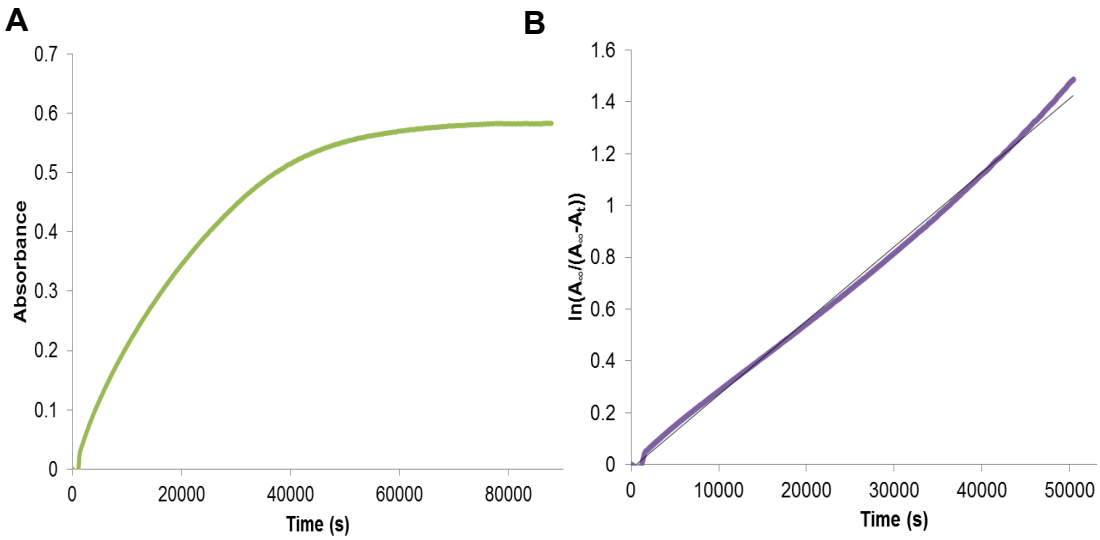

Figure 4.8. Copolymerization of equimolar quantities of cyclohexene oxide and phthalic anhydride in the presence of 4.05 mM (salen)CrCl and one equivalent of $PPNN_3$ in 2.5 mL of toluene at 80 °C. **A**. Absorbance of the growth of the 1738 cm^{-1} band of the polyester *vs* time. **B**. Plot of $\ln(A_\infty/A_\infty - A_t)$ *vs* time.

The copolymerization reactions of equimolar quantities of phthalic anhydride and cyclohexene oxide at a constant catalyst concentration were monitored by *in situ* infrared spectroscopy over a temperature range of 40 °C. **Table 4.2** lists the rate constants obtained from the linear plots in **Figure 4.9** as a function of temperature, with an Eyring plot of these data shown in **Figure 4.10**. The $\Delta H^{\neq}$ and $\Delta S^{\neq}$ values derived from **Figure 4.10** for the copolymerization of PA and CHO were determined to be 67.5 kJ/mol and -95.3 J/mol, respectively, with $\Delta G^{\neq}$ being 101 kJ/mol at 80 °C.

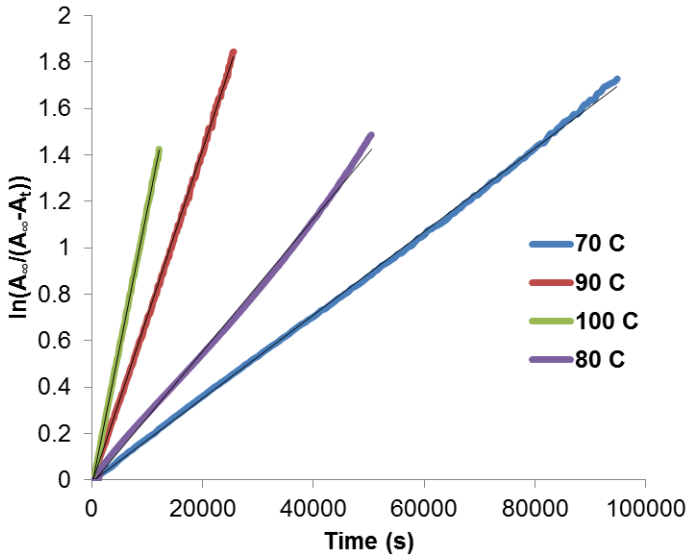

Figure 4.9. First-order plots for the copolymerization of PA and CHO as a function of temperature.

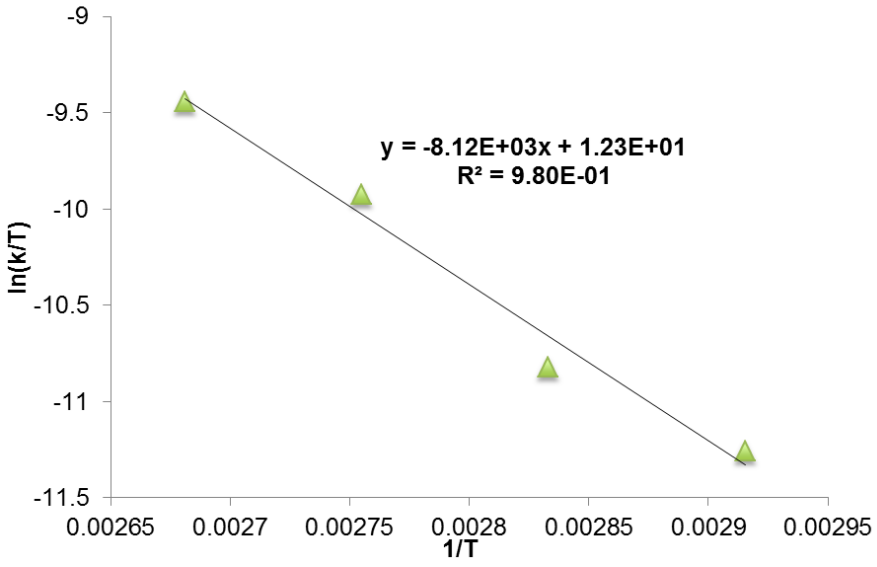

Figure 4.10. Eyring plot of the PA and CHO copolymerization reaction, with $R^2 = 0.980$.

Table 4.2. Temperature Dependent Rate Constants for the Copolymerization of PA and CHO.[a] [a]Reaction conditions: (salen)CrCl/$PPNN_3$/PA/CHO = 1:1:200:200, where the [(salen)CrCl] = 4.05 x 10^{-3} M in toluene solution. [b]Determined by GPC in tetrahydrofuran using monodisperse polystyrene standards.

Temperature (^{o}C)	k_3 x 10^3 M^{-1}-sec^{-1}	Mn (PDI)[b]
70.0	4.42	13,000 (1.12)
80.0	7.06	--------
90.0	17.8	18,000 (1.13)
100.0	29.6	17,000 (1.12)

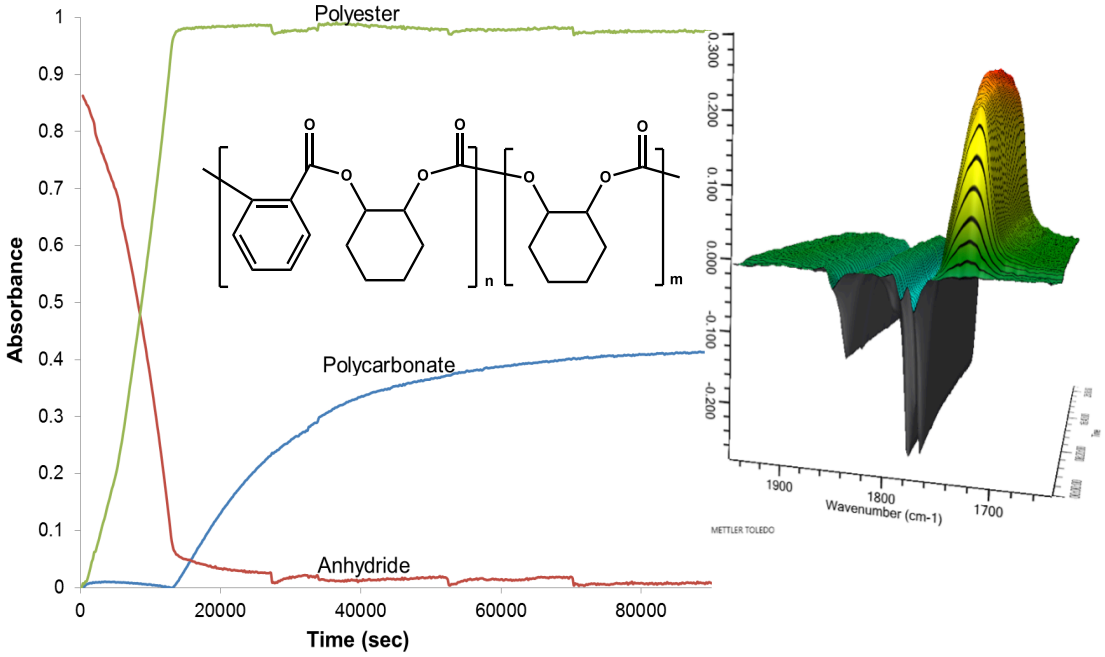

Figure 4.11. *In situ* FTIR analysis of block copolymerization process. Reaction conditions used were (salen)CrCl/PPNCl/PA/CHO = 1:3:200:200 under 500 psi CO_2, 80^{o}C with 19 mL toluene (solvent, volume totaling 25 mL). Deconvolution was performed by ReactIR ic10 software. Green line = polyester growth (1738 cm^{-1}, red line = anhydride consumption (1770 cm^{-1}), and blue line = polycarbonate growth (1750 cm^{-1}). The three-dimensional surface of the reaction is shown in the insert on the right.

Consistent with earlier studies by Coates and coworkers employing β-diiminate zinc catalysts, the terpolymerization of cyclohexene oxide, phthalic anhydride, and CO_2 catalyzed by (salen)CrCl and $PPNN_3$ afforded in a one pot synthesis a diblock copolymer of polyester and polycarbonate (**Figure 4.11**).[61] As noted in **Figure 4.12** this observation requires that the route governed by k_2 to be much faster that the pathway proceeding *via* CO_2 insertion and subsequent polycarbonate formation. This has been interpreted as resulting from a slower rate of CO_2 insertion *vs* cyclic anhydride into the metal alkoxide intermediate.[44] Alternatively, since CO_2 insertion into metal-alkoxides is highly reversible and generally thought to be non-rate-limiting, this behavior may be the result of a much slower ring-opening step of the metal-carbonate intermediate with the epoxide monomer, a process driven by k_4 in **Figure 4.12**.[62] Differential scanning calorimetry analysis of the resulting polymer revealed it to be a well-defined copolymer with two distinct T_g values (70 ^oC for PA/CHO and 115 ^oC PCHC).

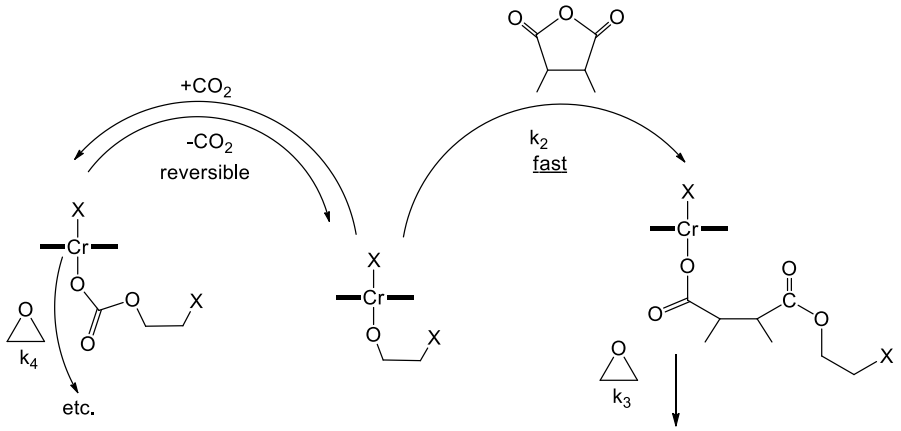

Figure 4.12. Scheme describing competitive CO_2/anhydride incorporation into polyester-block-polycarbonate

The reaction rates for the copolymerization of cyclohexene oxide with various cyclic anhydrides observed under similar reaction conditions provided relative reactivities of CHA > PA > CHE. Additionally, employing the CHA monomer while varying the epoxide under identical reaction conditions afforded a reactivity trend of PO > CHO ≳ SO (**Figure 4.13**). However, the cyclic ether, oxetane, was essentially unreactive under these reaction conditions.

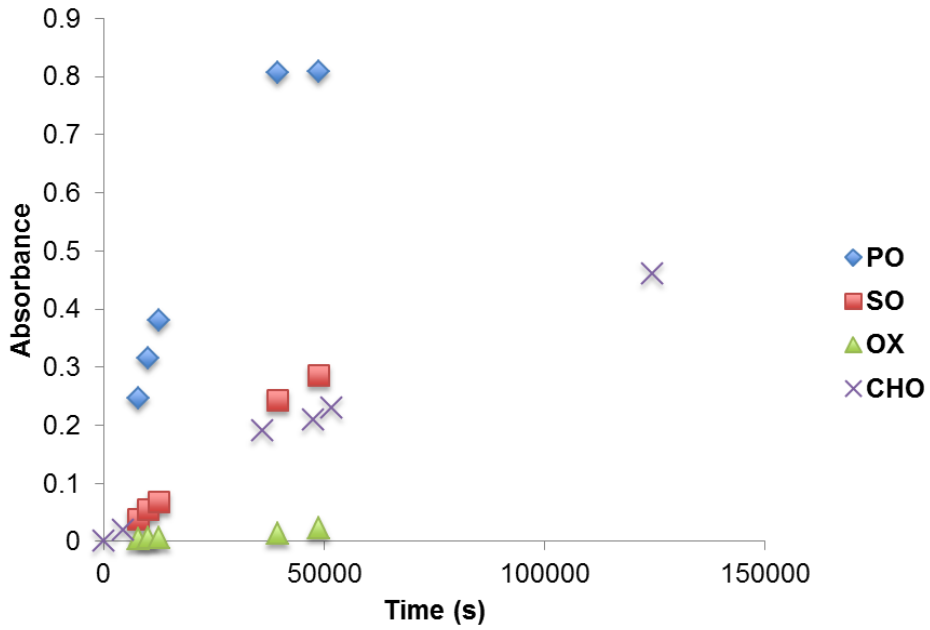

Figure 4.13. Comparison of Epoxides: Polymer growth vs. time – Reactions were performed in sealed NMR tubes using 2.0 mL d_8 toluene as solvent. 200 eq appropriate epoxide was added to tube, then was dissolved in a stock solution of 1.8 mL d_8 toluene, 300 mg CHA (200 eq), 6.3 mg (salen)CrCl (1 eq), and 5.7 mg $PPNN_3$ (1 eq). The tubes were then heated to 80°C and allowed to react until 100% conversion was achieved.

Thermal Properties of Copolymers. The glass transition temperatures of the various polyesters synthesized from the monomers listed in **Figure 4.2** utilizing a (salen)CrCl/$PPNN_3$ catalyst system in toluene at 80 ^oC were determined by differential scanning calorimetry (DSC) analysis. These data, along with the corresponding molecular weight data for selected copolymers obtained from GPC measurements, are summarized in **Table 4.3**. As anticipated, the steric bulk of the pendant groups and rigidity of the monomeric structure have a direct effect on the T_g of the resultant polyester. That is, in general the T_g values increased with epoxides in the order CHO > SO > PO, and increased with cyclic anhydrides in the order CHE > PA $\gtrsim$ CHA > MA > SA. Specifically, the glass transition temperature found for the polyesters formed from propylene oxide and CHE, PA, MA, and SA were 28, 45, -23, and -45 ^oC, respectively.

Table 4.3. GPC and DSC data for selected polyesters. [a]Sample was synthesized using both $PPNN_3$ and (salen)CrCl. [b]Sample was synthesized using only PPNCl as initiator.

Polyester (cyclic anhydride/epoxide)	M_n (x 10^{-3})	M_w (x 10^{-3})	PDI	T_g (^oC)
CHE/CHO	10	14	1.34	91
CHA/CHO	9.2	9.7	1.06	79
CHE/SO	5.7	6.5	1.14	53
MA/CHO	8.5	20	2.3	50
PA/SO	19	24	1.27	54
CHA/SO	-	-	-	32
PA/CHO[a]	18	20	1.13	70
PA/CHO[b]	14	15	1.07	-

Similarly, the copolymer provided by the alternative coupling of SA with CHO or SO displayed corresponding T_g values of 35 and 1.5 ^oC.

The range of T_g values achievable from the alternating ring-opening copolymerization of epoxides and cyclic anhydrides is over 130 ^oC, with a high T_g of 90 ^oC for the copolymer from CHE and CHO and a low T_g of -45 ^oC for that produced from SA and PO. Furthermore, it has been shown that only a small percentage of cross linking can drastically increase the T_g of resultant polyesters. In this regard, we have observed two vastly different T_g parameters (-23 and 28 ^oC) for maleic anhydride/propylene oxide copolymer samples obtained from very similar synthetic procedures.

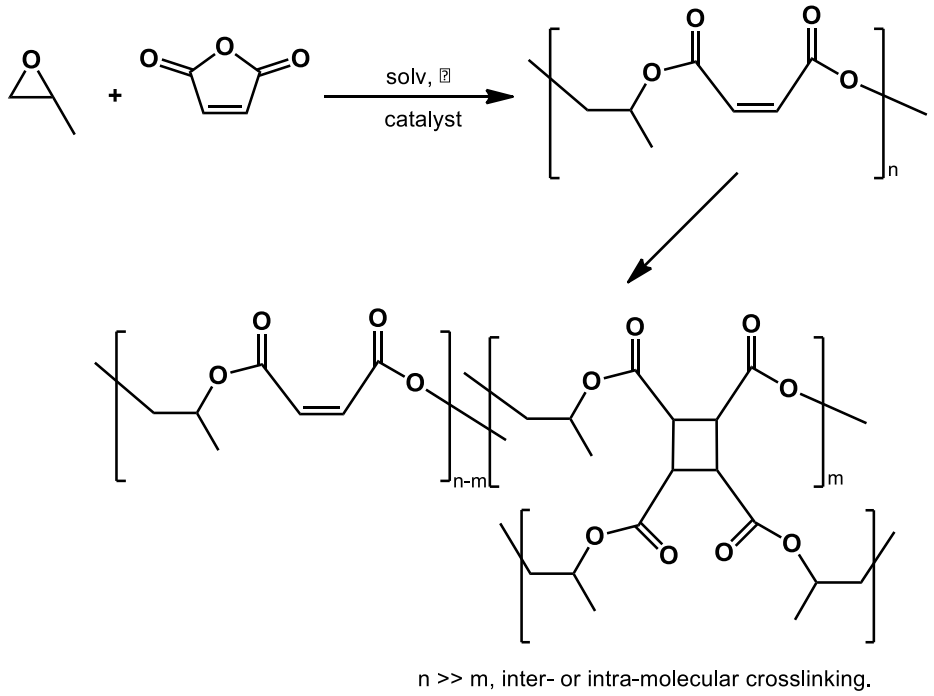

Figure 4.14. Scheme describing potential photochemical crosslinking mechanism of MAPO polymer

We speculate here that this is due to a spontaneous photodimerization reaction as indicated in **Figure 4.14**. Consistent with the suggestions is the observation that copolymer from MA and epoxides have the broadest polydispersity indices (~2.3) of all polyester synthesized in this report. That is, the other polyester synthesized displayed narrow polydispersity indices (< 1.30) with M_w values of about 10,000 or greater.

Future Work

Further studies of the copolymerization of cyclic anhydrides with epoxides will focus on several topics: the kinetic study of metal-free anion-initiated polymerization, discovery of new monomers, and incorporation of bifunctional monomers for use as crosslinkers.

As shown in this study, the reaction of epoxide and anhydride to produce polyester proceeds in the absence of a single-site metal catalyst, albeit more slowly. The anion-initiated process is interesting for industrial applications because the removal of metal catalyst is typically a concern for polymers produced using catalysts. Additionally, the narrow molecular weight distributions obtained using the anion-initiated process indicates that it proceeds by a chain-growth mechanism. Although it is clear that the metal need not be present for the reaction to occur, it does participate when present, as evidenced by the selective incorporation of anhydride prior to CO_2 in the polyester-block-polycarbonate reactions. At this point it is still unclear as to precisely what factors influence the reactivity of the co-monomers with respect to anions and

transition metal complexes, but further kinetic studies should elucidate aspects of the mechanism.

Although several anhydride monomers have been reported in this study, only three epoxides were studied extensively. Preliminary studies have been performed utilizing epoxides such as limonene oxide and glycidol, both of which have proven to be active. As mentioned previously, the incorporation of limonene oxide represents the potential to synthesize a polyester composed of 100% renewable resources by mass. Glycidol, due to its pendant alcohol group, is a desirable monomer due to potential biomedical applications of any resultant polymer. Interestingly, the alcohol group, which would render glycidol totally unreactive for the CO_2/epoxide copolymerization reaction, has little to no effect on the anhydride/epoxide copolymerization process. Additionally, initial samples of the glycidol/CHO polymer have proven to be at least partially water-soluble.

The potential use of bifunctional monomers has been discussed previously in Chapter III. In an analogous reaction, it is possible to use either a bifunctional anhydride, such as pyromellitic dianhydride, or a bifunctional epoxide, once again such as 1,3-butylenediepoxide or bisphenol-A diglycidyl ether to produce one pot crosslinked polyesters.

Conclusions

Herein, we have reported kinetic studies of the alternating ring-opening copolymerization of various epoxides with cyclic acid anhydrides to afford polyesters of

high molecular weights and narrow molecular weight distributions using a (salen)CrCl catalyst in the presence of onium salts. The activation parameters for the process involving phthalic anhydride/cyclohexene oxide monomers in toluene solution were determined to be $\Delta H^{\neq} = 67.5$ kJ-mol^{-1} and $\Delta S^{\neq} = -95.3$ J-mol^{-1}, where the rate determining step was ring-opening of the epoxide by the enchained anhydride. For a given cyclic anhydride, cyclohexane anhydride, the relative rate of coupling with epoxide decreased in the order PO > CHO $\gtrsim$ SO, whereas, for cyclohexene oxide the relative reactivity order with anhydrides was CHA > PA > CHE. This catalytic system was also shown to terpolymerize epoxide/cyclic anhydride/CO_2 to afford diblock copolymers with very little tapering, thereby providing a one-step synthesis of poly(ester-*co*-carbonate). In the polyester product resulting from the ring-opening polymerization of maleic anhydride and propylene oxide two vastly different T_gs were observed at -23 and 28 ^{o}C. We have proposed the higher T_g value to be the result of some degree of cross-linking by photoinduced dimerization. Further efforts are being directed at providing a more definitive assessment of this possibility.

V. QUANTIFYING THE ENERGY BARRIERS OF THE RING SLIP OF 2,5-DIMETHYLPYRROLE MANGANESE CARBONYL COMPLEXES*

Introduction to Collaboration with Texas A&M Qatar

The latter chapters of this dissertation were studies performed in collaboration with the laboratories of Dr. Ashfaq Bengali of Texas A&M Qatar. Dr. Bengali and the laboratories of Dr. Darensbourg have collaborated, at this point, for nearly five years with the research having resulted in multiple peer reviewed publications in ACS journals. The collaboration, which continues to be funded by the Qatar Research Foundation, has provided multiple students from the Darensbourg laboratories, myself included, the opportunity to travel to Doha, Qatar to perform studies using the instrumental setup described in the introduction of this dissertation. Many thanks are due to Dr. Bengali and the rest of Texas A&M Qatar for their graciousness and the opportunities afforded to our research program.

This research was primarily the project of Dr. Bert Swennenhuis, a postdoctoral research formerly employed by Dr. Bengali. My role in the collaboration was primarily to perform some of the "slower" FT-IR observations, to synthesize starting materials for use by the Bengali labs, and to perform structural characterization of various complexes *via* X-ray crystallography.

Introduction

The mechanism of ligand substitution reactions from transition metal containing organometallic complexes remains an important area of research.[128,72,129] The primary motivation for these studies comes from the ability of such complexes to promote both stoichiometric and catalytic transformations of organic compounds.[130] Most often, the active metal containing species is generated by ligand loss from a precursor complex followed by binding of a substrate molecule. Fundamental information regarding the energetics and mechanism of ligand substitution is therefore desirable. Ligand substitution from metal complexes containing the η^5-cyclopentadienyl (Cp) ligand is of particular interest since highly reactive reduced hapticity complexes can be generated as intermediates in the reactions.[68,131] The incoming ligand can then occupy the resulting open coordination site on the metal thereby providing a low energy pathway for the substitution reaction. For example, the associative substitution of a CO ligand from $CpM(CO)_2$ [M = Co, Rh, Ir] is thought to occur by way of a "ring slipped" intermediate formed by an η^5-η^3 haptotropic shift of the Cp ligand.[74] The ring slip mechanism was supported by observation of the unusually high associative lability of the (η^5-Indenyl)$Rh(CO)_2$ complex.[73] The traditional explanation for this high reactivity was attributed to the "indenyl effect" whereby the η^3 indenyl intermediate is stabilized by the rearomatization of the benzene ring (**Figure 5.1**). Recent theoretical studies have provided an alternate explanation for this effect.[132,77] These calculations have suggested that the origin of the indenyl effect is based on both the weaker η^5 binding of the indenyl ligand to the metal center and to a lower energy for the η^3 intermediate relative to Cp.

More pertinent to the current study, other systems also appear to exhibit this type of rate enhancement. For example, while $CpMn(CO)_3$ is thermally inert to CO substitution, its N-heterocycle analogue (η^5-C_4H_4N)$Mn(CO)_3$ reacts readily with phosphines and phosphites to form (η^5-C_4H_4N)$Mn(CO)_2(PR_3)$ complexes.[133,76,75] The pyrrole complex was estimated to react almost 10^8 times faster than the cyclopentadienyl analogue.[76] Basolo and co-workers convincingly established that CO displacement from the pyrrole complex proceeded by an associative mechanism by way of the 18 electron (η^3-C_4H_4N)$Mn(CO)_3(PR_3)$ ring slip intermediate. Because of the presence of the electron withdrawing nitrogen atom, the η^3 intermediate was proposed to be more energetically accessible than the equivalent carbocyclic complex. Furthermore, by employing substituted N-heterocycles such as 2,5 dimethyl- and 3,4 dimethyl pyrrole, it was established that in the pyrrole system, the nitrogen atom was contained within the allylic system of the η^3 intermediate.[76,75] We were interested in determining whether such mechanistic generalizations for the N-heterocyclic relative to the carbocyclic systems could be made in the displacement of ligands that, unlike CO, are weakly coordinated to transition metal centers. For example, would substitution of Solv from (η^5-C_4H_4N)$Mn(CO)_2$(Solv) also demonstrate rate enhancement relative to $CpMn(CO)_2$(solv) when Solv is a weakly coordinated solvent or solute present in large excess (**Figure 5.2**)?

Addressing this issue is important since ring slipped or lower hapticity organometallic intermediates are often invoked in catalytic and stoichiometric reactions.[131,134,135,136,137,138,139,140,141] In several such homogeneous reactions, the solvent

is weakly coordinated to the metal center, and establishing the possible accessibility of a ring slipped intermediate in the displacement of the solvent is important.[142]

We report in this paper a comparison between the reactivity of the (η^5-DMP)$Mn(CO)_2$(Solv) [DMP = 2,5 dimethylpyrrole] and $CpMn(CO)_2$(Solv) complexes [Solv = cyclohexane (CyH), η^2-benzene (Bz), 1-bromohexane (Br-hex), tetrahydrofuran (THF), and η^2-cyclooctene]. These solvents were chosen because of their different binding strengths to the Mn center, spanning a range from ~8 to 34 kcal/mol.[143,144,145,71,146,147] Furthermore, comparison of the reactivity differences between the N-heterocyclic and carbocyclic systems is facilitated since the displacement of these solvents from $CpMn(CO)_2$ has already been investigated. Given the large range of reaction time scales, a variety of time-resolved infrared techniques were employed to include step-scan, rapid-scan FTIR, and laser flash photolysis. In addition, DFT calculations were performed on all the complexes to lend support for the experimental findings. Surprisingly, unlike the displacement of CO from the related complexes, rate enhancement was not observed in the case of relatively weakly coordinated ligands. However, both associative (ring slip) and dissociative channels are predicted to contribute to the displacement of the stronger 2 bound cyclooctene from the (η^5-DMP)$Mn(CO)_2$ fragment.

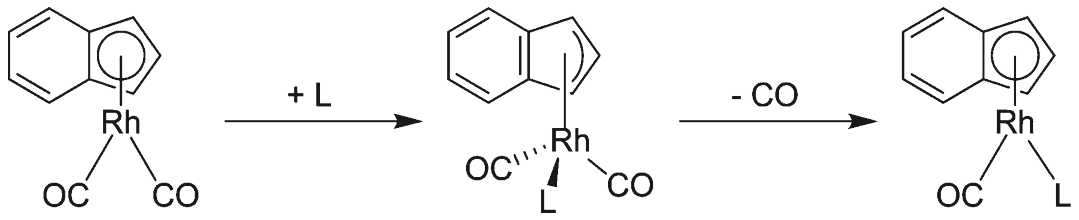

Figure 5.1. Proposed ring-slip mechanism for ligand substitution in (indenyl)Rh complex.

Experimental and Theoretical Methods

Kinetic experiments were performed using a Bruker Vertex 80 FTIR with step-scan and rapid-scan capabilities. Sample photolysis was conducted using the third harmonic (355 nm) of a Continuum Surelite I-10 Nd:YAG laser operating at 1 Hz. A syringe pump was used to flow solution through a temperature controlled 0.5 mm path length IR cell with CaF_2 windows (Harrick Scientific) to ensure that a fresh solution was photolyzed with every shot of the laser. The temperature was monitored by a thermocouple located close to the photolysis solution and maintained by a water circulator to within (0.1^{o} C. All spectra were obtained at 8 cm^{-1} resolution.

Some experiments were conducted using a flash photolysis apparatus employing infrared detection. The temporal profile of the photogenerated intermediates were probed with infrared light from a water cooled CO probe laser (1600-1920 cm^{-1}). The infrared output was attenuated by absorptive filters (OD = 2.5) prior to merging with the UV photolysis beam. The colinear IR/UV beams were passed through the sample cell following which the UV was split from the IR beam which was detected with a liquid

nitrogen cooled MCT detector. The signal was sent to a 1 GHz digital storage oscilloscope for processing.

The photolysis solutions were 3-4 mM in the Mn complex in cyclohexane solvent. To this solution, either benzene, 1-bromohexane or THF was added to yield a 1.12 M, 2.85 and 3.08 M solution in these solvents, respectively. The appro- priate amount of incoming ligand, either THF, 2,6-lutidine, or cyclooctene was added prior to photolysis. The reaction rates were studied over a 30 K temperature range.

Longer time scale kinetic experiments involving the Mn-(η^2-cyclooctene) complexes were conducted by photolyzing an 11.0 mL solution of the parent tricarbonyl (4 mM) in n-heptane solvent in the presence of 0.70 M cyclooctene under Ar. To the resulting solution containing the Mn-(η^2-cyclooctene) complex the appropriate amounts of 2-picoline and n-heptane were added, and the solution was heated to the required temperature (358 K). IR spectra were subsequently obtained at known time intervals.

All experiments were conducted under pseudo first order conditions. Observed rate constants (k_{obs}) were determined from a first order fit to the absorbance versus time profile of either the reactant or the product complexes. Activation parameters were calculated from the temperature dependence of the second order rate constants obtained from the k_{obs} versus [L] plots. Errors in the kinetic parameters were obtained from linear fits to the data as reported by the data analysis program Kaleidagraph.

The(η^5-DMP)$Mn(CO)_3$and$CpMn(CO)_2$(η^2-cyclooctene) complexes were synthesized according to literature procedures. The $CpMn(CO)_2$(η^2-cyclooctene) complex

had a small amount of parent tricarbonyl present, and since this complex is thermally unreactive the product was not purified further. The DMP complex was relatively unstable in solution at room temperature and was therefore synthesized, isolated as a yellow oil, dissolved in cyclohexane, and the resulting solution frozen. The frozen solutions were stable for several weeks. All solvents and reagents were anhydrous grade and of >99% purity (Aldrich) and used as received. 2-Picoline was freshly distilled under a nitrogen atmosphere, and cyclooctene was filtered over neutral alumina prior to use.

The structure, stabilities, and vibrational frequencies of all ground state, transition state, and intermediate complexes were studied using the Gaussian 03 program employing the B3LYP functional.[148,149] The transition metal, C, N, H, Br, and O atoms were described by the 6-31G* basis set. Bond dissociation enthalpies (BDEs) were calculated as the difference in enthalpy between the product $XMn(CO)_2$(Solv) and the reactant $XMn(CO)_2$ Solv enthalpies [X = η^5-DMP and Cp]. Transition state structures were modeled based on the studies of Veiros and were confirmed by frequency calculations which showed only one imaginary frequency along the reaction coordinate.[132,77]

Results and Discussion

As in the case of the analogous $CpMn(CO)_3$ system[23-28], photolysis of (η^5-DMP)$Mn(CO)_3$ in the presence of solvent yields the appropriate solvated species, (η^5-DMP)$Mn(CO)_2$-(Solv). For example, as shown in **Figure 5.3**, the (η^5-DMP)Mn-

$(CO)_2$(THF) complex with CO stretching absorbances at 1935 and 1864 cm^{-1} is formed upon photolysis of (η^5-DMP)- $Mn(CO)_3$ in the presence of THF.

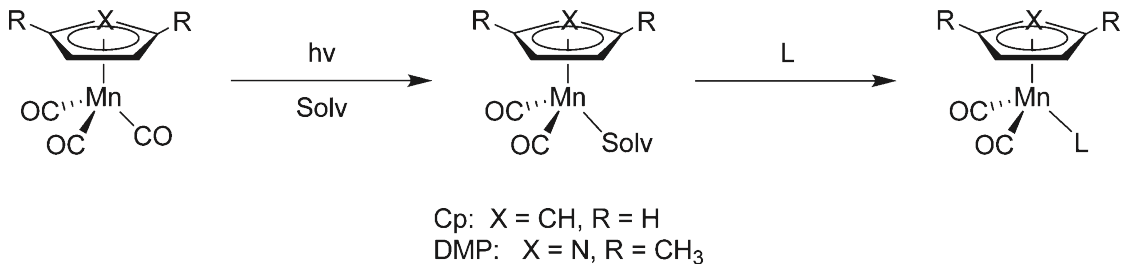

Figure 5.2. Scheme of photolytic CO removal, subsequent solvent replacement, and solvent displacement by the incoming ligand, L.

From the change in the intensity of the parent CO bands upon photolysis, the conversion to the solvate complex is estimated to be 20%. As shown in **Table 5.1**, for all solvates studied, the CO stretching frequencies are similar for the DMP and Cp complexes suggesting that the electron density on the Mn center is not significantly affected when the carbocyclic Cp ligand is replaced with DMP. The electron-withdrawing tendency of the nitrogen atom is likely offset by the inductive effect of the CH_3 groups resulting in similar donor characteristics for the DMP and Cp ligands.

The reaction of (η^5-DMP)$Mn(CO)_2$(Solv) with ligand L, shown in **Figure 5.4** in the case of Solv = 1-bromohexane and L = 2,6-lutidine, results in the displacement of the weakly bound solvent molecule to form the (η^5-DMP)$Mn(CO)_2$L complex. All substitution reactions studied displayed a linear relationship between k_{obs} and [L], as

illustrated by the displacement of CyH from (η^5-DMP)Mn(CO)$_2$(CyH) by THF shown in **Figure 5.5**. The linear behavior of k_{obs} as a function of [L] does not assist in the assignment of a displacement mechanism since it is consistent with either a dissociative, associative, or interchange pathway.[150]

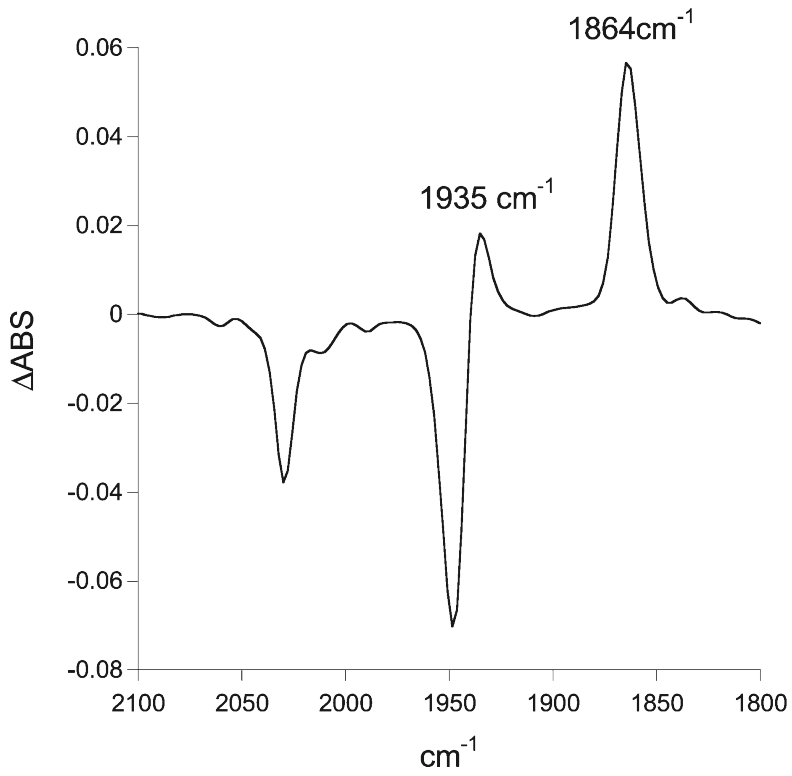

Figure 5.3. Difference spectra obtained upon photolysis of a cyclohexane solution of (η^5-DMP)Mn(CO)3 in the presence of THF at 293 K. The positivepeaksareduetotheformationofthe(η^5-DMP)Mn(CO)$_2$(THF) complex, and the negative peaks are associated with depletion of parent upon photolysis.

However, as discussed below, the agreement between the activation parameters and the calculated Mn-Solv binding strengths supports a dissociative or I_d mechanism of solvent substitution in all cases.

Unlike what is observed in the Cp system, the kobs versus [L] plots for DMP display significant non-zero intercepts. Experiments performed in the absence of incoming ligand (i.e., [L] = 0) confirmed that the non-zero intercepts are primarily due to the decomposition of the (η^5-DMP)Mn-$(CO)_2$(Solv) complex by an undetermined pathway.

Table 5.1. CO Stretching Frequencies for the $XMn(CO)_2$(Solv) [X = η^5-DMP or Cp] Complexes in Cyclohexane Solvent at 298 K. In some cases the position of only one band is listed since the remaining band is obscured by the CO absorbance of the parent tricarbonyl.

solv	Nu_{CO} DMP (cm^{-1})	$Nu_{CO,}$ Cp (cm^{-1})
Cyclohexane	1893	1958, 1891
Benzene	1898	1955, 1893
1-bromohexane	1882	1876
tetrahydrofuran	1935, 1864	1931, 1860
cyclooctene	1962, 1902	1959, 1897

For example, at 293 K in the absence of incoming ligand, the (η^5-DMP)$Mn(CO)_2$(CyH) complex exhibited a single exponential decay with k_{obs} = 1.3 x 10^5 s^{-1} similar to an intercept of 1.9 x 10^5 s^{-1} obtained at this temperature (**Figure 5.5**). By contrast, the intercept for the Cp system is smaller by a factor of 4.

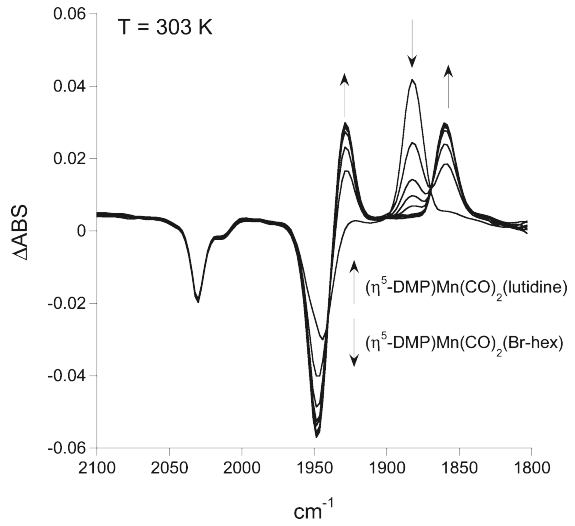

Figure 5.4. Reaction of the initially formed (η^5-DMP)Mn(CO)$_2$(Br-hex) complex with 2,6-lutidine in cyclohexane at 303 K. Photolysis was conducted in the presence of [1-bromohexane] = 2.85 M and [2,6-lutidine] = 0.43 M in cyclohexene solution. Spectra were obtained at 600 ms intervals. The CO band at 1950 cm^{-1} is a composite of the E vibrational mode of the parent tricarbonyl and the A_1 mode of the Br-hex solvate.

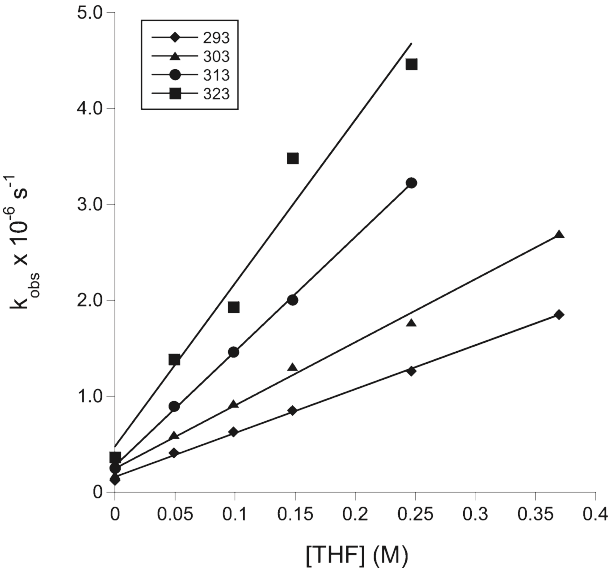

Figure 5.5. Plot of k_{obs} versus [THF] for the reaction of (η^5-DMP)Mn(CO)$_2$(CyH) with THF in cyclohexane at several temperatures.

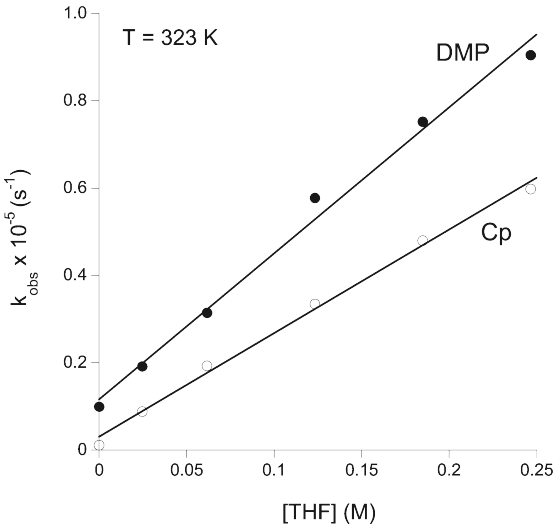

Figure 5.6. Plot of kobs versus [THF] for the reaction of $XMn(CO)_2(\eta^2\text{-Bz})$ [X = η^5-DMP, Cp] with THF at 323 K in cyclohexane solvent. The similar slope for the two plots suggests the lack of a significant rate enhancement upon replacement of Cp with the DMP ligand. The intercept for the DMP system is larger than for Cp although, as explained in the text, this does not imply a different displacement mechanism.

The larger background decay rate constants for the DMP complexes are probably due to the fact that the η^5 coordinated DMP ligand in the parent tricarbonyl can also act as a nucleophile toward the $(\eta^5\text{-DMP})Mn(CO)_2(Solv)$ complex.[151] Similar non-zero intercepts were also observed previously for the displacement of CO by $P(OEt)_3$ from the $(\eta^5\text{-DMP})Mn(CO)_3$ complex.[75] Alternatively, the solvent adduct can react with the parent complex, yielding a dinuclear species with a bridging CO group, as was observed by Poliakoff et al. for $CpMn(CO)_3$.[152] Also, as noted earlier, $(\eta^5\text{-DMP})Mn(CO)_3$ is inherently more unstable than the analogous carbocyclic complex resulting in a larger background decay rate. On the basis of the data, it is reasonable to conclude that the non-zero intercepts are not due to a parallel solvent displacement pathway.

As shown in **Figure 5.6** and in **Table 5.2**, for all the systems studied, the second order rate constants obtained from the slopes of the k_{obs} versus [L] plots are within a factor of 10 for the DMP and Cp systems with very similar activation parameters. These results are in dramatic contrast to the large enhancement in CO substitution rates observed upon replacement of Cp with pyrrole or DMP as the π cyclic ligand.[11-13] Since thermal displacement of CO from CpMn(CO)3 is not observed, the rate enhancement cannot be quantified. However, given the fact that CO substitution occurs within hours from the DMP complex at elevated temperatures while in the case of $CpMn(CO)_3$ no substitution occurs for days, the rate enhancement is significant. In early studies, Basolo estimates a 10^6-10^8 fold rate enhancement.[153] As shown in **Table 5.2**, theoretical calculations demonstrate that the Mn- Solv binding strength is unaffected by replacement of the Cp carbocycle with the heterocyclic DMP ligand. Since previous studies have shown that displacement of solvent by an incoming ligand follows either a dissociative or an I_d pathway for many $CpMn(CO)_2(Solv)$ complexes,[23-28] the almost identical activation parameters and calculated Mn-Solv binding strengths indicate a similar substitution mechanism for the DMP system. The data therefore point to a lack of $\eta^5 - \eta^3$ ring slippage in the displacement of solvent from (η^5-DMP)$Mn(CO)_2(Solv)$.

These results are in marked contrast to earlier substitution studies performed by Basolo which provided convincing evidence for an associative $\eta^5 - \eta^3$ haptotropic shift-based ring slip mechanism for the substitution of CO from (η^5-C_4H_4N)$Mn(CO)_3$ and (η^5-DMP)$Mn(CO)_3$.[11-13]

		(η^5-DMP)Mn(CO)$_2$(solv)			CpMn(CO)$_2$(solv)		
Solv/L	**k_{DMP}/k_{Cp}**	**$\Delta H^{\neq}$(kcal/mol)**	**BDE (kcal/mol)**	**$\Delta S^{\neq}$ (e.u.)**	**$\Delta H^{\neq}$ (kcal/mol)**	**BDE[a] (kcal/mol)**	**$\Delta S^{\neq}$ (e.u.)**
CyH/THF	3.7	7.8 ± 0.7	7.4	-1.0 ± 2.0	7.2 ± 0.6[b]	7.6	-6.2 ± 3.5[b]
Bz/THF	1.6	14.9 ± 1.4	13.6	+12.5 ± 4.5	14.8 ± 1.4	11.1	+11.7 ± 5.0
Br-hex/lutidine	0.4	21.1 ± 0.4	24.7	+11.8 ± 1.0	18.3 ± 0.6	24.7	+4.2 ± 1.0
THF/cyclooctene	0.1	22.1 ± 0.5	25.5	+5.5 ± 1.5	23.4 ± 2.0[c]	25.9	+17.7 ± 5.0[c]
CO/P(OEt)$_3$	~ 10^6	26.4 ± 0.8[d]	54.9	-19.4 ± 1.0[d]		55.2	

Table 5.2. Comparison of the kinetic parameters for the DMP and Cp systems.a For a given solvent (Solv) and incoming ligand (L) the slopes of the k_{obs} versus [L] plots were used to determine the ratio, k_{DMP}/k_{Cp}, at 293 K. In all cases the relative rate constants for a given solvate were obtained with the same incoming ligand L. [a] Calculated values. [b] Ref 143. [c] Ref 146 [d] Ref

Their observations indicated that the rate increase for thermal substitution of CO from heterocyclic (η^5-ligand)Mn fragments was greatly increased relative to the analogous carbocyclic Mn complexes. Thus, for example, the observed activation enthalpy of 26.5 kcal/ mol for the displacement of CO from (2,5-DMP)$Mn(CO)_3$ by P(OEt)3 is considerably less than the calculated Mn-CO bond strength of 55 kcal/mol. The primary difference between the CO and the Solv displacement reactions is that the Mn-Solv binding enthalpies ranging from 10 to 25 kcal/mol are considerably weaker than the Mn-CO interaction. Thus, if the transition state for the $\eta^5 - \eta^3$ hapticity shift is higher in energy than the strength of the weak (η^5-DMP)$Mn(CO)_2$-Solv bond, a dissociative pathway will be accessed and rate enhancement relative to the Cp system will not be observed. While $\Delta H^{\neq}$ for a dissociative process should be less than the BDE, the correlation between $\Delta H^{\neq}$ and BDE is always evident. For the (η^5-DMP)$Mn(CO)_3$ complex, the 3 transition state enthalpy is lower than the calculated 55 kcal/mol Mn-CO BDE (vide infra) and therefore rate enhancement is observed.

In an attempt to determine the lower limit of the Mn-Solv binding enthalpy when rate enhancement may be observed, we chose to study the displacement of the more strongly bound cyclooctene ligand from the Cp and DMP complexes. The experimentally determined[147] BDE of 34.9 kcal/mol for the $CpMn(CO)_2$-(η^2-cyclooctene) interaction is intermediate between the calculated value of 52-55 kcal/mol for the Mn-CO BDE when rate enhancement is observed and 24 kcal/mol for the Mn-THF BDE[146] when it is not.

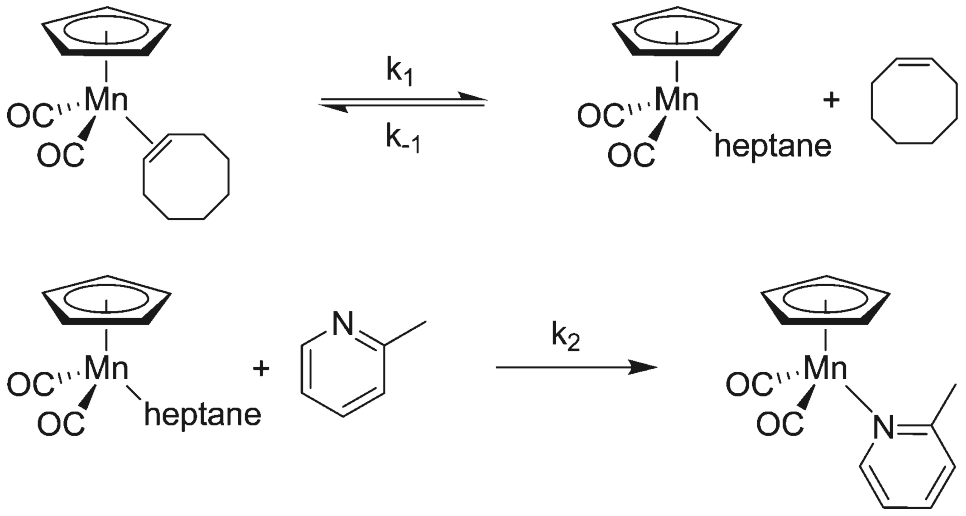

Figure 5.7. Rates describing the displacement of olefin from manganese center by picoline.

The invariance of k_{obs} with ligand concentration in the case of the Cp complex suggests that a dissociative mechanism is operative with the disruption of the $CpMn(CO)_2(\eta^2$-cyclooctene) bond as the rate limiting step (**Figure 5.7**). Unlike the other solvents, important differences in the mechanism of substitution of the η^2 bound cyclooctene ligand from the DMP and Cp systems are observed. As shown in **Figure 5.8**, a plot of k_{obs} versus [2-picoline] is linear for the DMP system while for the carbocyclic analogue, k_{obs} does not vary with [2-picoline]. This observation points to a difference in the mechanism of alkene substitution from the Mn center.

Previous studies by Angelici and Loewen have convincingly demonstrated that displacement of a variety of alkenes, including cyclooctene, from the $CpMn(CO)_2(\eta^2$-alkene) complexes follow a dissociative mechanism.[147]

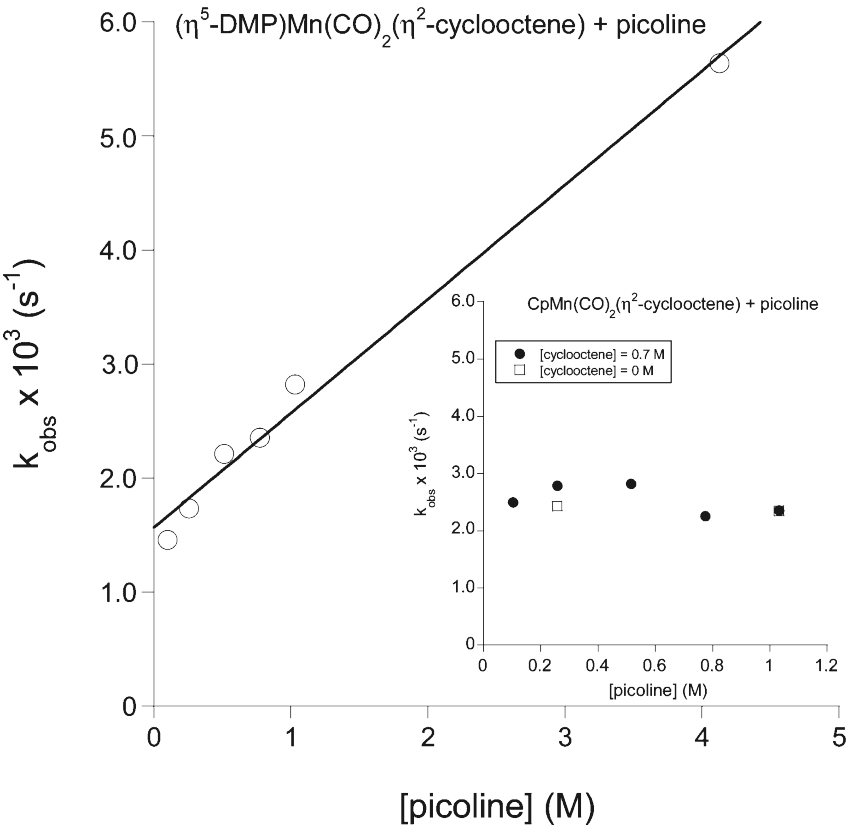

Figure 5.8.Plot of k_{obs} versus [2-picoline] at 358 K for the displacement of cyclooctene from the DMP and Cp complexes by 2-picoline in heptane. Note that while the plot is linear for the DMP system, as shown in the inset, kobs does not vary with [2-picoline] for the Cp complex.

Our results are therefore not surprising. The $CpMn(CO)_2$-(heptane) complex is a likely intermediate since it has been observed previously.[154] Applying the steady state assumption yields,

$$k_{obs} = \frac{k_1}{\frac{k_{-1}}{k_2}\left\{\frac{[\text{cyclooctene}]}{[\text{picoline}]}\right\} + 1}$$

Equation 5.1.

In the current experiments, [cyclooctene]/[2-picoline] was varied from 7 to 0.7. The observed lack of k_{obs} dependence on [2-picoline] can therefore be explained if $k_{-1}/k_2 < 0.1$. Under these conditions, k_{obs} will approach a limiting value of k_1 and will be insensitive to the [2-picoline] as observed. A ratio of 0.1 is not unreasonable since previous studies have demon- strated that the related complex CpMn(CO)2(cyclohexane) reacts with cyclopentene 3-4 times slower than with pyrrolidine, corresponding to a k_{-1}/k_2 ratio of 0.25.[143] Also, the reaction of $CpMn(CO)_2$(heptane) with silanes was found to be as much as nine times slower than with PPh_3 ($k_{-1}/k_2 \sim 0.1$).[155] Thus, the average value of $2.5 \pm 0.3\ 10^{-3}\ s^{-1}$ for k_{obs} at 358 K can be assigned to k_1 in good agreement with a previously reported value of $1.93\ 10^{-3}\ s^{-1}$ at 353 K.[147] To further confirm this interpretation of the kinetic results and to establish the value of k_1 under present experimental conditions, the $CpMn(CO)_2(\eta^2$-cyclooctene) complex was isolated and its reaction with 2-picoline studied with [cyclooctene] = 0 M. According to eq 1, $k_{obs} = k_1$ under these conditions. Values of $2.4\ 10^{-3}\ s^{-1}$ and $2.3\ 10^{-3}\ s^{-1}$ were obtained for k_{obs} with [2-picoline] = 0.25 and 1.0 M, respectively. The agreement between this value of k_1 and that obtained from the in situ experiments in the presence of both cyclooctene and 2-picoline provides confirmation that the invariance of k_{obs} upon

[2-picoline] is due to the saturation of the rate constant under the conditions of the experiment.

In contrast to the Cp system, k_{obs} for the displacement of cyclooctene from the (η^5-DMP)Mn(CO)$_2$ fragment increases linearly with [2-picoline]. The theoretical calculations detailed below (**Table 5.3**) suggest that in the case of Solv = cyclooctene, the enthalpy of the 3 associative transition state is similar to the Mn-(η^2-cyclooctene) binding enthalpy. Thus, it is reasonable to suggest that both associative and dissociative channels are accessible for the substitution of cyclooctene from the DMP complex. The overall reaction mechanism is presented in **Figure 5.9**. Applying the steady state assumption to the intermediate (η^5-DMP)Mn(CO)$_2$(heptane) and (η^3-DMP)Mn(CO)$_2$(η^2-cyclooctene)(2-picoline) complexes, and further assuming that $k_{-1} < k_2$ as discussed for the Cp system, yields the k_{obs} versus [2-picoline] dependence shown in eq 2. Thus, a plot of k_{obs} versus [2-picoline] should be linear with a non-zero intercept yielding k_1, as observed in **Figure 5.5**.

Table 5.3. Calculated enthalpic parameters for the reaction: (η^5-DMP)Mn(CO)$_2$-(solv) + L → (η^5-DMP)Mn(CO)$_2$L. The enthalpy of the associative transition state (η^3-TS) and η^3 intermediate (η^3-I) for two Solv/L combinations along with the Mn-Solv binding enthalpies are presented.

Solv/L	η^3-TS (kcal/mol)	η^3-I (kcal/mol)	Mn-solv BDE (kcal/mol)
THF/C_2H_4	29.2	22	25.5
C_2H_4/pyridine	28.4	-	31.8

As discussed earlier, the kobs versus [L] plots for the DMP systems tend to have non-zero intercepts because of the higher background decay rate of the complexes. However, unlike the other solvents, for Solv = cyclooctene, the background decay rate obtained in the absence of incoming ligand was 16 times less than the intercept of the k_{obs} versus [cyclooctene] plot. This observation suggests that the non-zero intercept is not primarily due to the decomposition of the (η^5-DMP)Mn(CO)$_2$(η^2-cyclooctene) complex, but rather is evidence for the presence of another substitution pathway. Importantly, the k_1 value of $1.6 \pm 0.1\ 10^{-3}\ s^{-1}$ for the DMP system is similar to that of the Cp complex. This agreement is consistent with the expectation that the binding enthalpies of the η^2-cyclooctene solvent are not likely to differ for the two complexes.

The kinetic results for the DMP system are therefore consistent with concurrent associative and dissociative channels for the displacement of η^2 coordinated cyclooctene by 2-picoline. Importantly, while the overall substitution mechanism differs when Cp is replaced with DMP, there is no rate enhancement since the activation enthalpies for the associative and dissociative pathways are similar in the latter case. The data obtained in the current investigation suggests that for the (η^5-DMP)Mn(CO)$_2$(Solv) systems, the transition from a dissociative to associative substitution pathway occurs when the activation barrier approaches 33 kcal/mol, the binding enthalpy of cyclooctene to the Mn center.

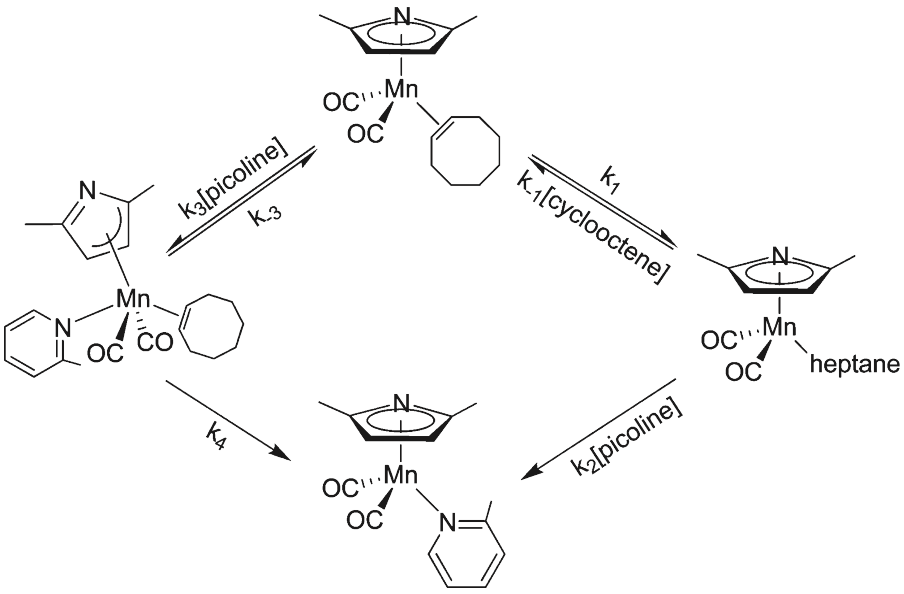

Figure 5.9. Mechanism describing dual associative/dissoaciatve pathways of olefin substitution from $(DMP)Mn(CO)_2$ fragment.

Thus, this value can be assigned to the enthalpic cost required to both disrupt the aromaticity of the pyrrole ligand and expand the coordination number on the Mn center to accommodate the incoming ligand as the 3 intermediate is formed. Rate enhancement relative to the Cp system is therefore expected only for the displacement of ligands that are bound to the Mn center by more than 33 kcal/mol. In such cases, the ring slipped transition state is predicted to be more energetically accessible than the dissociative one leading to an increase in the substitution rate. To gain a better understanding of the systems involved and to provide supporting evidence for the experimental results, DFT calculations were performed on the relevant compounds.

Theoretical Modeling

The binding strengths of various solvents to the metal center in the $CpMn(CO)_2$ and (η^5-DMP)$Mn(CO)_2$ fragments are presented in **Table 5.2**. Good agreement with the experimental values suggests the level of theory applied is appropriate for modeling the systems under investigation. The calculated geometries for a typical solvated complex are shown in **Figure 5.10** for the $CpMn(CO)_2THF$ and (η^5-DMP)$Mn(CO)_2THF$ molecules. The results indicate that replacement of Cp with the DMP ligand does not affect either the strength of the Mn-Solv bond or the geometry of the solvated complex. These results are consistent with the observation that the CO stretching vibrations of the DMP and Cp complexes are nearly identical, suggestive of similar electron density on both metal centers.

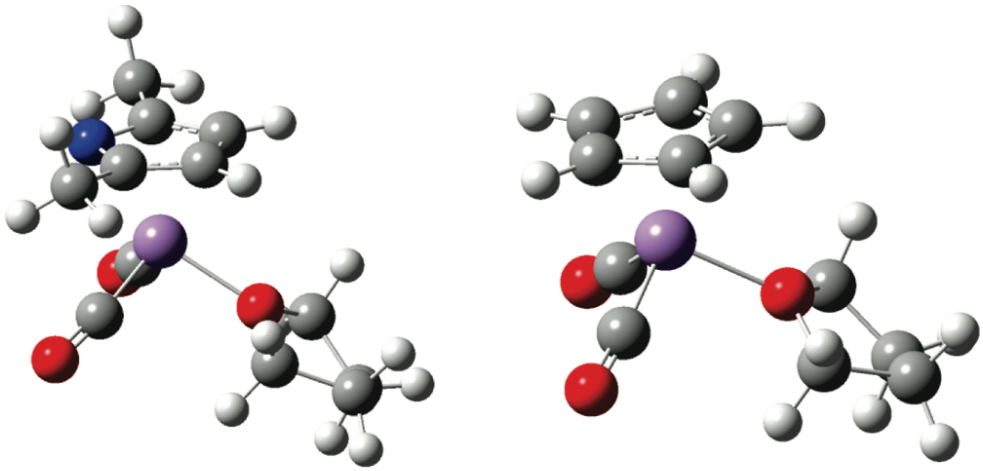

Figure 5.10. Calculated structures for the (a)(η^5-DMP)$Mn(CO)_2(THF)$ and (b) $CpMn(CO)_2THF$ molecules. The geometries and THF binding strengths are similar for both complexes.

The enthalpies of transition states and intermediates for some $\eta^5 - \eta^3$ ring slipped reactions were calculated for the Cp and DMP complexes. The most favorable η^3 transition state structure for the DMP system is one in which the nitrogen atom is not part of the allylic system, consistent with the enhanced steric bulk because of the presence of the CH_3 groups at the 2,5 positions. However, the calculated difference in enthalpy between the structures with and without nitrogen participation in the allylic system is <1.0 kcal/mol, and the two isomers can therefore be considered as isoenergetic.

The modeling results shown in **Figure 5.11** are consistent with the experimental data. For example, in the reaction of $CpMn(CO)_3$ with PH_3, the ring slipped transition state, (η^3-Cp)$Mn(CO)_3PH_3$, is 43 kcal/mol higher than the ground state. By contrast, in the DMP system the η^3 transition state is energetically more accessible at 32.9 kcal/mol. Interestingly, this activation enthalpy is similar to the calculated value of 30 kcal/mol for the η^3 transition state accessed in the displacement of CO from the (η^5-Indenyl)$Mn(CO)_3$ complex by PH_3.[132] Importantly, the associative transition state for the DMP complex is significantly lower in energy relative to the 54.9 kcal/mol Mn-CO BDE. It is therefore not surprising that substitution of CO from the DMP complex proceeds by an associative mechanism and shows a significant rate enhancement relative to the Cp system. The η^3 transition state energy for the DMP complex compares favorably to the experimental value of 26.4 kcal/mol for the displacement of CO by $P(OEt)_3$.[75] However, when P(n-Bu)$_3$ was used as the incoming ligand, an activation barrier of 15.7 kcal/mol was reported.

The enthalpic profiles for the weakly solvated complexes studied here have the same basic characteristics. For example, displacement of THF by C_2H_4 (model for cyclooctene used in the experiments) by a ring slip pathway demonstrates a relatively more accessible enthalpic profile for DMP versus Cp. Importantly however, as shown in **Figure 5.12**, the key difference from the CO substitution profile is that even for DMP, the η^3 transition state at 29.2 kcal/mol is higher in energy than the calculated value of 25.5 kcal/mol for the Mn-THF bond dissociation enthalpy. Consequently, the lower energy dissociative channel is utilized for the substitution of THF. Since the Mn-THF binding strength remains virtually unaffected when DMP is replaced by Cp, rate enhancement is not observed.

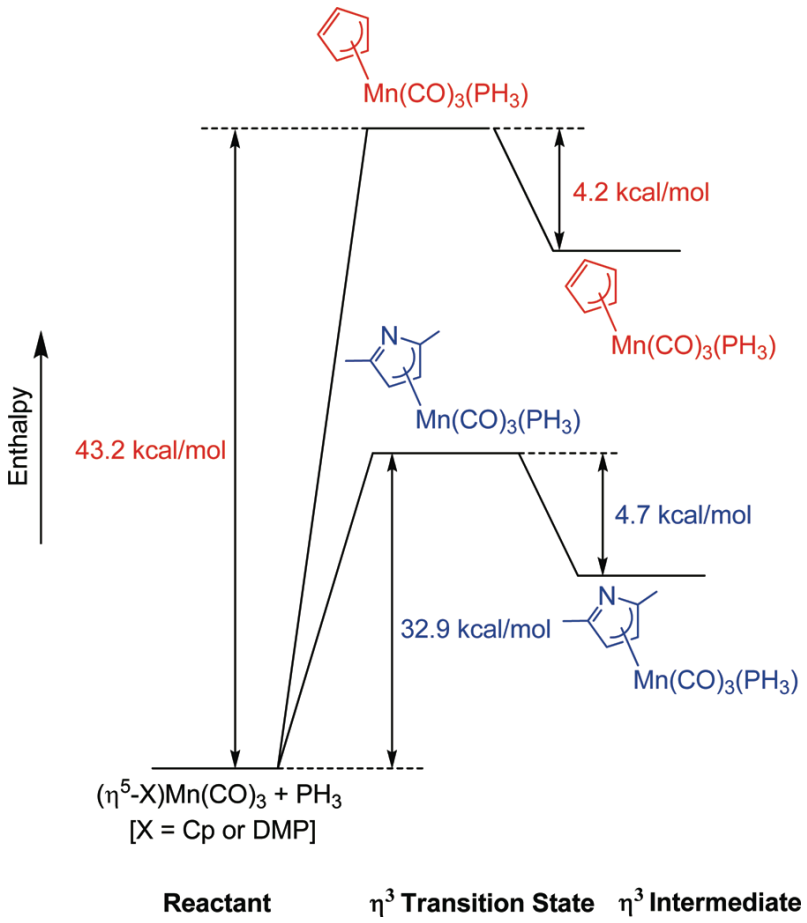

Figure 5.11. Enthalpy diagram for the displacement of CO from (η^5-X)-$Mn(CO)_3$ PH3 where X = Cp and DMP. The η^3 transition state is energetically more accessible for the DMP system.

The structures of the η^3 transition state and intermediate are shown in **Figure 5.13**. The 2.11 A˚ Mn-O bond distance in the transition state is similar to that found in the ground state structure (2.09 A˚). Furthermore, the incoming C_2H_4 ligand is loosely associated with the metal center as evident by the relatively long 2.82 A˚ bond distance between the center of the bond and Mn. Taken together these bond distances suggest there is relatively little bond breaking and making in the transition state. Thus, the higher

enthalpy of the transition state relative to the ground state is primarily due to the electronic and structural deformation of the DMP ligand as it undergoes a $\eta^5 - \eta^3$ haptotropic shift.

As shown in **Table 5.3**, unlike THF, the calculations suggest that for Solv = ethylene, the transition state energies for the associative and dissociative channels are similar. In the (η^5-DMP)Mn(CO)$_2$-(η^2-C_2H_4) pyridine system, the η^3 transition state is predicted to lie 28.4 kcal/mol higher than the ground state while the Mn-(η^2-C_2H_4) binding enthalpy is calculated to be only 3 kcal/mol higher at 31.8 kcal/mol. Consequently, for the cyclooctene system, it is reasonable to suggest that both substitution channels are accessed in the displacement reaction. As discussed earlier, the kinetic data are consistent with this prediction. Since the transition state enthalpies for the two pathways are calculated to be similar, rate enhancement relative to the Cp system is not observed.

Despite the variation in the solvent/ligand combinations, the activation enthalpies of the corresponding η^3 transition states are similar at 28.4, 29.2, and 32.9 kcal/mol for the C_2H_4/ pyridine, THF/C_2H_4, and CO/PH_3 systems, respectively. Consistent with the experimental results, the similar activation enthalpies suggest that the η^3 transition state is accessible for the displacement of solvents with Mn-Solv BDEs in excess of 33 kcal/mol. Rate enhancement is therefore not expected for weaker bound solvents.

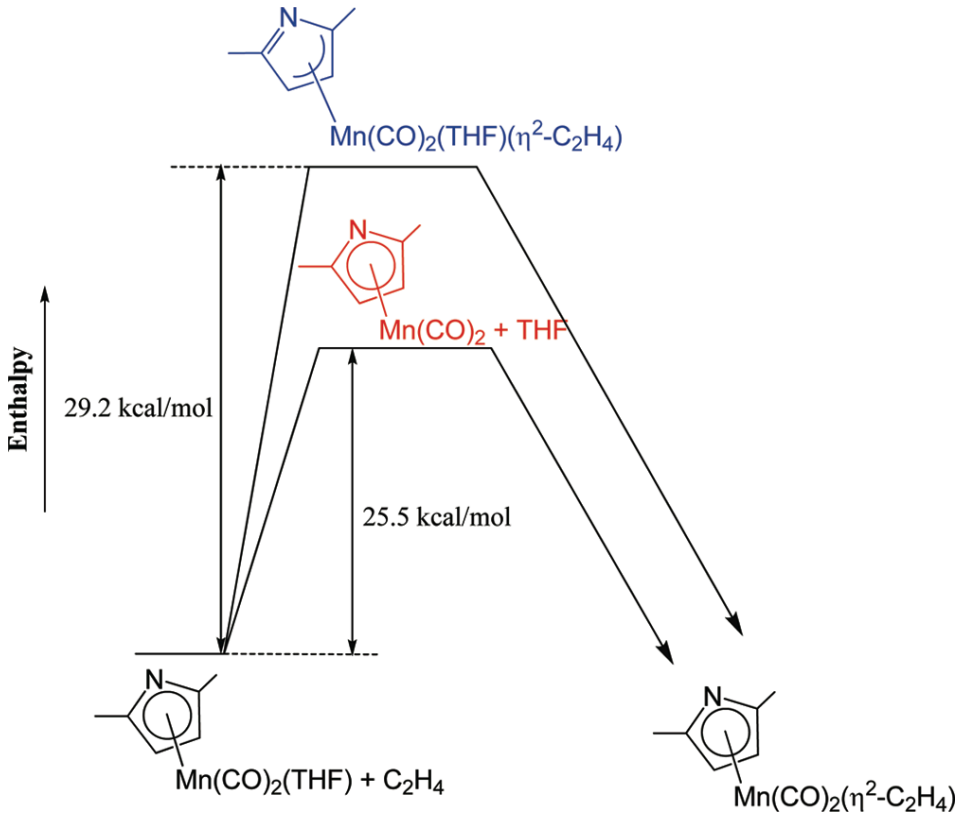

Figure 5.12. Enthalpy profile for the substitution of THF from the (-DMP)- $Mn(CO)_2$ fragment by C_2H_4. Unlike CO displacement, the dissociative channel for THF substitution has a lower enthalpy than the associative pathway.

Conclusions

The results of the kinetic study demonstrate that for the (η^5-DMP)$Mn(CO)_2$(Solv) complexes, the associative η^5 - η^3 ring slip substitution pathway becomes competitive with the dissociative channel only when the Mn-Solv bond dissociation enthalpy is >33 kcal/mol. Thus, unlike CO substitution, rate enhancement relative to the Cp system is not observed in the displacement of weakly bound solvents

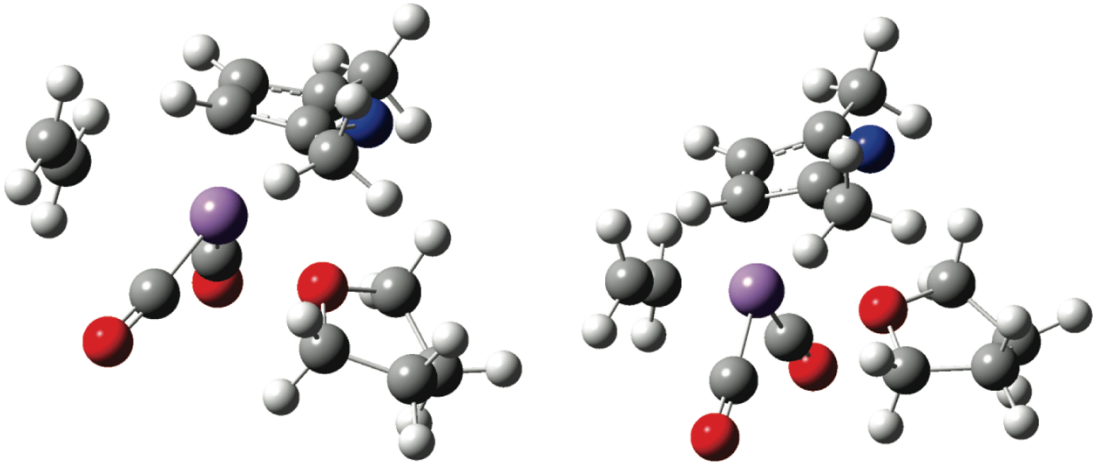

Figure 5.13. Calculated structures of the (η^3-DMP)Mn(CO)$_2$(THF)(η^2-C_2H_4) transition state and intermediate.

For these solvents, the close agreement between the calculated BDEs and the activation enthalpies suggest that the solvent displacement for both the DMP and the Cp complexes proceeds by a dissociative or I_d mechanism. While for the stronger bound cyclooctene ligand rate enhancement is not observed, experimental evidence supported by theoretical calculations demonstrates the accessibility of both dissociative and associative substitution channels.

Previous theoretical studies have calculated a 30 kcal/mol barrier for the η^5 - η^3 ring slip of the indenyl ligand in the displacement of CO from (η^5-Indenyl)Mn(CO)$_3$ by PH_3.[132] This activation energy is similar to that of the DMP complex (32.9 kcal/mol) and suggests that substitution of weakly coordinated solvents from the indenyl complexes

will display the same characteristics as observed for the DMP system. In initial experiments no significant rate enhancement was observed for the substitution of THF or 1-bromohexane from (η^5-Fluorenyl)Mn(CO)$_2$(Solv).

The results of the present study demonstrate that caution must be exercised when extrapolating the results of experiments that provide evidence for an associative ring slip pathway in ligand substitutions. Systems that demonstrate rate enhancement for the substitution of strongly coordinated ligands may not show the same effect for weaker bound substrates.

VI. KINETIC AND THEORETICAL COMPARISONS OF TRIS(PYRAZOLYL)BORATE AND CYCLOPENTADIENYL MANGANESE COMPLEXES*

Introduction

The scorpionate ligand, hydridotris(1-pyrazolyl)borate (Tp), is often considered as an equivalent of the more commonly used cyclopentadienyl (Cp) ligand in transition-metal-containing organometallic complexes.[156,157,158] Als vthough both Tp and Cp are facially coordinating six-electron anionic donors, they have different steric and electronic characteristics.[159] With estimated cone anglesof 262^{o} for Tp and 150^{o} for Cp, the former ligand is considerably more sterically demanding than Cp. However, the relative electron donor characteristics of the two ligands are not so straightforward and vary with the identity of the metal center, its oxidation state, and other coordinated ligands.[159] In some instances, steric factors have been judged to play a primary role in influencing the reactivity trends.[160] For example, a computational study of C-H activation by Re complexes found that while oxidative addition of methane to $CpRe(CO)_2$ was exothermic, the same transformation was endothermic for $TpRe(CO)_2$.[161] Steric differences between the Tp and Cp ligands were thought to play a primary role in the calculated reactivity difference. However; in some cases, differences in reactivity are the result of an electronic effect. For example, dissociation of the triflate

*Reprinted (adapted) with permission from Swennenhuis, B. H. G.; Poland, R.; DeYonker, N. J.; Webster, C. E.; Darensbourg, D. J.; Bengali, A. A. *Organometallics* **2011**, *30*, 3054–3063. Copyright 2011 ACS publications

ligand from the more sterically encumbered $TpMe_2(PMe_3)Ir$-(Me)OTf ($TpMe_2$ = hydridotris(3,5-dimethylpyrazolyl)borate) complex was found to be slower than from the analogous Cp* complex, pointing to an electronic ,rather than a steric, effect imposed by the $TpMe_2$ ligand.[162] Also, trends in the relative stabilities of the Cp*- and Tp-Ru carbyne complexes were attributed to differences in the relative electron-donating abilities of the Cp* and Tp ligands.[163]

In general, the Tp ligand enforces a six-coordinate environment around the metal center, while the Cp systems exhibit more flexible geometries.[78,164,165,166,167] In contrast to the commonly observed seven-coordinate "piano stool" geometry for Cp-ligated metal centers, similar structures are quite rare for the Tp systems. In some instances the differences in reactivity can be explained by the strong preference for octahedral geometry in the Tp system. For example, reaction of $TpMo(CO)_3^-$ with CH_3I yields the quasi-six-coordinate acyl complex $TpMo(CO)_2(\eta^2\text{-}COCH_3)$, while the same reaction with $CpMo(CO)_3^-$ yields the sevencoordinate $CpMo(CO)_3(CH_3)$ complex.[10-13] Preference for octahedral binding was also observed in $TpRu^{2+}$ complexes, where the dissociation of CH_3CN from $[TpRu(CH_3CN)_3]^+$ was 8 orders of magnitude slower than that from the corresponding Cp system.[168] Similarly, ligand displacement rates were also found to be significantly slower from the $TpOs^{2+}$ complexes than from the analogous Cp^*Os^{2+} counterparts, a likely consequence of the strongly directional character of the frontier orbitals of the TpM fragment, which favors an octahedral ligand arrangement around the metal center.[168,169]

Given the importance of organometallic complexes in promoting a variety of organic transformations, the development of new species with reactivity patterns different from those that incorporate the ubiquitous Cp ligand is of considerable interest.

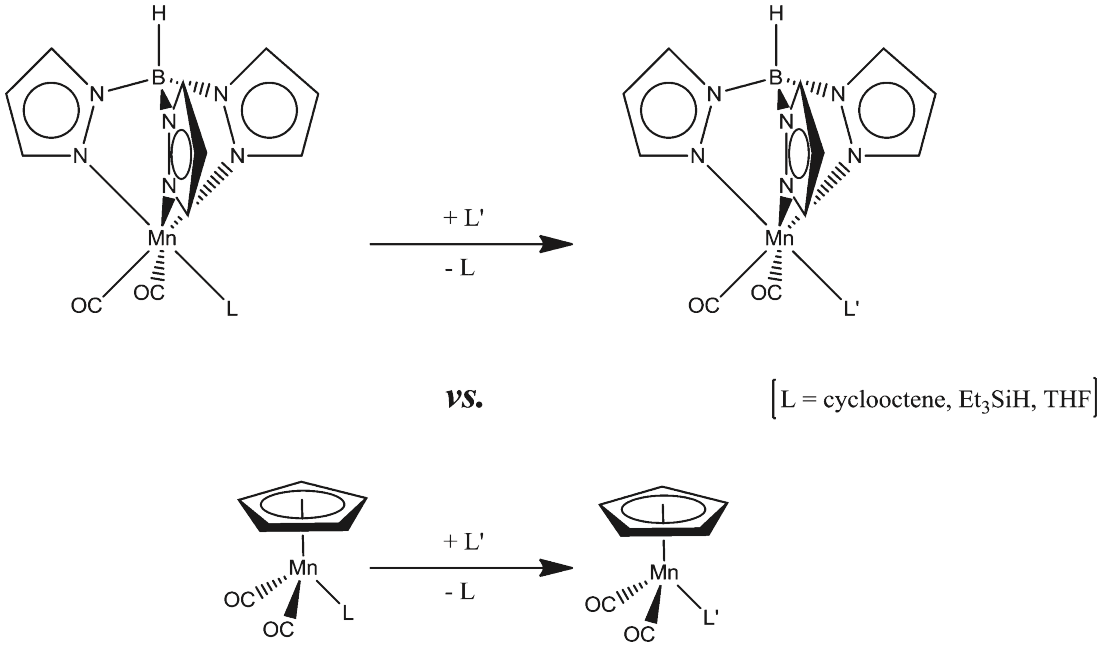

Figure 6.1. Ligand substitution in $TpMn(CO)_2L$ and $CpMn(CO)_2L$ complexes

There is therefore a need to better understand the effect of non-Cp-based ligands upon the reactivity of the related complexes. While the interactions of several ligands with the $CpMn(CO)_2$ fragment have been studied extensively,[170,171] little information is available for the Tp analogue. We therefore report in this paper an experimental and theoretical investigation into the displacement of weakly coordinated ligands from the $TpMn(CO)_2$ fragment (**Figure 6.1**). The results point to a dramatic difference in the displacement

rates and energetics of ligands such as triethylsilane, cyclooctene, and THF from the $TpMn(CO)_2$ and $CpMn(CO)_2$ systems.

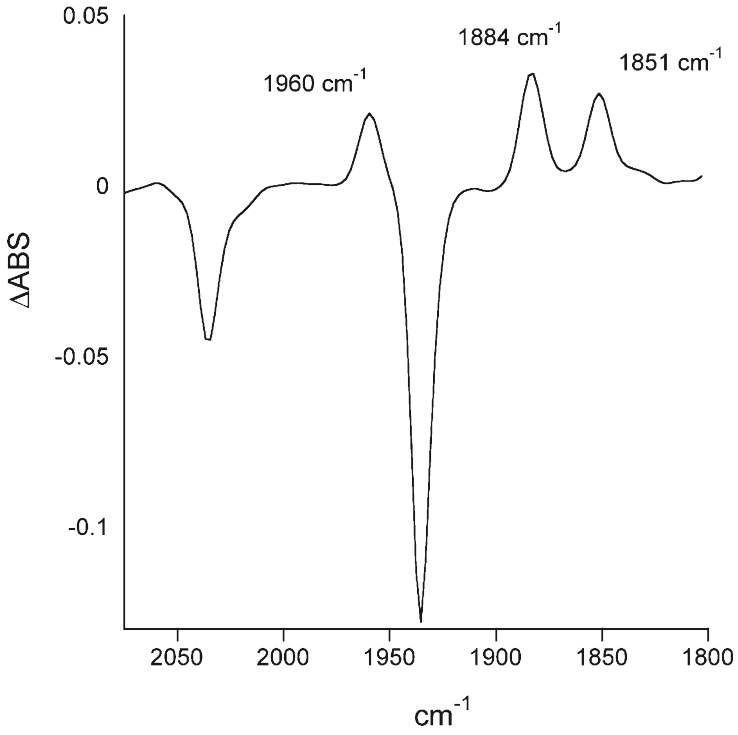

Figure 6.2. Difference spectra obtained 12.5 μs after photolysis of a cyclohexane solution of $TpMn(CO)_3$ in the presence of cyclooctene (2.11 M) and THF (0.45 M) at 296 K. Negative peaks are associated with depletion of the parent upon photolysis. Positive peaks are due to the CO stretching bands of the $TpMn(CO)_2(\eta^2$-cyclooctene) 1960/ 1884 cm^{-1}) and $TpMn(CO)_2$(THF) (1851 cm^{-1}) complexes. The second CO band for the THF species is not observed in this experiment, due to overlap with the parent band. Under some conditions, however, it is observed at 1946 cm^{-1}.

Experimental and Theoretical Methods

Time-resolved IR spectra (microseconds to seconds) were obtained using a Bruker Vertex 80 FTIR equipped with step-scan and rapid-scan capabilities (2200-1800 cm^{-1}). Sample photolysis was conducted using the third harmonic (355 nm) of a Nd:YAG laser (Continuum Surelite I-10) operating at 1-10 Hz.

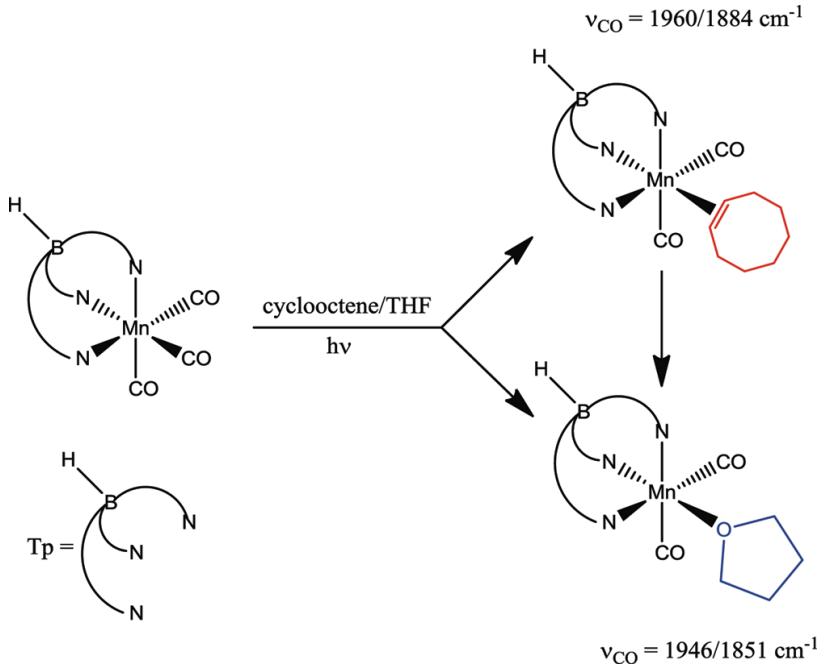

Figure 6.3. Mechanism of photolytic CO displacement and subsequent ligand replacement by cyclooctene and THF in $TpMn(CO)_2$, the THF adduct of which is more stable than the cyclooctene adduct.

A syringe pump was used to flow solution through a temperature-controlled 0.5 mm path length IR cell with CaF_2 windows (Harrick Scientific) to ensure that a fresh solution was photolyzed with every shot of the laser. The temperature was monitored by a thermocouple located close to the photolysis solution and maintained by a water

circulator to within (0.1 ^{o}C. All spectra were obtained at 8 cm^{-1} resolution. Once the IR spectra of all reactive species were identified using the instrumentation described above, kinetic data were obtained using a flash photolysis apparatus employing infrared detection. The temporal profile of the photogenerated intermediates was probed with infrared light from a water-cooled CO probe laser (1600-1920 cm^{-1}). The infrared output was tuned to the desired wavenumber and attenuated by absorptive filters (OD = 2.5) prior to merging with the UV photolysis beam. The collinear IR/UV beams were passed through the sample cell, following which the UV beam was split from the IR beam which was detected with a liquid nitrogen cooled MCT detector (Kolmar Technologies, 50 ns rise time). The signal was sent to a 1GHz digital storage oscilloscope (LeCroy 9415) for processing.

All solvents and ligands were of anhydrous grade (Aldrich) and >99% purity and used as received, unless stated otherwise. Triethylsilane and THF were distilled under nitrogen, and cyclooctene was passed through a column of alumina prior to use to remove any peroxide impurities. $TpMn(CO)_3$ was synthesized according to a literature procedure.[172,173] The photolysis solution contained ~1 mM of $TpMn(CO)_3$ in n-heptane or cyclohexane solvent with either 1.9 M triethylsilane or 3.1 M cyclooctene and the appropriate amount of THF as the displacing ligand. All kinetic experiments were conducted under pseudo-first-order conditions, with the concentration of the incoming ligand at least 10 times larger than that of the reactant complexes. Observed rate constants (k_{obs}) were obtained from first-order exponential fits to either the decay or growth of the reactant and product complexes, respectively, as a function of time. The

errors in the reported rate constants and other kinetic parameters were obtained from least-squares analysis of the data as implemented by the software program KaleidaGraph.

All computations were performed using the Gaussian09 software package. Energies, optimized geometries, and unscaled harmonic vibrational frequencies were obtained using density functional theory.[149] Both the hybrid B3LYP15[148] and pure BVP8616[174,175,176] functional were used with default grid parameters (Default pruned fine grids (75 radial shells, 302 angular points) for energies and default pruned coarse grids for gradients and Hessians (35 radial shells, 110 angular points)).

Table 6.1. Experimental CO Stretching (cm^{-1}) and Force Constants (10^2 N/m) for a variety of $XMn(CO)_2L$ (X = Tp, Cp) complexes at 298 K in cyclohexane solution with some THF added to aid in the solubility of the Tp system. *a* Neat $HSiEt_3$. Unlike other ligands, ν_{CO} values for the $HSiEt_3$, eomplexes are different since the natures of silane binding to the Tp and Cp metal center are somewhat different (*vide infra*).

L	Tp		Cp	
	ν_{CO} (cm^{-1})	k_{CO}, k_1	ν_{CO} (cm^{-1})	k_{CO}, k_1
CO	2034, 1936	15.92, 0.786	2027, 1944	15.93, 0.665
Cyclooctene	1960, 1884	14.92, 0.589	1961, 1902	15.07, 0.460
$HSiEt_3$[a]	1952, 1871	14.76, 0.625	1977, 1913	15.28, 0.503
Tetrahydrofuran	1946, 1851	14.56, 0.728	1934, 1863	14.56, 0.544
Pyridine	1936, 1849	14.47, 0.665	1934, 1868	14.60, 0.507
N_2	1977, 1913	15.28, 0.502	1979, 1928	15.41, 0.402

The basis set for manganese and rhenium atoms was the Hay and Wadt basis set and effective core potential (ECP) combination (LANL2DZ)[177] as modified by Couty and Hall (Mn, 341/341/41; Re, 341/341/21),[178] where the two outermost p functions

have been replaced by a split of the optimized Mn/ Re 4p/6p function, respectively. All carbon, boron, nitrogen, silicon, and hydrogen atoms utilized the 6-31G(d') basis set (The 6-31G(d') basis set has the d polarization functions for C, N, and O taken from the 6-311G basis set, instead of the original arbitrarily assigned value of 0.8 used in the 6-31G(d) basis set. Foresman, J. B.; Frisch, A. Exploring Chemistry with Electronic Structure Methods, 2nd ed.; Gaussian, Inc., Pittsburgh, PA, p 110).[179]

Spherical harmonic d functions were used throughout; i.e., there are five angular basis functions per d function. The Hessian of the energy was computed at all stationary points to designate them as either minima or transition states (first-order saddle points). Zero-point energies (ZPE) and thermal enthalpy corrections for bond dissociation energies (BDEs) were computed at 298.15 K and 1 atm. With pure DFT functionals such as BVP86, metal-complex carbonyl harmonic stretching frequencies are systematically too small, which enhances fortuitous agreement with anharmonic experimental observations. Therefore, only BVP86 harmonic vibrational frequencies will be discussed in the text, and B3LYP harmonic vibrational frequencies will be reported in the Supporting Information.

Results and Discussion

(a). TpMn(CO)3 + Cyclooctene. As shown in **Figure 6.3**, photolysis of a cyclohexane solution of $TpMn(CO)_3$ in the presence of cyclooctene and THF results in the formation of two dicarbonyl species absorbing at 1960/1884 and 1946/1851 cm^{-1}. The lower wavenumber species is assigned to the $TpMn(CO)_2(THF)$ complex, since photolysis of $TpMn(CO)_3$ in a cyclohexane/THF solution yields a species with similar CO stretching bands. On the basis of the established photochemistry of the analogous Cp system, the second transient is assigned to the $TpMn(CO)_2(\eta^2$-cyclooctene) complex.[170,171] Due to the low solubility of TpMn(CO)3 in alkanes and alkenes, it was not possible to photolyze the compound in the presence of only cyclooctene, since THF was required to aid in the solubility. As suggested by a reviewer, we have computed the geometries of the CH σ-bound $TpMn(CO)_2$(cyclooctene) and $CpMn(CO)_2^-$ (cyclooctene) complexes. With the BVP86 functional, these complexes are energetically disfavored relative to their η^2-bound counterparts by ~11 and ~14 kcal/mol, respectively. We predict a low barrier of rearrangement between σ-bound and π-bound complexes and thus a short lifetime for any σ-bound species. As shown in **Table 6.1**, the similar CO stretching frequencies and respective force constants for several Tp and Cp complexes suggest that the metal electron density does not vary significantly in the two systems.[180]

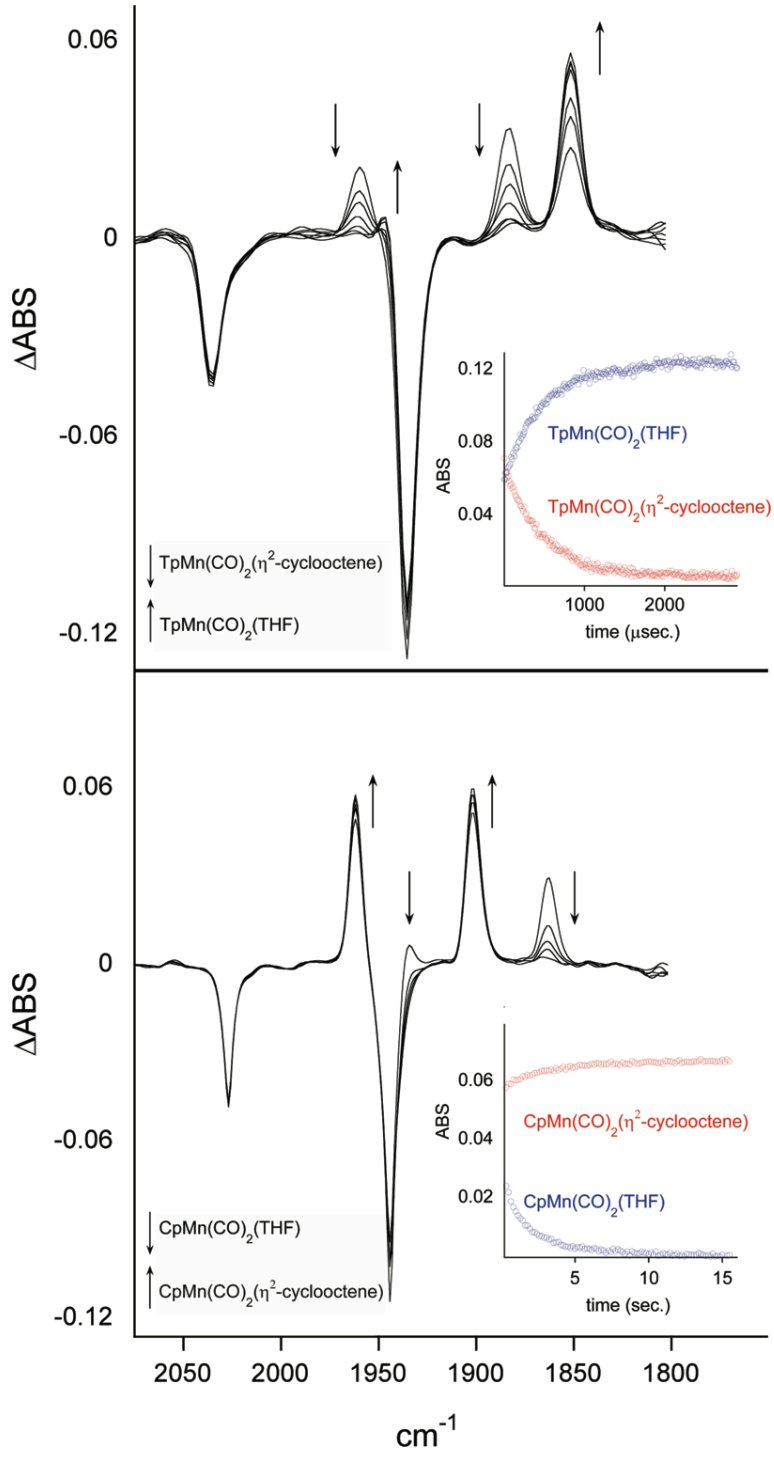

Figure 6.4. Photolysis of (a) $TpMn(CO)_3$ and (b) $CpMn(CO)_3$ conducted in the presence of cyclooctene (2.11 M) and THF (0.45 M) in cyclohexane at 296 K.

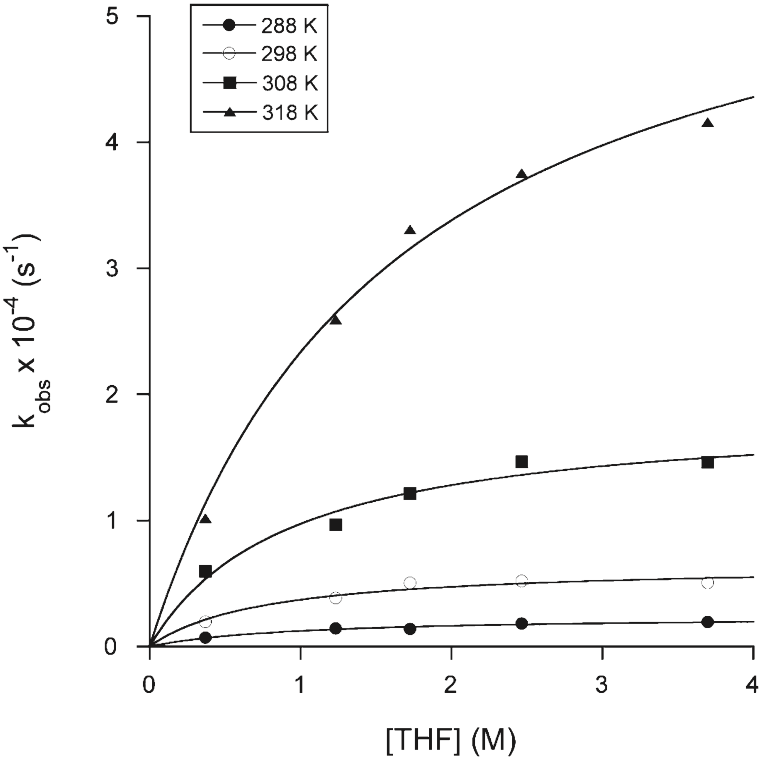

Figure 6.5. Plot of k_{obs} vs [THF] at several temperatures for the displacement of cyclooctene from $TpMn(CO)_2(\eta^2$-cyclooctene by THF. The cyclohexane solution was 3.1 M in cyclooctene with the appropriate amount of THF added. The saturation behavior of k_{obs} suggests a dissociative mechanism of ligand displacement from the Mn center.

This observation is consistent with a previous comparison which ranked the relative donor abilities of the Tp and Cp ligands toward a Mn(I) metal center as Cp*~ $Tp^{Me}{}_2$ > Cp ~ Tp.[159] Although the Tp and Cp species have similar electron densities, the kinetic profiles of the respective η^2-cyclooctene complexes are dramatically different and the relative stabilities of the Mn(η^2-cyclooctene) and Mn-THF complexes are reversed. This reversal is confirmed by DFT computations which, unlike the case for the Cp complexes, suggest stronger binding of the THF ligand to the $TpMn(CO)_2$ fragment

relative to cyclooctene (vide infra). These results are unlike those for $CpMn(CO)_2L$ complexes, where cyclooctene is significantly preferred to THF.

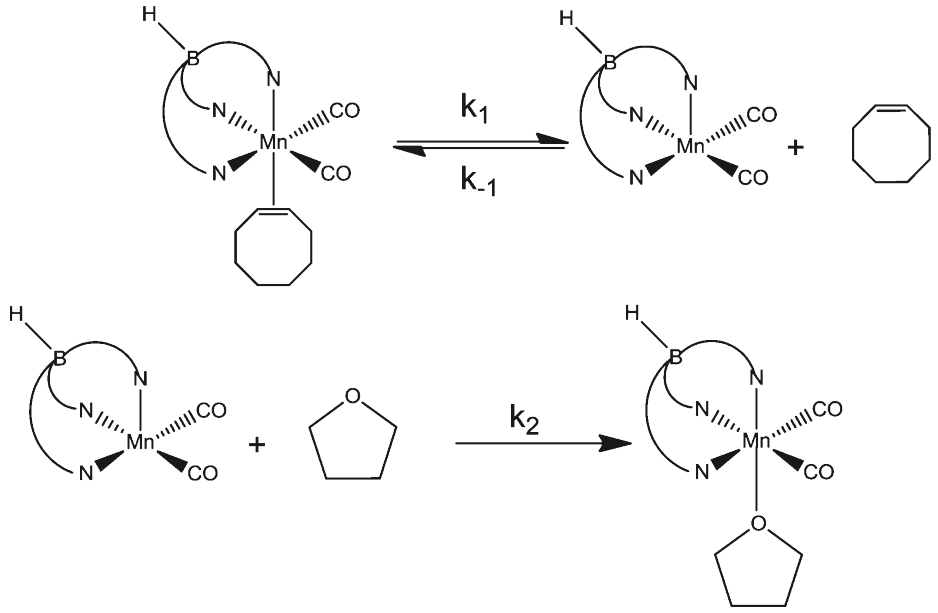

Figure 6.6. Mechanism of cycloctene displacement by THF from $TpMn(CO)_2$.

As shown in **Figure 6.4**, while TpMn(CO)2(η^2-cyclooctene) reacts with THF to form the $TpMn(CO)_2$(THF) complex, photolysis of $CpMn(CO)_3$ in the presence of cyclooctene and THF results in the opposite reactivity. Thus, the initially formed THF complex is converted to $CpMn(CO)_2$(η^2-cyclooctene), a species that has previously been isolated and characterized.[147] In the presence of even small amounts of THF, the $TpMn(CO)_2$(η^2-cyclooctene) complex disappears within a few milliseconds at roomtemperature, suggestive of weaker binding of the cyclooctene ligand to the metal center, in dramatic contrast to the Cp system.

Table 6.2. Rate constants obtained from fits to the k_{obs} vs THF data for the reaction: $TpMn(CO)_2L + THF \rightarrow TpMn(CO)_2THF + L$ at several temperatures

Temp (K)	L = cyclooctene		L = $HSiEt_3$	
	10^{-3} k_1 (s^{-1})	k_2/k_{-1}	10^{-3} k_1 (s^{-1})	k_2/k_{-1}
288	2.4 ± 0.2	3.2 ± 0.9		
293			17.9 ± 1.4	3.0 ± 0.5
298	6.5 ± 0.7	4.0 ± 1.5		
303			38.3 ± 2.0	3.3 ± 0.4
308	18.7 ± 1.9	3.4 ± 1.0		
313			74.9 ± 6.5	5.0 ± 1.3
318	61.3 ± 4.4	2.0 ± 0.3	102.0 ± 5.0	6.0 ± 1.0

Interestingly, the alkene and THF complexes of the analogous $CpRe(CO)_2$ and $TpRe(CO)_2$ fragments do not display reversed relative stabilities and for both complexes the alkene adducts are more stable than the THF analogues.[181,182] The difference in relative stability between the Mn and Re systems may be attributed to both steric and electronic factors. The larger Re metal center is expected to be more sterically accessible to an alkene ligand, and an enhanced π back-bonding interaction with the more diffuse d orbitals of the third-row metal would result in stronger binding of the alkene relative to THF. The saturation behavior of k_{obs} as a function of [THF] shown in **Figure 6.5** points to a mechanism involving reversible loss of the cyclooctene ligand to generate an intermediate complex which reacts with THF to form the final $TpMn(CO)_2(THF)$ product (**Figure 6.6**).

Application of the steady-state assumption to the $TpMn(CO)_2$ intermediate results in the kobs dependence shown in eq 1.

$$k_{\text{obs}} = \frac{k_1 k_2[\text{THF}]}{k_{-1}[\text{cyclooctene}] + k_2[\text{THF}]}$$

Equation 6.1. Steady state equation.

Consistent with eq 1, k_{obs} is found to be inversely dependent on [cyclooctene]. For example, at 293 K with n-heptane as the diluent and [THF] = 1.23 M, kobs = 1068, 2375, and 4286 s^{-1} at cyclooctene concentrations of 6.91, 3.07, and 1.54 M, respectively. This inverse dependence implies reversible dissociation of the cyclooctene ligand and is inconsistent with other mechanisms that may lead to the limiting behavior of k_{obs} such as reversible dechelation of one arm of the Tp ligand. DFT calculations confirm that dechelation of one arm of the Tp ligand is a higher energy process than MnL bond dissociation. Previous studies have shown that displacement of cyclooctene by an incoming ligand also proceeds by a similar dissociative mechanism for the Cp complex.[147] There is therefore no evidence of a mechanistic difference in the displacement of cyclooctene from either the Tp or Cp complexes. A fit of the kobs vs [THF] data to eq 1 yields the values of k_1 and the selectivity ratio k_2/k_{-1} shown in **Table 6.2**.

Using literature values for the activation parameters, $k_1 \sim 3 \times 10^{-8}$ s^{-1} at 288 K for the dissociation of the cyclooctene ligand from $CpMn(CO)_2(\eta^2$-cyclooctene). Combined with the present results, this rate constant yields the ratio $k_1(Tp)/k_1(Cp) \sim 10^{11}$ at 288 K. An Eyring analysis (**Figure 6.7**) yields activation parameters of $\Delta H_1^{\ddagger} = 18.8 \pm 1.0$ kcal/mol and $\Delta S_1^{\ddagger} = +23 \pm 3$ e.u for the k_1 step, with the former value providing an

estimate for the strength of the $TpMn(CO)_2$-(η^2-cyclooctene) bond. Good agreement with a theoretical estimate of 15.5 kcal/mol for the TpMn(CO)2!(!2-cyclooctene) binding enthalpy provides confirmation of the dissociative nature of the transition state. In contrast, the $CpMn(CO)_2$(η^2-cyclooctene) binding enthalpy has previously been estimated at 34.9 kcal/mol by employing a similar kinetic analysis,[147] significantly higher than for the Tp system and in reasonable agreement with the computed BVP86 BDE of 32.3 kcal/mol. The approximately 15 kcal/mol lower binding enthalpy of cyclooctene to the $TpMn(CO)_2$ fragment and the resulting 10^{11}-fold enhancement in reactivity is quite surprising, considering the similar electronic characteristics of the Tp and Cp systems, and points to a steric factor for the reactivity difference. Further evidence that steric effects may play a role in determining the overall bond strength is provided by DFT calculations, which predict a BDE of 20.9 kcal/mol for the $TpMn(CO)_2$-(η^2-ethylene) interaction, ~5 kcal/mol higher than that of cyclooctene.

The observed large rate enhancement of ligand displacement following replacement of the Cp coligand with Tp is rare. There are, however, several examples of a slower displacement rate of ligands from Tp-complexed metals in comparison to the Cp analogues.[162,168,169,183] Interestingly, most of these instances involve second- and third-row transition metals. The smaller size of the first-row Mn center could be expected to result in a more sterically encumbered binding pocket when complexed to the larger Tp ligand, leading to a weaker interaction with the cyclooctene ligand. The larger steric footprint of the Tp ligand and the relative inaccessibility of the Mn center is

also apparent from the space-filling model of the $TpMn(CO)_3$ and $CpMn(CO)_3$ complexes (**Figure 6.8**).[184]

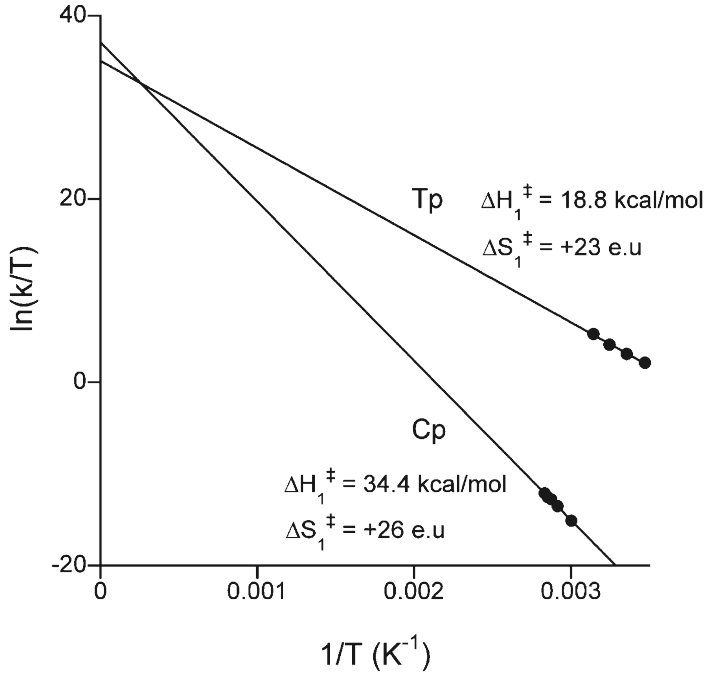

Figure 6.7. The dissociation of cyclooctene from $CpMn(CO)_2(\eta^2$-cyclooctene)[147] and $TpMn(CO)_2(\eta^2$-cyclooctene).The plots have been extrapolated to more clearly demonstrate the difference in slopes, which is related to the binding enthalpy difference in the Cp and Tp systems. The y intercepts for both systems yield similar positive $\Delta S^{\neq}$ values, consistent with a dissociative displacement mechanism.

The crystal structure data for $TpMn(CO)_3$ were reported by: Joachim, J. E.; J. Organomet. Chem. 1993, 448, 119. Data were collected at ambient temperature, and the structure was refined in the space group P3. Cell parameters were a = 11.522(4) Å, c = 7.933(3) Å, V = 912.061 Å3, R = 6.9%. The structure was later shown to belong to the P¯3 space group by: Marsh, R. E. Acta Crystallogr., Sect. B 2002, 58, 62. We recollected

the crystal structure data for $TpMn(CO)_3$ as shown in **Figure 6.8**, but at 77 K and refined the structure in the space group $P^{-}3$. Cell parameters were a = 11.3823(7) Å, c = 7.8487(10) Å, V = 880.62(14) Å3, R = 3.04%. While steric considerations undoubtedly play a role, electronic effects cannot be completely ruled out in explaining the weaker ligand binding to $TpMn(CO)_2$. Curtis et al. have proposed that the differences in stability between some Cp- and Tp- coordinated metal systems may arise as a result of strong directional character in the frontier orbitals of the latter system.[165] Consistent with this explanation, more recent theoretical studies have also indicated that the HOMO and LUMO of the $CpRe(CO)_2$ fragment are more diffuse than those of the $TpRe(CO)_2$ fragment.[161] This more directional character in the Tp system may result in poorer overlap with the π and π* orbitals of the cyclooctene ligand, resulting in both a weaker L→metal π and metal→L π back-bonding interaction and hence a lower binding enthalpy as observed. As discussed later, DFT calculations also suggest that the trans influence of the pyrazolyl nitrogen may impact the TpMn-L BDEs.

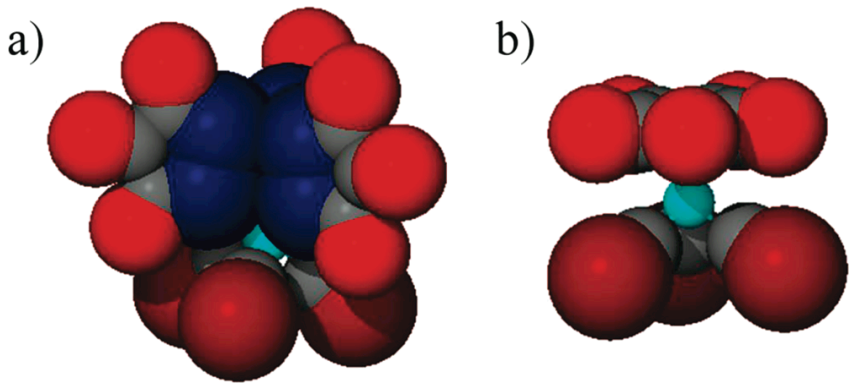

Figure 6.8. Space-filling models of (a) $TpMn(CO)_3$ and (b) $CpMn(CO)_3$

Weaker binding to the $TpMn(CO)_2$ fragment is also observed in the case of the THF ligand. As shown in **Figure 6.9**, photolysis of $CpMn(CO)_3$ in THF at 296 K yields the previously observed $CpMn(CO)_2(THF)$ complex with a lifetime of ~500 s.[146] Under similar conditions, the $TpMn(CO)_2$-(THF) complex has a shorter lifetime of ~20 s. A complete kinetic analysis of the Tp reaction could not be performed, since the reaction lifetimes fall in a region that is difficult to probe by the existing instrumentation. Nonetheless, the relative lifetimes suggest weaker binding of THF in the Tp complex compared to the Cp system. Free energies of activation were determined by computing direct transition states of L dissociation using DFT. In good agreement with experimental measurements, the computed lifetime of $CpMn(CO)_2(THF)$ is approximately 17.5 times greater than that of $TpMn(CO)_2(THF)$. Without a sophisticated treatment of transition state theory, magnitudes of computed lifetimes are expected to be in poor agreement with experiment. However, qualitative trends in relative lifetimes can be reliably discussed. DFT computations also provide THF binding enthalpies of 22.5 and 16.5 kcal/mol for the Cp and Tp complexes, respectively. The difference in reactivity is not as extreme as in the case of the cyclooctene ligand, however. It may be speculated that the steric bulk of the Tp complex does not impact the binding of the smaller THF ligand to the extent that it does the larger cyclooctene molecule.

(b). $TpMn(CO)_3$ + HSiEt3. The photolysis of $CpMn(CO)_3$ in the presence of $HSiEt_3$ has been well studied on both the ultrafast and longer time scales. These existing data provide an excellent opportunity to compare the reactivities of the Cp and Tp systems with silanes. For the Cp system, the ultrafast reactions are complicated but

essentially involve the initial formation of both Si-H and C-H coordinated π complexes within a few picoseconds upon photolysis of $CpMn(CO)_3$ in pure $HSiEt_3$.[185]

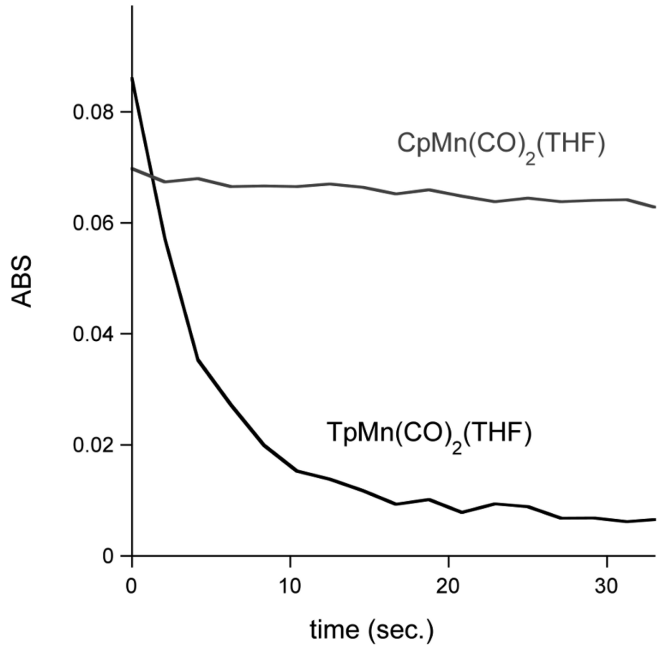

Figure 6.9. Relative stabilities of $CpMn(CO)_2(THF)$ and $TpMn(CO)_2(THF)$ complexes at 293 K. Photolysis of the parent tricarbonyl complexes in pure THF was conducted in the absence of other ligands, and the absorbances at 1860 and 1852 cm^{-1} for the Cp and Tp analogues, respectively, were monitored.

These weakly solvated complexes undergo Si-H oxidative addition on a picosecond to nanosecond time scale, forming the final $CpMn(CO)_2(H)(SiEt_3)$ product. Longer time scale studies (hours) by Yang and coworkers focused on the reductive elimination of triethylsilane from $CpMn(CO)_2(H)(SiEt_3)$ and reported a dissociative mechanism for the reaction with an activation enthalpy of 27.4 kcal/mol.[186]

Theoretical modeling[185] and crystal structures of several $CpMn(CO)_2$/silane complexes indicate that the Si-H bond is not completely dissociated in the final complex. Thus, it is perhaps more proper to refer to the final species as a Si-H η^2-coordinated sigma complex rather than an oxidatively added silane complex in which the Si-H bond is completely broken. However, for the sake of consistency with earlier studies, the final stable product of $CpMn(CO)_3/HSiEt_3$ photolysis will be referred to as $CpMn(CO)_2(H)(SiEt_3)$.

As shown in **Figure 6.10**, photolysis of $CpMn(CO)_3$ in neat $HSiEt_3$ on the microsecond time scale results only in the formation of a single dicarbonyl product with CO bands at 1913 and 1977 cm^{-1}. This species is assigned to the previously observed and well-characterized $CpMn(CO)_2(H)(SiEt_3)$ complex.[185,186] Unlike the Cp system, photolysis of $TpMn(CO)_3$ in pure $HSiEt_3$ results in the initial formation of a single dicarbonyl species with CO stretching absorbances at 1871 and 1952 cm^{-1}, which then decays within several milliseconds to form another dicarbonyl complex absorbing at 1913 and 1977 cm^{-1}. This higher wavenumber species is assigned to the $TpMn(CO)_2N_2$ complex, since the related CO absorbances are not observed when the photolysis solution is purged with Ar but reappear when the experiment is conducted in the presence of N_2. As shown in **Figure 6.11**, further confirmation for this assignment is provided by the observation of a band at 2180 cm^{-1} (computed at the BVP86 level of theory to occur at 2179 cm^{-1}), which is due to the "NN stretch of the end-on-bound N_2 ligand. The related $CpMn(CO)_2N_2$ complex has also been observed previously and is surprisingly stable.[187] Although the concentration of free N_2 in the photolysis solution,

estimated at ~7 mM, is much lower than that of $HSiEt_3$, the nitrogen complex is nonetheless observed, since the computed Mn-N_2 bond strength (26.2 kcal/mol) is significantly greater than that for Mn-$HSiEt_3$ (11.5 kcal/mol).

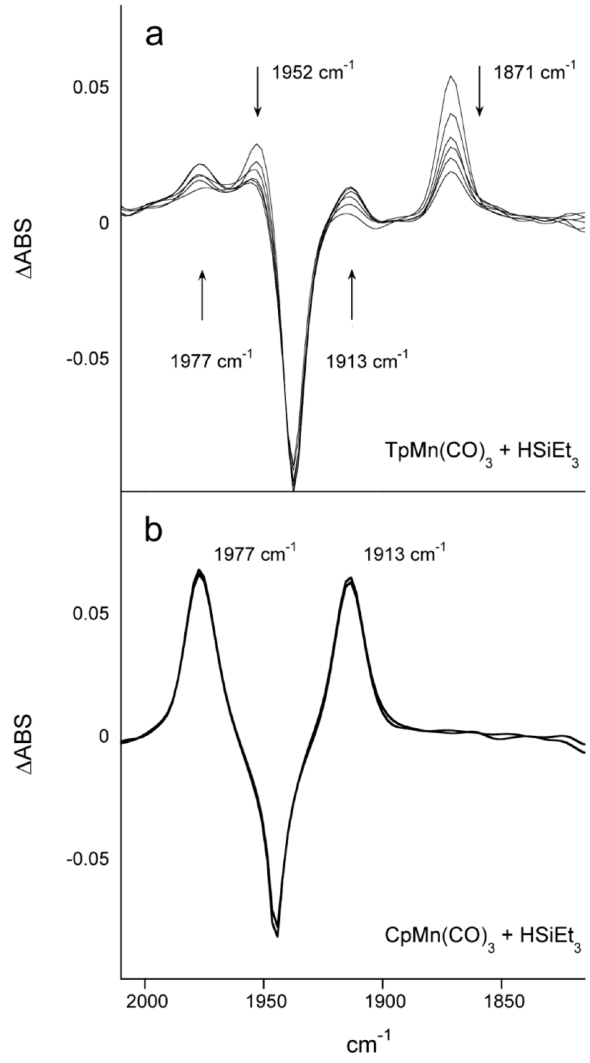

Figure 6.10. Photolysis of (a) $TpMn(CO)_3$ and (b) $CpMn(CO)_3$ in neat $HSiEt_3$ at 295 K. The Tp spectra were obtained at 0, 1, 7, 10.5, 14, and 17.5 ms after photolysis. For $CpMn(CO)_3$ only the spectra after 250 μs and 17.5 ms after photolysis are shown. The second CO band of the parent tricarbonyl complexes is not shown.

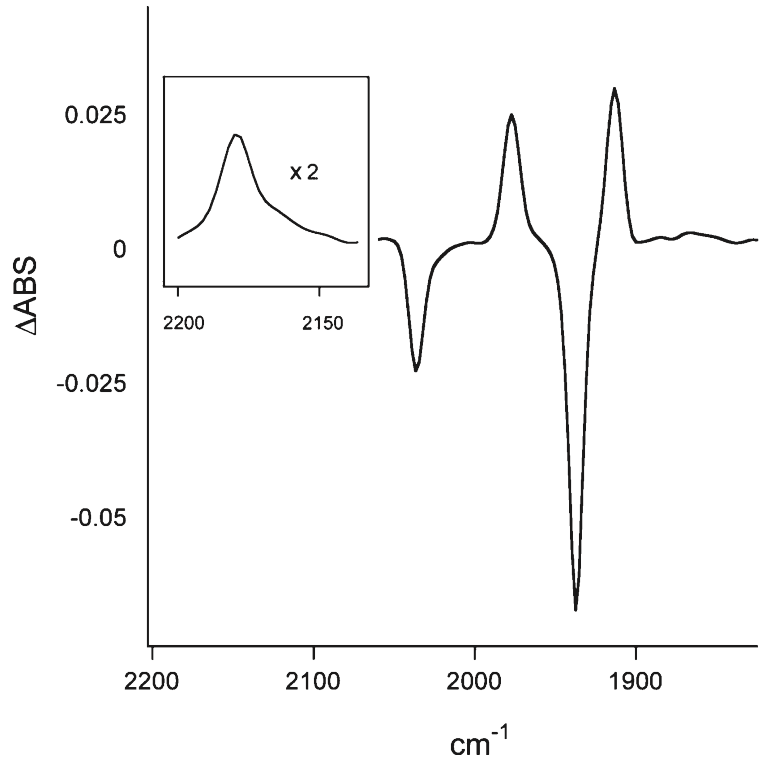

Figure 6.11. Difference spectra obtained upon photolysis of a cyclohexane/$HSiEt_3$ (100:4) solution of $TpMn(CO)_3$ purged with N_2 at 297 K. The spectrum was obtained 1 s after photolysis. The positive peaks at 2180, 1977, and 1914 $^{cm-1}$ are due to the $TpMn(CO)_2N_2$ complex.

With added THF, photolysis of a n-heptane solution of $TpMn(CO)_3$ with 1.9 M $HSiEt_3$ yields the initial low-wavenumber complex which completely converts to $TpMn(CO)_2(THF)$ within a few hundred microseconds (**Figure 6.12**). This observation suggests that the initial species contains an intact $TpMn(CO)_2$ unit with loosely coordinated silane that is displaced by the incoming THF ligand. This species is most likely either a metal C-H or Si-H coordinated π complex. Some C-H oxidative addition reactions proceed by way of a π complex, and more appropriately, such complexes have been observed on the ultrafast time scale in the $CpMn(CO)_3/HSiEt_3$

system.[185] In the present case, however, it is more likely that the loosely bound silane complex is a Si-H rather than C-H solvate.

Thus, when a n-heptane solution of $TpMn(CO)_3$ under identical conditions of [THF] but without added $HSiEt_3$ is photolyzed, only the $TpMn(CO)_2(THF)$ complex is observed. If C-H coordination of the ethyl group of the silane were occurring, we would expect to detect a C-H coordinated heptane complex on the same time scale, which is not observed. This conclusion is supported by DFT computations, which predict the ethyl C-H coordinated silane π complex to be 8.6 kcal/mol higher in energy (with ZPE and thermal corrections at 298.15 K) than the Si-H bound species.

Calculations suggest different modes of $HSiEt_3$ binding to the metal center in the Tp and Cp systems. As shown in **Figure 6.13**, for the Cp complex, a traditional η^2-type binding of the Si-H bond to the Mn center is predicted. Interestingly, however, for the Tp system a hydro-bridged type structure is preferred (/Mn-H-Si ~ 140^o). A comparable intermediate for the Cp system is unlikely, since it would be expected to convert to the stable piano-stool-type η^2 form in an almost barrierless reaction, as suggested by the ultrafast studies.[185] Attempts to theoretically model a hydro-bridged form of the Cp system were unsuccessful, as geometry optimizations collapse to the η^2 or $CpMn(CO)_2(H)(SiEt_3)$ complex. This difference in binding geometry is likely due to the strong preference for octahedral geometry in the Tp system, while the Cp complexes appear to exhibit more flexible structures.

As shown in **Figure 6.14**, a complete kinetic profile for the reaction of $TpMn(CO)_2(HSiEt_3)$ with THF was obtained. Similar to the case for the cyclooctene

system, k_{obs} shows a nonlinear dependence on [THF] and the reaction profile is consistent with a dissociative substitution pathway.

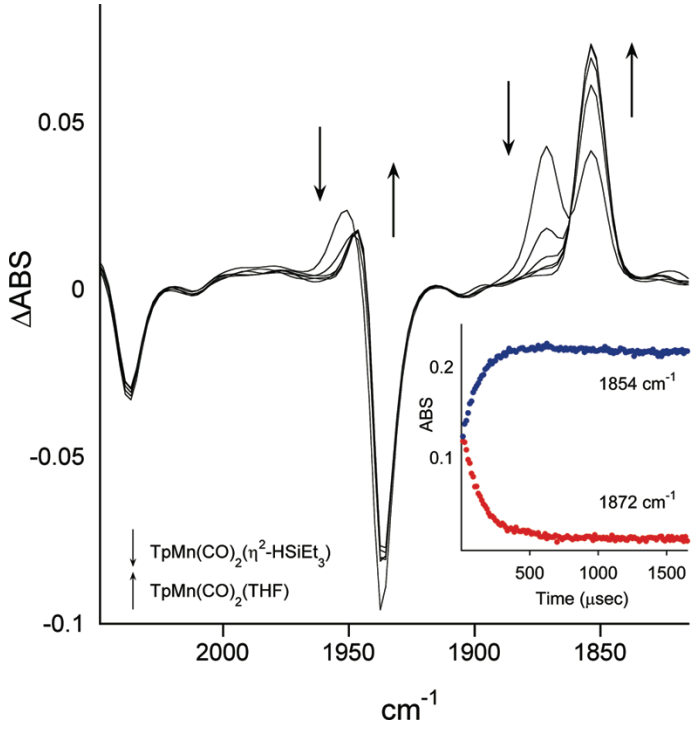

Figure 6.12. Reaction of the initially formed $TpMn(CO)_2(HSiEt_3)$ complex with THF at 295 K. Photolysis was conducted in the presence of $HSiEt_3$ (1.9 M) and THF (0.25 M) in n-heptane. Spectra were obtained 0, 122, 244, 366, 488, and 1000 μs after photolysis.

The relevant kinetic parameters are presented in **Table 6.2**. The temperature dependence of k_1 yields $\Delta H_1^{\ddagger} = 12.2 \pm 0.7$ kcal/mol and $\Delta S_1^{\ddagger} = +4 \pm 2$ e.u.Within experimental error, the invariance of the selectivity ratio k_2/k_{-1} with temperature suggests similar activation barriers for the reaction of the proposed TpMn- $(CO)_2$ intermediate with either THF or $HSiEt_3$. Assuming a fully dissociated transition state, the activation enthalpy is

expected to provide an estimate for the strength of the $TpMn(CO)_2$-($HSiEt_3$) π interaction and is in good agreement with a calculated value of 11.5 kcal/mol (see below). Using literature activation parameters for the displacement of $HSiEt_3$ from the $CpMn(CO)_2$ fragment,[186] $k_1(Tp)/k_1(Cp) \sim 10^8$ at 303 K. The faster rate for the Tp system is likely due in part to the different binding mode of the silane.

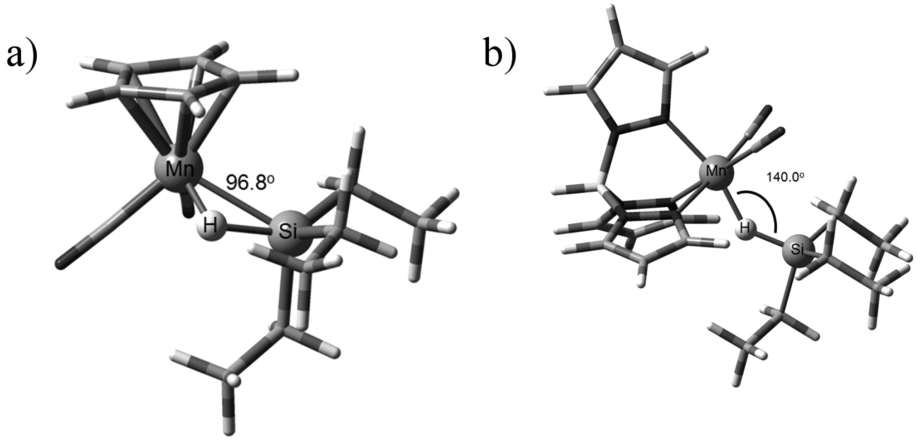

Figure 6.13. Calculated BVP86 geometries for (a) $CpMn(CO)_2(HSiEt_3)$ and (b) $TpMn(CO)_2(HSiEt_3)$.

(c). Theoretical Modeling of Bond Dissociation Energies/ Enthalpies. In agreement with the experimental findings, DFT calculations predict weaker binding of ligands such as $HSiEt_3$, cyclooctene, and THF to the metal center in the Tp relative to Cp complexes. In an attempt to deduce trends in binding versus ligand (X and L) characteristics, bond dissociation enthalpies were computed for X = Cp, Cp*, and Tp for a variety of ligands (L) related to this investigation. The computed BDEs are presented

in **Table 6.3**. Our theoretical values are within 4 kcal/ mol of all BDEs with known experimental determinations.

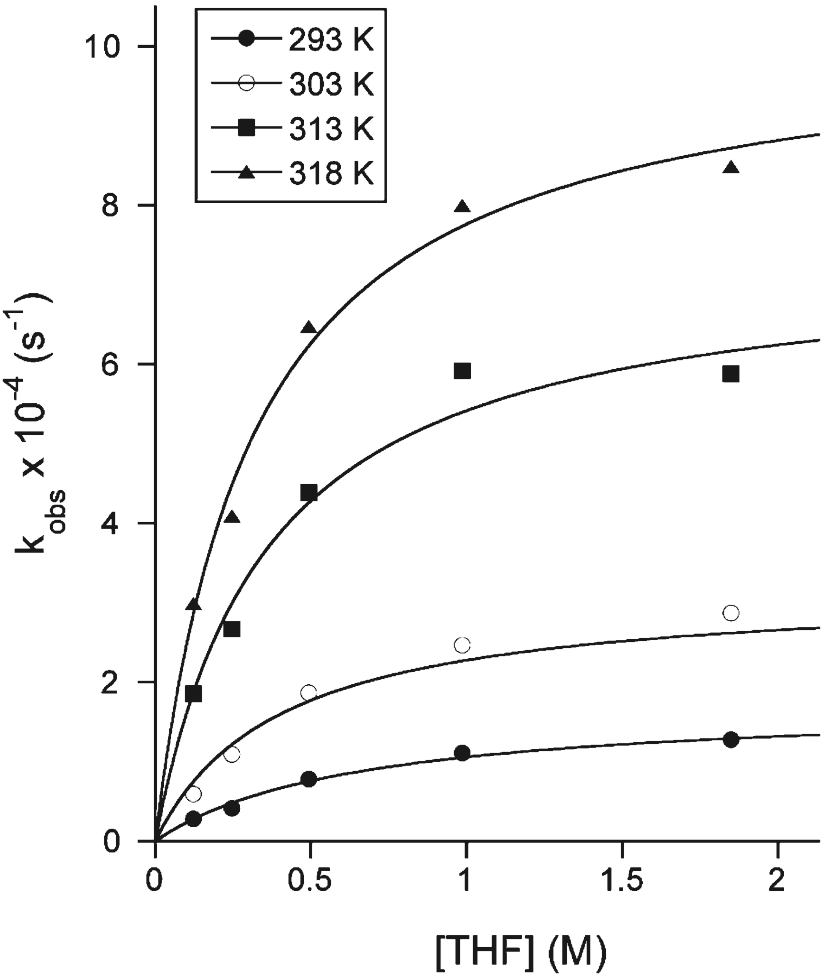

Figure 6.14. Plot of kobs vs [THF] at different temperatures for the displacement of $HSiEt_3$ from the $TpMn(CO)_2(HSiEt_3)$ complex by THF. The n-heptane solution was 1.9 M in $HSiEt_3$ with the appropriate amount of THF added. The limiting behavior of k_{obs} indicates a dissociative mechanism for the reaction.

On the basis of indirect experiments using photoacoustic calorimetry, Yang and co-workers report a lower bound of 54.8 kcal/mol for the gas-phase Mn-CO bond enthalpy

in $CpMn(CO)_3$.[186] Our computed value of 61.6 kcal/mol is in fair agreement with this reported experimental lower limit.

Table 6.3. Mn-L bond dissociation enthalpies in $XMn(CO)_2$-L complexes.[a] Bond dissociation enthalpies have been calculated using zero-point corrected energies and thermal enthalpy corrections at 298.15 K. All values are in kcal/mol and were obtained using the BVP86 functional.[b] Reference 32. [c] Reference 37. [d] Reference 35. [e] Reference 24. [f] This work.

L	X = Cp		X = Cp*	X = Tp	
	Theory	**Experimental**	**Theory**	**Theory**	**Experimental**
CO	61.6		60.6	48.1	
Triethylsilane	27.2	28.1[d]	23.0	11.5	12.2[f]
THF	22.5	24.0[b]	19.8	16.5	
Ethane	8.4	8.6[c]	6.2	2.9	
Cyclooctene	32.3	34.4	23.5	15.5	18.8[f]
Pyridine	34.6		31.8	28.9	
H_2	22.7		22.0	10.5	
N_2	35.1		35.0	26.2	
Ar	3.1		1.9	0.3	
ethylene				20.9	

The binding of ethane (a conformationally rigid approximation of n-heptane) is quite weak for both the Tp and Cp complexes, and the theoretical value of 8.4 kcal/mol for X = Cp is in good agreement with historical estimates of 8-10 kcal/mol for Mn-hydrocarbon interactions.[188,189] Overall, there does not seem to be a clear relationship between the flexibility or steric bulk of L and the corresponding binding enthalpies. Modifying the X ligand, however, does show some obvious trends. The triethylsilane BDE is most affected by changing X = Cp/Cp* to Tp. This is likely due to the change in bonding type of the $HSiEt_3$ ligand from an η^2coordination with X = Cp/Cp* to the hydrobridged coordination of X = Tp. An increase in the computed Mn-Si and terminal

Mn-H bond lengths shows correlation with slightly weaker binding capability when X = Cp* and with more substantial weakening for X = Tp. For $CpMn(CO)_2$-($HsiEt_3$), r_e (Mn-H) = 1.569 Å and re(Mn!Si) = 2.502 Å, in comparison to the Cp*Mn(CO)2(HsiEt3) values of re- (Mn!H) = 1.581 Å and r_e (Mn!Si) = 2.553 Å and TpMn-$(CO)_2$($HsiEt_3$) bond lengths of r_e (Mn-H) = 1.708 Å and r_e (Mn-Si) = 3.062 Å.

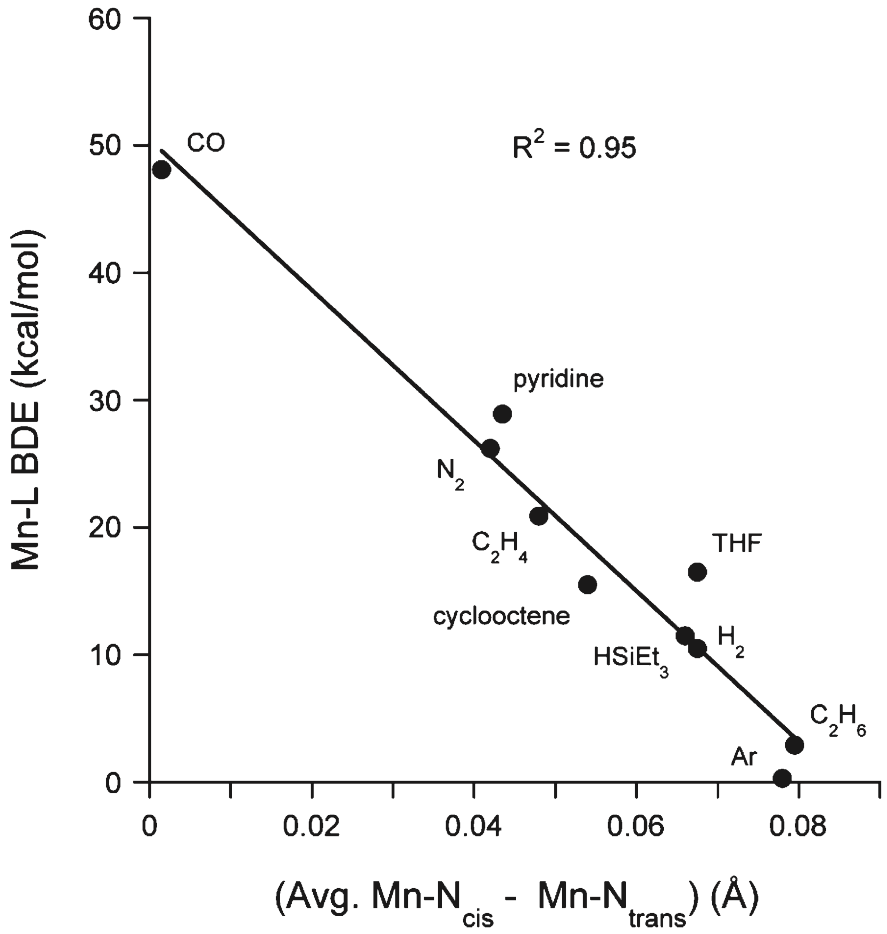

Figure 6.15. Relationship between the MnL bond dissociation enthalpy and the length of the MnN_{trans} bond relative to the average MnL_{cis} bond length in $TpMn(CO)_2L$ complexes.

Replacement of Cp with Cp* does not affect the Mn-L binding strengths for the smaller ligands L = N_2, H_2, CO, Ar. This observation is not surprising, since the binding of these small molecules is expected to be the least influenced by the larger steric bulk of the Cp* ligand. The similar BDEs do suggest, however, that the relatively better donor ability of Cp* compared to Cp does not impact the overall Mn-L bond strengths. As a reviewer suggested, the electronic differences between Cp and Cp* are not expected to significantly impact metal-ligand interactions unless the metal is highly electronegative, which is not the case here. The weaker binding of larger molecules such as cyclooctene and triethylsilane in the Cp* relative to the Cp system can then be attributed to steric effects. Unlike the Cp/Cp* system, even small-molecule binding enthalpies are considerably smaller for the Tp complexes. These findings suggest that the impact of electronic and steric factors upon ligand binding in the Tp system cannot easily be separated.

The weaker ligand binding to the $TpMn(CO)_2$ fragment may be a consequence of the octahedral geometry adopted by the complex, which places L trans to the nitrogen on one arm of the Tp ligand. Thus, if the pyrazolyl nitrogen exhibits a stronger trans influence than the other ligands studied here, weaker Mn-L binding is to be expected. In addition to square-planar complexes, structural trans effects in octahedral complexes have been well documented.[190] Since coordination of L results in a distortion of the Tp ligand relative to L = CO, the difference in the calculated average Mn-N_{cis} and Mn-N_{trans} bond lengths was evaluated as a function of the Mn-L binding enthalpies to isolate the influence of L upon the Mn-N_{trans} interaction. As shown in **Figure 6.15**, the data suggest

that a decrease in the Mn-L binding enthalpy is accompanied by a shortening of the Mn-N_{trans} bond relative to the Mn-N_{cis} interaction. Since for all ligands the Mn-N_{trans} bond is shorter than the average Mn-N_{cis} bond length, it is reasonable to suggest that the ligands investigated exhibit a trans influence weaker than that of CO. The crystal structure of the $TpTc(CO)_2(PPh_3)$ complex also exhibits a Tc-N_{trans} bond length that is 0.05 Å shorter than Tc-N_{cis}, which was attributed to the possible trans influence of the CO ligands.[191] This finding provides anecdotal evidence that the weaker ligand binding may be due, in part, to the adoption of an octahedral geometry in the Tp complexes and the resulting trans influence of the pyrazolyl nitrogen. In this regard it is important to note that if steric considerations were the primary factor in determining the stability of the $TpMn(CO)_2L$ complexes, then the results of the present study suggest that L = PR_3 complexes with bulky R groups would be relatively unstable.

However, a variety of $PzB(Pz)_3Mn(CO)_2PR_3$ (Pz = pyrazolyl) and $TpMe_2Mn(CO)_2PR_3$ complexes for R =C_6H_5, C_6H_{11},OC_6H_5 have been isolated and characterized.[192,193] It is therefore reasonable to conclude that both electronic and steric factors contribute to the overall trend in the Mn-L binding enthalpies in the Tp complexes relative to the Cp system and assessing the specific influence of each contribution is difficult.

Conclusions

The displacement of L = cyclooctene, $HSiEt_3$ from the respective photolytically generated $TpMn(CO)_2L$ complexes was studied. Like the analogous Cp complexes, substitution of these ligands from the Mn center proceeds by a dissociative mechanism. However, in dramatic contrast to the Cp system, the displacement rates are significantly higher. The cyclooctene and $HSiEt_3$ complexes react almost 10^{11} and 10^8 times faster, respectively, when Tp is the ancillary ligand. This difference in reactivity is a result of a significantly weaker $TpMn(CO)_2$-L interaction. In comparison to the Cp complexes, the ligand binding enthalpies are almost 50% lower, with kinetic analysis yielding estimates of 18.8 $\pm$ 1.0 kcal/mol and 12.2 $\pm$ 0.7 kcal/mol for the $TpMn(CO)_2$-cyclooctene and $TpMn(CO)_2$-$HSiEt_3$ bond enthalpies, respectively. The larger steric bulk of the Tp ligand is a factor in the weaker binding of the ligands. However, electronic effects also contribute to the difference in the ligand binding enthalpies, since DFT calculations confirm that small ligands such as CO, N_2, and H_2 are also bound significantly more weakly to the $TpMn(CO)_2$ fragment. The computational results are consistent with the experimental findings and predict different binding modes of the $HSiEt_3$ ligand to the Mn center in the Cp and Tp complexes. An η^2 interaction between the Si-H bond and the $CpMn(CO)_2$ fragment is predicted, whereas a Mn-H-$SiEt_3$ hydro-bridged type structure is calculated for the Tp complex, which is consistent with the octahedral enforcer role of the Tp ligand. On the basis of the successful calibration of computed CO vibrational stretching frequencies and good agreement of calculated BDEs with experiment for X =

Cp, Tp, theory can be used to design and validate characterization of novel ligands for $XMn(CO)_2L$ complexes.

VII. CONCLUSIONS

It is widely apparent that many benefits stand to be reaped from the utilization of cheap, renewable, and benign resources to produce materials such as plastic. A variety of factors affect this, including the implications of global warming due to CO_2 as a waste product, the non-renewable nature of the Earth's fossil fuel reserves, and the ever-rising cost of fossil fuels. In order to utilize conventionally unreactive molecules such as CO_2, metal catalysts such as the ones in this study are typically utilized.

The metal-catalyzed copolymerization of CO_2 and epoxides represents a potential source for polycarbonate material that can be produced on a large scale and can potentially utilize 100% renewable monomers by mass. Currently, only poly(ethylene carbonate) and poly(propylene carbonate) are produced industrially from CO_2 and epoxides. One major problem with the CO_2/epoxides coupling approach to polycarbonate synthesis is that the exact structure of BPAPC cannot be replicated, and in order to produce a polymer with similar properties it is necessary to closely copy this structure. Inherently, it is very difficult to synthesize a polycarbonate with a similarly useful structure from epoxides and CO_2. In order to someday achieve properties comparable to BPAPC, the discovery of new, useful monomers is necessary. At this point, the most-studied epoxides for CO_2 coupling are cyclohexene oxide, which yields a polycarbonate too brittle to be of use, and propylene oxide, which yields a useful polymer lacking thermal excellence. Recent advances in the Darensbourg laboratories have yielded poly(indene carbonate), the CO_2/epoxide-produced polycarbonate with the

highest T_g ever reported for this process at ~135 ^oC. Because more epoxides must be utilized to fully realize the potential of this polycarbonate production process, more active and selective catalysts must be developed.

This dissertation has initially focused on the (salan)CrX catalyst and its ability as a highly-active, selective catalyst for polycarbonate production from the coupling of CO_2 and epoxides. The (salan)Cr catalyst, when compared to the typical (salen)Cr catalyst, is more selective for polycarbonate production, allows near-quantitative CO_2 insertion into polymer evidenced by lack of ether-linkages, and shows an increased reactivity for aliphatic epoxides such as propylene oxide. (salan)CrX catalyzes living copolymerizations and can be used to incrementally synthesize block-terpolymers as evidenced by the synthesis of a poly(propylene carbonate)-block-poly(cyclohexylene carbonate)-block-poly(viny-cyclohexylene carbonate) terpolymer.

In using a catalyst such as (salan)CrX which can be used effectively to catalyze the coupling of multiple epoxides with CO_2, it is possible to synthesize random terpolymers by subjecting mixtures of epoxide to polymerization conditions. The process of terpolymerization can be used to synthesize a polycarbonate with tunable properties based on the mole fraction of epoxide used in the monomer feed. In addition, the reactivity of the individual epoxides in the monomer feed mixture can be influenced by the monomer mole fraction ratio. This leads to possibilities of increasing the reaction rate of inactive epoxides by including a typically more reactive epoxide, such as propylene or ethylene oxide. The reactivity ratios, determined through Fineman-Ross analysis, demonstrate a temperature dependence based on the presence of aliphatic

epoxides that are more likely to produce cyclic carbonate as a byproduct, *ie.* propylene oxide. Poly(cyclohexene carbonate) production becomes more favored as the temperature of terpolymerization is increased above room temperature.

Another topic explored in this dissertation is the copolymerization of epoxides with cyclic anhydrides to produce polyesters. This process is very robust, as evidenced by its ability to be run in much less scrupulously dry and air-free conditions than in the case of polycarbonate synthesis. Although polyesters inherently do not possess the level of thermal excellence associated with polycarbonates, the robustness of this process allows for an extra measure of creativity. Due to the wide availability of active monomers, it is possible to achieve a very wide range (>100 ^{o}C) of glass transition temperatures simply through proper monomer selection. The addition of bifunctional monomers as crosslinkers opens the door for a multitude of further modifications that can be made to the polymers, including the potential synthesis of a polymer with very useful properties being composed of renewable monomers over 90% by mass.

The metal-catalyzed copolymerization of cyclic anhydrides and epoxides proceeds *via* a chain-growth mechanism (with obtained PDIs typically around 1.1-1.3) which is desirable compared to the typical step-growth mechanism of polyester synthesis. Certain polyesters, such as the very useful poly(propylene fumarate), suffer from an extreme synthetic difficulty using the traditional step-growth synthesis. The anhydride/epoxide copolymerization process makes the synthesis of poly(propylene fumarate) much simpler, in addition to making it more effective at achieving higher molecular weights.

It is hopeful that this dissertation serves as an indicator that it is possible, through creativity and effective research, to synthesize materials from non-petroleum resources that are competitive with analogous petroleum-based polymers in terms of mechanical and thermal properties. In addition, the area of anhydride/epoxide copolymerization has been somewhat underutilized as a research topic as of late. Hopefully others will use this research as an example and expand and surpass what has been reported here in an attempt to create materials that will lessen mankind's reliance on fossil fuels.

The second part of this dissertation, which focused on FT-IR-based study of ligand substitution in manganese complexes, also serves as an example of the importance of fundamental chemical research. The mechanism of ligand substitution in (η^5-ligand)M(CO)$_x$ complexes has been historically attributed to the indenyl effect, although it has been proven that the effect is not necessarily the most energy-efficient pathway. Carbocycles such as the cyclopentadienyl (Cp) ligand have a destabilized reduced hapticity η^3 intermediate which makes the associative indenyl effect unobtainable. Complexes with stabilized η^3 intermediates typically have added functionality which helps to stabilize the ring-slipped structure, such as a heteroatom in the case of 2,5-dimethylpyrrole or the benzene ring to assist in dearomatization of indene. The kinetic studies presented in this dissertation have helped to elucidate this commonly referenced mechanism and determine that for the (DMP)Mn(CO)$_2$ fragment, an energy of ~34.0 kJ/mol is necessary to initiate the reduced hapticity "ring-slip" mechanism for ligand substitution.

It is also important to realize that FT-IR, while an excellent analytical tool, must be utilized with care. The trispyrazolyl borate (Tp) ligand, generally considered to be a simple electronic mimic of Cp, has been proven to cause different ligand stabilities for the $Cp(CO)_2$ fragment. Olefin substitution has been proven to occur as high 10^8 times faster than in $TpMn(CO)_2$ than in $CpMn(CO)_2$. This is because the increased diffuseness of the Mn orbitals in $TpMn(CO)_2$ cause the complex to be more stable for binding of what are typically considered to be weak ligands, such as THF. The $TpMn(CO)_2(THF)$ complex is in fact more stable than its olefin analogue, which is in stark contrast to the $CpMn(CO)_2$ fragment.

To conclude, it is hoped that this dissertation serves as an example of the importance of elucidation of catalytic mechanism when studying organometallic complexes. Kinetic and mechanistic studies, which can be performed using FT-IR as an analytical technique, yield very useful data regarded the reaction mechanism undergone by catalysts. Understanding of these mechanisms is paramount for understanding how to improve and optimize these catalytic systems.

REFERENCES

(1) Keeling, R. CO_2 Concentration at Mauna Loa Observatory, HI, Scripps Institution of Oceanography. (scrippsco2.ucsd.edu/). (accessed January 2012).

(2) Rohde, R. Atmospheric Transmission, Global Warming Art Project. (www.globalwarmingart.com/wiki/file:atmospheric_transmission_png) (accessed January 2012).

(3) Aresta, M. *Utilization of Greenhouse Gases* ACS Symposium Series; American Chemical Society, **2003.** *852*, 2–39.

(4) Xu; Moulijn, J. A. *Energy Fuels* **1996**, *10*, 305–325.

(5) Nashawi, I. S.; Malallah, A.; Al-Bisharah, M. *Energy Fuels* **2010**, *24*, 1788–1800.

(6) Anastas, P. *Green Catalysis*, Wiley-VCH; Weinheim, Germany, 2009.

(7) Tans P., Recent Mauna Loa CO_2, Earth System Research Laboratory: Global Monitoring Divison. (www.esrl.noaa.gov/gmd/ccgg/trends/). (accessed January 2012).

(8) Aresta, M.; Dibenedetto, A. *Dalton Trans.* **2007**, *28*, 2975–2992.

(9) Finney, B. Phase diagram of CO_2, Wikimedia Commons. (commons.wikimedia.org/wiki/file:carbon_dioxide_pressure-temperature_phase_diagram.svg). (accessed January 2012)

(10) Otsuka, E. Urea synthesis using excess ammonia. *United States Patent 3005849*. **1961**.

(11) Riduan, S. N.; Zhang, Y.; Ying, J. Y. *Angew. Chem., Int. Ed.* **2009**, *48*, 3322–3325.

(12) Taylor, D. K.; Keiper, J. S.; DeSimone, J. M. *Ind. Eng. Chem. Res.* **2002**, *41*, 4451–4459.

(13) Wai, C. M.; Hunt, F.; Ji, M.; Chen, X. *J. Chem. Educ.* **1998**, *75*, 1641.

(14) Omae, I. *Catal. Today* **2006**, *115*, 33–52.

(15) Sakakura, T.; Choi, J.-C.; Yasuda, H. *Chem. Rev.* **2007**, *107*, 2365–2387.

(16) Mathers, R.; Meier, M. *Green Polymerization Methods*; Wiley-VCH; Weinheim, Germany. 2011.

(17) Darensbourg, D. J.; Horn, A.; Moncada, A. I. *Green Chem. 12*, 1376–1379.

(18) Darensbourg, D. J.; Moncada, A. I.; Wei, S.-H. *Macromolecules 44*, 2568–2576.

(19) Darensbourg, D. J. *Chem. Rev.* **2007**, *107*, 2388–2410.

(20) Darensbourg, D. J.; Yarbrough, J. C. *J. Am. Chem. Soc.* **2002**, *124*, 6335–6342.

(21) Darensbourg, D. J.; Andreatta, J. R.; Moncada, A. I. Polymers from Carbon Dioxide: Polycarbonates, Polythiocarbonates, and Polyurethanes, from Carbon Dioxide as a Chemical Feedstock. Wiley-VCH Verlag GmbH & Co. KGaA; Weihnheim, Germany. 213–248.

(22) Darensbourg, D. J.; Stafford, N. W.; Katsurao, T. *J. Mol. Catal. A-Chemical.* **1995**, *104*, L1–L4.

(23) Thayer, A. *Chemical and Engineering News* **2012**, *90*, 11–12.

(24) Stephens, M. P. *Polymer Chemistry: An Introduction*. Oxford University Press; New York, 1999.

(25) Goldhaber, S. B.; Chessin, R. L. *Environ. Sci. Technol.* **1997**, *31*, 568A–573A.

(26) Lubick, N. *Environ. Sci. Technol.* **2009**, *43*, 3406.

(27) Chapin, R. E.; Adams, J.; Boekelhedie, K; Gray, L.E.; Hayward, S.W. et al. NTP-CERHR Expert Panel Report On The Reproductive And Developmntal Toxicity Of Bisphenol A; US Department of Health and Human Services, **2007**.

(28) Peeples, L. Toxic Chemical BPA Under Attack, But Alternatives May Not Be Safer, Experts Say. Huffington Post. (www.huffingtonpost.com/2012/02/23/toxic-chemical-bpa-alternatives_n_1297222.html). (accessed February 2012).

(29) *Phosgene.* Materials Safety Data Sheet No. G-67, The Boc Group, Murray Hill, NJ, (June 1) 1995, (159.121.82.250/CR2K_SubDB/MSDS/PHOSGENE.PDF). (Accessed January 2012).

(30) Sakakura, T.; Saito, Y.; Okano, M.; Choi, J.-C.; Sako, T. *J. Org. Chem.* **1998**, *63*, 7095–7096.

(31) Fan, G.-Z.; Zhao, H.-T.; Duan, Z.-X.; Fang, T.; Wan, M.-H.; He, L.-N. *Catal. Sci. Technol.* **2011**, *1*, 1138–1141.

(32) Koning, C.; Wildeson, J.; Parton, R.; Plum, B.; Steeman, P.; Darensbourg, D. J. *Polymer* **2001**, *42*, 3995–4004.

(33) Darensbourg, D. J.; Wilson, S. J. *J. Am. Chem. Soc.* **2011**, *133*, 18610–18613.

(34) Novomer Homepage. (www.novomer.com). (accessed January 2012).

(35) Ren, W.-M.; Liu, Y.; Wu, G.-P.; Liu, J.; Lu, X.-B. *J. Polym. Sci., Part A: Polym. Chem.* **2011**, *49*, 4894–4901.

(36) Wu, G.-P.; Wei, S.-H.; Lu, X.-B.; Ren, W.-M.; Darensbourg, D. J. *Macromolecules 43*, 9202–9204.

(37) Byrne, C. M.; Allen, S. D.; Lobkovsky, E. B.; Coates, G. W. *J. Am. Chem. Soc.* **2004**, *126*, 11404–11405.

(38) Liu, Q.; Zou, Y.; Bei, Y.; Qi, G.; Meng, Y. *Mater. Lett.* **2008**, *62*, 3294–3296.

(39) Darensbourg, D. J.; Moncada, A. I.; Wei, S.-H. *Macromolecules 44*, 2568–2576.

(40) Inoue, S.; Koinuma, H.; Tsuruta, T. *J. Polym. Sci., Part B: Polym. Lett.* **1969**, *7*, 287–292.

(41) Aida, T.; Inoue, S. *J. Am. Chem. Soc.* **1985**, *107*, 1358–1364.

(42) Cheng, M.; Moore, D. R.; Reczek, J. J.; Chamberlain, B. M.; Lobkovsky, E. B.; Coates, G. W. *J. Am. Chem. Soc.* **2001**, *123*, 8738–8749.

(43) Brule, E.; Guo, J.; Coates, G. W.; Thomas, C. M. *Macromol. Rapid Commun.* **2011**, *32*, 169–185.

(44) Coates, G. W.; Moore, D. R. *Angew. Chem., Int. Ed.* **2004**, *43*, 6618–6639.

(45) Darensbourg, D. J.; Ulusoy, M.; Karroonnirum, O.; Poland, R. R.; Reibenspies, J. H.; Cetinkaya, B. *Macromolecules* **2009**, *42*, 6992–6998.

(46) Li, B.; Wu, G.-P.; Ren, W.-M.; Wang, Y.-M.; Rao, D.-Y.; Lu, X.-B. *J. Polym. Sci., Part A: Polym. Chem.* **2008**, *46*, 6102–6113.

(47) Darensbourg, D. J.; Yarbrough, J. C.; Ortiz, C.; Fang, C. C. *J. Am. Chem. Soc.* **2003**, *125*, 7586–7591.

(48) Nakano, K.; Kamada, T.; Nozaki, K. *Angew. Chem., Int. Ed.* **2006**, *45*, 7274–7277.

(49) Seong, J. E.; Na, S. J.; Cyriac, A.; Kim, B.-W.; Lee, B. Y. *Macromolecules* **2009**, *43*, 903–908.

(50) Luinstra, G. A. *Polym. Rev.* **2008**, *48*, 192–219.

(51) Shi, L.; Lu, X.-B.; Zhang, R.; Peng, X.-J.; Zhang, C.-Q.; Li, J.-F.; Peng, X.-M. *Macromolecules* **2006**, *39*, 5679–5685.

(52) Sujith, S.; Min, J. K.; Seong, J. E.; Na, S. J.; Lee, B. Y. *Angewandte Chemie-International Edition* **2008**, *47*, 7306–7309.

(53) Fineman, M.; Ross, S. D. *Journal of Polymer Science* **1950**, *5*, 259–262.

(54) Sax, L. *Environ. Health Perspect.* **2010**, *118*, 445–448.

(55) Inoue, S.; Kitamura, K.; Tsuruta, T. *Makromol. Chem.* **1969**, *126*, 250–65.

(56) Fischer, R. F. *J. Polym. Sci.* **1960**, *44*, 155–172.

(57) Lukaszczyk, J.; Jaszcz, K. *React. Funct. Polym.* **2000**, *43*, 25–32.

(58) Chen, X.; Zhang, Y.; Shen, Z. *Chin. J. Polym. Sci.* **1997**, *15*, 262–272.

(59) Hua, Z.; Qi, G.; Chen, S. *J. Appl. Polym. Sci.* **2004**, *93*, 1788–1792.

(60) DiCiccio, A. M.; Coates, G. W. *J. Am. Chem. Soc.* **2011**, *133*, 10724–10727.

(61) Huijser, S.; HosseiniNejad, E.; Sablong, R.; de, J.; Koning, C. E.; Duchateau, R. *Macromolecules* **2011**, *44*, 1132–1139.

(62) Jeske, R. C.; Rowley, J. M.; Coates, G. W. *Angew. Chem., Int. Ed.* **2008**, *47*, 6041–6044.

(63) Kasper, F. K.; Tanahashi, K.; Fisher, J. P.; Mikos, A. G. *Nat. Protoc.* **2009**, *4*, 518–525.

(64) Elschenbroich, C. *Organometallics*; Wiley-VCH; Weinheim, Germany, 2006.

(65) Wilkinson, G.; Rosenblum, M.; Whiting, M. C.; Woodward, R. B. *J. Am. Chem. Soc.* **1952**, *74*, 2125–2126.

(66) Dunitz, J. D.; Orgel, L. E.; Rich, A. *Acta Crystallogr.* **1956**, *9*, 373–375.

(67) Angelici, R. J.; Loewen, W. *Inorg. Chem.* **1967**, *6*, 682–686.

(68) Basolo, F. *J. Organomet. Chem.* **1990**, *383*, 579–86.

(69) Andreatta, J. R.; Cieslinski, G. B.; Batool, M.; Sun, X. Z.; George, M. W.; et al. *Inorg. Chem.* **2009**, *48*, 7787–7793.

(70) Swennenhuis, B. H. G.; Poland, R.; DeYonker, N. J.; Webster, C. E.; Darensbourg, D. J.; Bengali, A. A. *Organometallics* **2011**, *30*, 3054–3063.

(71) Bengali, A. A.; Fan, W. Y. *Organometallics* **2008**, *27*, 5488–5493.

(72) Basolo, F. *Coord. Chem. Rev.* **1982**, *43*, 7–15.

(73) Ji, L. N.; Rerek, M. E.; Basolo, F. *Organometallics* **1984**, *3*, 740–745.

(74) Schuster-Woldan, H. G.; Basolo, F. *J. Am. Chem. Soc.* **1966**, *88*, 1657–1663.

(75) Kershner, D. L.; Basolo, F. *J. Am. Chem. Soc.* **1987**, *109*, 7396–7402.

(76) Kershner, D. L.; Rheingold, A. L.; Basolo, F. *Organometallics* **1987**, *6*, 196–198.

(77) Calhorda, M. J.; Romao, C. C.; Veiros, L. F. *Chem. Eur. J.* **2002**, *8*, 868–875.

(78) Becker, E.; Pavlik, S.; Kirchner, K. *Adv. Organomet. Chem.* **2008**, *56*, 155–197.

(79) Darensbourg, D. J.; Mackiewicz, R. M.; Phelps, A. L.; Billodeaux, D. R. *Acc. Chem. Res.* **2004**, *37*, 836–844.

(80) Darensbourg, D. J.; Fitch, S. B. *Inorg. Chem.* **2007**, *46*, 5474–5476.

(81) Darensbourg, D. J.; Fitch, S. B. *Inorg. Chem.* **2008**, *47*, 11868–11878.

(82) Balsells, J.; Carroll, P. J.; Walsh, P. J. *Inorg. Chem.* **2001**, *40*, 5568–5574.

(83) Demadis, K. D.; Meyer, T. J.; White, P. S. *Inorg. Chem.* **1998**, *37*, 3610–3619.

(84) Casiraghi, G.; Casnati, G.; Puglia, G.; Sartori, G.; Terenghi, G. *J. Chem. Soc., Perkin Trans. 1* **1980**, 1862–5.

(85) Darensbourg, D. J.; Mackiewicz, R. M.; Rodgers, J. L.; Fang, C. C.; Billodeaux, D. R.; Reibenspies, J. H. *Inorg. Chem.* **2004**, *43*, 6024–6034.

(86) Tshuva, E. Y.; Goldberg, I.; Kol, M. *J. Am. Chem. Soc.* **2000**, *122*, 10706–10707.

(87) Davidson, M. G.; O'Hara, C. T.; Jones, M. D.; Keir, C. G.; Mahon, M. F.; Kociok-Koehn, G. *Inorg. Chem.* **2007**, *46*, 7686–7688.

(88) Clegg, W.; Davidson, M. G.; Graham, D. V.; Griffen, G.; Jones, M. D.; Kennedy, A. R.; O'Hara, C. T.; Russo, L.; Thomson, C. M. *Dalton Trans.* **2008**, 1295–1301.

(89) Peri, D.; Meker, S.; Shavit, M.; Tshuva, E. Y. *Chem.--Eur. J.* **2009**, *15*, 2403–2415.

(90) Xiao, Y.; Wang, Z.; Ding, K. *Macromolecules* **2006**, *39*, 128–137.

(91) Cohen, C. T.; Chu, T.; Coates, G. W. *J. Am. Chem. Soc.* **2005**, *127*, 10869–10878.

(92) Leighton, J. L.; Jacobsen, E. N. *J. Org. Chem.* **1996**, *61*, 389–390.

(93) Darensbourg, D. J.; Moncada, A. I. *Inorg. Chem.* **2008**, *47*, 10000–10008.

(94) Hormnirun, P.; Marshall, E. L.; Gibson, V. C.; White, A. J. P.; Williams, D. J. *J. Am. Chem. Soc.* **2004**, *126*, 2688–2689.

(95) Ren, W.-M.; Liu, Z.-W.; Wen, Y.-Q.; Zhang, R.; Lu, X.-B. *J. Am. Chem. Soc.* **2009**, *131*, 11509–11518.

(96) Chisholm, M. H.; Zhou, Z. *J. Mater. Chem.* **2004**, *14*, 3081–3092.

(97) Sugimoto, H.; Inoue, S. *J. Polym. Sci., Part A: Polym. Chem.* **2004**, *42*, 5561–5573.

(98) Nakano, K.; Hashimoto, S.; Nozaki, K. *Chem. Sci.* **2010**, *1*, 369–373.

(99) Kember, M. R.; Buchard, A.; Williams, C. K. *Chem. Commun.* **2011**, *47*, 141–163.

(100) Klaus, S.; Lehenmeier, M. W.; Anderson, C. E.; Rieger, B. *Coord. Chem. Rev.* **2011**, *255*, 1460–1479.

(101) Darensbourg, D. J.; Kudaroski, R. A. *Adv. Organomet. Chem.* **1983**, *22*, 129–68.

(102) Leitner, W. *Coord. Chem. Rev.* **1996**, *153*, 257–284.

(103) Gibson, D. H. *Chem. Rev.* **1996**, *96*, 2063–2095.

(104) Louie, J.; Gibby, J. E.; Farnworth, M. V.; Tekavec, T. N. *J. Am. Chem. Soc.* **2002**, *124*, 15188–15189.

(105) Takimoto, M.; Nakamura, Y.; Kimura, K.; Mori, M. *J. Am. Chem. Soc.* **2004**, *126*, 5956–5957.

(106) Takaya, J.; Iwasawa, N. *J. Am. Chem. Soc.* **2008**, *130*, 15254–15255.

(107) Boogaerts, I. I. F.; Nolan, S. P. *J. Am. Chem. Soc.* **2010**, *132*, 8858–8859.

(108) Urakawa, A.; Jutz, F.; Laurenczy, G.; Baiker, A. *Chem.--Eur. J.* **2007**, *13*, 3886–3899.

(109) Jessop, P. G.; Joo, F.; Tai, C.-C. *Coord. Chem. Rev.* **2004**, *248*, 2425–2442.

(110) Getty, A. D.; Tai, C.-C.; Linehan, J. C.; Jessop, P. G.; Olmstead, M. M.; Rheingold, A. L. *Organometallics* **2009**, *28*, 5466–5477.

(111) Darensbourg, D. J.; Wildeson, J. R.; Yarbrough, J. C.; Reibenspies, J. H. *J. Am. Chem. Soc.* **2000**, *122*, 12487–12496.

(112) Quan, Z.; Min, J.; Zhou, Q.; Xie, D.; Liu, J.; Wang, X.; Zhao, X.; Wang, F. *Macromol. Symp.* **2003**, *195*, 281–286.

(113) Ren, W.-M.; Zhang, X.; Liu, Y.; Li, J.-F.; Wang, H.; Lu, X.-B. *Macromolecules* **2010**, *43*, 1396–1402.

(114) Eno, S.; Egami, H.; Uchida, T.; Katsuki, T. *Chem. Lett.* **2008**, *37*, 632–633.

(115) Matsumoto, K.; Saito, B.; Katsuki, T. *Chem Commun.* **2007**, 3619–3627.

(116) Darensbourg, D. J.; Frantz, E. B.; Andreatta, J. R. *Inorg. Chim. Acta* **2007**, *360*, 523–528.

(117) Darensbourg, D. J.; Rodgers, J. L.; Mackiewicz, R. M.; Phelps, A. L. *Catal. Today* **2004**, *98*, 485–492.

(118) Gao, L. J.; Xiao, M.; Wang, S. J.; Meng, Y. Z. *J. Appl. Polym. Sci.* **2008**, *108*, 1037–1043.

(119) Gao, L. J.; Du, F. G.; Xiao, M.; Wang, S. J.; Meng, Y. Z. *J. Appl. Polym. Sci.* **2008**, *108*, 3626–3631.

(120) Darensbourg, D. J.; Holtcamp, M. W. *Macromolecules* **1995**, *28*, 7577–7579.

(121) Cherian, A. E.; Sun, F. C.; Sheiko, S. S.; Coates, G. W.*J. Am. Chem. Soc.* **2007**, *129*, 11350–11351.

(122) Liu, B.; Gao, Y.; Zhao, X.; Yan, W.; Wang, X. *J. Polym. Sci., Part A: Polym. Chem.* **2010**, *48*, 359–365.

(123) Darensbourg, D. J.; Fang, C. C.; Rodgers, J. L. *Organometallics* **2004**, *23*, 924–927.

(124) Williams, C. K.; Hillmyer, M. A. *Polym. Rev.* **2008**, *48*, 1–10.

(125) Lenz, R. W.; Marchessault, R. H. *Biomacromolecules* **2005**, *6*, 1–8.

(126) Maeda, Y.; Nakayama, A.; Kawasaki, N.; Hayashi, K.; Aiba, S.; Yamamoto, N. *Polymer* **1997**, *38*, 4719–4725.

(127) Jeske, R. C.; DiCiccio, A. M.; Coates, G. W. *J. Am. Chem. Soc.* **2007**, *129*, 11330–11331.

(128) Darensbourg, D. J. *Adv. Organomet. Chem.* **1982**, *21*, 113–150.

(129) Howell, J. A. S.; Burkinshaw, P. M. *Chem. Rev.* **1983**, *83*, 557–599.

(130) Cornils, B.; Herrmann, W. A. *J. Catal.* **2003**, *216*, 23–31.

(131) O'Connor, J. M.; Casey, C. P. *Chem. Rev.* **1987**, *87*, 307–318.

(132) Veiros, L. F. *Organometallics* **2000**, *19*, 3127–3136.

(133) Ji, L. N.; Kershner, D. L.; Rerek, M. E.; Basolo, F. *J. Organomet. Chem.* **1985**, *296*, 83–94.

(134) Marder, T. B.; Roe, D. C.; Milstein, D. *Organometallics* **1988**, *7*, 1451–1453.

(135) Borrini, A.; Diversi, P.; Ingrosso, G.; Lucherini, A.; Serra, G. *J. Mol. Catal.* **1985**, *30*, 181–195.

(136) Foo, T.; Bergman, R. G. *Organometallics* **1992**, *11*, 1801–1810.

(137) Schmid, M. A.; Alt, H. G.; Milius, W. *J. Organomet. Chem.* **1996**, *514*, 45–49.

(138) Llinas, G. H.; Day, R. O.; Rausch, M. D.; Chien, J. C. W. *Organometallics* **1993**, *12*, 1283–1288.

(139) Garrett, C. E.; Fu, G. C. *J. Org. Chem.* **1998**, *63*, 1370–1371.

(140) McFarlane, K. L.; Lee, B.; Fu, W.; van, E.; Ford, P. C. *Organometallics* **1998**, *17*, 1826–1834.

(141) Chin, R. M.; Baird, B.; Jarosh, M.; Rassman, S.; Barry, B.; Jones, W. D. *Organometallics* **2003**, *22*, 4829–4832.

(142) Wax, M. J.; Bergman, R. G. *J. Am. Chem. Soc.* **1981**, *103*, 7028–7030.

(143) Lugovskoy, S.; Lin, J.; Schultz, R. H. *Dalton Trans.* **2003**, 3103–3110.

(144) Bengali, A. A.; Fan, W. Y.; Abdulrazak, K. T. *Organometallics* **2009**, *28*, 3123–3128.

(145) Bengali, A. A. *Organometallics* **2000**, *19*, 4000–4003.

(146) Coleman, J. E.; Dulaney, K. E.; Bengali, A. A. *J. Organomet. Chem.* **1999**, *572*, 65–71.

(147) Angelici, R. J.; Loewen, W. *Inorg. Chem.* **1967**, *6*, 682–686.

(148) Becke, A. D. *J. Chem. Phys.* **1993**, *98*, 5648–5652.

(149) Lee, C.; Yang, W.; Parr, R. G. *Phys. Rev. B: Condens. Matter* **1988**, *37*, 785–789.

(150) Schultz, R. H. *Int. J. Chem. Kinet.* **2004**, *36*, 427–433.

(151) Pyshnograeva, N. I.; Setkina, V. N.; Andrianov, V. G.; Struchkov, Y. T.; Kursanov, D. N. *J. Organomet. Chem.* **1978**, *157*, 431–436.

(152) Creaven, B. S.; Dixon, A. J.; Kelly, J. M.; Long, C.; Poliakoff, M. *Organometallics* **1987**, *6*, 2600–2605.

(153) Kershner, D. L.; Rheingold, A. L.; Basolo, F. *Organometallics* **1987**, *6*, 196–198.

(154) Yang, P. F.; Yang, G. K. *J. Am. Chem. Soc.* **1992**, *114*, 6937–6938.

(155) Hester, D. M.; Sun, J.; Harper, A. W.; Yang, G. K. *J. Am. Chem. Soc.* **1992**, *114*, 5234–5240.

(156) Trofimenko, S. *Chem. Rev.* **1993**, *93*, 943–980.

(157) Trofimenko, S. *Accounts Chem. Res.* **1971**, *4*, 17–22.

(158) Trofimenko, S. *J. Am. Chem. Soc.* **1967**, *89*, 3170–3177.

(159) Tellers, D. M.; Skoog, S. J.; Bergman, R. G.; Gunnoe, T. B.; Harman, W. D. *Organometallics* **2000**, *19*, 2428–2432.

(160) Besora, M.; Vyboishchikov, S. F.; Lledos, A.; Maseras, F.; Carmona, E.; Poveda, M. L. *Organometallics* **2010**, *29*, 2040–2045.

(161) Bergman, R. G.; Cundari, T. R.; Gillespie, A. M.; Gunnoe, T. B.; Harman, W. D.; Klinckman, T. R.; Temple, M. D.; White, D. P. *Organometallics* **2003**, *22*, 2331–2337.

(162) Tellers, D. M.; Bergman, R. G. *J. Am. Chem. Soc.* **2000**, *122*, 954–955.

(163) Beach, N. J.; Williamson, A. E.; Spivak, G. J. *J. Organomet. Chem.* **2005**, *690*, 4640–4647.

(164) Curtis, M. D.; Shiu, K. B.; Butler, W. M. *J. Am. Chem. Soc.* **1986**, *108*, 1550–1561.

(165) Curtis, M. D.; Shiu, K. B. *Inorg. Chem.* **1985**, *24*, 1213–1218.

(166) Curtis, M. D.; Shiu, K. B.; Butler, W. M. *Organometallics* **1983**, *2*, 1475–1477.

(167) Piper, T. S.; Wilkinson, G. *J. Inorg. Nucl. Chem.* **1956**, *3*, 104–124.

(168) Ruba, E.; Simanko, W.; Mereiter, K.; Schmid, R.; Kirchner, K. *Inorg Chem* **2000**, *39*, 382–384.

(169) Dickinson, P. W.; Girolami, G. S. *Inorg. Chem.* **2006**, *45*, 5215–5224.

(170) Caulton, K. G. *Coord. Chem. Rev.* **1981**, *38*, 1–43.

(171) Cowan, A. J.; Poritus, P.; Kawanami, H. K.; Jina, O. S.; Grills, D. C.; Sun, X.-Z.; McMaster, J.; George, M. W. *Proc. Natl. Acad. Sci. U. S. A.* **2007**, *104*, 6933–6938.

(172) Trofimenko, S. *J. Amer. Chem. Soc.* **1969**, *91*, 588–595.

(173) Joachim, J. E.; Apostolidis, C.; Kanellakopulos, B.; Maier, R.; Marques, N.; Meyer, D.; Mueller, J.; Pires, de M.; Nuber, B.; et, al. *J. Organomet. Chem.* **1993**, *448*, 119–129.

(174) Becke, A. D. *Phys. Rev. A: Gen. Phys.* **1988**, *38*, 3098–3100.

(175) Perdew, J. P.; Zunger, A. *Phys. Rev. B: Condens. Matter* **1981**, *23*, 5048–5079.

(176) Vosko, S. H.; Wilk, L.; Nusair, M. *Can. J. Phys.* **1980**, *58*, 1200–1211.

(177) Hay, P. J.; Wadt, W. R. *J. Chem. Phys.* **1985**, *82*, 299–310.

(178) Couty, M.; Hall, M. B. *J. Comput. Chem.* **1996**, *17*, 1359–1370.

(179) Hariharan, P. C.; Pople, J. A. *Theor. Chim. Acta* **1973**, *28*, 213–222.

(180) Cotton, F. A.; Kraihanzel, C. S. *J. Am. Chem. Soc.* **1962**, *84*, 4432–4438.

(181) Gunnoe, T. B.; Sabat, M.; Harman, W. D. *J. Am. Chem. Soc.* **1998**, *120*, 8747–8754.

(182) Casey, C. P.; Rutter, E. W. *J. Am. Chem. Soc.* **1989**, *111*, 8917–8919.

(183) Bengali, A. A.; Mezick, B. K.; Hart, M. N.; Fereshteh, S. *Organometallics* **2003**, *22*, 5436–5440.

(184) Farrugia, L. J.; Evans, C.; Lentz, D.; Roemer, M. *J. Am. Chem. Soc.* **2009**, *131*, 1251–1268.

(185) Yang, H.; Asplund, M. C.; Kotz, K. T.; Wilkens, M. J.; Frei, H.; Harris, C. B. *J. Am. Chem. Soc.* **1998**, *120*, 10154–10165.

(186) Hester, D. M.; Sun, J.; Harper, A. W.; Yang, G. K. *J. Am. Chem. Soc.* **1992**, *114*, 5234–5240.

(187) Yang, J.; N'Guessan, B. R.; Dedieu, A.; Grills, D. C.; Sun, X.-Z.; George, M. W. *Organometallics* **2009**, *28*, 3113–3122.

(188) Ishikawa, Y.; Brown, C. E.; Hackett, P. A.; Rayner, D. M. *Chem. Phys. Lett.* **1988**, *150*, 506–510.

(189) Klassen, J. K.; Selke, M.; Sorensen, A. A.; Yang, G. K. *J. Am. Chem. Soc.* **1990**, *112*, 1267–1268.

(190) Coe, B. J.; Glenwright, S. J. *Coord. Chem. Rev.* **2000**, *203*, 5–80.

(191) Alberto, R.; Herrmann, W. A.; Kiprof, P.; Baumgaertner, F. *Inorg. Chem.* **1992**, *31*, 895–899.

(192) Schoenberg, A. R.; Anderson, W. P. *Inorg. Chem.* **1972**, *11*, 85–87.

(193) Joachim, J. E.; Apostolidis, C.; Kanellakopulos, B.; Meyer, D.; Nuber, B.; Raptis, K.; Rebizant, J.; Ziegler, M. L. *J. Organomet. Chem.* **1995**, *492*, 199–210.

APPENDIX A

SUPPLEMENTARY ^{1}H NMR DATA FOR CHAPTER IV

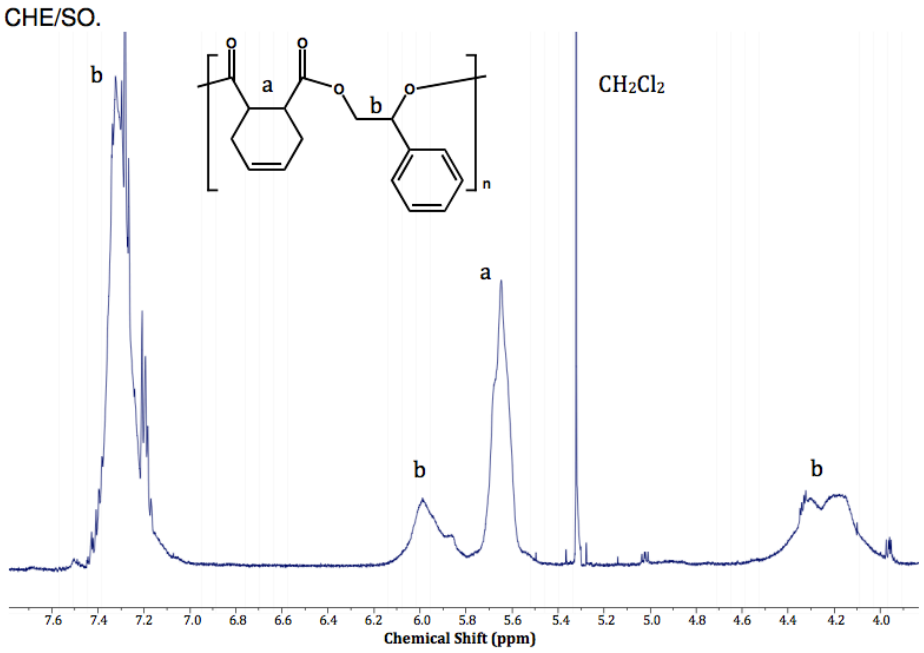

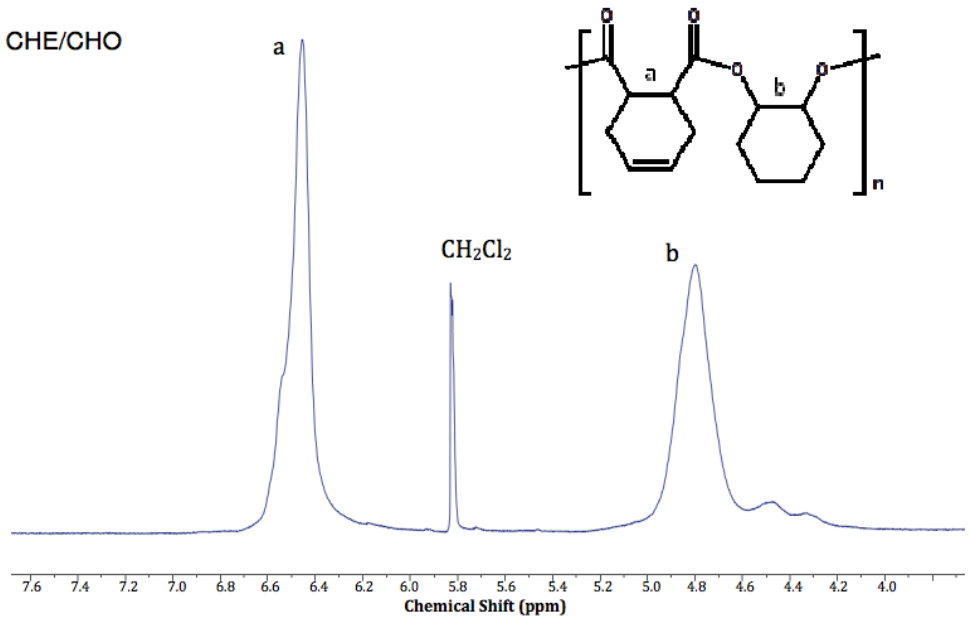

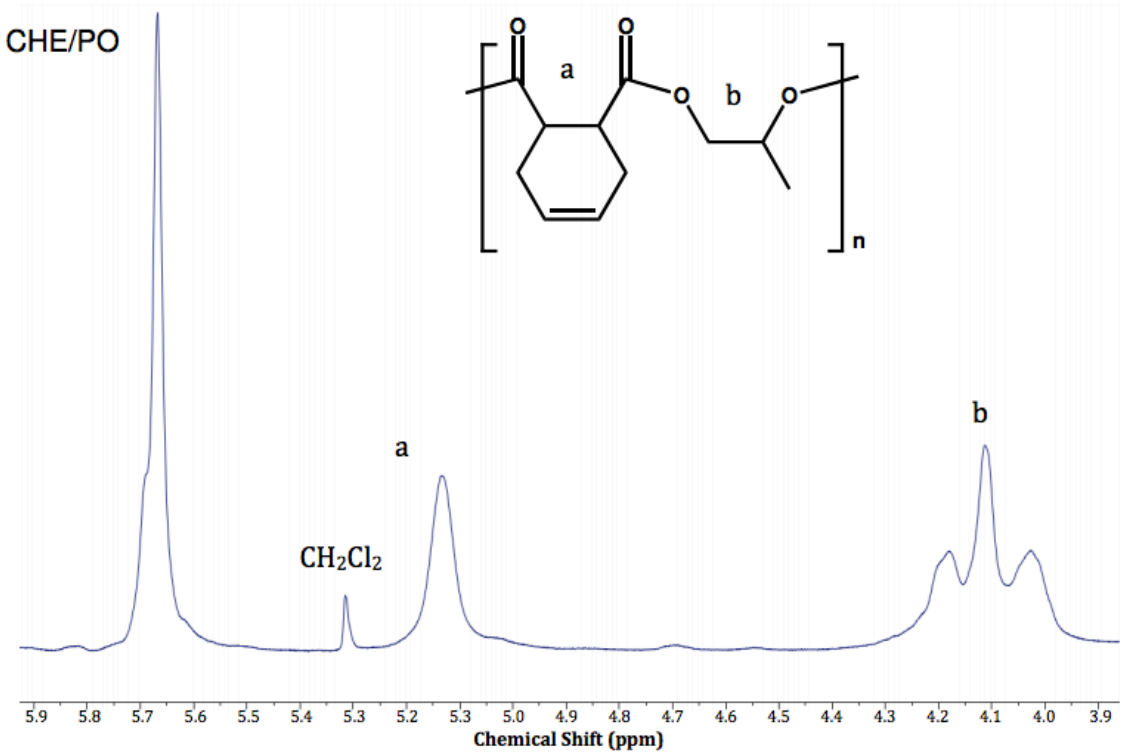
CHE/PO
a
b
n
a
b
CH_2Cl_2
5.9 5.8 5.7 5.6 5.5 5.4 5.3 5.2 5.3 5.0 4.9 4.8 4.7 4.6 4.5 4.4 4.3 4.2 4.1 4.0 3.9
Chemical Shift (ppm)

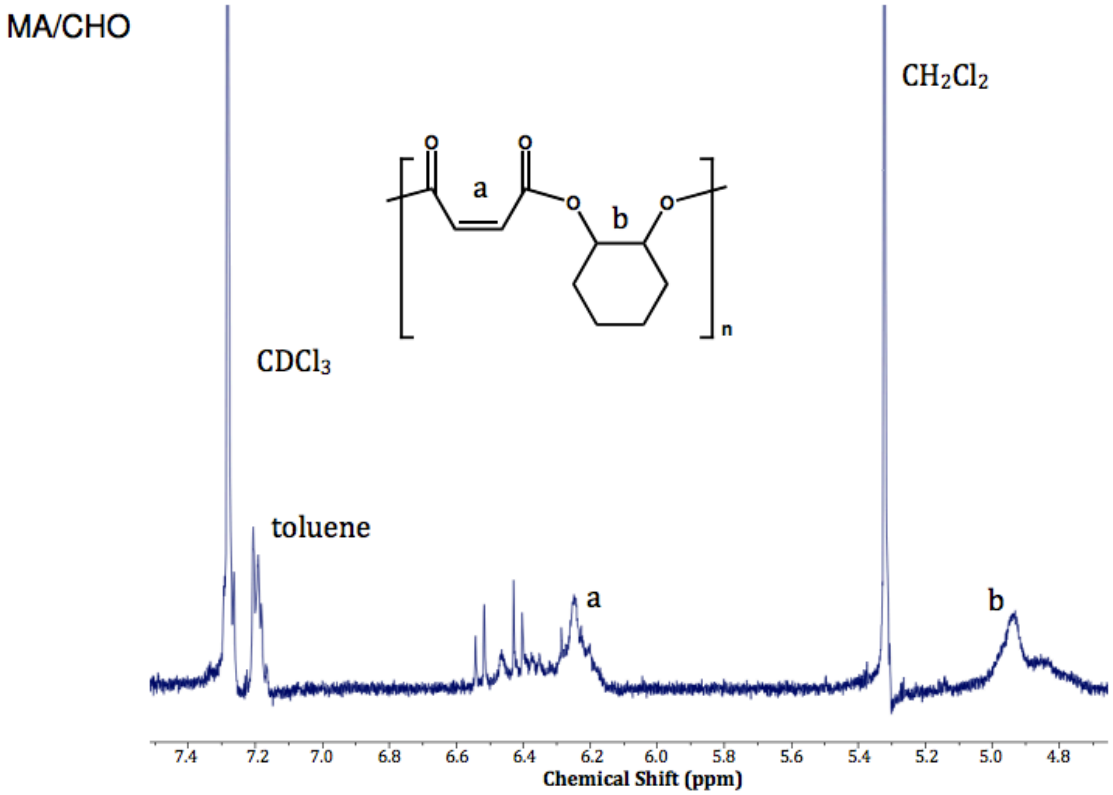
MA/CHO
a
b
n
CH_2Cl_2
$CDCl_3$
toluene
a
b
7.4 7.2 7.0 6.8 6.6 6.4 6.2 6.0 5.8 5.6 5.4 5.2 5.0 4.8
Chemical Shift (ppm)

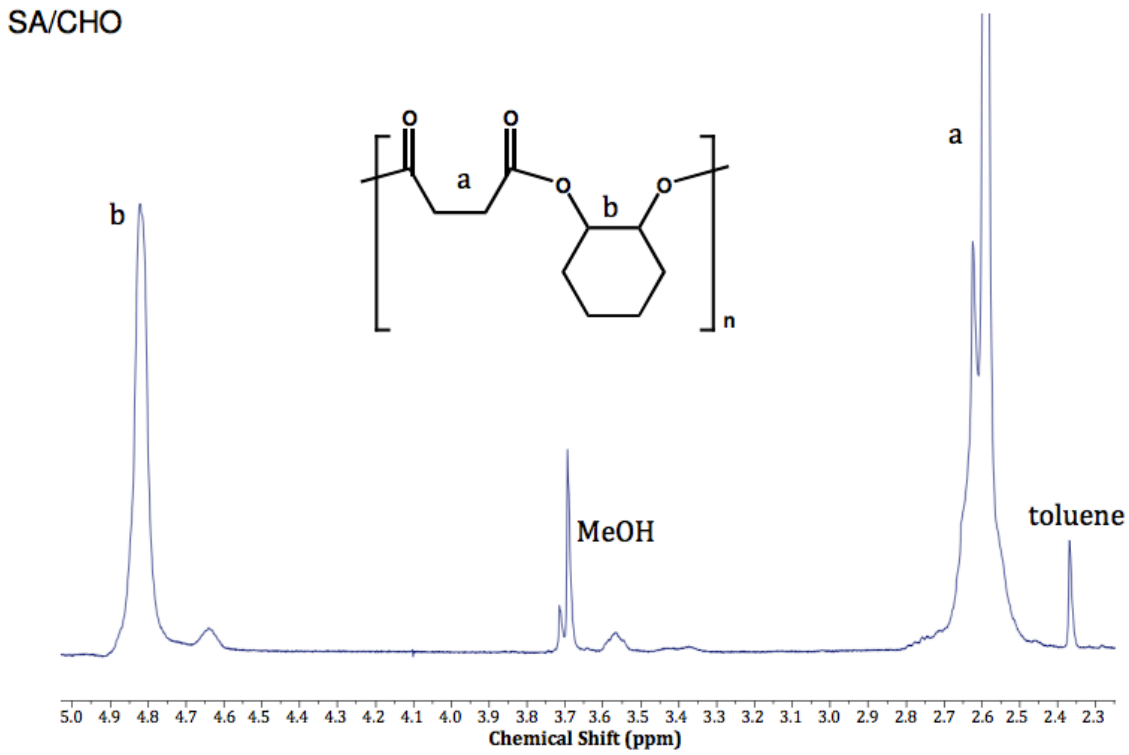
SA/CHO
b
a
b
MeOH
toluene
5.0 4.9 4.8 4.7 4.6 4.5 4.4 4.3 4.2 4.1 4.0 3.9 3.8 3.7 3.6 3.5 3.4 3.3 3.2 3.1 3.0 2.9 2.8 2.7 2.6 2.5 2.4 2.3
Chemical Shift (ppm)

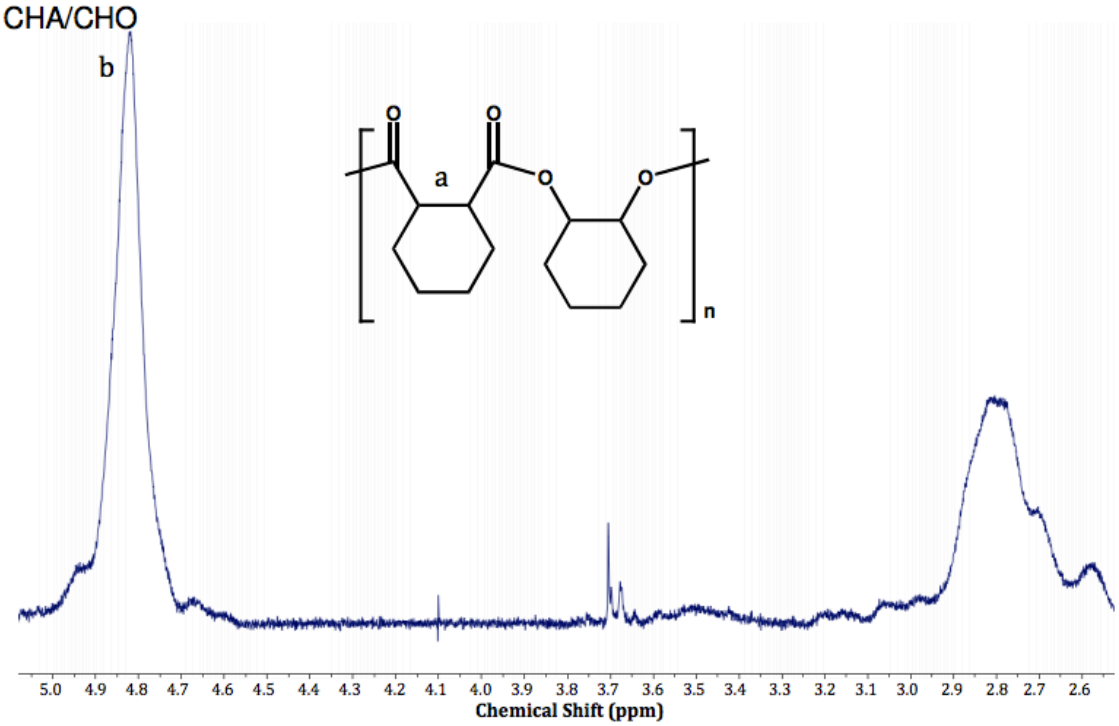
CHA/CHO
b
a
5.0 4.9 4.8 4.7 4.6 4.5 4.4 4.3 4.2 4.1 4.0 3.9 3.8 3.7 3.6 3.5 3.4 3.3 3.2 3.1 3.0 2.9 2.8 2.7 2.6
Chemical Shift (ppm)

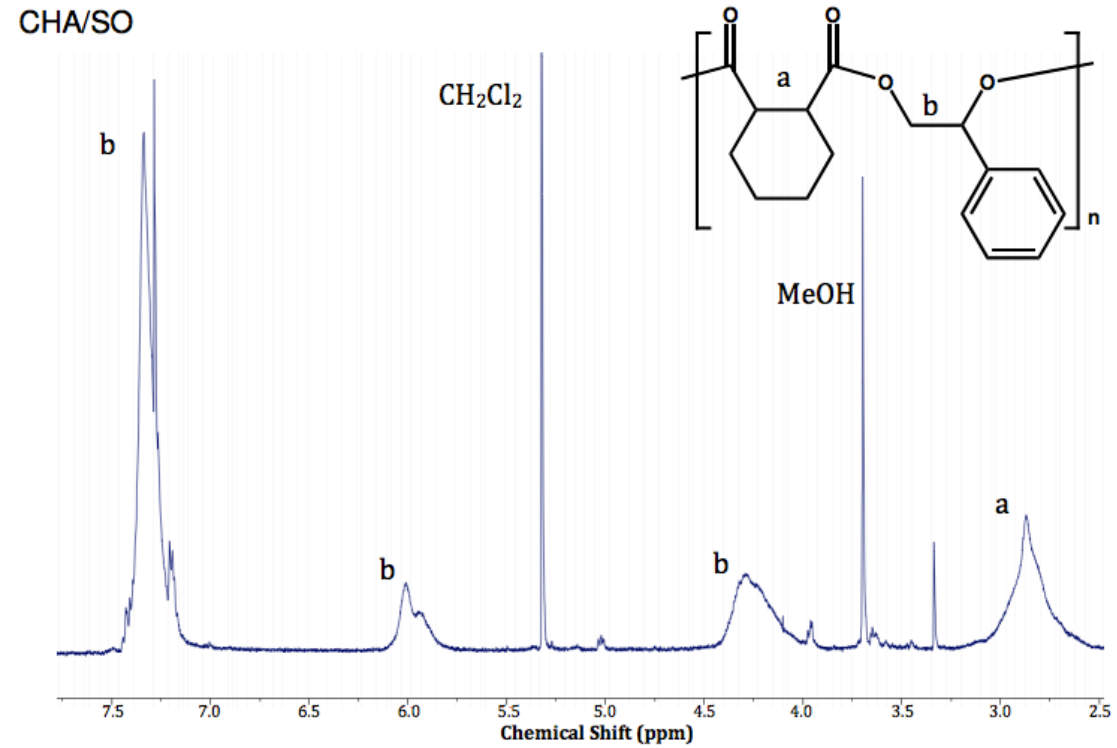
CHA/SO
CH_2Cl_2
MeOH
a
b
n
Chemical Shift (ppm)

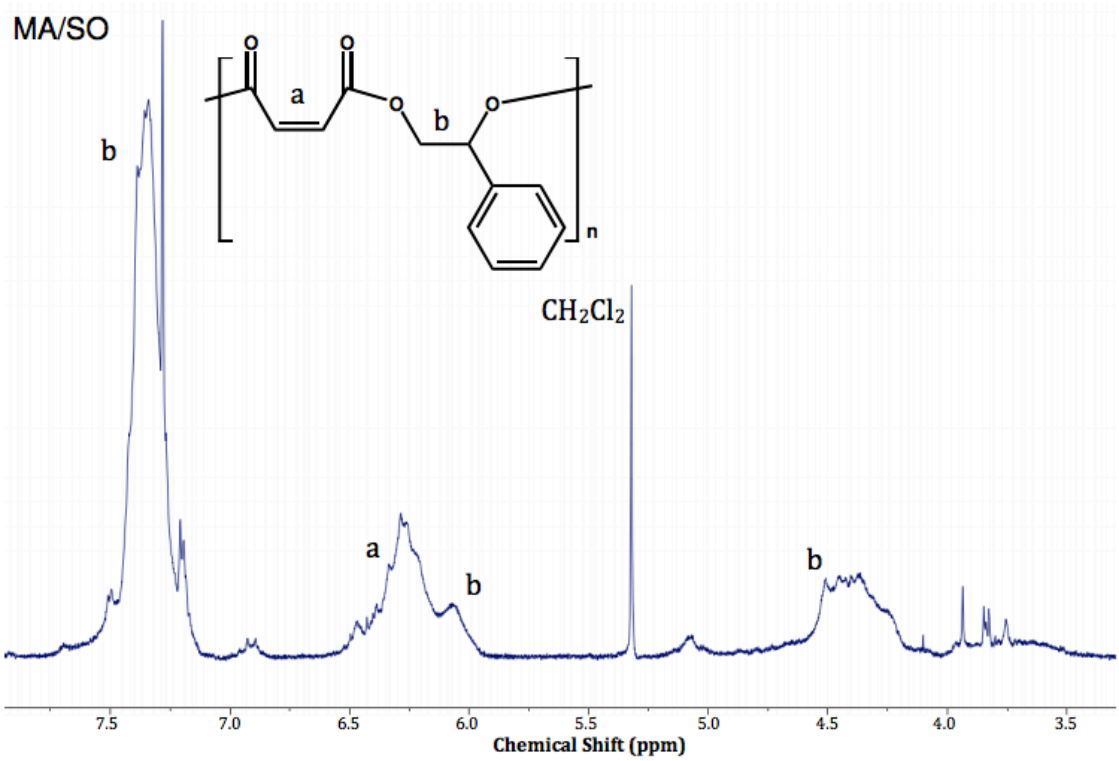
MA/SO
CH_2Cl_2
a
b
n
Chemical Shift (ppm)

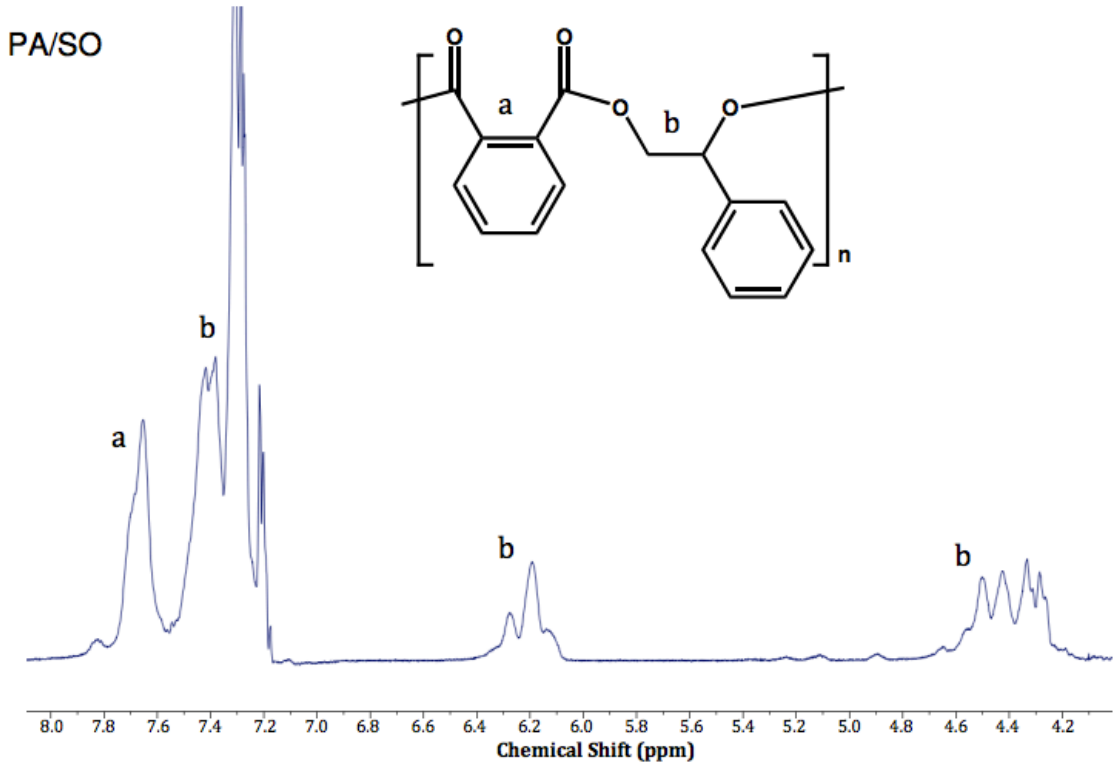
PA/SO
a
b
b
b
b
8.0 7.8 7.6 7.4 7.2 7.0 6.8 6.6 6.4 6.2 6.0 5.8 5.6 5.4 5.2 5.0 4.8 4.6 4.4 4.2
Chemical Shift (ppm)

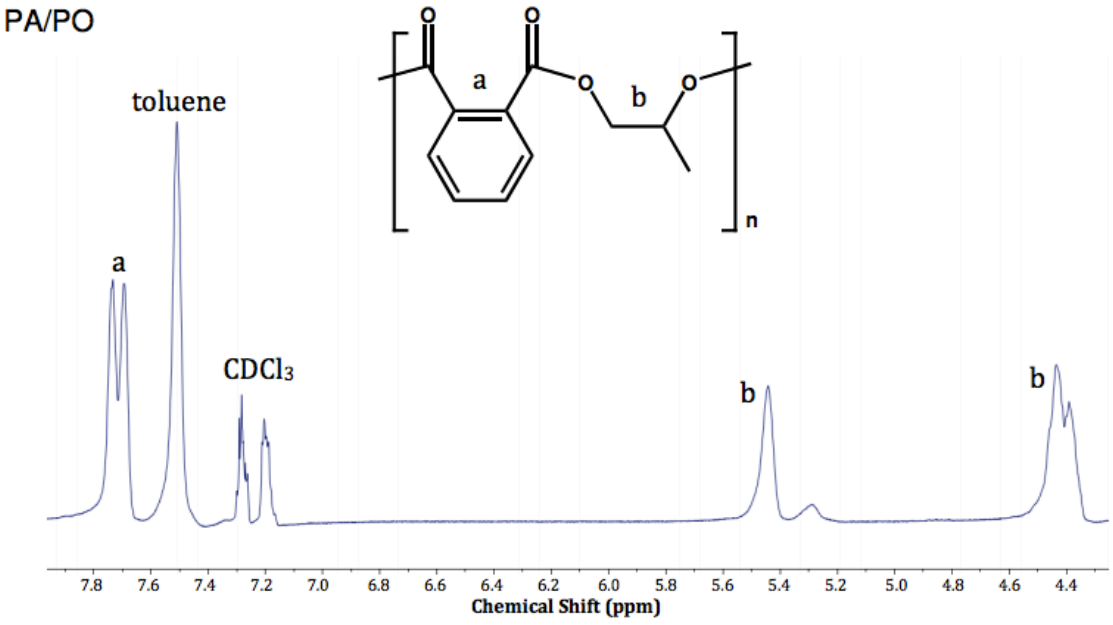
PA/PO
toluene
a
CDCl3
b
b
7.8 7.6 7.4 7.2 7.0 6.8 6.6 6.4 6.2 6.0 5.8 5.6 5.4 5.2 5.0 4.8 4.6 4.4
Chemical Shift (ppm)

PA/CHO-block-PCHC

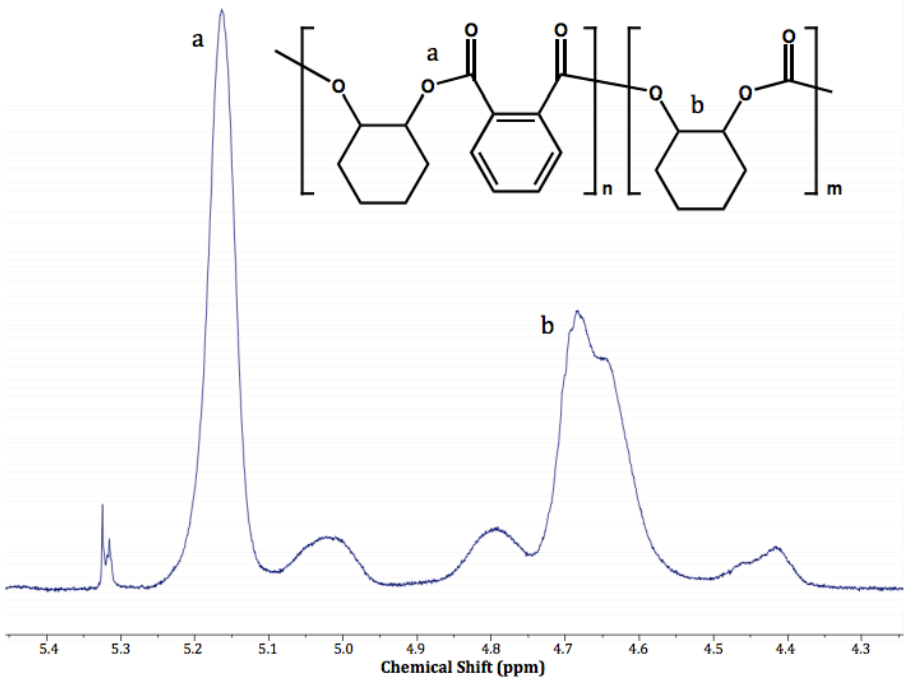

MA/PO

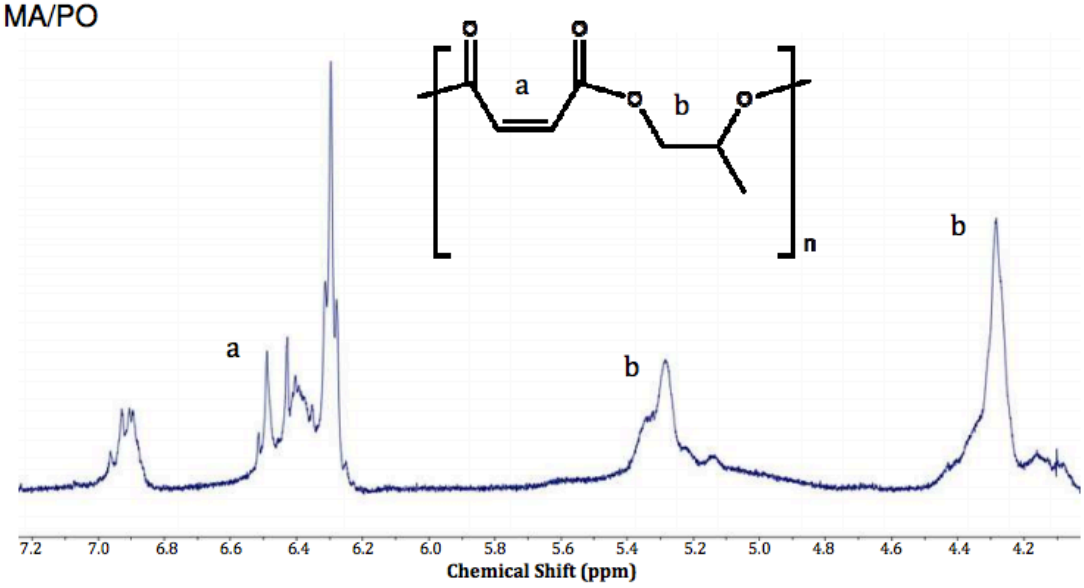

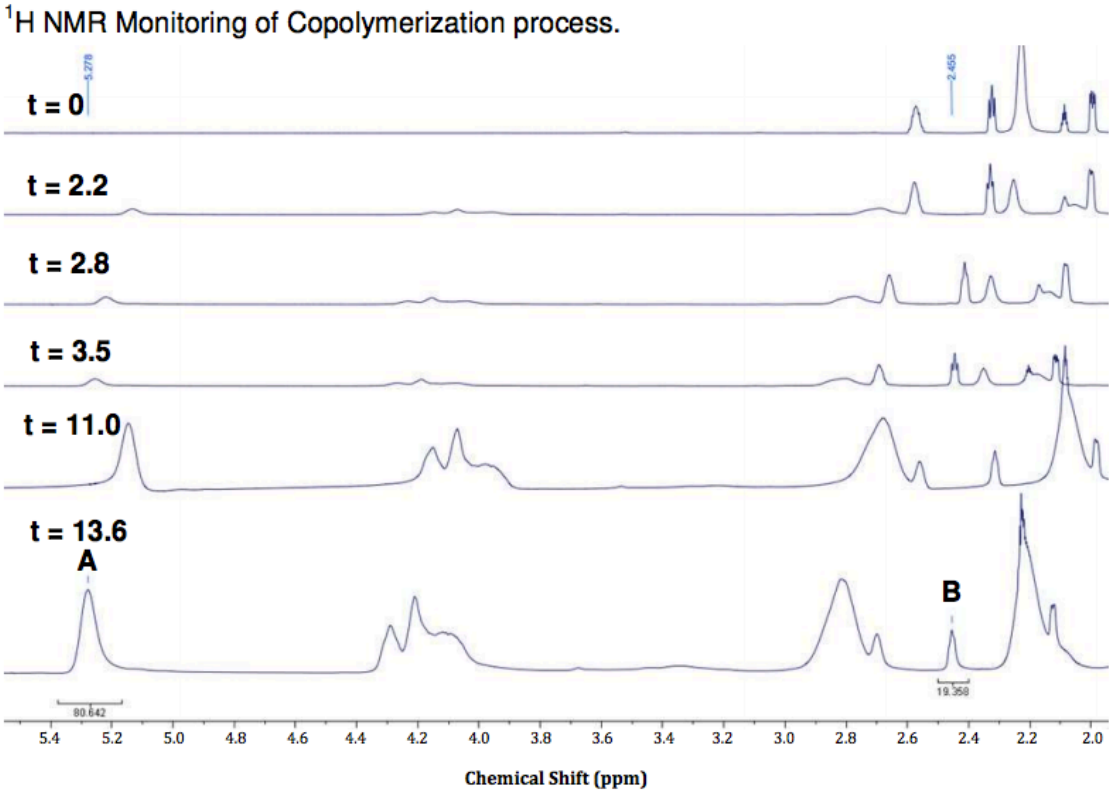

Representative ^{1}H NMR overlay, PO + CHA. Time is represented in hours. To determine % conversion PO monomer asymmetric methylene peak (Peak B) was integrated against CHAPO methine peak from PO monomeric unit (Peak A). Time is reported in hours. Reaction coordinates are provided in Figure 4-13.

APPENDIX B

SUPPORTING CRYSTALLOGRAPHIC DATA FOR CHAPTER 6

Structure B-1: $TpMn(CO)_3$

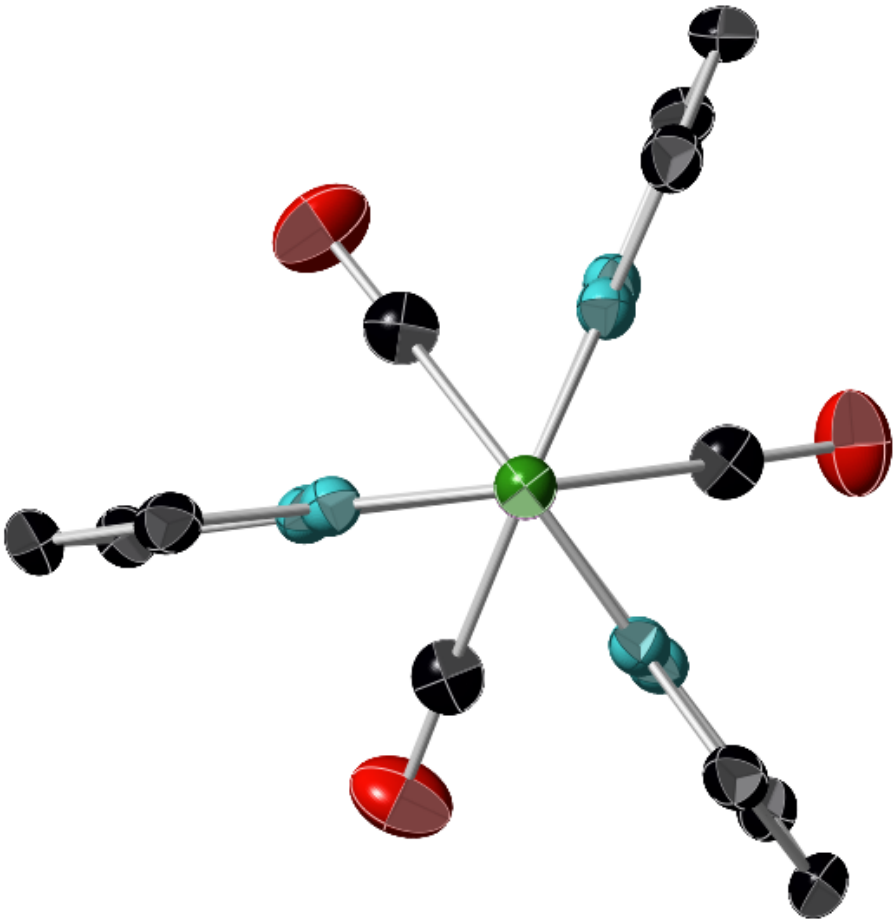

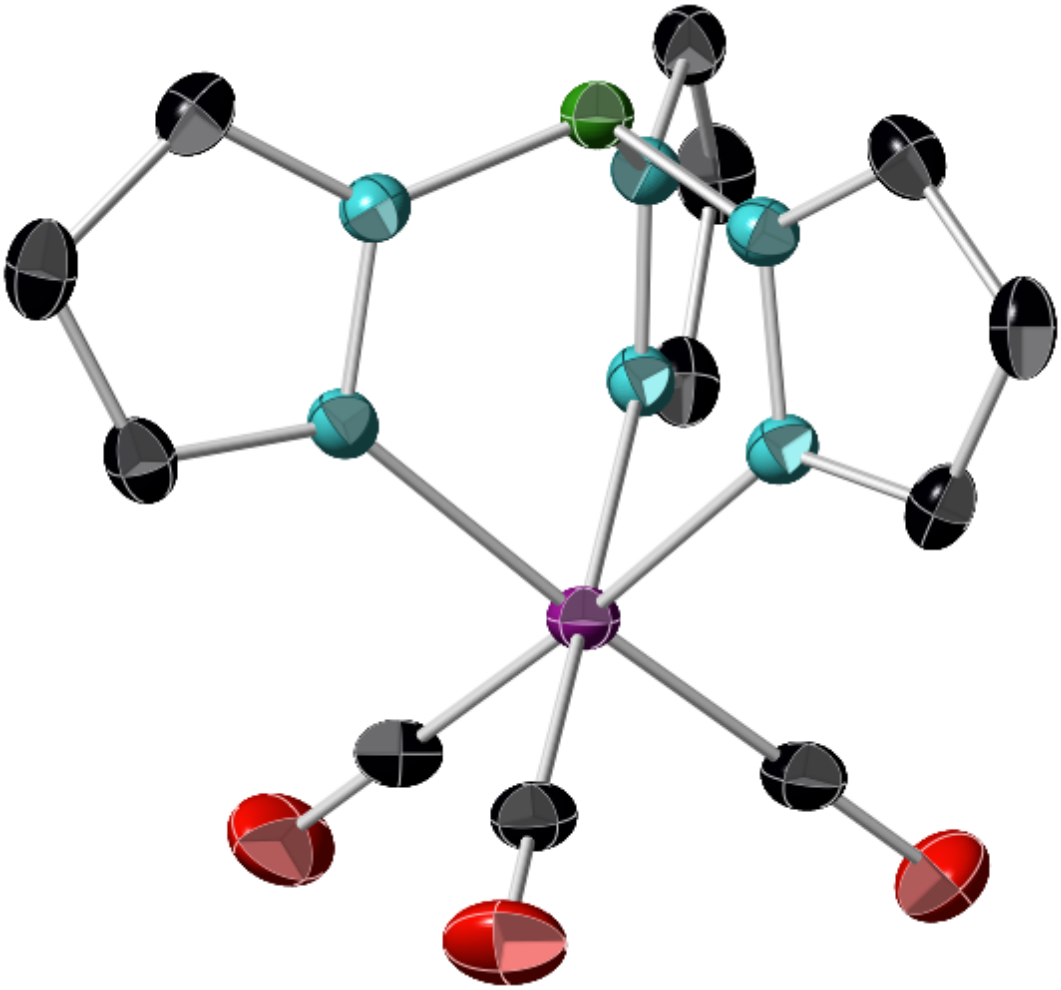

Table B-1. Crystal data and structure refinement for rp009_0m.

Identification code	rp009_0m
Empirical formula	C12 H10 B Mn N6 O3
Formula weight	352.01
Temperature	77(2) K
Wavelength	0.71073 Å
Crystal system	Hexagonal

Space group	P-3
Unit cell dimensions	a = 11.3823(7) Å a= 90°.
	b = 11.3823(7) Å b= 90°.
	c = 7.8487(10) Å g = 120°.
Volume	880.62(14) Å3
Z	2
Density (calculated)	1.328 Mg/m3
Absorption coefficient	0.769 mm-1
F(000)	356
Crystal size	0.2 x 0.2 x 0.2 mm3
Theta range for data collection	2.07 to 26.74°.
Index ranges	-14<=h<=14, -14<=k<=14, -9<=l<=9
Reflections collected	9672
Independent reflections	1254 [R(int) = 0.0742]
Completeness to theta = 26.74°	100.0 %
Absorption correction	Semi-empirical from equivalents
Max. and min. transmission	0.9721 and 0.9721
Refinement method	Full-matrix least-squares on F^2
Data / restraints / parameters	1254 / 0 / 73
Goodness-of-fit on F^2	1.090
Final R indices [I>2sigma(I)]	R1 = 0.0286, wR2 = 0.0835
R indices (all data)	R1 = 0.0308, wR2 = 0.0843

Largest diff. peak and hole 0.966 and -0.285 e.Å-3S91

Table B-2. Atomic coordinates (x 10^4) and equivalent isotropic displacement parameters (Å^{2}x 10^3) for rp009_0m. U(eq) is defined as one third of the trace of the orthogonalized U^{ij} tensor.

	x	y	z	U(eq)
B(1)	3333	6667	6319(4)	20(1)
C(1)	2024(2)	5368(2)	969(2)	26(1)
C(2)	3276(2)	4058(2)	3635(2)	24(1)
C(3)	3225(2)	3441(2)	5180(2)	28(1)
C(4)	3231(2)	4313(2)	6397(2)	24(1)
Mn(1)	3333	6667	2281(1)	19(1)
N(3)	3273(1)	5379(1)	5610(2)	19(1)
N(4)	3300(1)	5233(1)	3890(2)	19(1)
O(1)	1204(2)	4542(2)	132(2)	41(1)

Table B-3. Bond lengths [Å] and angles [°] for rp009_0m

B(1)-N(3)#1	1.5363(17)
B(1)-N(3)#2	1.5363(17)

Bond lengths [Å] and angles [°] for rp009_0m

B(1)-N(3)	1.5363(17)
C(1)-O(1)	1.144(2)
C(1)-Mn(1)	1.8064(18)
C(2)-N(4)	1.339(2)
C(2)-C(3)	1.388(3)
C(2)-H(3)	0.9300
C(3)-C(4)	1.375(2)
C(3)-H(2)	0.9300
C(4)-N(3)	1.342(2)
C(4)-H(1)	0.9300
Mn(1)-C(1)#1	1.8064(18)
Mn(1)-C(1)#2	1.8064(18)
Mn(1)-N(4)#1	2.0487(14)
Mn(1)-N(4)#2	2.0487(14)
Mn(1)-N(4)	2.0487(14)
N(3)-N(4)	1.3622(19)
N(3)#1-B(1)-N(3)#2	107.64(12)
N(3)#1-B(1)-N(3)	107.64(12)
N(3)#2-B(1)-N(3)	107.64(12)

Bond lengths [Å] and angles [°] for rp009_0m

O(1)-C(1)-Mn(1)	179.25(17)
N(4)-C(2)-C(3)	110.50(15)
N(4)-C(2)-H(3)	124.8
C(3)-C(2)-H(3)	124.8
C(4)-C(3)-C(2)	104.92(15)
C(4)-C(3)-H(2)	127.5
C(2)-C(3)-H(2)	127.5
N(3)-C(4)-C(3)	108.56(15)
N(3)-C(4)-H(1)	125.7
C(3)-C(4)-H(1)	125.7
C(1)#1-Mn(1)-C(1)	90.74(8)
C(1)#1-Mn(1)-C(1)#2	90.74(8)
C(1)-Mn(1)-C(1)#2	90.74(8)
C(1)#1-Mn(1)-N(4)#1	91.17(7)
C(1)-Mn(1)-N(4)#1	92.01(7)
C(1)#2-Mn(1)-N(4)#1	176.63(7)
C(1)#1-Mn(1)-N(4)#2	92.01(7)
C(1)-Mn(1)-N(4)#2	176.63(7)
C(1)#2-Mn(1)-N(4)#2	91.17(7)
N(4)#1-Mn(1)-N(4)#2	85.98(6)

Bond lengths [Å] and angles [°] for rp009_0m

C(1)#1-Mn(1)-N(4)	176.63(7)
C(1)-Mn(1)-N(4)	91.17(7)
C(1)#2-Mn(1)-N(4)	92.01(7)
N(4)#1-Mn(1)-N(4)	85.98(6)
N(4)#2-Mn(1)-N(4)	85.98(6)
C(4)-N(3)-N(4)	109.77(13)
C(4)-N(3)-B(1)	131.33(16)
N(4)-N(3)-B(1)	118.87(15)
C(2)-N(4)-N(3)	106.25(13)
C(2)-N(4)-Mn(1)	133.36(12)
N(3)-N(4)-Mn(1)	120.39(10)

Symmetry transformations used to generate equivalent atoms:

#1 -x+y,-x+1,z #2 -y+1,x-y+1,z

Table B-4. Anisotropic displacement parameters ($Å^2 x\ 10^3$) for rp009_0m. The anisotropic displacement factor exponent takes the form: $-2\pi^2[\ h^2 a^{*2} U^{11} + ... + 2\ h\ k\ a^* b^*\ U^{12}]$

U^{11}	U^{22}	U^{33}	U^{23}	U^{13}	U^{12}

B(1)	21(1)	21(1)	18(1)	0	0	10(1)
C(1)	29(1)	31(1)	18(1)	1(1)	2(1)	15(1)
C(2)	21(1)	21(1)	30(1)	-4(1)	2(1)	11(1)
C(3)	24(1)	21(1)	41(1)	3(1)	1(1)	14(1)
C(4)	22(1)	24(1)	27(1)	6(1)	-1(1)	12(1)
Mn(1)	21(1)	21(1)	15(1)	0	0	10(1)
N(3)	19(1)	20(1)	18(1)	1(1)	0(1)	9(1)
N(4)	18(1)	20(1)	19(1)	-1(1)	1(1)	9(1)
O(1)	36(1)	43(1)	31(1)	-11(1)	-8(1)	9(1)

Table 5. Hydrogen coordinates (x 10^4) and isotropic displacement parameters ($Å^2$x 10^3) for rp009_0m.

	x	y	z	U(eq)
H(3)	3291	3705	2572	31(5)
H(2)	3194	2618	5354	34(5)
H(1)	3209	4184	7569	32(5)

VITA

Ross Rivers Poland was born to Shep and Mary Poland. Ross graduated from high school with honors in May, 2003. He then enrolled in Rose-Hulman Institute of Technology pursing a Bachelors of Science in Chemistry in the Fall of 2003. He graduated from Rose-Hulman with a B.S. in Chemistry and minor in Language and Literature in May, 2007. A month later, Ross joined the research laboratories of Dr. Donald J. Darensbourg at Texas A&M University. He receieved his Ph.D. in Inorganic Chemistry in May of 2012. In April of 2012, Ross began his career in industrial chemistry as a Fuel Additive Chemist for Baker Hughes Inc. in Sugarland, TX.

Ross may be reached *via* electronic mail at polandrr@gmail.com. Any physical mail may be addressed to PO Box 647 Wharton, TX 77488.